ornl

OAK RIDGE NATIONAL LABORATORY

MARTIN MARIETTA

ORNL/TM-10569

Radiation Exposure Inside Reinforced Concrete Buildings at Nagasaki

W. A. Rhoades
R. L. Childs
D. T. Ingersoll

OPERATED BY
MARTIN MARIETTA ENERGY SYSTEMS, INC.
FOR THE UNITED STATES
DEPARTMENT OF ENERGY

ORNL/TM-10569

Engineering Physics and Mathematics Division

RADIATION EXPOSURE INSIDE REINFORCED CONCRETE BUILDINGS AT NAGASAKI

W. A. Rhoades, R. L. Childs,* and D. T. Ingersoll

DATE PUBLISHED — May 1989

*Computing and Telecommunications Division

Prepared for the
Defense Nuclear Agency Under
Interagency Agreement No. 40-65-A1

Prepared by the
OAK RIDGE NATIONAL LABORATORY
Oak Ridge, Tennessee 37831
operated by
MARTIN MARIETTA ENERGY SYSTEMS, INC.
for the
U.S. DEPARTMENT OF ENERGY
under contract DE-AC05-84OR21400

CONTENTS

ABSTRACT

The biological effects on the residents of Hiroshima and Nagasaki due to initial-irradiation exposure during the nuclear attacks of World War II was recognized immediately as an important source of information. After the war, an extensive effort gathered data concerning the locations of individuals at the time of the attack and their subsequent medical histories. The data from personnel located in reinforced concrete buildings are particularly significant, since large groups of occupants received radiation injury without complications due to blast and thermal effects.

In order to correlate the radiation dose with physiological effects, the dose to each individual must be calculated. Enough information about the construction of the buildings was available after the war to allow a radiation transport model to be constructed, but the accurate calculation of penetration into such large, thick-walled three-dimensional structures was beyond the scope of computing technology until recently. Now, the availability of Cray vector computers and the development of a specially-constructed discrete ordinates transport code, TORT, have combined to allow the successful completion of such a study.

This document describes the radiation transport calculations and tabulates the resulting doses by source component and individual case location. An extensive uncertainty analysis is also included. These data are to be used in another study as input to a formal statistical analysis, resulting in a new value for the LD50 dose, i.e., the dose at which the mortality risk is 50%.

1. OVERVIEW

1.1 OBJECTIVE AND SIGNIFICANCE OF THE STUDY

Since the end of World War II (WWII), numerous studies have been directed toward correlating the radiation exposure at Hiroshima and Nagasaki with the resulting risk of fatality. This information is important to military and civilian agencies in planning effective response to a nuclear attack or accident.

The information from the WWII exposures has certain advantages over information gained from other sources. The rate of dose delivery was very high, as it would be in an attack or accident situation. The locations and the shielding situations of the exposed personnel were carefully catalogued after the war, and the dose can thus be calculated more accurately than the dose in many accident situations. The personnel were in relatively good health, given the hardships of wartime life, and thus more representative of potential exposure victims than the subjects of clinical radiation treatment.

Accordingly, the determination of the actual radiation dose to personnel, the incidence of radiation-induced fatality, and the correlation between these data have received the most intensive kind of analytical attention. A very early study appears to have started in or about 1946.[1,2] A collection of unpublished studies dating to about 1954 includes rudimentary line-of-sight shielding estimates.[3] The effort has continued to such an extent that a 1987 conference of the American Nuclear Society featured an entire session on the WWII dose evaluation. At that session, Loewe stated the case for the WWII evaluation: "The public significance derives from the fact that the medical records of exposed survivors represent the only body of data relevant to radiation risk evaluation that applies to effects of whole-body radiation on humans, which includes a relatively large statistical sample representing a general population, and for which record details are available on a generally consistent basis."[4] It is the intent of this study to add to the existing body of knowledge by evaluating the dose to certain exposed personnel more accurately than has previously been possible.

1.2 COHORT SELECTION

The data collected by the postwar efforts of the Atomic Bomb Casualty Commission (ABCC),[3] the subsequent Radiation Effects Research Foundation (RERF), and others include a vast number of individual histories, but only a much smaller subset was appropriate to this study. The desirable properties of such a subset include:

- a mixture of survival and fatalities within a group of relatively similar circumstance,
- a high fraction of fatalities due to radiation effects uncomplicated by mechanical injury or burns,

- detailed medical reports on fatalities from which the cause of death can be determined,
- an accurate description of the location and position of the personnel, and
- a detailed description of the surroundings sufficient to allow determination of the radiation exposure.

The histories of personnel not protected by buildings or terrain features did not meet these criteria. Levin reports that most unprotected persons as far away as 2400 m who were not killed by debris received fatal burns, but the nuclear radiation dose at that distance was quite non-lethal.[5] SAIC reports that over 50% of the survivors in the RERF data base were inside residential dwellings at the time of the attack, and they have conducted a sophisticated analysis of those cases.[6] In general, those houses protected their occupants from most of the thermal radiation, and they also reduced the nuclear radiation by factors that sometimes exceeded 4. Houses roughly 700 to 1200 m from the hypocenter below the weapon had doses appropriate to this type of study. The analysis of those cases is complicated, however, by the fact that blast and fire injuries were widespread among that group. It is well known that nuclear radiation exposures in ordinarily non-lethal amounts enhance the effects of relatively minor injuries, making interpretation difficult.

The subject of this study, originally suggested by Dikewood Division of Kaman Sciences, Albuquerque, NM, is the analysis of exposure to personnel inside reinforced concrete buildings at ranges of roughly 500 m. These heavy, earthquake-proof structures protected their occupants from thermal radiation, as did the residences, but the basic structure of the buildings remained relatively intact, and significant groupings of radiation victims relatively free of other injuries were found. The study concentrated on buildings at Nagasaki, since there is significantly less uncertainty in the radiation source data for that city.

1.3 BUILDING SELECTION

The first building selected, "Building A," was the main building of the Chinzei School, located roughly 500 m southwest of ground zero (GZ). This building consisted of four stories and a basement. The interior was dominated by heavy concrete support structure and internal walls dividing each floor into rooms. The third floor included an auditorium at the north end that extended past the fourth floor to the roof. The roof collapsed at the time of the blast, and all personnel on the third and fourth floors died during that day. The remaining personnel received doses ranging from well past the survival limit to well below it. It will be seen that the building attenuated the incident radiation by factors ranging from about 4 near windows facing the blast to 50 and higher. A wooden structure stood on the same grounds as the concrete building, but it was of no importance to this study.

The other building, "Building C," was the south wing of the Shiroyama school, located roughly 500 m west of GZ. The school complex had additional wings, but they contained no cases of interest to this study. The building consisted of only three floors, with all of the personnel located on the second and third. The lowest doses in this building were sufficient to cause serious radiation injury.

1.4 EXTERNAL RADIATION SOURCES

The radiation field external to the buildings had been calculated as a part of another study.[7] The external sources significant to this study included:

- prompt gammas arriving directly from the weapon,
- prompt neutrons arriving directly from the weapon,
- prompt gammas from air/ground neutron capture (n,gamma), and
- delayed gammas from the weapon debris.

All of the prompt sources were furnished by Pace,[8] while the delayed sources were furnished by Gritzner.[9] Each source was used to construct a detailed space-direction-energy source description around the outer surface of the buildings.

1.5 INTERIOR DOSE CALCULATION

In order to calculate the transport of radiation inside each building, a detailed geometric description of the structure was required. This was assembled from blueprints, sketches, photographs, etc. largely from Refs. 1–3 and associated files. A well-proven two-dimensional (2-D) transport code, DOT,[10] was literally taken apart and rebuilt to perform the three-dimensional (3-D) calculations required by this study. Extensive testing and comparison supported the validity of the new code, TORT.[11] Each of the external sources was used separately, so that each contribution to the total could be identified.

The dose rates as a function of position were obtained by folding energy-dependent response functions developed by Pace[8] and Ryman[12] with the fluxes obtained from TORT. Separate functions were obtained for:

- tissue free in air (FIA),
- small intestine average (SI), and
- bone marrow average (BM).

In a separate effort, Stohler and associates[13] evaluated the extensive files of personnel locations and injuries. The histories were screened in order to reject cases in which the radiation effect was accompanied by significant non-nuclear injury or where the location and fate of the victims could not be determined with confidence. The doses in the specific locations of the applicable cases were obtained by interpolating the TORT data. The effect of positional uncertainty was obtained by examining the effect of small displacements representing that uncertainty.

1.6 RESULTS

In addition to tables of doses and positional uncertainties, contour plots of dose inside the building were obtained. Using the fatality information provided by Dikewood, the "transition range" of mixed mortality was estimated. A detailed uncertainty analysis was performed. These results and their determination will be discussed at length in the following sections. Subsequent studies are to apply formal statistical methods to arrive at a new value for the LD50 dose, i.e., the dose at which the mortality risk is 50%.

1.7 DATA REFERENCES

In later sections, it will be found that much of the data relating to the construction of the buildings was collected in the period following WWII, and it was collected in feet and inches. It is beyond the scope of this project to reverse that fact, and so many references to building dimensions will be in those units. To do otherwise would thwart checking and reliability. The reader may be assured that all calculations reported herein were performed in proper metric units, and the results will be reported accordingly.

2. BASIC NUCLEAR DATA

2.1 CROSS SECTION LIBRARIES

Three sets of cross section data were used in the concrete building studies, although only the largest set was used in the final dose determination:

Neutron groups	Gamma groups	Total groups	Application
13	7	20	Preliminary method studies
37	21	58	Early production runs
46	23	69	Final production runs

The largest library, the 69-group set, is a current DNA standard called "DABL-69."[14] It was based on the fine-group VITAMIN-E collection,[15,16] and all final doses tabulated herein were calculated with these data. Certain preliminary data were calculated using a 58-group library using an older energy structure[17] with data from VITAMIN-E. A 20-group library was prepared by additional weighting of the 58-group data.

The energy boundaries for these libraries are shown in Tables 2.1–2.3. It can be seen that each of the smaller libraries is a subset of the now-standard 69-group set. The nuclide content of the 20-group set, listed in Table 2.4, is smaller than that of the larger sets, but it sufficed to mix the simple materials needed for this study. The 20-group and 58-group libraries are limited to P_3 cross section expansion, while the 69-group library has P_5 capability.

Table 2.1 DNA 20-group cross section library group energy boundaries

Group	Neutron group boundaries (eV)	Group	Gamma group boundaries (eV)
1	1.964E+7[a]	1	2.0E+7
2	1.000E+7	2	8.0E+6
3	6.376E+6	3	6.0E+6
4	3.012E+6	4	3.0E+6
5	1.108E+6	5	1.0E+6
6	5.502E+5	6	4.5E+5
7	1.576E+5	7	1.0E+5
8	5.248E+4		1.0E+4
9	1.059E+4		
10	1.234E+3		
11	1.013E+2		
12	1.068E+1		
13	1.125E+0		
	1.E−5		

[a]Read as 1.964×10^7.

2.2 KERMA RESPONSE FUNCTIONS

The dose in these calculations is evaluated by folding kerma response functions with the flux at a given point. Kerma is defined as: "...the total kinetic energy of all the charged particles liberated by neutron and gamma rays in a small volume of a given material divided by the mass of the material in that volume element."[7] This definition is compatible with the definition of dose in rad units defined by Goldstein.[18] For these purposes, however, the centiGray (cGy) unit will be used. Doses in centiGrays are numerically equal to doses in rads. The definition of kerma does not include the kinetic energy of neutral recoil atoms, and so kerma would be slightly less than the total energy deposition.

Our first application of this concept is the "free-in-air" (FIA) soft tissue kerma, i.e. the kerma in an infinitesimal particle of soft tissue at a given point. Since this kerma is independent of direction, the resulting response function is dependent only upon energy. Accordingly, the kerma can be determined by folding the response function with the scalar flux at any location. The free-in-air kerma response functions for the 20-group and 69-group libraries, determined by Pace, are listed in Tables 2.5 and 2.6.[8] These were obtained from the data of Kerr by reducing Kerr's responses[19] to the VITAMIN-E group structure using the VITAMIN-E weighting spectrum, performing a 1-D air-transport calculation with a point source representing the weapon leakage, and further reducing the data to the final group

Table 2.2 DNA 58-group cross section library group energy boundaries

Group	Neutron energy range (eV)	Group	Gamma energy range (eV)
1	1.964030E+07—1.690461E+07	1	1.400000E+07—1.000000E+07
2	1.690461E+07—1.491830E+07	2	1.000000E+07—8.000000E+06
3	1.491830E+07—1.419070E+07	3	8.000000E+06—7.000000E+06
4	1.419070E+07—1.384030E+07	4	7.000000E+06—6.000000E+06
5	1.384030E+07—1.252320E+07	5	6.000000E+06—5.000000E+06
6	1.252320E+07—1.221400E+07	6	5.000000E+06—4.000000E+06
7	1.221400E+07—1.105170E+07	7	4.000000E+06—3.000000E+06
8	1.105170E+07—1.000000E+07	8	3.000000E+06—2.500000E+06
9	1.000000E+07—9.048370E+06	9	2.500000E+06—2.000000E+06
10	9.048370E+06—8.187310E+06	10	2.000000E+06—1.500000E+06
11	8.187310E+06—7.408180E+06	11	1.500000E+06—1.000000E+06
12	7.408180E+06—6.376280E+06	12	1.000000E+06—7.000000E+05
13	6.376280E+06—4.965850E+06	13	7.000000E+05—4.500000E+05
14	4.965850E+06—4.723670E+06	14	4.500000E+05—3.000000E+05
15	4.723670E+06—4.065700E+06	15	3.000000E+05—1.500000E+05
16	4.065700E+06—3.011940E+06	16	1.500000E+05—1.000000E+05
17	3.011940E+06—2.385210E+06	17	1.000000E+05—7.000000E+04
18	2.385210E+06—2.306860E+06	18	7.000000E+04—4.500000E+04
19	2.306860E+06—1.826840E+06	19	4.500000E+04—3.000000E+04
20	1.826840E+06—1.108030E+06	20	3.000000E+04—2.000000E+04
21	1.108030E+06—5.502320E+05	21	2.000000E+04—1.000000E+04
22	5.502320E+05—1.576440E+05		
23	1.576440E+05—1.110900E+05		
24	1.110900E+05—5.247520E+04		
25	5.247520E+04—2.478750E+04		
26	2.478750E+04—2.187490E+04		
27	2.187490E+04—1.059460E+04		
28	1.059460E+04—3.354630E+03		
29	3.354630E+03—1.234100E+03		
30	1.234100E+03—5.829470E+02		
31	5.829470E+02—1.013010E+02		
32	1.013010E+02—2.902319E+01		
33	2.902319E+01—1.067700E+01		
34	1.067700E+01—3.059020E+00		
35	3.059020E+00—1.125350E+00		
36	1.125350E+00—4.139940E−01		
37	4.139940E−01—1.000010E−05		

Table 2.3 DNA 69-group cross section library group energy boundaries

Group	Neutron energy range (eV)	Group	Gamma energy range (eV)
1	1.964030E+07—1.690461E+07	1	2.000000E+07—1.400000E+07
2	1.690461E+07—1.491830E+07	2	1.400000E+07—1.200000E+07
3	1.491830E+07—1.419070E+07	3	1.200000E+07—1.000000E+07
4	1.419070E+07—1.384030E+07	4	1.000000E+07—8.000000E+06
5	1.384030E+07—1.252320E+07	5	8.000000E+06—7.000000E+06
6	1.252320E+07—1.221400E+07	6	7.000000E+06—6.000000E+06
7	1.221400E+07—1.105170E+07	7	6.000000E+06—5.000000E+06
8	1.105170E+07—1.000000E+07	8	5.000000E+06—4.000000E+06
9	1.000000E+07—9.048370E+06	9	4.000000E+06—3.000000E+06
10	9.048370E+06—8.187310E+06	10	3.000000E+06—2.500000E+06
11	8.187310E+06—7.408180E+06	11	2.500000E+06—2.000000E+06
12	7.408180E+06—6.376280E+06	12	2.000000E+06—1.500000E+06
13	6.376280E+06—4.965850E+06	13	1.500000E+06—1.000000E+06
14	4.965850E+06—4.723670E+06	14	1.000000E+06—7.000000E+05
15	4.723670E+06—4.065700E+06	15	7.000000E+05—4.500000E+05
16	4.065700E+06—3.011940E+06	16	4.500000E+05—3.000000E+05
17	3.011940E+06—2.385210E+06	17	3.000000E+05—1.500000E+05
18	2.385210E+06—2.306860E+06	18	1.500000E+05—1.000000E+05
19	2.306860E+06—1.826840E+06	19	1.000000E+05—7.000000E+04
20	1.826840E+06—1.422740E+06	20	7.000000E+04—4.500000E+04
21	1.422740E+06—1.108030E+06	21	4.500000E+04—3.000000E+04
22	1.108030E+06—9.616400E+05	22	3.000000E+04—2.000000E+04
23	9.616400E+05—8.208500E+05	23	2.000000E+04—1.000000E+04
24	8.208500E+05—7.427360E+05		
25	7.427360E+05—6.392790E+05		
26	6.392790E+05—5.502320E+05		
27	5.502320E+05—3.688320E+05		
28	3.688320E+05—2.472350E+05		
29	2.472350E+05—1.576440E+05		
30	1.576440E+05—1.110900E+05		
31	1.110900E+05—5.247520E+04		
32	5.247520E+04—3.430670E+04		
33	3.430670E+04—2.478750E+04		
34	2.478750E+04—2.187490E+04		
35	2.187490E+04—1.059460E+04		
36	1.059460E+04—3.354630E+03		
37	3.354630E+03—1.234100E+03		
38	1.234100E+03—5.829470E+02		
39	5.829470E+02—2.753640E+02		
40	2.753640E+02—1.013010E+02		
41	1.013010E+02—2.902319E+01		
42	2.902319E+01—1.067700E+01		
43	1.067700E+01—3.059020E+00		
44	3.059020E+00—1.125350E+00		
45	1.125350E+00—4.139940E−01		
46	4.139940E−01—1.000010E−05		

Table 2.4 Contents of the DNA 20-group library[a]

ID no.=	1	TITLE= p0	H-1	MINX(1301/1) XLACS(1002) 08-14-85 17
ID no.=	2	TITLE= p1	H-1	MINX(1301/1) XLACS(1002) 08-14-85 17
ID no.=	3	TITLE= p2	H-1	MINX(1301/1) XLACS(1002) 08-14-85 17
ID no.=	4	TITLE= p3	H-1	MINX(1301/1) XLACS(1002) 08-14-85 17
ID no.=	21	TITLE= p0	B-10	1305/1 09-30-80 174n MINX VITAMIN-E
ID no.=	22	TITLE= p1	B-10	1305/1 09-30-80 174n MINX VITAMIN-E
ID no.=	23	TITLE= p2	B-10	1305/1 09-30-80 174n MINX VITAMIN-E
ID no.=	24	TITLE= p3	B-10	1305/1 09-30-80 174n MINX VITAMIN-E
ID no.=	25	TITLE= p0	B-11	1160/0 09-29-80 174n MINX VITAMIN-E
ID no.=	26	TITLE= p1	B-11	1160/0 09-29-80 174n MINX VITAMIN-E
ID no.=	27	TITLE= p2	B-11	1160/0 09-29-80 174n MINX VITAMIN-E
ID no.=	28	TITLE= p3	B-11	1160/0 09-29-80 174n MINX VITAMIN-E
ID no.=	29	TITLE= p0	C	1306/1 09-29-80 174n MINX VITAMIN-E
ID no.=	30	TITLE= p1	C	1306/1 09-29-80 174n MINX VITAMIN-E
ID no.=	31	TITLE= p2	C	1306/1 09-29-80 174n MINX VITAMIN-E
ID no.=	32	TITLE= p3	C	1306/1 09-29-80 174n MINX VITAMIN-E
ID no.=	33	TITLE= p0	N-14	1275/1 08-16-81 174n MINX VITAMIN-E
ID no.=	34	TITLE= p1	N-14	1275/1 08-16-81 174n MINX VITAMIN-E
ID no.=	35	TITLE= p2	N-14	1275/1 08-16-81 174n MINX VITAMIN-E
ID no.=	36	TITLE= p3	N-14	1275/1 08-16-81 174n MINX VITAMIN-E
ID no.=	37	TITLE= p0	O-16	1276/1 09-29-80 174n MINX VITAMIN-E
ID no.=	38	TITLE= p1	O-16	1276/1 09-29-80 174n MINX VITAMIN-E
ID no.=	39	TITLE= p2	O-16	1276/1 09-29-80 174n MINX VITAMIN-E
ID no.=	40	TITLE= p3	O-16	1276/1 09-29-80 174n MINX VITAMIN-E
ID no.=	45	TITLE= p0	Na-23	1311/1 09-29-80 174n MINX VITAMIN-E
ID no.=	46	TITLE= p1	Na-23	1311/1 09-29-80 174n MINX VITAMIN-E
ID no.=	47	TITLE= p2	Na-23	1311/1 09-29-80 174n MINX VITAMIN-E
ID no.=	48	TITLE= p3	Na-23	1311/1 09-29-80 174n MINX VITAMIN-E
ID no.=	49	TITLE= p0	Mg	1312/1 08-14-81 174n MINX VITAMIN-E
ID no.=	50	TITLE= p1	Mg	1312/1 08-14-81 174n MINX VITAMIN-E
ID no.=	51	TITLE= p2	Mg	1312/1 08-14-81 174n MINX VITAMIN-E
ID no.=	52	TITLE= p3	Mg	1312/1 08-14-81 174n MINX VITAMIN-E
ID no.=	53	TITLE= p0	Al-27	1313/1 11-12-80 174n MINX VITAMIN-E
ID no.=	54	TITLE= p1	Al-27	1313/1 11-12-80 174n MINX VITAMIN-E
ID no.=	55	TITLE= p2	Al-27	1313/1 11-12-80 174n MINX VITAMIN-E
ID no.=	56	TITLE= p3	Al-27	1313/1 11-12-80 174n MINX VITAMIN-E
ID no.=	57	TITLE= p0	Si	1314/1 11-15-80 174n MINX VITAMIN-E
ID no.=	58	TITLE= p1	Si	1314/1 11-15-80 174n MINX VITAMIN-E
ID no.=	59	TITLE= p2	Si	1314/1 11-15-80 174n MINX VITAMIN-E
ID no.=	60	TITLE= p3	Si	1314/1 11-15-80 174n MINX VITAMIN-E
ID no.=	61	TITLE= p0	P-31	1315/1 08-07-81 174n MINX VITAMIN-E
ID no.=	62	TITLE= p1	P-31	1315/1 08-07-81 174n MINX VITAMIN-E
ID no.=	63	TITLE= p2	P-31	1315/1 08-07-81 174n MINX VITAMIN-E
ID no.=	64	TITLE= p3	P-31	1315/1 08-07-81 174n MINX VITAMIN-E
ID no.=	65	TITLE= p0	S	1347/1 08-09-81 174n MINX VITAMIN-E
ID no.=	66	TITLE= p1	S	1347/1 08-09-81 174n MINX VITAMIN-E
ID no.=	67	TITLE= p2	S	1347/1 08-09-81 174n MINX VITAMIN-E
ID no.=	68	TITLE= p3	S	1347/1 08-09-81 174n MINX VITAMIN-E
ID no.=	73	TITLE= p0	Ar	8824 08-23-81 174n MINX VITAMIN-E
ID no.=	74	TITLE= p1	Ar	8824 08-23-81 174n MINX VITAMIN-E

Table 2.4 Cont'd

ID no.=	75	TITLE= p2	Ar	8824	08-23-81	174n	MINX	VITAMIN-E
ID no.=	76	TITLE= p3	Ar	8824	08-23-81	174n	MINX	VITAMIN-E
ID no.=	77	TITLE= p0	K	1150/1	08-16-81	174n	MINX	VITAMIN-E
ID no.=	78	TITLE= p1	K	1150/1	08-16-81	174n	MINX	VITAMIN-E
ID no.=	79	TITLE= p2	K	1150/1	08-16-81	174n	MINX	VITAMIN-E
ID no.=	80	TITLE= p3	K	1150/1	08-16-81	174n	MINX	VITAMIN-E
ID no.=	81	TITLE= p0	Ca	1320/3	10-22-83	174n	MINX	VITAMIN-E
ID no.=	82	TITLE= p1	Ca	1320/3	10-22-83	174n	MINX	VITAMIN-E
ID no.=	83	TITLE= p2	Ca	1320/3	10-22-83	174n	MINX	VITAMIN-E
ID no.=	84	TITLE= p3	Ca	1320/3	10-22-83	174n	MINX	VITAMIN-E
ID no.=	93	TITLE= p0	Cr	1324/1	10-29-80	174n	MINX	VITAMIN-E
ID no.=	94	TITLE= p1	Cr	1324/1	10-29-80	174n	MINX	VITAMIN-E
ID no.=	95	TITLE= p2	Cr	1324/1	10-29-80	174n	MINX	VITAMIN-E
ID no.=	96	TITLE= p3	Cr	1324/1	10-29-80	174n	MINX	VITAMIN-E
ID no.=	97	TITLE= p0	Mn-55	1325/2	11-19-83	174n	MINX	VITAMIN-E
ID no.=	98	TITLE= p1	Mn-55	1325/2	11-19-83	174n	MINX	VITAMIN-E
ID no.=	99	TITLE= p2	Mn-55	1325/2	11-19-83	174n	MINX	VITAMIN-E
ID no.=	100	TITLE= p3	Mn-55	1325/2	11-19-83	174n	MINX	VITAMIN-E
ID no.=	101	TITLE= p0	Fe	1326/3	10-22-83	174n	MINX	VITAMIN-E
ID no.=	102	TITLE= p1	Fe	1326/3	10-22-83	174n	MINX	VITAMIN-E
ID no.=	103	TITLE= p2	Fe	1326/3	10-22-83	174n	MINX	VITAMIN-E
ID no.=	104	TITLE= p3	Fe	1326/3	10-22-83	174n	MINX	VITAMIN-E
ID no.=	109	TITLE= p0	Ni	1328/2	11-16-83	174n	MINX	VITAMIN-E
ID no.=	110	TITLE= p1	Ni	1328/2	11-16-83	174n	MINX	VITAMIN-E
ID no.=	111	TITLE= p2	Ni	1328/2	11-16-83	174n	MINX	VITAMIN-E
ID no.=	112	TITLE= p3	Ni	1328/2	11-16-83	174n	MINX	VITAMIN-E
ID no.=	177	TITLE= p0	U-235	1395/1	10-04-80	174n	MINX	VITAMIN-E
ID no.=	178	TITLE= p1	U-235	1395/1	10-04-80	174n	MINX	VITAMIN-E
ID no.=	179	TITLE= p2	U-235	1395/1	10-04-80	174n	MINX	VITAMIN-E
ID no.=	180	TITLE= p3	U-235	1395/1	10-04-80	174n	MINX	VITAMIN-E
ID no.=	181	TITLE= p0	U-238	1398/1	11-15-80	174n	MINX	VITAMIN-E
ID no.=	182	TITLE= p1	U-238	1398/1	11-15-80	174n	MINX	VITAMIN-E
ID no.=	183	TITLE= p2	U-238	1398/1	11-15-80	174n	MINX	VITAMIN-E
ID no.=	184	TITLE= p3	U-238	1398/1	11-15-80	174n	MINX	VITAMIN-E
ID no.=	225	TITLE= p0	Ba-138	1353/1	04-20-85	174n	MINX	VITAMIN-E
ID no.=	226	TITLE= p1	Ba-138	1353/1	04-20-85	174n	MINX	VITAMIN-E
ID no.=	227	TITLE= p2	Ba-138	1353/1	04-20-85	174n	MINX	VITAMIN-E
ID no.=	228	TITLE= p3	Ba-138	1353/1	04-20-85	174n	MINX	VITAMIN-E
ID no.=	601	TITLE= p1	VOID					
ID no.=	602	TITLE= p2	VOID					
ID no.=	603	TITLE= p3	VOID					
ID no.=	604	TITLE= p4	VOID					

[a] The last portion of the title identifies the 58-group set that was the source of the data.

structure using the energy spectrum from the 1-D calculation. The FIA data presented in the tables are appropriate to the Nagasaki weapon at a radius of about 500 m. Table 2.5 also shows a uranium fission spectrum determined by collapsing a VITAMIN-E spectrum.

Table 2.6 shows two additional response functions determined by Ryman[12] for kerma in the small intestine and in bone marrow. The details of how these were derived are given in Appendix C. Since the definition of kerma as stated applies rigorously only to a "small volume," we must keep in mind that its application to an extended organ or system implies a suitable averaging process. The directional and spatial distributions have been suppressed in this averaging, so the responses can be applied in the same manner as the FIA responses.

2.3 MATERIAL COMPOSITIONS

While the geometry of the buildings was quite complex, the problems required only a simple set of material mixtures: concrete, earth, air, wood, and plaster. The compositions of these mixtures are displayed in Table 2.7, together with the actual ID numbers of the library components selected. The compositions of reinforced concrete, earth, and air were suggested by Pace.[8] The concrete is a blend appropriate to Japanese construction. The earth and air are those used in the Nagasaki air/ground transport calculations.[7] The air is applicable to altitudes of 0–125 m, and the proper amount of water has been included. The wood composition was provided by Cramer.[20] The plaster composition is from Refs. 21 and 22.

Table 2.5 DNA 20-group kerma response and fission functions

Group	Free-in-air soft-tissue kerma $\left[\frac{\text{cGy}\cdot\text{cm}^2}{\text{particle}}\right]$	Uranium fission fraction
1	6.436170E−09	1.28590E−3
2	5.178320E−09	1.93572E−2
3	4.320830E−09	1.96362E−1
4	3.029480E−09	4.45441E−1
5	2.009000E−09	1.92053E−1
6	1.246700E−09	1.19599E−1
7	6.384700E−10	2.07240E−2
8	2.515560E−10	4.71858E−3
9	5.379590E−11	4.40788E−4
10	6.456820E−12	1.85985E−5
11	1.144110E−12	4.33011E−7
12	1.916860E−12	1.48864E−8
13	9.835310E−12	5.61681E−10
14	2.936730E−09	0
15	1.982150E−09	0
16	1.455200E−09	0
17	8.320870E−10	0
18	3.765940E−10	0
19	1.404140E−10	0
20	1.131930E−10	0

Table 2.6 DNA 69-group kerma response functions

Group	Free-in-air $\frac{cGy \cdot cm^2}{particle}$	Small intestine $\frac{Gy \cdot cm^2}{particle}$	Bone marrow $\frac{Gy \cdot cm^2}{particle}$
1	0.0	0.0	0.0
2	7.077370E−09[a]	4.426527E−11	4.772557E−11
3	6.854930E−09	4.242363E−11	4.686905E−11
4	6.744980E−09	4.272550E−11	4.597830E−11
5	6.488640E−09	3.950927E−11	4.206632E−11
6	6.381350E−09	3.866144E−11	4.051942E−11
7	6.333820E−09	3.560847E−11	3.937926E−11
8	5.989160E−09	3.566422E−11	3.937441E−11
9	5.771130E−09	3.296186E−11	3.660641E−11
10	5.515770E−09	2.931333E−11	3.409208E−11
11	5.471970E−09	2.685140E−11	3.202864E−11
12	5.118050E−09	2.489206E−11	3.053506E−11
13	4.718830E−09	2.278859E−11	2.757607E−11
14	4.578040E−09	1.854872E−11	2.487749E−11
15	4.436460E−09	1.630944E−11	2.352912E−11
16	4.203620E−09	1.317658E−11	1.959037E−11
17	3.554380E−09	1.026234E−11	1.669800E−11
18	3.325070E−09	9.639425E−12	1.501879E−11
19	3.216030E−09	7.465329E−12	1.307756E−11
20	2.916400E−09	5.736491E−12	1.060127E−11
21	2.638570E−09	4.031827E−12	8.443888E−12
22	2.525510E−09	2.993088E−12	6.835394E−12
23	2.227480E−09	2.899945E−12	6.105845E−12
24	2.060070E−09	2.809753E−12	6.000444E−12
25	1.938130E−09	2.372944E−12	5.247199E−12
26	1.792150E−09	2.233542E−12	4.719108E−12
27	1.649400E−09	1.723456E−12	3.962127E−12
28	1.297760E−09	1.573431E−12	2.972716E−12
29	1.021680E−09	1.380759E−12	2.380207E−12
30	8.114740E−10	1.334669E−12	1.910536E−12
31	5.690210E−10	1.238254E−12	1.577307E−12
32	3.630200E−10	1.175168E−12	1.357668E−12
33	2.610050E−10	1.160076E−12	1.235696E−12
34	2.132010E−10	1.162470E−12	1.229365E−12
35	1.541070E−10	1.109893E−12	1.183093E−12
36	6.520750E−11	1.135166E−12	1.131684E−12
37	2.295970E−11	1.121648E−12	1.105471E−12
38	9.602990E−12	1.121044E−12	1.163116E−12
39	4.134630E−12	1.159321E−12	1.146539E−12
40	2.106530E−12	1.097105E−12	1.187130E−12
41	1.079640E−12	1.148725E−12	1.143656E−12
42	9.180880E−13	1.131138E−12	1.221251E−12
43	1.265990E−12	1.124283E−12	1.272104E−12
44	2.198230E−12	1.145612E−12	1.281946E−12
45	3.585080E−12	1.142234E−12	1.237433E−12
46	8.100940E−12	1.106108E−12	1.220370E−12

Table 2.6 Cont'd

Group	Free-in-air (FIA)	Small intestine (SI)	Bone marrow (BM)
46	0.0	0.0	0.0
47	3.175600E−09	2.544366E−11	2.769750E−11
48	2.761200E−09	2.178194E−11	2.403630E−11
49	2.351700E−09	1.806358E−11	2.000330E−11
50	2.052500E−09	1.564311E−11	1.739900E−11
51	1.852210E−09	1.380293E−11	1.563240E−11
52	1.645670E−09	1.248159E−11	1.339117E−11
53	1.436400E−09	1.061882E−11	1.165841E−11
54	1.216860E−09	1.704023E−12	9.403036E−12
55	1.036000E−09	7.084599E−12	8.113812E−12
56	9.026680E−10	6.171013E−12	6.816419E−12
57	7.580870E−10	4.883398E−12	5.514999E−12
58	5.893170E−10	3.671165E−12	4.077272E−12
59	4.266030E−10	2.523286E−12	2.837419E−12
60	2.957870E−10	1.683161E−12	1.937082E−12
61	1.951130E−10	1.068689E−12	1.263538E−12
62	1.083820E−10	5.968414E−13	7.139559E−13
63	5.296280E−11	3.327378E−13	3.743490E−13
64	3.494150E−11	2.118065E−13	2.453518E−13
65	3.110080E−11	1.469365E−13	1.601847E−13
66	4.846280E−11	7.815564E−14	1.019230E−13
67	1.049700E−10	1.238341E−14	5.347652E−14
68	3.395990E−10	0.0	1.055788E−14

Table 2.7 Library nuclide selections and material compositions

	Library ID numbers		Atomic densities (atoms/b·cm)				
Nuclide	20-group	69-group	Conc.	Earth	Air	Wood	Plaster
H−1	1	1	8.488E−3	3.521E−2	1.311E−6	2.377E−2	3.247E−2
B−10	33	49	2.21E−6	–	–	–	–
B−11	37	55	8.94E−6	–	–	–	–
C	41	61	9.681E−4	1.806E−3	–	1.426E−2	–
N−14	45	67	–	–	3.676E−5	–	–
O−16	49	75	4.852E−2	3.857E−2	1.052E−5	1.189E−2	4.870E−2
Na−23	57	85	1.158E−3	2.556E−4	–	–	–
Mg	61	91	4.907E−4	–	–	–	–
Al− 27	65	97	2.836E−3	2.816E−3	–	–	–
Si	69	103	1.277E−2	6.806E−3	–	–	–
P−31	73	109	3.112E−5	–	–	–	–
S	77	115	4.698E−5	–	–	–	8.117E−3
Ar	85	127	–	–	2.198E−7	–	–
K	89	133	4.931E−4	1.510E−4	–	–	–
Ca	93	139	3.113E−3	2.267E−4	–	–	8.117E−3
Cr	105	157	5.794E−6	–			
Mn−55	109	163	1.645E−5	1.796E−5			
Fe	113	169	6.721E−4	8.247E−4			
Ni	125	187	1.026E−6				
Cl	81	121	–	7.512E−6			
Ti	97	145	–	1.034E−4			

3. PROMPT EXTERNAL SOURCE

3.1 METHOD

The general method of calculation of prompt source used in the building calculations was as follows:

- the source of prompt neutrons and gammas in the weapon was determined from a weapon hydrodynamics calculation,
- the leakage from the weapon was determined by a radiation transport calculation,
- a static, analytical first-collision-source calculation throughout the surrounding air and ground was performed by applying the GRTUNCL code[23] to the weapon leakage,
- the source was transported from its first-collision site using the 2-D discrete ordinates code DOT, which produced directional fluence output files,
- the VISTA code was used to select and normalize the directional fluence in the vicinity of the buildings of interest, and
- the DOTTOR code was used to interpolate the RZ-geometry VISTA files to form a boundary source file on an XYZ-geometry surrounding the building.

A description of the calculation of weapon leakage and transport to the site of the buildings is given in Ref. 7. The weapon leakage calculation was performed under the direction of Whalen.[7] First, a coupled neutronic-hydrodynamic code calculated the source of neutrons and gammas. Then, a special version of the MCNP code calculated the escape of particles from the weapon mass. The neutron leakage spectrum was characterized by the leakage of relatively low-energy particles in the range 0.1–1 keV due to repeated scatters by light nuclei in the explosive material surrounding the weapon. Whalen points out that those particles did not govern the dose to personnel in the ranges of interest, however, and another peak at roughly 5 MeV, a peak of much lower magnitude, was the primary contributor to personnel dose. The gamma energy was distributed widely between 0.1 MeV and 5 MeV.

An experimental spectrum measurement was performed as a part of the ICHIBAN program, and comparisons of these results failed to show agreement with Whalen's calculations. An older measurement that did confirm Whalen's calculations was discovered, however, and they are now believed correct.

In the air/ground transport calculation, the emission from the Nagasaki weapon was represented as an isotropic point source at a height of 503 m above sea level. The GRTUNCL code performed an analytical calculation of the first-collision source, i.e., the distribution of particles after their first flight from the point source, in

cylindrical (RZ) geometry. Since the new source was distributed in space over a large volume, it formed a better starting condition for the subsequent discrete ordinates calculation. Given the output of GRTUNCL, the DOT 2-D discrete ordinates code[10] then calculated the fluence of particles in the air and ground out to a distance of about 2,000 m. The DOT output was produced in a very fine 240-direction mesh.

The cross sections used in the GRTUNCL and DOT calculations were in the same group structure as the 69-group set described earlier, but to get accurate results at large distances, it was necessary to weight the VITAMIN-E data over the spectrum calculated by a 1-D ANISN[24] calculation in a selected number of radial zones. This gave, in effect, several cross section libraries, each appropriate to a specific distance from the weapon, from which the desired accuracy was obtained.

As one of its options, DOT can produce an output file of all of the directional fluence information over a selected band of heights. Due to the large size of this output file, however, it was not practical for DOT to supply output with precisely the correct normalization and ordering needed, and an auxiliary code called VISTA was used to perform this and other services. VISTA selects a subset of heights and radial positions in the vicinity of the volume being studied, determines the correct final normalization, and sorts the data into a format suitable for subsequent processing. VISTA is an updated version of the VISA code used in the VCS code system.[25,26]

The VISTA file was then used with the DOTTOR code[27] to construct a boundary source on a surface enclosing the building being studied. DOTTOR is given both the DOT and TORT geometric grids and directional quadratures, after which it performs the transformation by interpolating the fluence data from one grid to the other.

3.2 CHOICE OF SOURCE SURFACE

It may be noted that the surface on which the TORT source is constructed must be such that the fluence entering the surface is not much perturbed by the presence of the building inside. In general, this can be satisfied in two ways:

- if the building is small with respect to a typical mean free path in air, so that escape from the building, scattering, and then re-entry into the building is relatively improbable, or
- if the source surface is so far away from the building that the scattering takes place inside the surface.

The dimensions of the buildings presently examined are sufficiently small that the probability of escape, scatter, and then re-entry is relatively small. Thus, a source surface immediately adjacent to the building is permissible. It may be noted that, since the rescatter phenomenon described is the only physical consideration in locating the surface, there would be no advantage in placing the surface at a greater distance unless the second criterion was satisfied. The second criterion would require a distance of hundreds of meters.

4. DELAYED EXTERNAL SOURCE

4.1 METHOD

The calculation of the fluence due to delayed sources is also described in Ref. 7. The sources referred to as "delayed" include radiation due to the the decay of short-term activation products, fission products, and delayed-neutron precursors in the time domain following 0.2 s. The nuclides from which these emissions occur were contained in the bomb debris and were carried upward from the detonation point in the fireball, propelled by bouyancy and shock effects. Although several sources of delayed radiation were calculated, only the delayed gammas were of such strength as to be of interest to this calculation.

The calculation of fluence at ground level due to the delayed gammas was especially difficult because the sources were constantly in motion, and because the thermal and pressure effects perturbed the atmosphere between the sources and the ground area of interest. The calculational procedure described in the reference was as follows:

- the emissions were determined as a function of time from previous experimental data,
- the flux as a function of distance for a constant point emission in a uniform air environment was determined by a 1-D ANISN calculation,
- the source location and perturbed air density at a set of discrete times were determined from the STLAMB hydrodynamics code,
- the flux was selected from the ANISN results at a radius providing an amount of air between source and observation point equivalent to the STLAMB result at the discrete times and was then normalized to the appropriate source at those times,
- the effect of ground scattering and absorption was included by a separate correction derived from the VCS code system,[25,26] and
- the resulting time-dependent flux at a given point was integrated to provide fluence.

The ANISN calculations were performed using the 38 gamma groups of the VITAMIN-E library, and these were then condensed to the 23 gamma groups of the 69-group library. The ground correction at the source height and range of interest proved to be on the order of 6%, so the accuracy of the correction was not a major concern.

Fluences from this calculation and from a somewhat similar delayed-neutron calculation were supplied by Gritzner.[9] The data file was in a format different from that of the prompt data, but a code called FIRE, developed by this study, was able

to transform the information into a form that VISTA could accept. At that point, the data were processed in the same manner as prompt files, resulting in a delayed source at the building surface. A bias of 5% was implied in the error estimates of Ref. 7, and this bias was eliminated by multiplying the doses from delayed gammas by 1.05 before use.

4.2 EARLY VS. LATE DELAYED SOURCE

It was also important to know the fraction of the delayed source arriving before the shock wave, since the shock wave rearranged much of the material inside the building. Gritzner provided data showing the time of shock arrival and the fraction of delayed gamma radiation arriving before the shock wave as a function of distance (Figs. 4.1–4.2). At the distances of concern in this study, about 500 m, 30% of the delayed gamma source arrived before the shock wave and is thus termed "early delayed source." The remainder is "late delayed source."

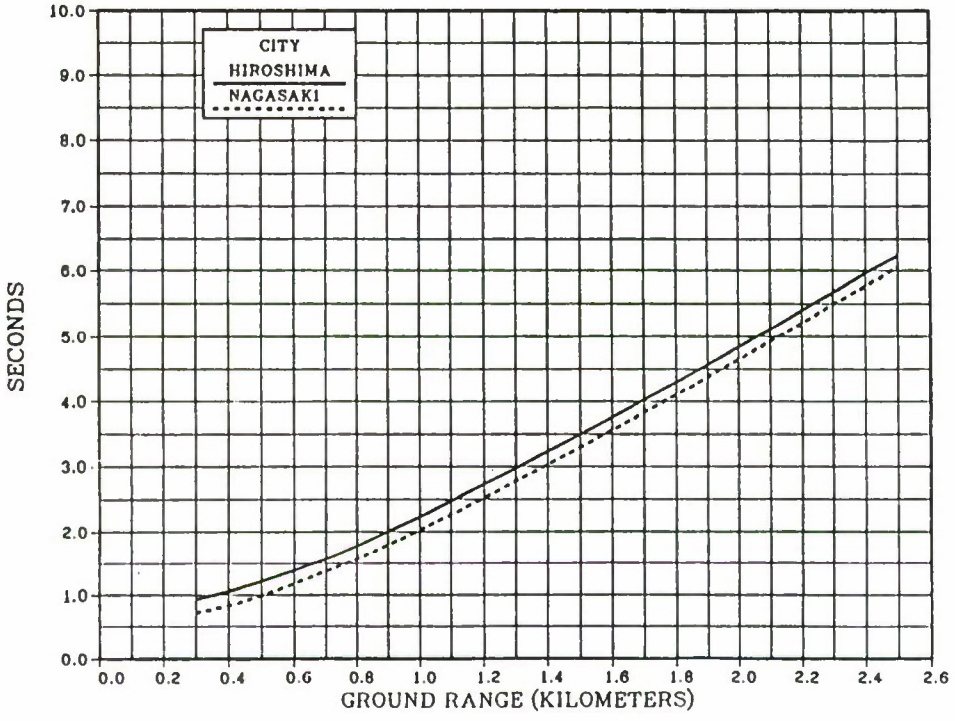

Figure 4.1 Blast wave time of arrival.

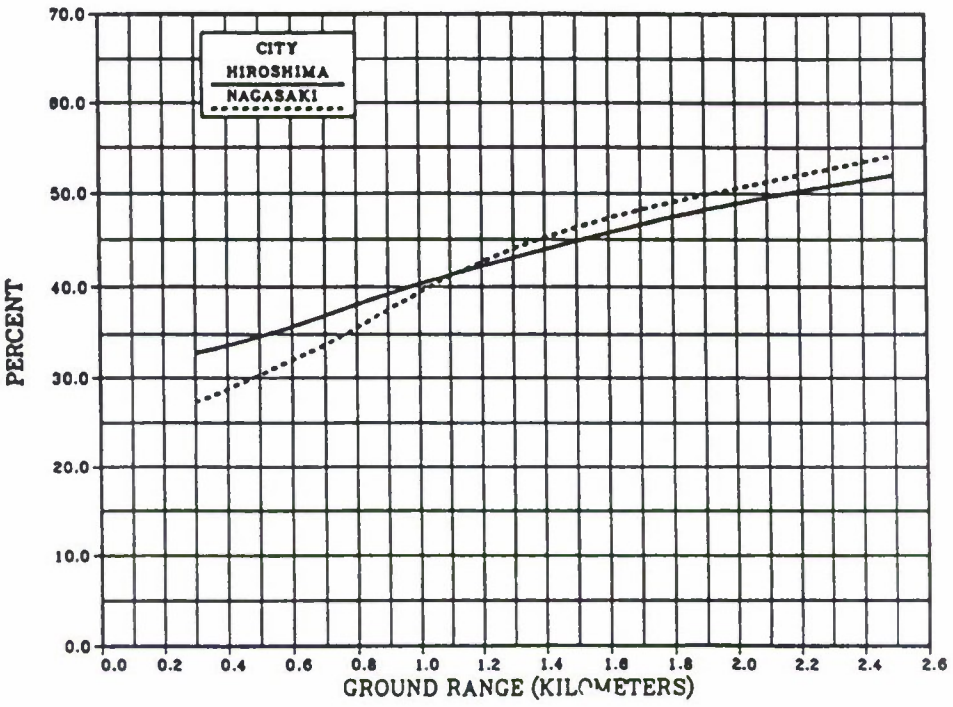

Figure 4.2 Percent debris gamma kerma prior to blast arrival.

5. SOLUTION TECHNIQUES AND MODELING PROCEDURES

5.1 MESH CONSIDERATIONS

It was recognized from the beginning that the buildings were too large to allow solution with traditional mesh spacing of a few centimeters in each direction. Most of the interior was filled with air, however, interrupted here and there by support material and internal walls. The air and internal material were sufficiently important to thwart a void-streaming calculation, but a compromise procedure using mesh cells large along the surfaces of the walls and floor but small in the direction through the material appeared practical.

Such a mesh would allow penetration directly through walls and floors to be calculated correctly, although it would not support the calculation of flow laterally through the solid material. This latter effect was considered negligible, an assumption similar to that employed in the ground layers of an air/ground transport problem. Penetration through the large support pillars would not be calculated adequately by this strategy, but the pillars were considered essentially opaque as compared to the easy streaming paths through the surrounding air.

5.2 TESTS OF HYPOTHETICAL BUILDINGS

5.2.1 English Building Study

Several approaches were used to test the validity of the overall calculations. The first tests of the method consisted of hypothetical concrete structures analyzed by both discrete ordinates and Monte Carlo methods.[28] Large intervals along the surface were used in a calculation of one-energy-group neutron penetration through the roof and second floor of a windowless, two-story building called the "English building" (Fig. 5.1). The source was isotropic, placed along the top of the building. Only the first group of a 13-group neutron library was solved.

In Fig. 5.2, the results of a Monte Carlo solution performed by the MORSE code[29] are indicated by points enclosed with circles. The circle size indicates the approximate degree of statistical convergence. The data represent flux values along a vertical traverse near one corner of the building. They show an attenuation of roughly a factor of 20 through the building.

The curves indicate the results of two TORT calculations using the weighted difference method and a preliminary version of the nodal method[30] with a coarse S_2 directional quadrature. Both results follow the general trend of the Monte Carlo data, finally diverging by about 20% at the end of the traverse. The nodal method shows excellent agreement with the Monte Carlo results.

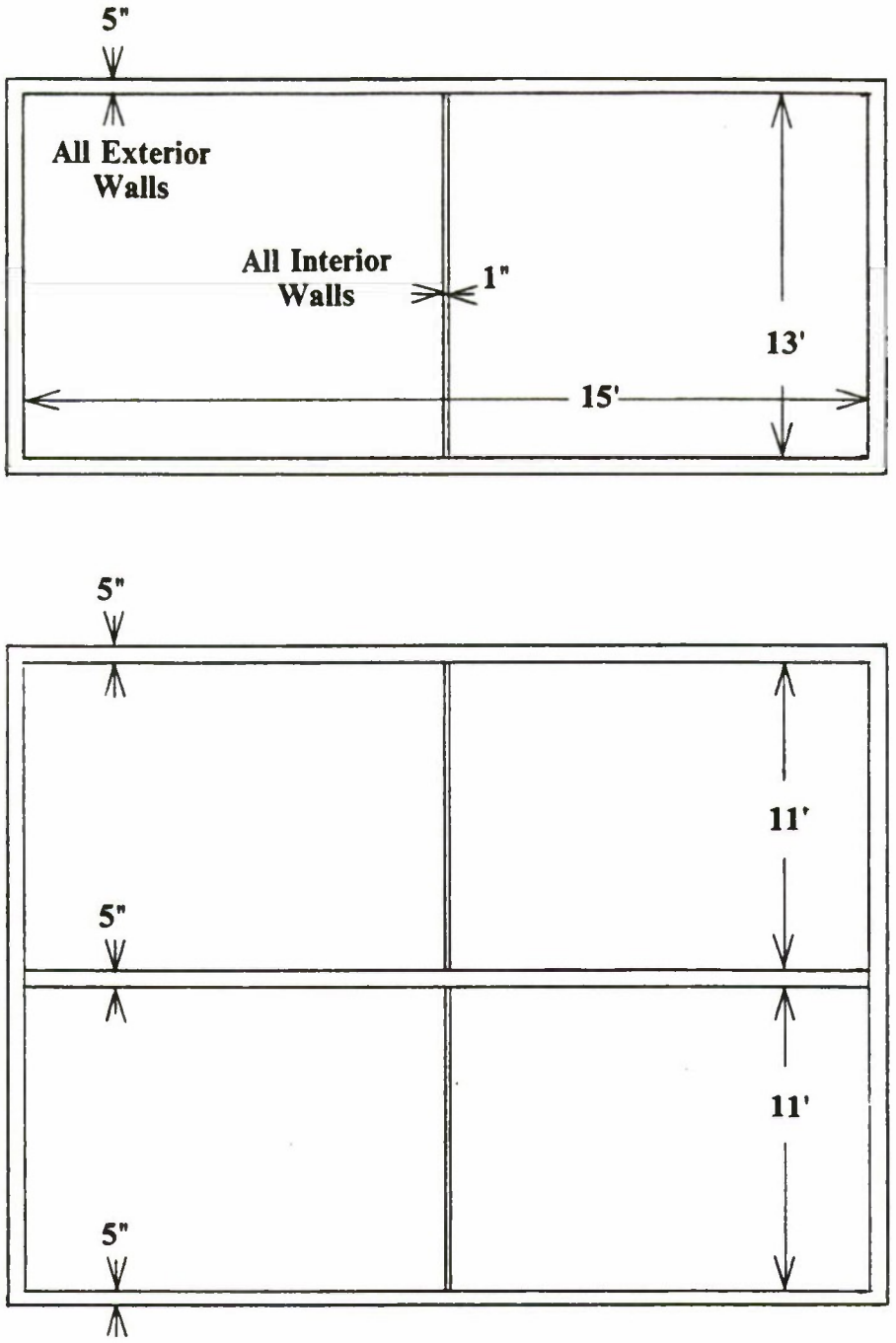

Figure 5.1 Windowless concrete building used to test large mesh intervals in roof and floor penetration.

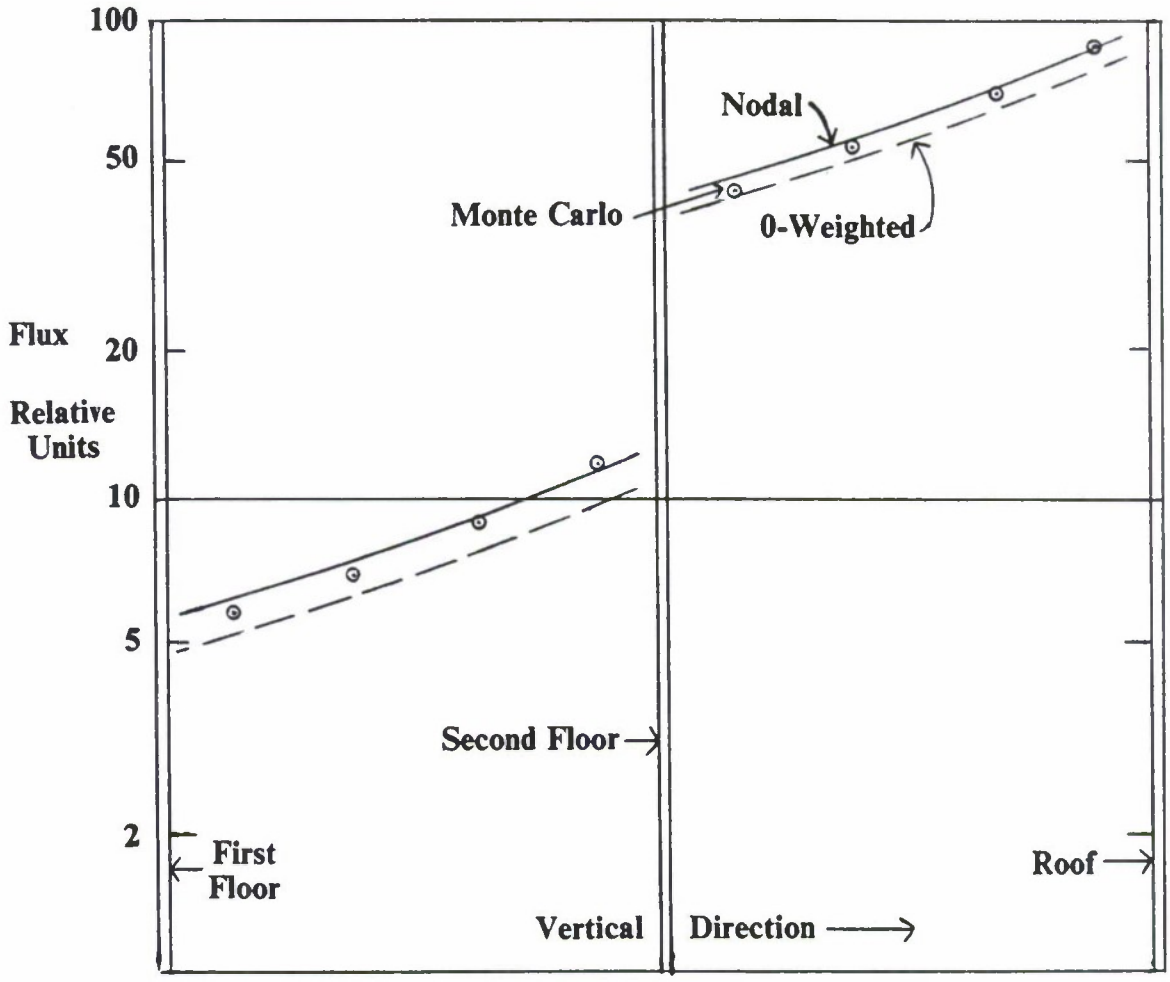

Figure 5.2 Comparison of nodal and 0-weighted TORT results with Monte Carlo results.

5.2.2 Early Metric Building Studies

Reference 28 also reported a study of a somewhat more complicated concrete building illustrated in Fig. 5.3. An internal wall and support pillar partially obstruct the streaming through the windows, as shown in Fig. 5.4. All energy groups of the 20-group cross section library were used. The incoming radiation was represented as an isotropic source distributed uniformly over the rear, top, and right faces as viewed in Fig. 5.3. Detector traverses across the front and rear walls at 1.5 m above the second floor were examined in detail.

The histograms of Fig. 5.5 show neutron dose calculated using P_1 scattering expansion, S_6 directional quadrature, and the weighted difference spatial treatment. The coarse mesh had intervals of approximately 1 m along the walls and 6 cm through the concrete. The medium mesh had the 1 m intervals refined by a factor of 3. The coarse mesh has clearly represented the average dose in each interval well; the only significant discrepancies are immediately in front of the window edges, where the coarse mesh cannot represent the details of the steep gradient.

The study also included a comparison with Monte Carlo calculations, represented by x's in the figure. Since the internal error estimator was considered unreliable in this application, calculations with two different random number seeds are represented. The discrepancy between the results of the two Monte Carlo calculations is an indication of the statistical uncertainty, and it is large in certain areas, especially between the windows and the outside walls. Considering this, the agreement with TORT appears satisfactory. It should be noted that the original paper included six Monte Carlo results between 0.5 m and -0.5 m, but those were later discovered to be invalid. A single new point has been added at 0.5 m in the present work, and its Monte Carlo convergence was about 20%.

Figure 5.6 shows the gamma dose from these same calculations. The tilt from right to left due to the source on the right wall is more pronounced than for the neutron dose. The two discrete ordinates results are in good agreement, and the extent of agreement with Monte Carlo is comparable to that of the neutron dose.

Reference 28 also reports the refining of the space mesh through the wall by a factor of 2 and the use of the finer S_{10} directional quadrature. Neither refinement was found to change the results significantly. A 10% change in concrete density produced increases in the doses as large as 22% in areas away from the windows, indicating a sensitivity to the concrete composition.

5.2.3 New Metric Building Studies with Open Windows

The studies reported in Ref. 28 also included a discrete ordinates calculaton performed with a low-order nodal procedure, but that application was not particularly successful. In the meantime, refinements to the nodal procedure have made it dependable, accurate, and acceptable in cost.[30] Also, a new procedure, the characteristic method, has been developed, and it is considered even more accurate than the nodal method.[31] Although the character method is not yet efficient enough for production use, it was applied in a comparison between the various methods.

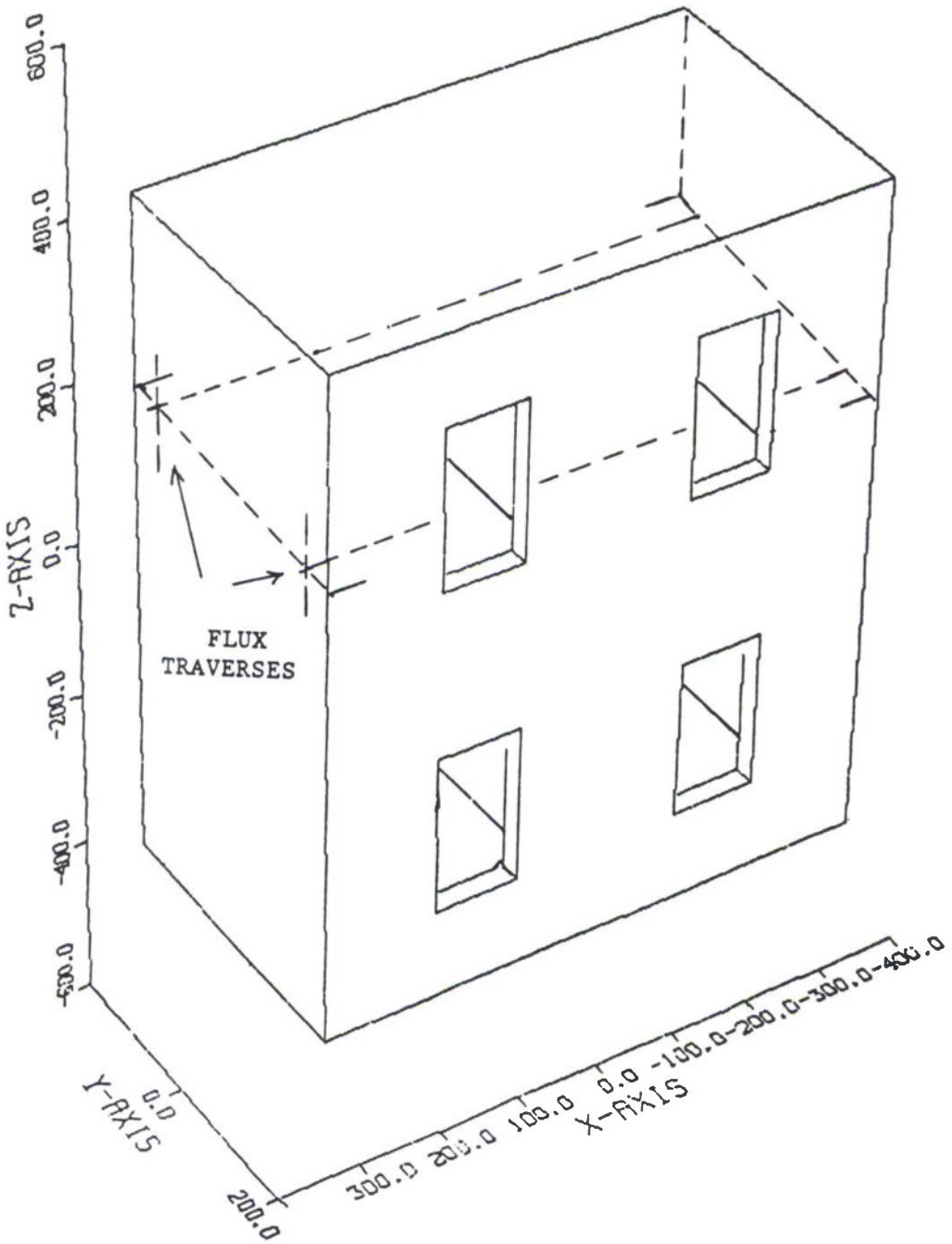

Figure 5.3 Four-room building for window streaming calculation.

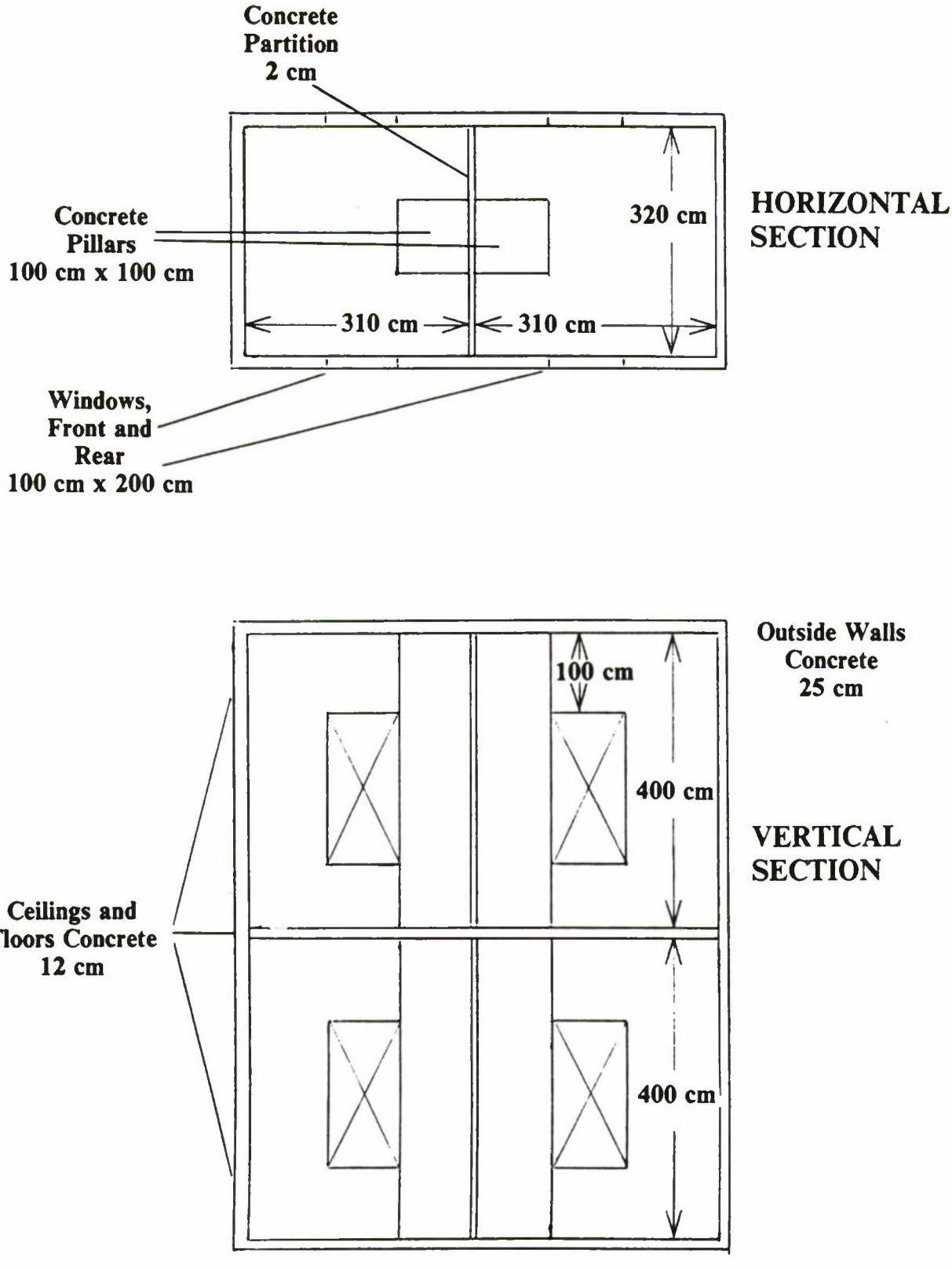

Figure 5.4 Internal construction of four-room building.

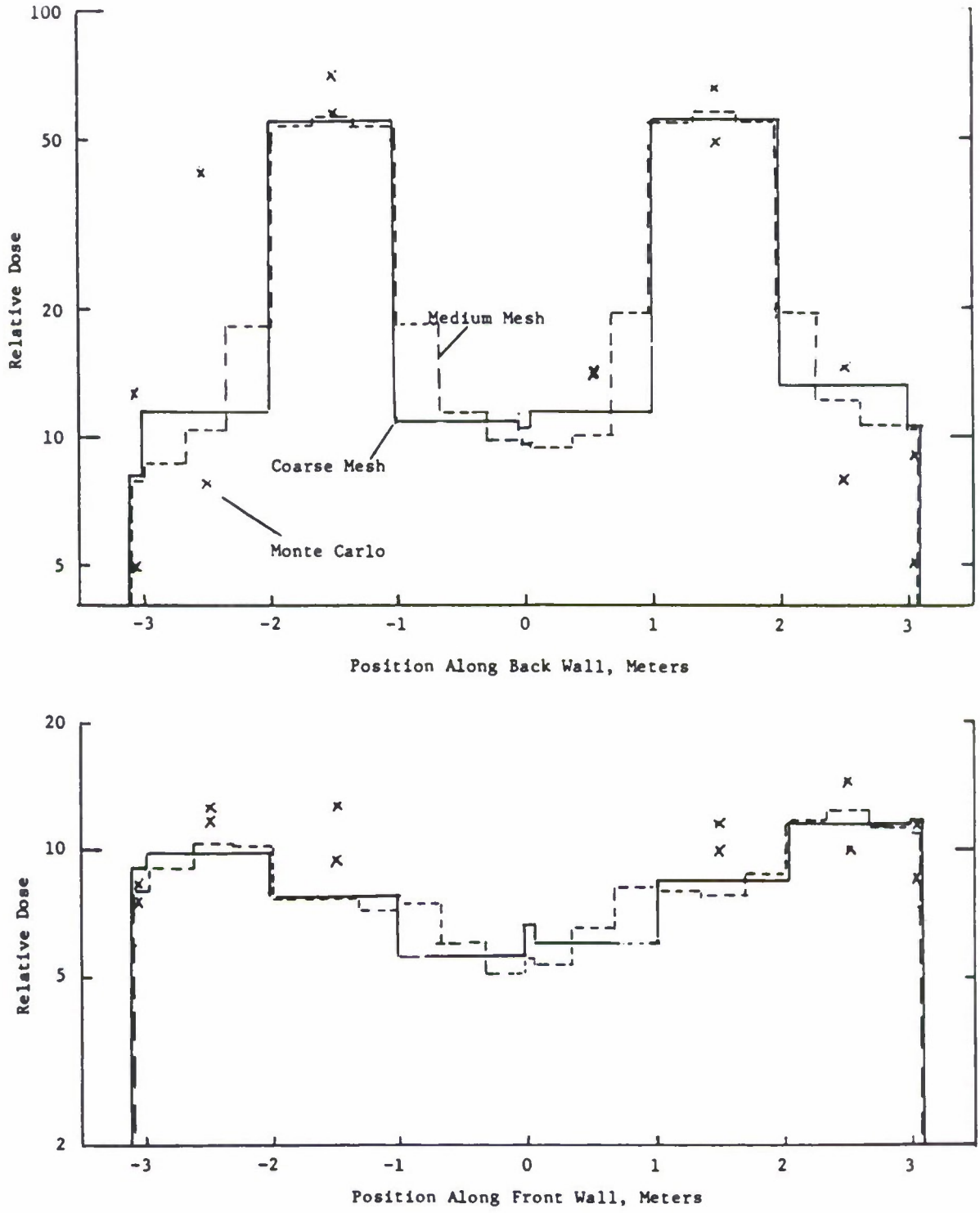

Figure 5.5 Comparison of coarse mesh vs. medium mesh discrete ordinates neutron dose vs. Monte Carlo results.

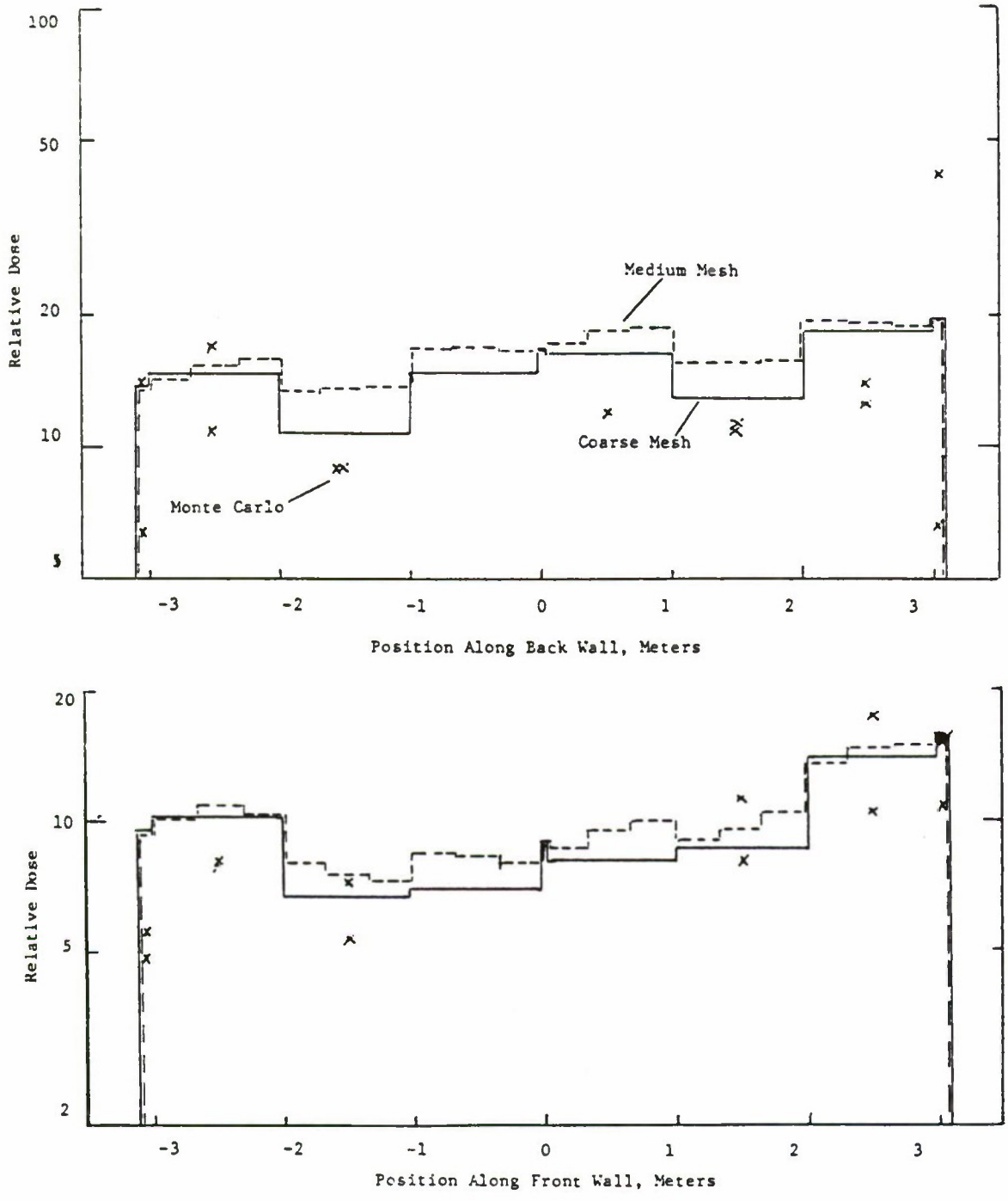

Figure 5.6 Comparison of coarse mesh vs. medium mesh discrete ordinates gamma dose vs. Monte Carlo results.

The same building model and cross section library were used. Since most of the dose in the Nagasaki buildings of interest arrived as gamma radiation, a gamma source spectrum representative of the prompt gamma flux at about 500 m was assumed (Table 5.1). The first comparison, which used the weighted difference method with theta (the method-adjustment parameter) set to 0.0, showed that increasing the scattering expansion from P_1 to P_3 produced no significant change (Fig. 5.7). (The widths of the 2-cm wall at the middle of the traverses and the 10-cm intervals at each end have been exaggerated in the plots for clarity.) The figure also shows that increasing the directional quadrature from S_6 to S_{10} produced little effect.

Table 5.1 Gamma source spectrum used in new metric building study

Energy group	Source
1	0.00000E+00
2	0.00000E+00
3	0.00000E+00
4	0.00000E+00
5	0.00000E+00
6	0.00000E+00
7	0.00000E+00
8	0.00000E+00
9	0.00000E+00
10	0.00000E+00
11	0.00000E+00
12	0.00000E+00
13	0.00000E+00
14	1.77410E+07
15	1.58037E+08
16	6.02292E+09
17	2.93931E+10
18	2.44920E+10
19	8.98607E+10
20	7.88103E+10

In comparing the various spatial treatments, the characteristic method was taken as the reference, based on its excellent performance in various mesh refinement studies and other comparisons. Figure 5.8 compares weighted difference results for various values of theta with characteristic results. Variations in the weighted difference results as large as 40% were found due to the value of the parameter theta. Historically, values of theta of 0.5 or larger have produced the best performance in comparison with other methods, but those values gave too little dose in this calculation everywhere except in the narrow intervals inside the center wall and at each end of the traverses. The non-physical peak in the concrete wall between the

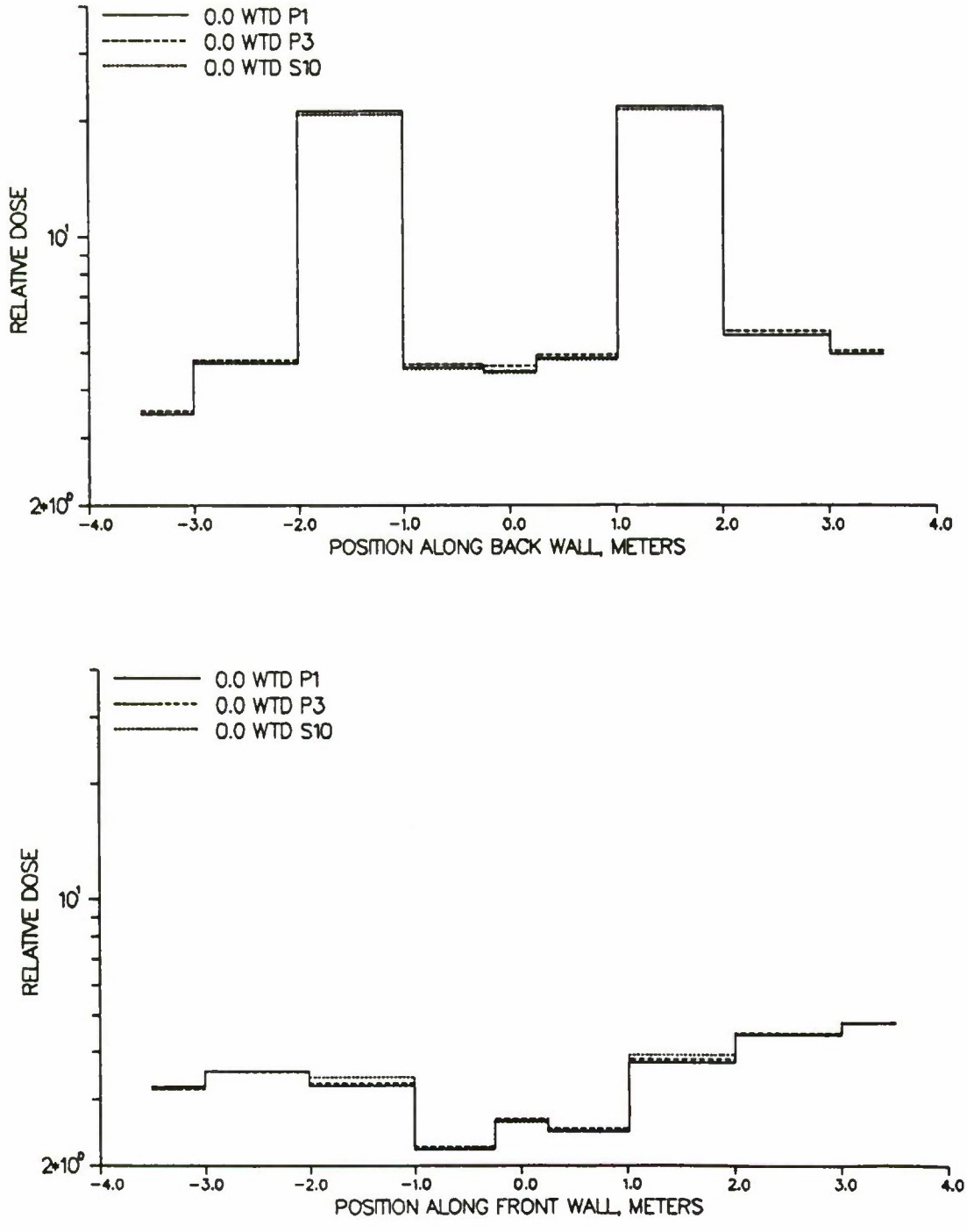

Figure 5.7 Dose traverses across metric building, isotropic source case, showing the effects of increasing the scattering order from P_1 to P_3 or the directional quadrature from S_6 to S_{10}; weighted difference calculation.

windows was especially pronounced with the non-zero thetas. With theta of 0.0, the results were better in some places and worse in others.

Figure 5.9 compares the nodal method with the characteristic. It is seen that the value of the adjustable nodal parameter is of no importance except in the 2-cm and 10-cm intervals mentioned above. In these, the largest value of theta uniformly produces the best agreement. Theoretically, the larger values of theta could result in spurious negative values and poor convergence, but no such problems were noted in these calculations.

The characteristic method has no adjustable parameter, but its formulation allows an uncommon flexibility in the treatment of flux shapes at the surfaces of each mesh cell. The standard method uses an approach similar to the nodal method in calculating the shapes, but an alternate method using a simpler approach is also available. Figure 5.10 compares these characteristic methods, showing that they give comparable results except inside the center wall. This study provides no basis for a preference, but other studies have indicated clear superiority for the standard version.

To make the problem more difficult, the source was isolated into a single direction with all direction cosines equal to -0.57355. As shown in Fig. 5.11, this skewed the dose traverses to the left and produced on the order of 10% maximum difference between the P_1 and P_3, but it indicated no need for finer quadrature for this case.

5.2.4 New Metric Building Studies with Closed Windows

Some of the more difficult locations in the large building are not properly characterized by radiation streaming through a window, but instead, by radiation penetrating through layers of heavy roof and floor material and across intervening internal air spaces. This situation was tested by deleting all of the windows in the metric building, placing the monodirectional source only on the roof, and moving the detectors to 1.5 m above the bottom floor. Thus, radiation reaching internal points is required to penetrate repeated layers of concrete and open air. Figure 5.12 shows a maximum difference of about 20% due to the scattering expansion in this case, but only a small effect due to quadrature, when weighted difference is used.

In Figure 5.13, the same comparisons are made with a nodal calculation. With this method, the effect of using the finer quadrature reaches 25% in some places, while the effect of P_3 exceeds 50%.

Figure 5.14 shows that no value of theta is really satisfactory for use with the weighted difference model, as was the case with window streaming. Figure 5.14 shows, once again, that the larger values of theta match the characteristic calculation best except in the thin intervals. The 0.0 value of theta produces results generally in disagreement by 30% or more except in the thin intervals.

Figure 5.15 shows that the nodal method matches the characteristic results closely for all values of theta except inside the center wall. Inside the wall, the value of 0.5 gave the best results.

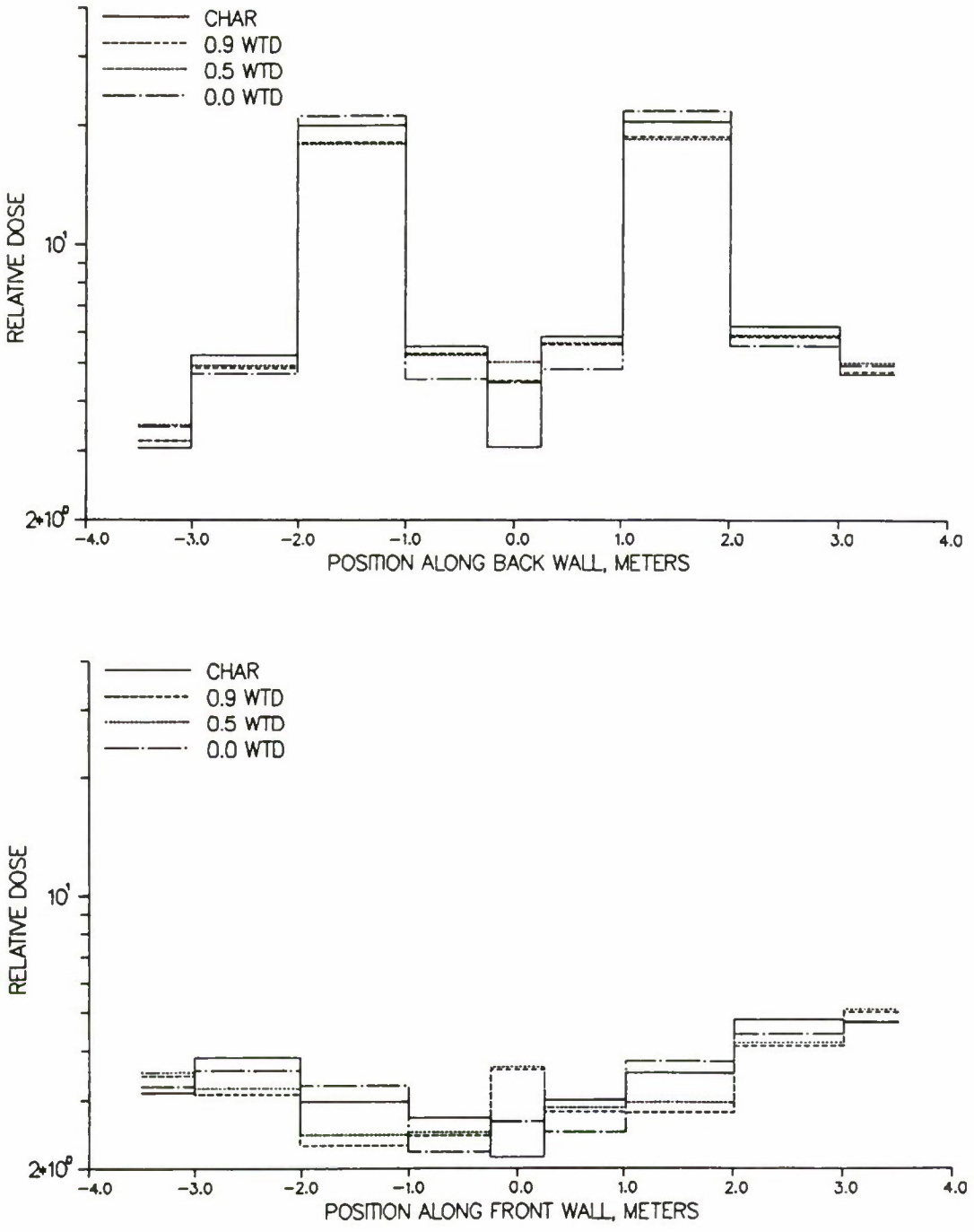

Figure 5.8 Dose traverses across metric building, isotropic source case, showing weighted difference results vs. characteristic results.

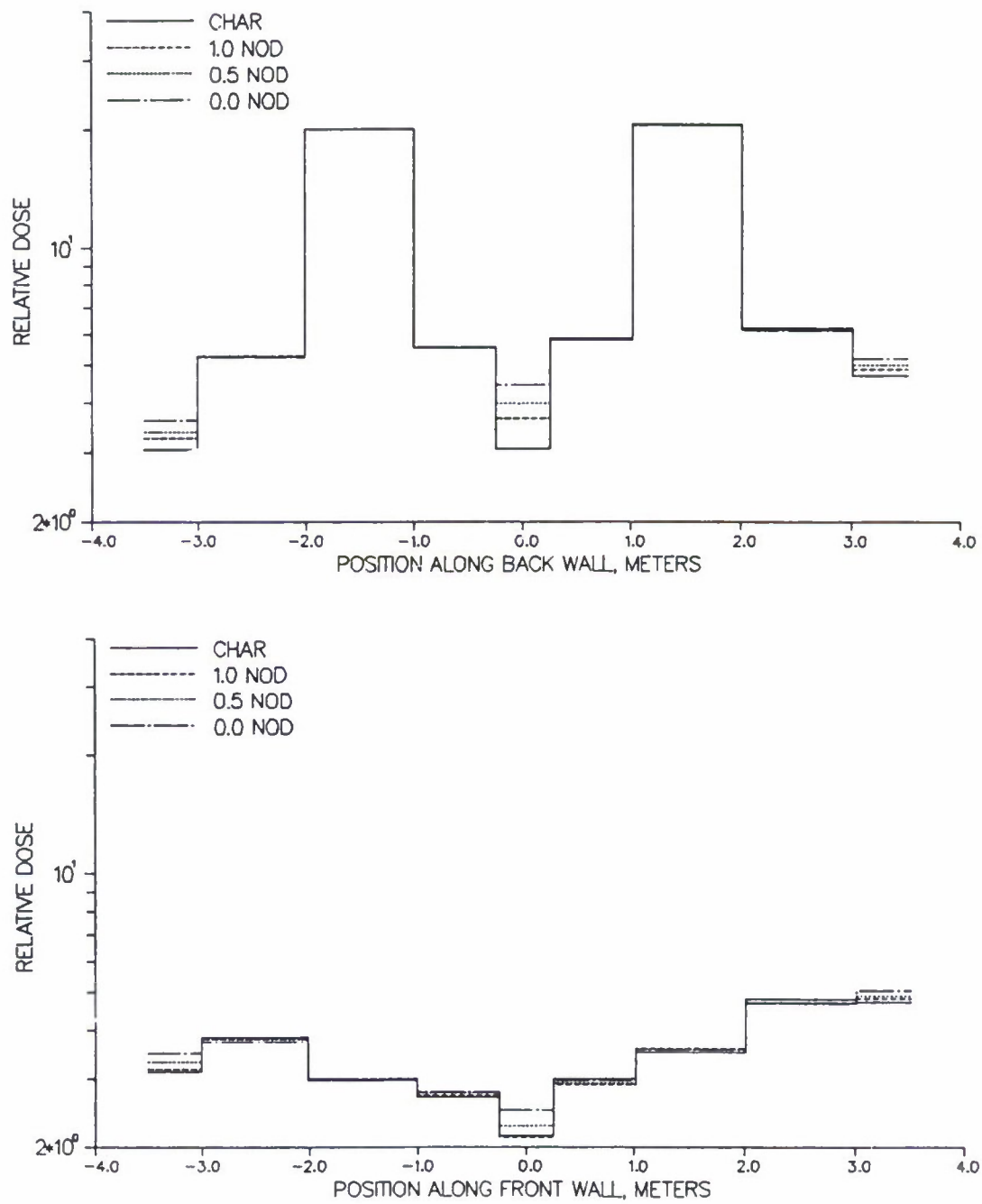

Figure 5.9 Dose traverses across metric building, isotropic source case, showing nodal results vs. characteristic results.

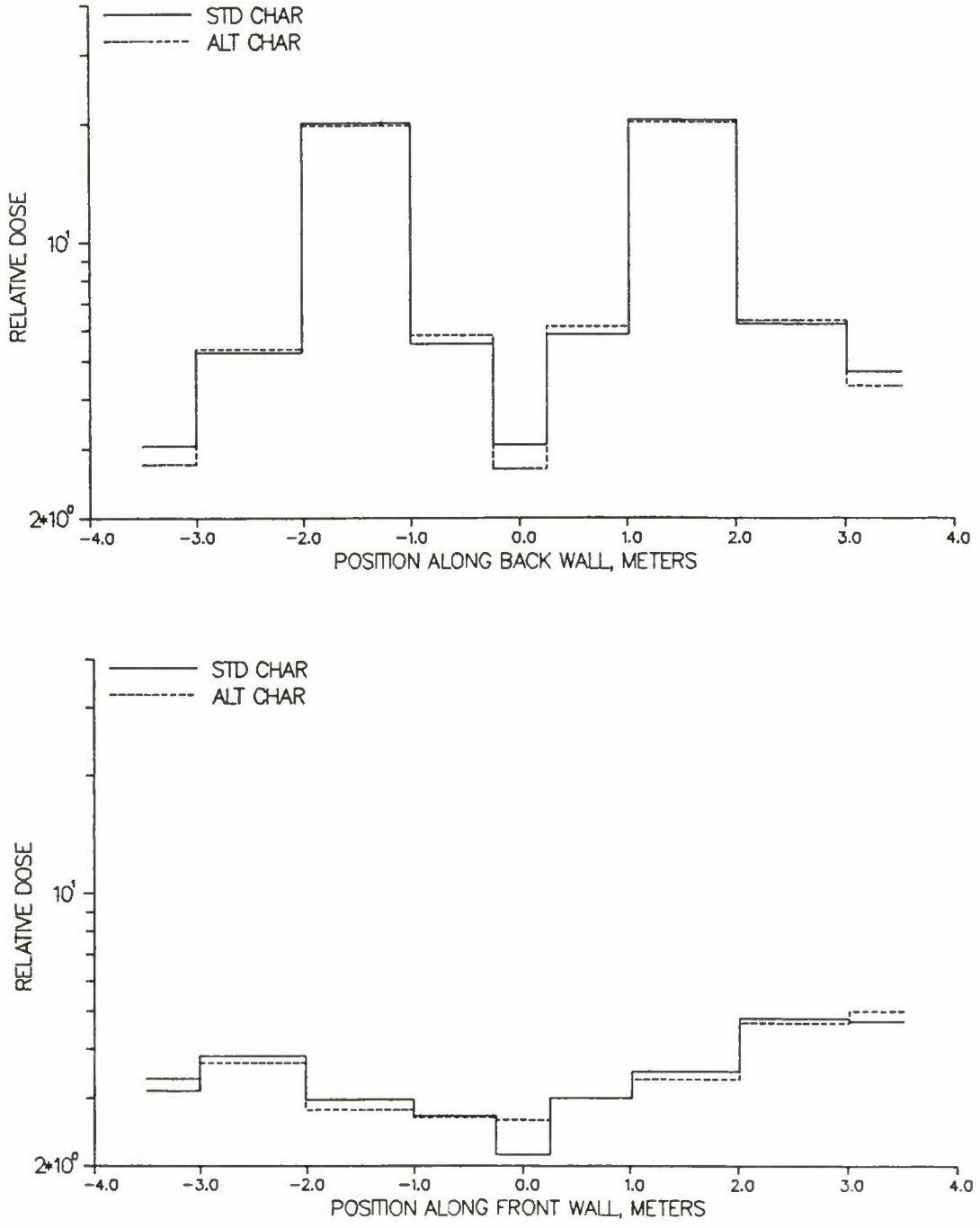

Figure 5.10 Dose traverse across metric building, isotropic source case, showing results of the standard characteristic method vs. an alternate characteristic method.

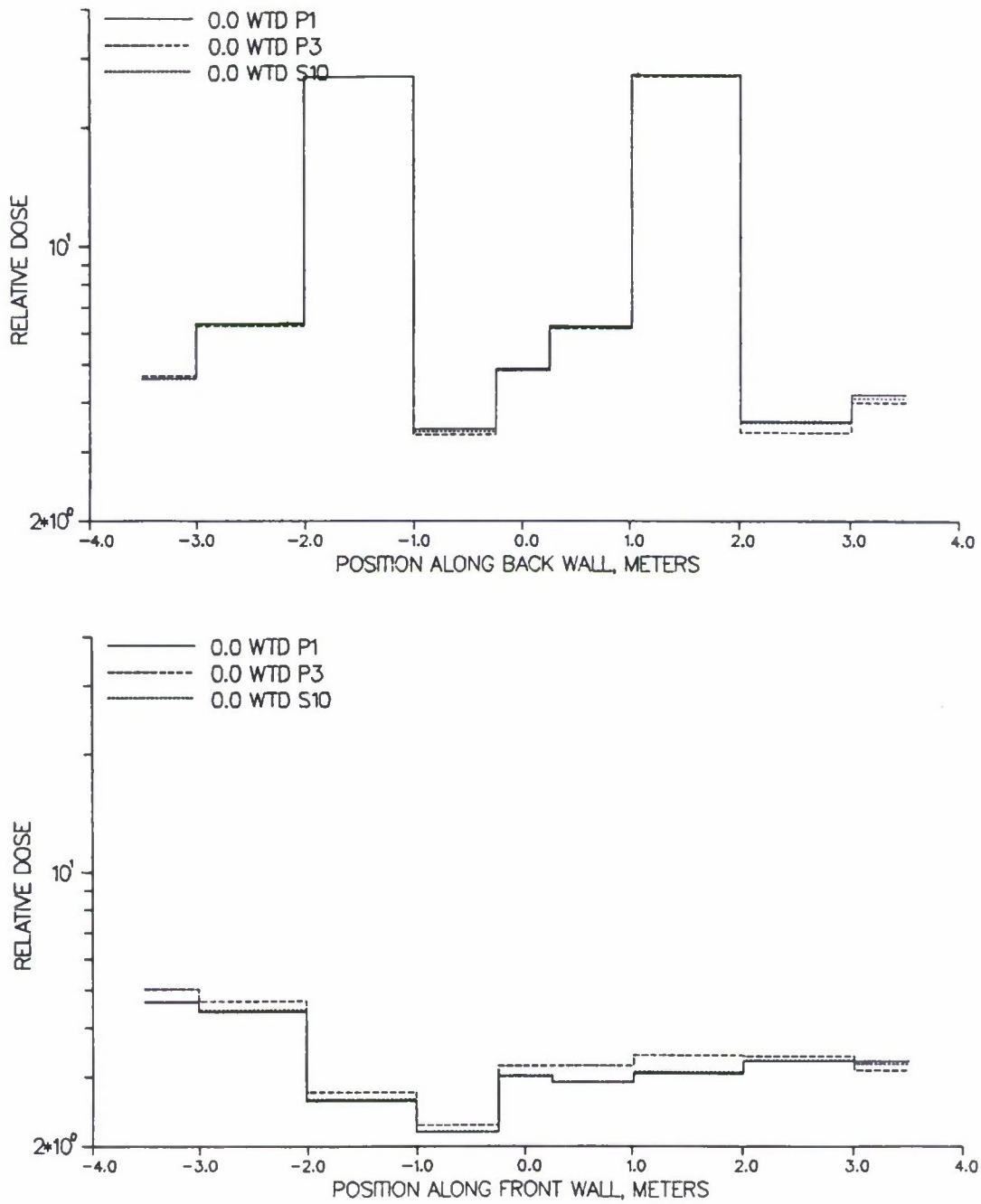

Figure 5.11 Dose traverses across metric building, monodirectional source case, showing the effects of increasing the scattering order from P_1 to P_3 or the directional quadrature from S_6 to S_{10}; weighted difference calculation.

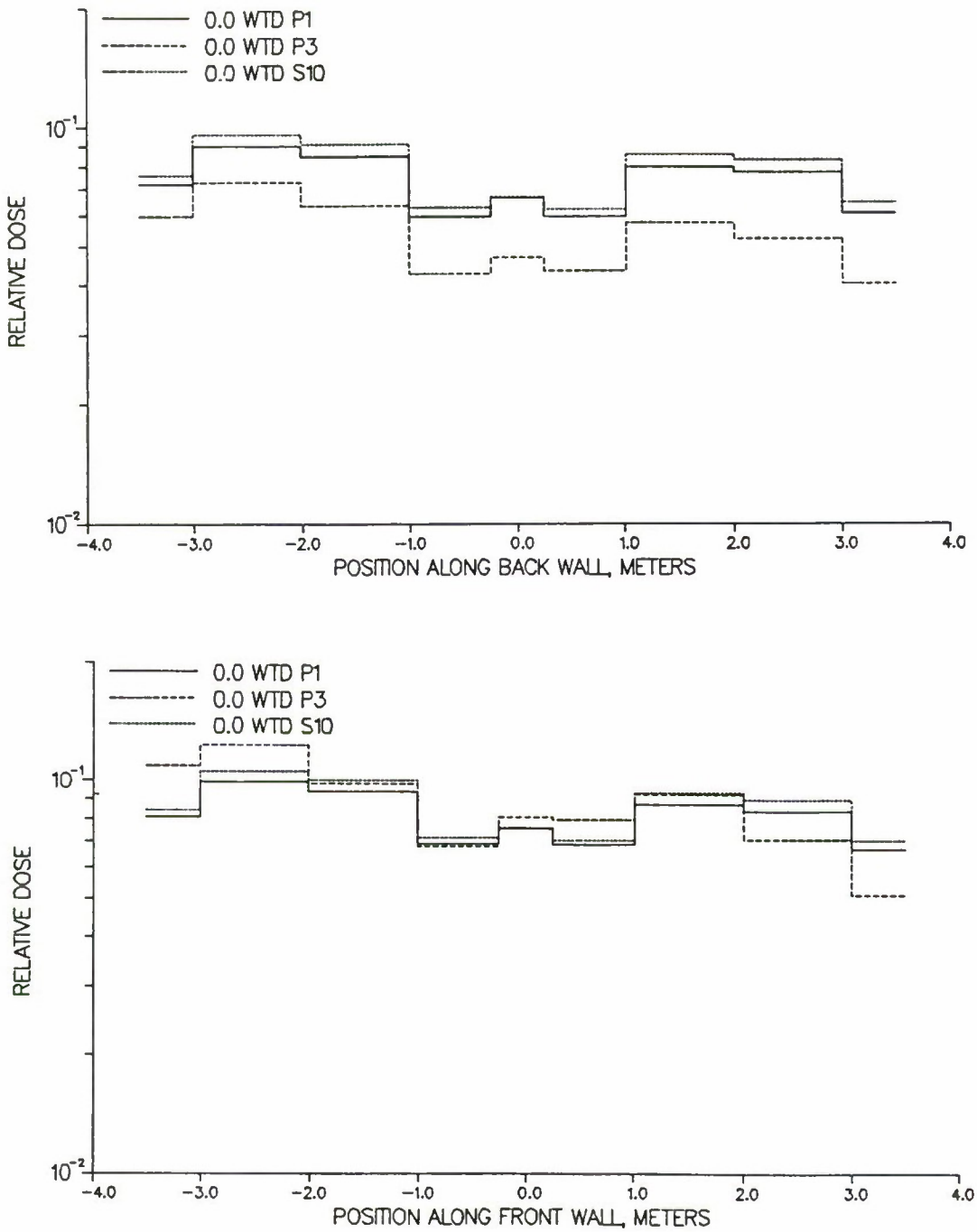

Figure 5.12 Dose traverse across metric building, monodirectional source case, windows closed, showing the effects of increasing the scattering order from P_1 to P_3 or the directional quadrature from S_6 to S_{10}; weighted difference calculation.

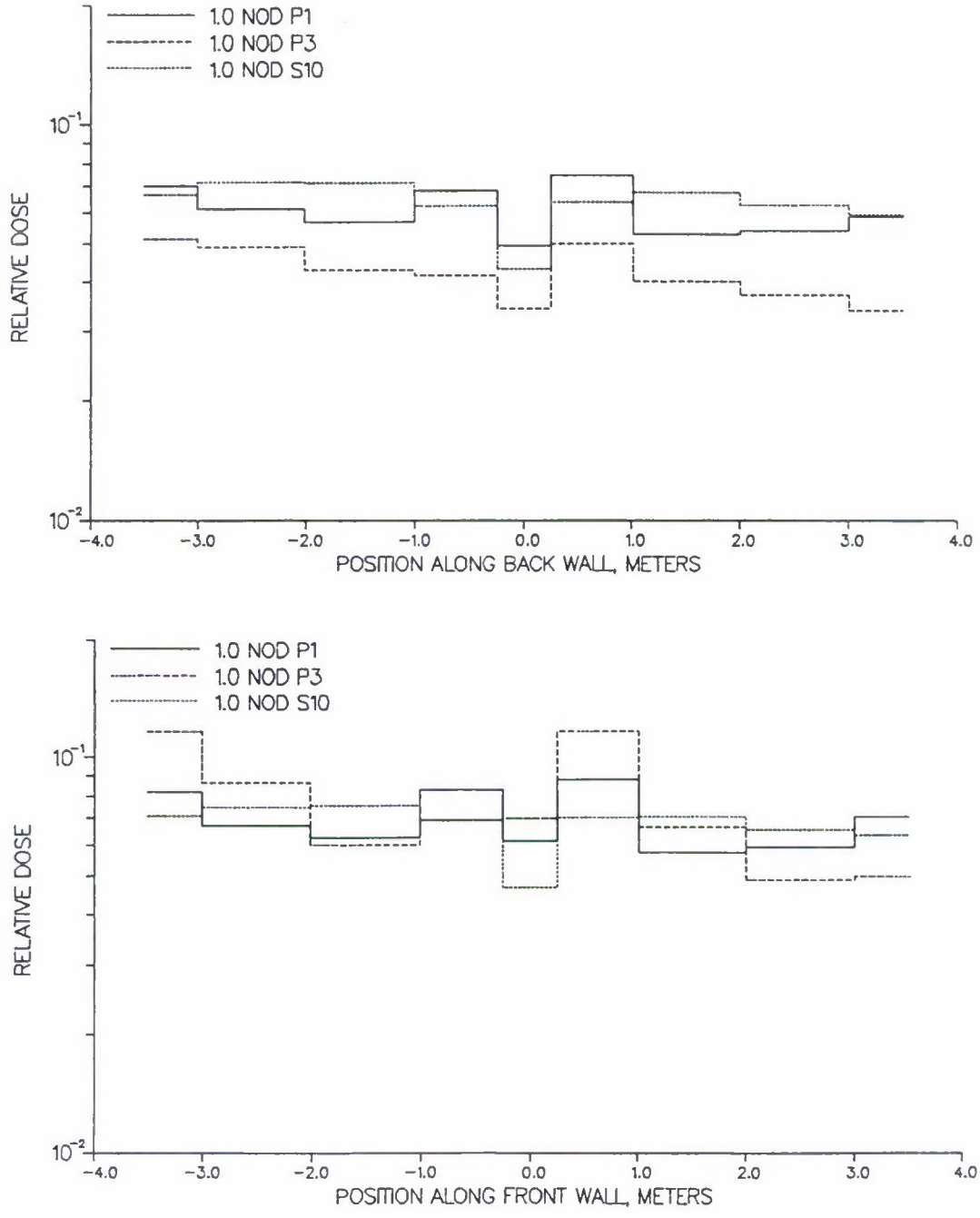

Figure 5.13 Dose traverses across metric building, monodirectional source, windows closed, showing the effects of increasing the scattering order from P_1 to P_3 or the directional quadrature from S_6 to S_{10}; nodal calculation.

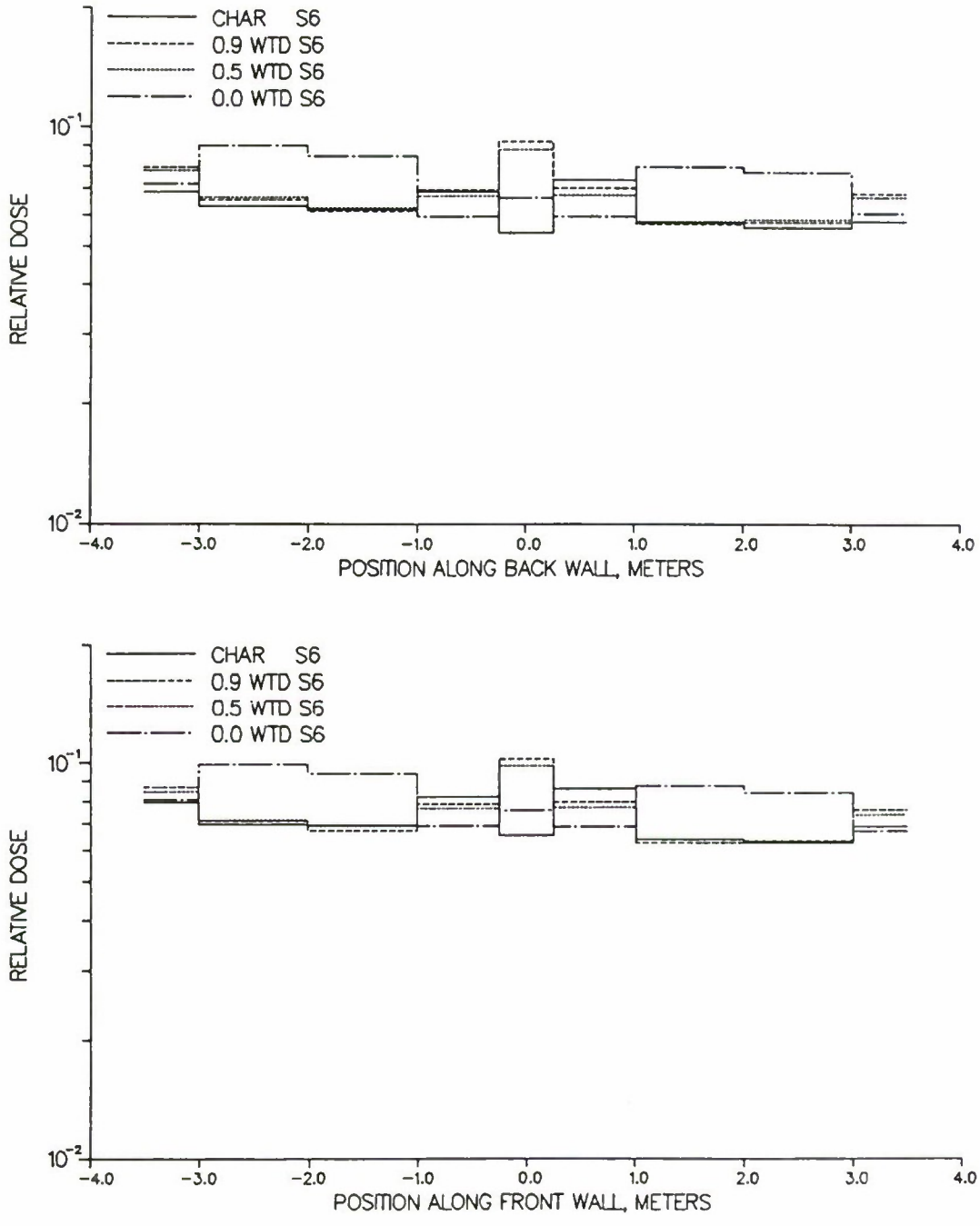

Figure 5.14 Dose traverses across metric building, monodirectional source, windows closed, showing weighted difference results vs. characteristic results.

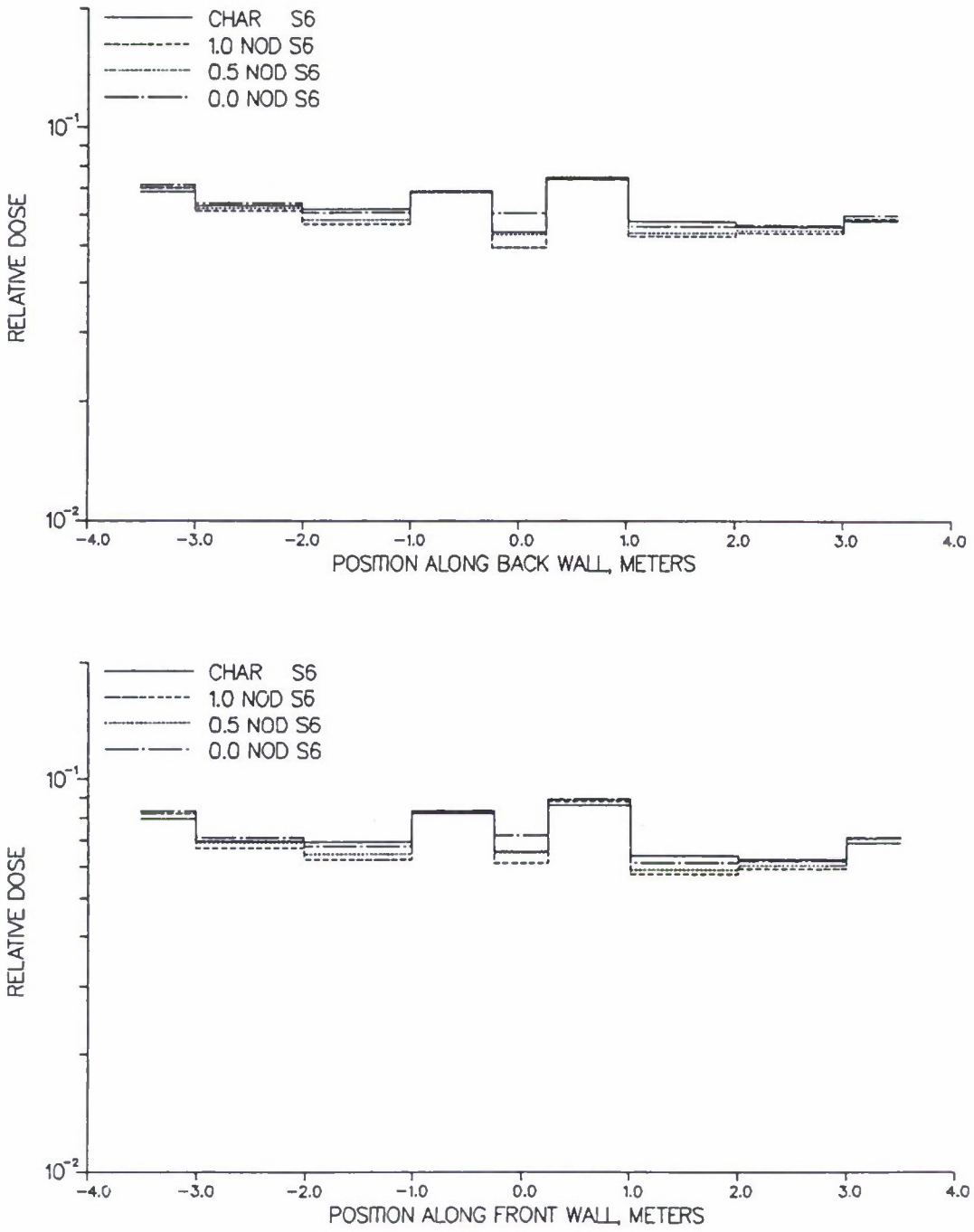

Figure 5.15 Dose traverses across metric building, monodirectional source, windows closed, showing nodal results vs. characteristic results.

With the characteristic results as the basis for comparison, these data indicate that the nodal method is much better than weighted difference for problems like those studied. The nodal results are generally insensitive to the value of the adjustable parameter except in the narrow intervals. In those locations, the larger parameter values are preferable to 0.0.

5.3 EXPERIMENTAL DATA FROM A MODEL BUILDING

The hypothetical concrete building studies were supplemented by a series of experiments, lead by Muckenthaler, on an actual building constructed at Oak Ridge's Tower Shield Facility.[32] This building was a one-story structure with two rooms separated by an optional internal wall and a movable support pillar (Figs. 5.16–5.18). An optional window faced the source, and four windows were open at the sides. Bonner-Ball neutron-detector traverses were made across the front and back rooms through the access provided by the lateral windows. By using three sizes of Bonner Balls, approximate spectral information was obtained. TLD gamma detectors were spaced frequently throughout the interior of the building. Extensive measurements of the external flux were taken before the building was constructed, and these served as a guide to the analysis.

A comparison of the measurements with TORT results showed neutron results in good agreement, on the order of 15% (Fig. 5.19).[33] The terms "zero-weighted" and "theta-weighted" indicate the weighted difference method with theta equal to 0.0 and 0.9, respectively. The gamma calculations showed agreement within 17% in areas touched by at least a portion of the direct beam, although errors immediately behind obstructions were occasionally as large as 50%.

The experimental building represented a more difficult computational problem than the Nagasaki buildings. Its single source was positioned at a distance such that the radiation was roughly monodirectional. In contrast, most of the locations in the lower floors of the Nagasaki buildings were affected by either scattered radiation penetrating the floors above or streaming through several windows. Thus, their uncertainty would not be so large as that of the positions directly behind the pillar in the experimental building.

5.4 NAGASAKI BUILDING TESTS

5.4.1 Early Methods Comparisons

Additional testing and comparisons were conducted on the first concrete building models of the Nagasaki buildings. The A1 model of the A building had the basic exterior walls, floors, windows, and internal support structure of the later models, but it had no internal walls or basement (Fig. 5.20). The weapon position was taken to be at a height of 503 m, at a ground range of 468 m, and in the direction used as a viewpoint for the figure.

ORNL-PHOTO 5181-84

Figure 5.16 The TORT Validation Experiment, shown facing the Tower Shield Reactor Port.

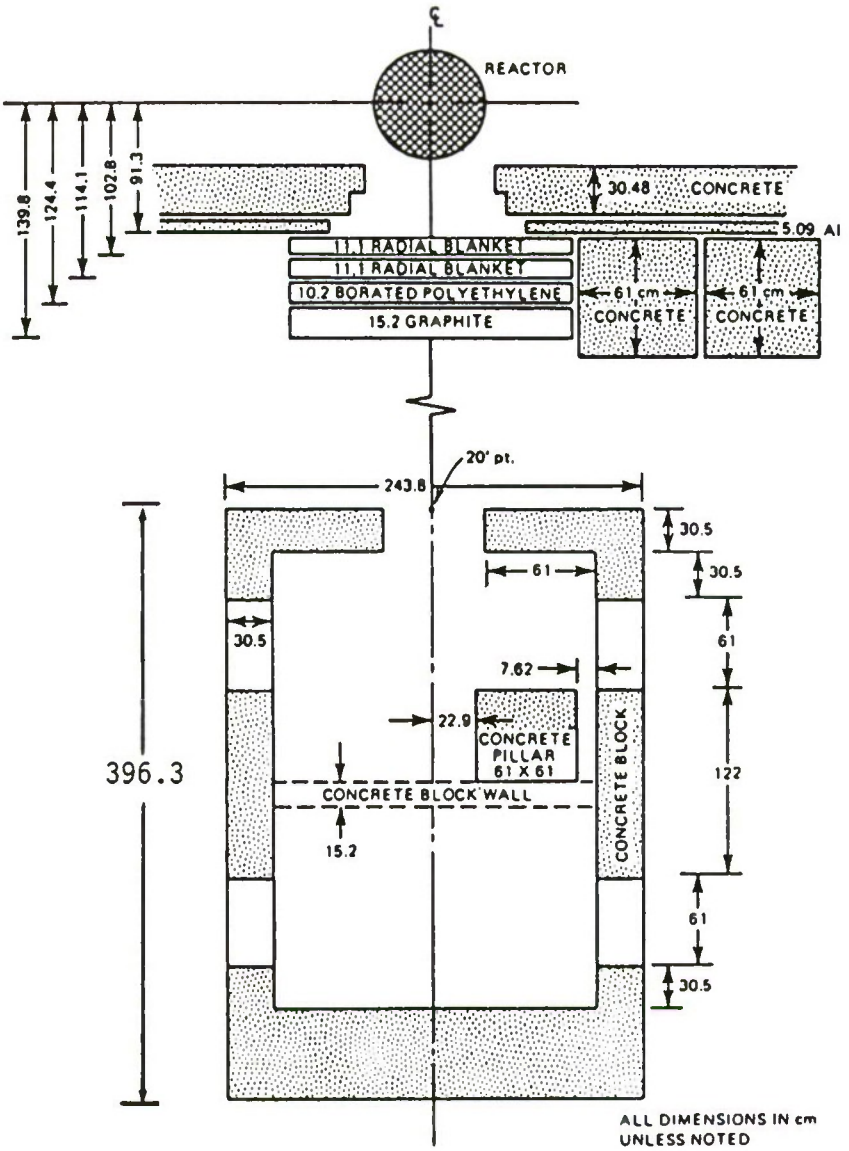

Figure 5.17 Schematic drawing of spectrum modifier and test building with pillar in offset position and front window open.

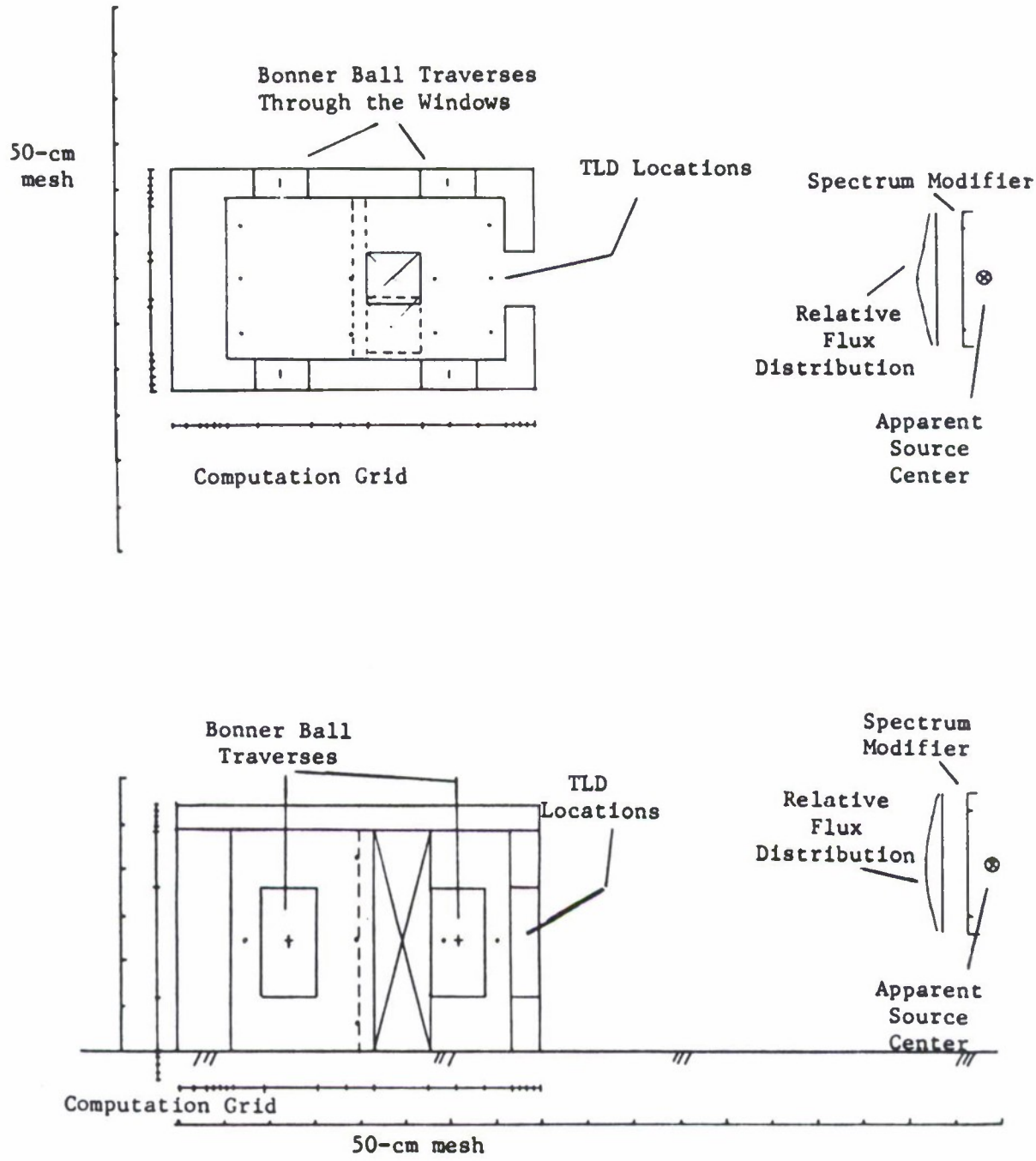

Figure 5.18 Scaled layout drawings showing relationship of source to building.

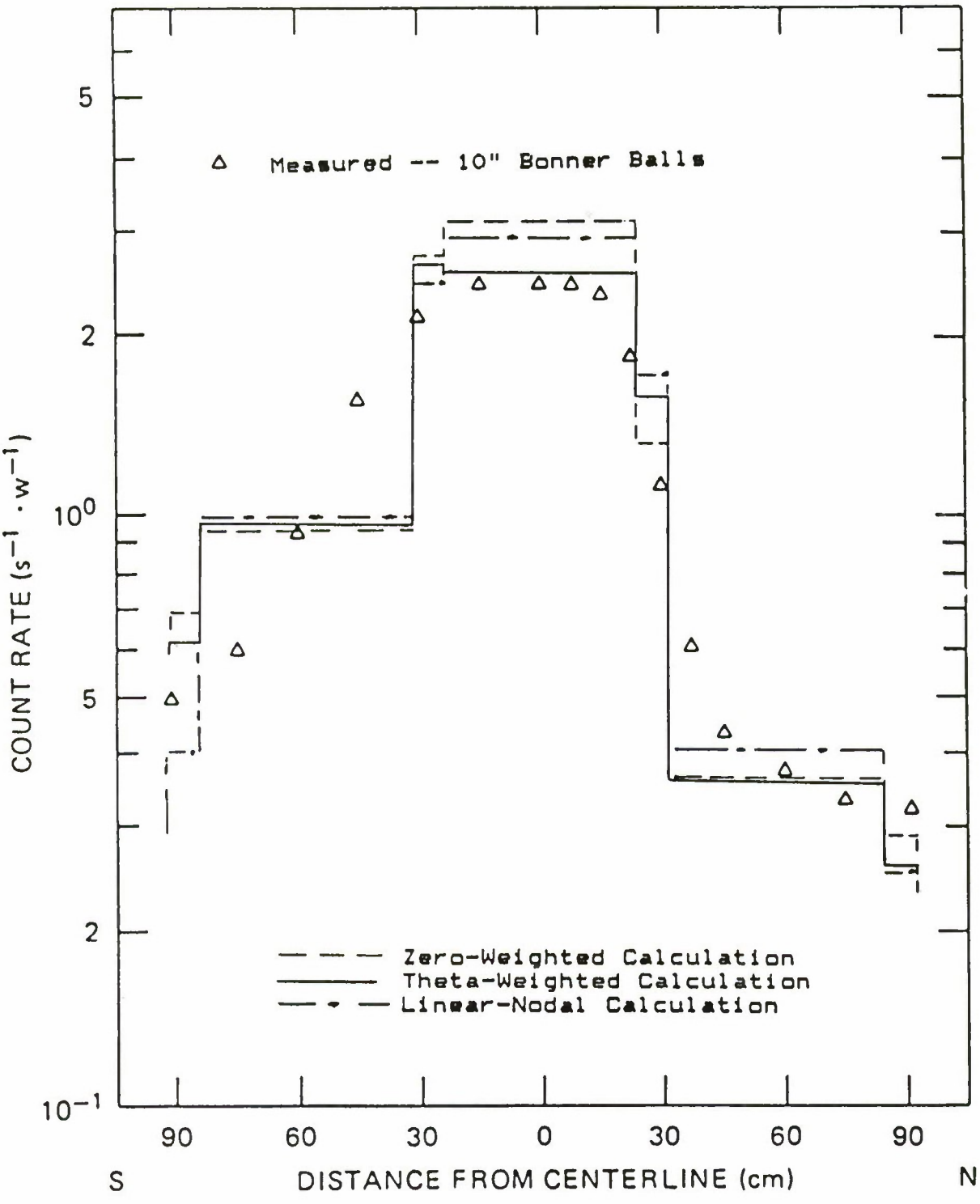

Figure 5.19 Comparison of experimental vs. calculated fast neutron flux traverse behind pillar in offset position.

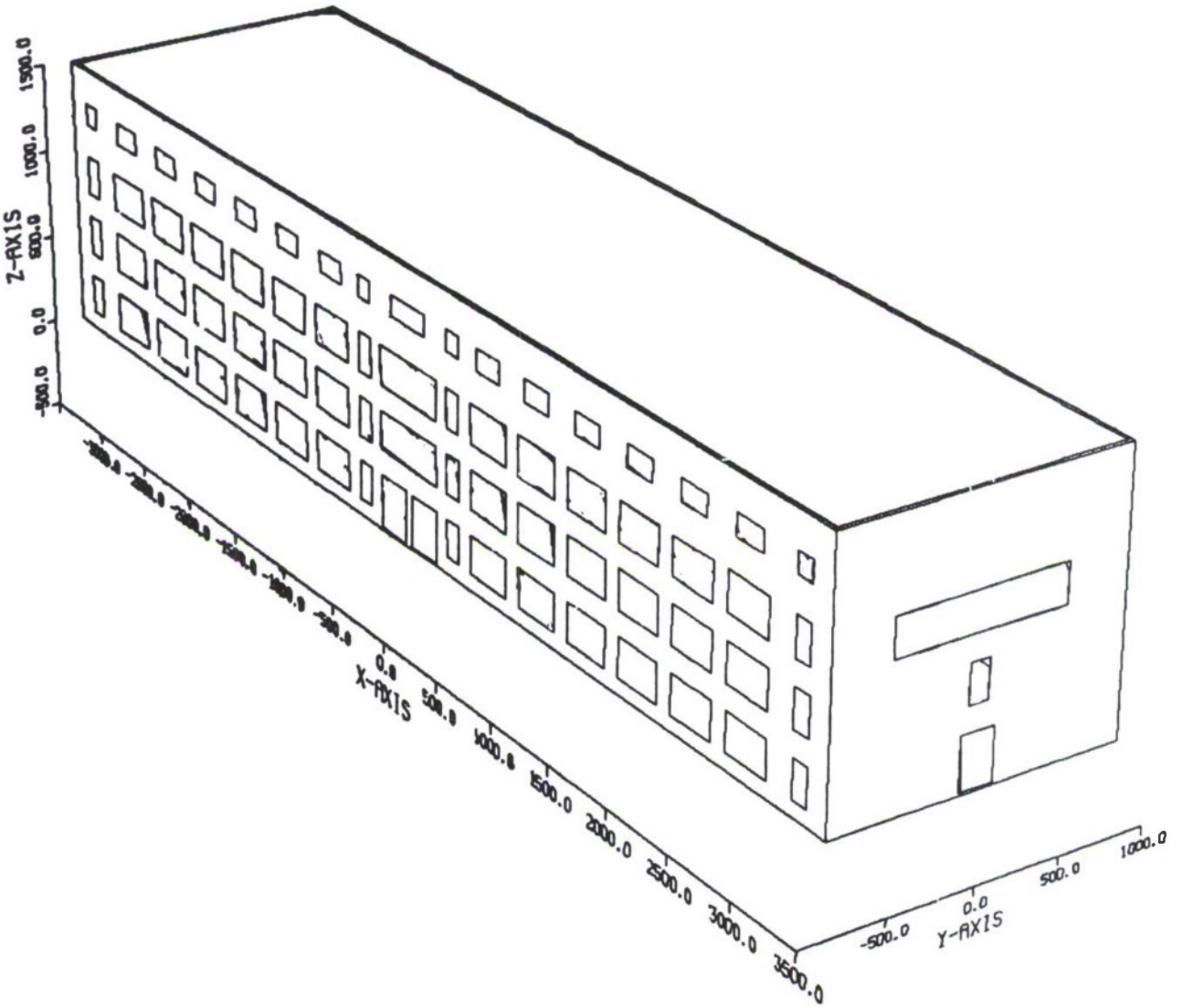

Figure 5.20 Discrete ordinates concrete building model of Building A (Chinzei School). (Dimensions in cm.)

The first study of this series was conducted using the 58-group cross section library and a preliminary version of the prompt gamma source on all surfaces of the building except the bottom. The gamma source was appropriate for this use, since gamma fluence causes most of the personnel dose in the buildings of interest. It also presents a more difficult test of the transport calculations. A weighted difference calculation with a theta of 0.3, a P_1 scattering expansion, and the S_6 directional quadrature was performed as a basis of comparison, after which various perturbations were examined.

Two points were selected for tabulation: Point 8, near a second-floor window facing the source, and Point 1, deep inside the building (Fig. 5.21). Both points were 1.55 m above their respective floor surfaces. Table 5.2 shows the resulting doses for several numerical methods and several values of the model adjustment parameter, theta. The table shows that increasing the directional quadrature in a weighted difference calculation from S_6 to S_{10} changes the dose near the window by only 3%, but a 17% change is found at Point 1 inside the building. A similar calculation, not shown, indicated a negligible effect on dose at Point 1 when the scattering expansion was increased from P_1 to P_3.

The table shows good agreement among all of the S_6 calculations for Point 8, with a span of only 7% between high and low values for the various methods and thetas. The data for Point 1 span a range of 62%, however. The sophisticated nodal and characteristic values are in close agreement, and the nodal results are independent of the value of theta. The weighted difference results agree with the other methods if a value of theta no smaller than 0.3 is chosen.

5.4.2 A Comparison with Monte Carlo

An approximate check on the methods is also available through an adjoint-scoring Monte Carlo calculation performed by Cramer using a model similar to the A1 model described above (Fig. 5.22).[34,35] The comparison is only approximate:

- the Monte Carlo model had a basement, certain other details were different from the discrete ordinates model, and
- Cramer indicated that his results were preliminary, not final, due to limitations in the method used.

These calculations used the 58-group cross section library with early versions of prompt neutron and gamma sources from the weapon. The Monte Carlo results consisted of relative doses calculated at Point 1 inside the building and at a radius of 500 m without the building (Table 5.3). In order to evaluate the dose ratio, doses calculated by the DOT code for 500 m and 468 m were used to adjust the Monte Carlo results to 468 m, the true range of Point 1. Finally, the (internal dose/external dose) ratios for Point 1 were obtained.

Table 5.4 shows the properly normalized doses calculated by the DOT code near the ground surface without the presence of the building, from which dose ratios comparable to the Monte Carlo results are calculated. In each case, the agreement

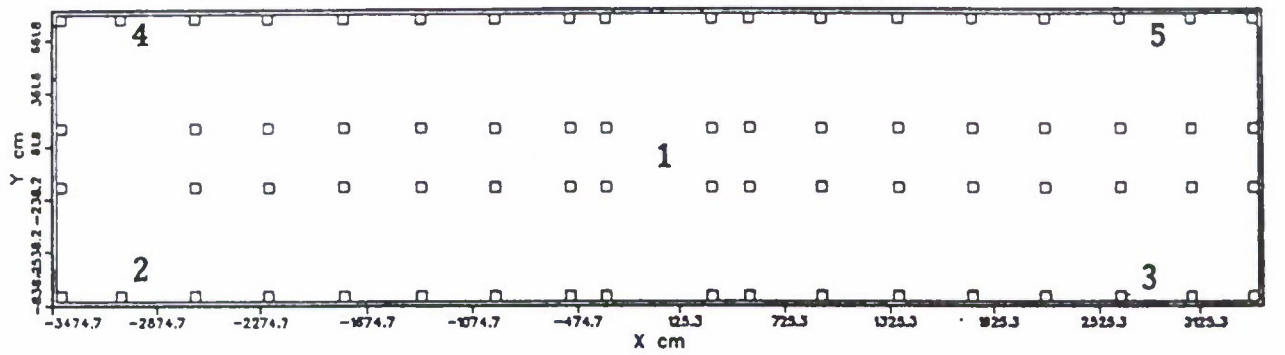

FIRST FLOOR

source

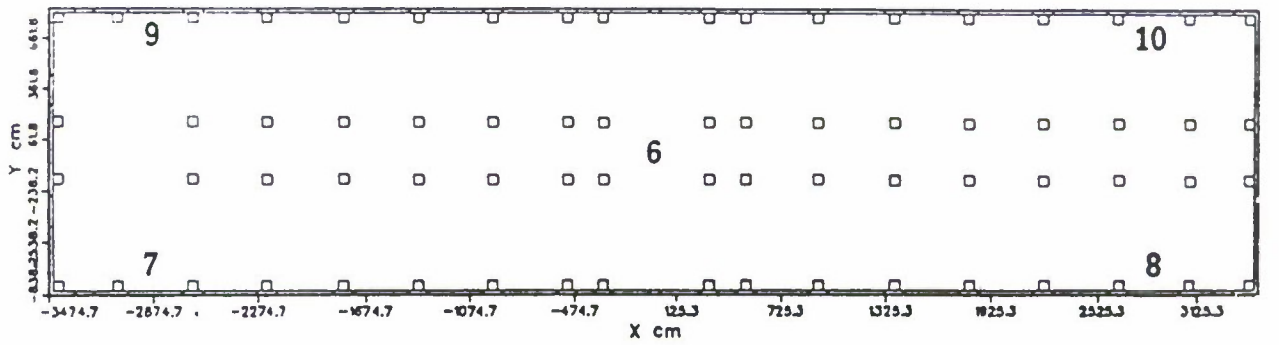

SECOND FLOOR

source

Figure 5.21 First-floor and second-floor layouts of Building A1, facing westward, showing key points 1 through 10.

Table 5.2 Prompt gamma dose in building A1 calculated by various methods

Method	Theta	Sn order	Point 1 dose	Point 8 dose
Weighted difference	0.3	10	27	312
Weighted difference	0	6	34	331
Weighted difference	0.1	6	29	322
Weighted difference	0.3	6	23	322
Weighted difference	0.5	6	21	323
Nodal	0	6	22	342
Nodal	1	6	22	344
Characteristic	–	6	21	339

Notes:

- All doses are in centiGray units (cGy).
- Point 1 is 1.55 m above the first floor at the center of the building.
- Point 8 is 1.55 m above the second floor near a window at the front of the building, facing the weapon.
- Building model Al was used.

is well within 2 standard deviations—excellent, considering the limitations indicated earlier.

5.4.3 Recent Methods Comparisons

In a final study, the same building model was used, with the minor alteration that the thin wood/plaster composite false ceiling on the fourth floor was replaced with wood. The newer 69-group library was used, together with the total source, including both prompt and delayed radiation. The delayed gamma radiation predominated in this source. Radiation at Point 1 and at Point 6, directly above on the second floor, were examined in detail.

The data of Table 5.5 show dose calculated by various weighted and nodal methods using three sets of directional quadrature. When these data are plotted in Figs. 5.23 and 5.24, it is evident why weighted difference seems satisfactory with S_6 and not with S_{10}. In fact, all of the curves intersect within the range shown, and three of them coincidentally intersect very near S_6. When the finer S_{10} quadrature is used, however, this agreement disappears, and the need for the nodal method is apparent.

One is left to speculate how the curves will approach the vertical axis. It is tempting to extrapolate linearly to the vertical axis, with the alarming conclusion

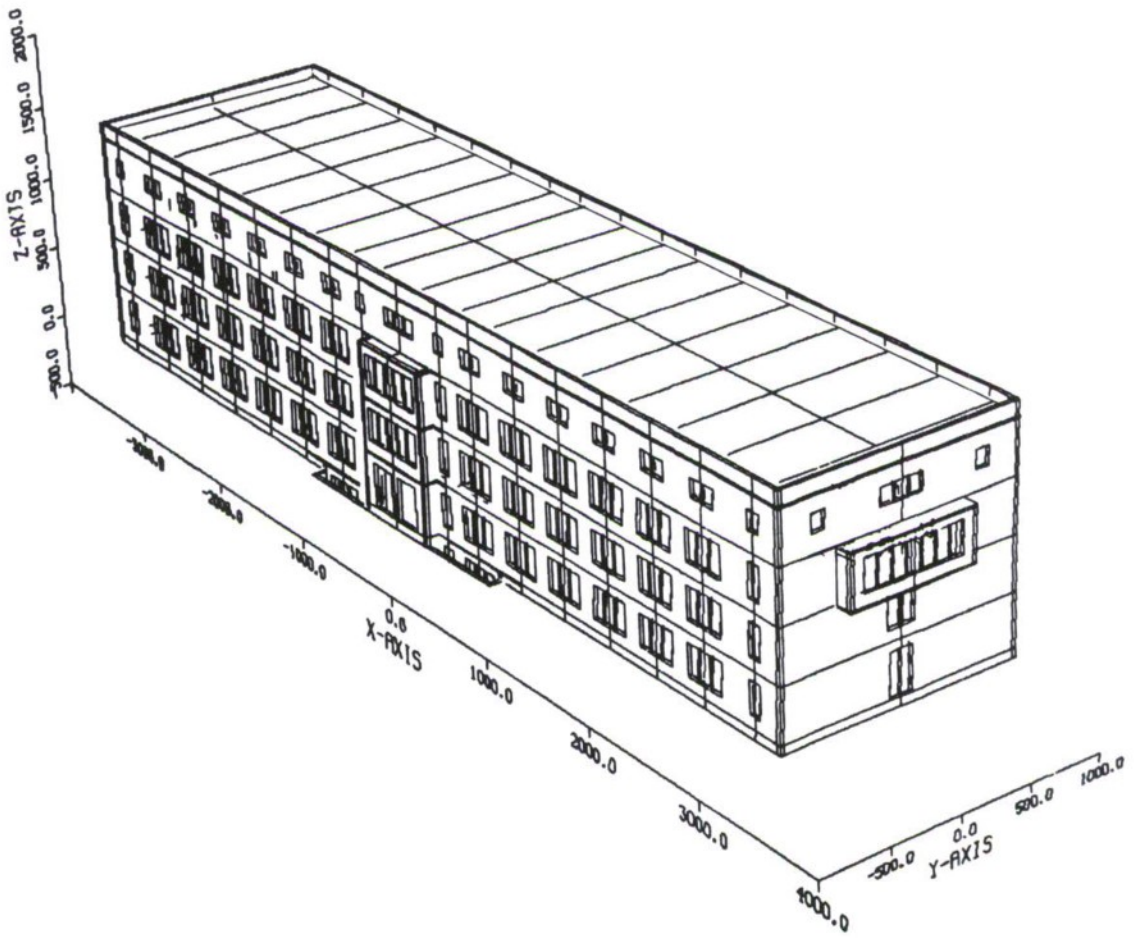

Figure 5.22 Monte Carlo building model for Building A (Chinzei School). (Dimensions in cm.)

Table 5.3 Building A1 Monte Carlo results

	Neutron	Gamma
DOT ext. dose, 500 m	7.18E−23	7.16E−22
DOT ext. dose, 468 m	8.53E−23	8.17E−22
MC ext. dose, 500 m	6.46E−23±2%	6.99E−22±3%
MC ext. dose, adjusted to 468 m	7.67E−23±2%	7.98E−22±3%
MC dose, point 1	5.46E−24±8%	2.91E−23±12%
Ratio, ext. dose to point 1 dose	14.0±8%	27±12%

Notes:

- MC indicates a Monte Carlo calculation.
- ext. indicates dose external to the building.
- All prompt gamma sources were used.
- Doses were reported in units of rads per source neutron.
- Uncertainty estimates indicate 1 standard deviation statistical convergence of the Monte Carlo.

Table 5.4 Comparison of doses calculated by discrete ordinates (DO) and Monte Carlo (MC)

		Dose (cGy)				Dose attenuation	
		Neutron	Building capture gamma	Other gamma	Total gamma	Neutron	Gamma
External	–	290	0	8700	8700	1.0	1.0
Point 8	DO	100	37	2700	2700	2.9	3.2
Point 1	DO	23	30	240	270	13	32
Point 1	MC	–	–	–	–	14 ± 8%	27 ± 12%

Table 5.5 Building A1 dose by various methods

Point	Type	Method	Dose (cGy)		
			S_4	S_6	S_{10}
1	neutron	weighted	12.3	14.9	17.5
1	neutron	nodal	11.0	15.9	22.1
6	neutron	weighted	15.3	17.6	19.8
6	neutron	nodal	15.0	19.0	24.3
1	gamma	weighted	205	214	250
1	gamma	nodal	166	216	316
6	gamma	weighted	433	350	419
6	gamma	nodal	449	349	483

that the results for fine mesh would not agree. There is no sound basis for that extrapolation, however. In related studies, it was observed that the advanced methods approached the final value quickly, overshot a bit, and then moved to the final value.

The effect of increasing the scattering expansion from P_1 to P_3 was also restudied in a case using the nodal method and the finer directional quadrature. The data of Table 5.6 show that neither neutron nor gamma dose are affected significantly by this change. A detailed comparison of data from the various energy groups provides additional insight. The data for Point 1 differ badly in the higher energy groups, but the lower groups are hardly affected at all, as illustrated in Table 5.7. One can speculate that the flux in the higher groups is quite directional, pointed away from the source, while the lower groups are driven by flux resulting from scatters and arriving from many directions. Depending on the hardness or softness of the flux spectrum, either behavior might predominate. Apparently, the behavior of the lower groups controls the accuracy requirement in this case.

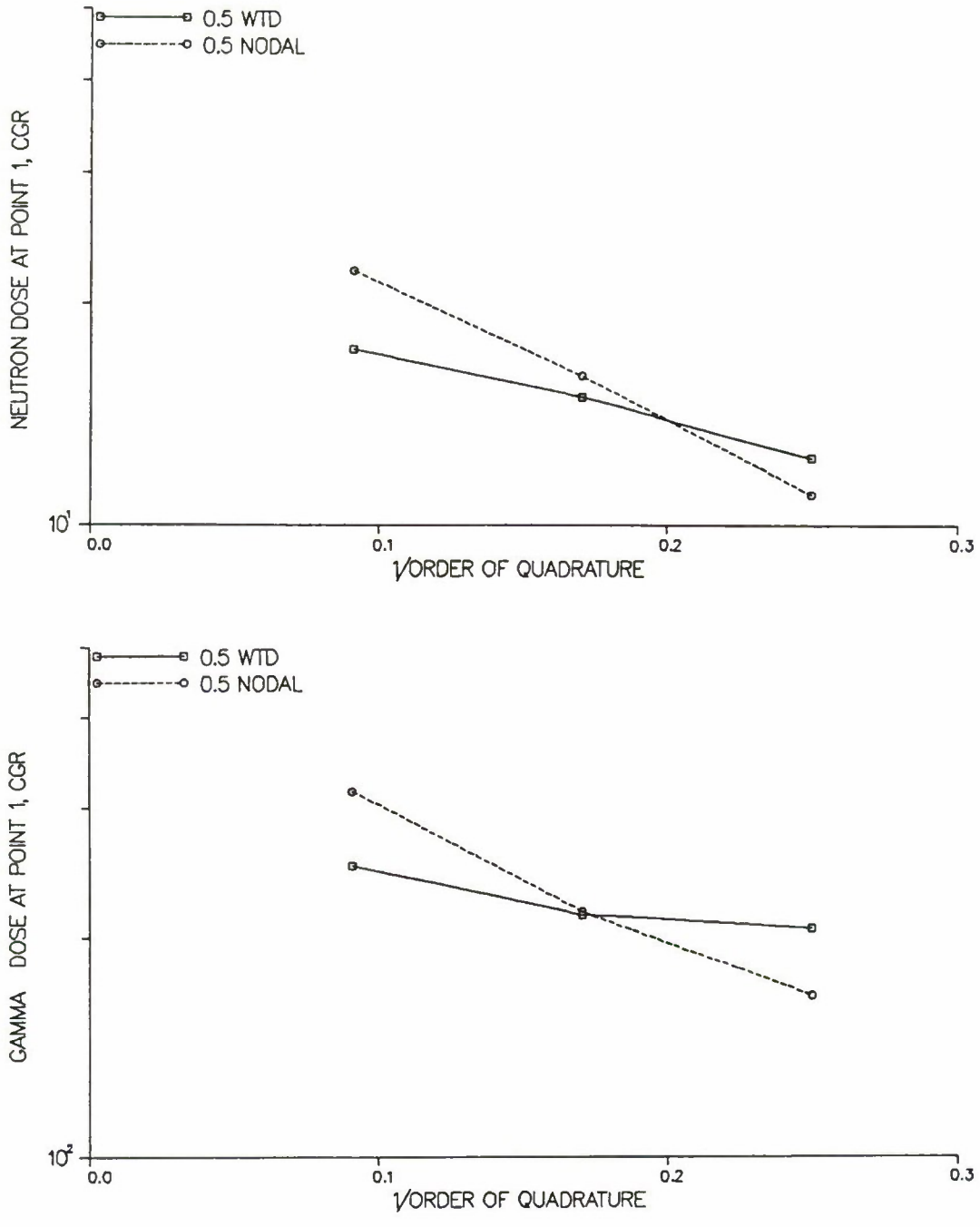

Figure 5.23 Variation of dose at Point 1 with order of quadrature and spatial method.

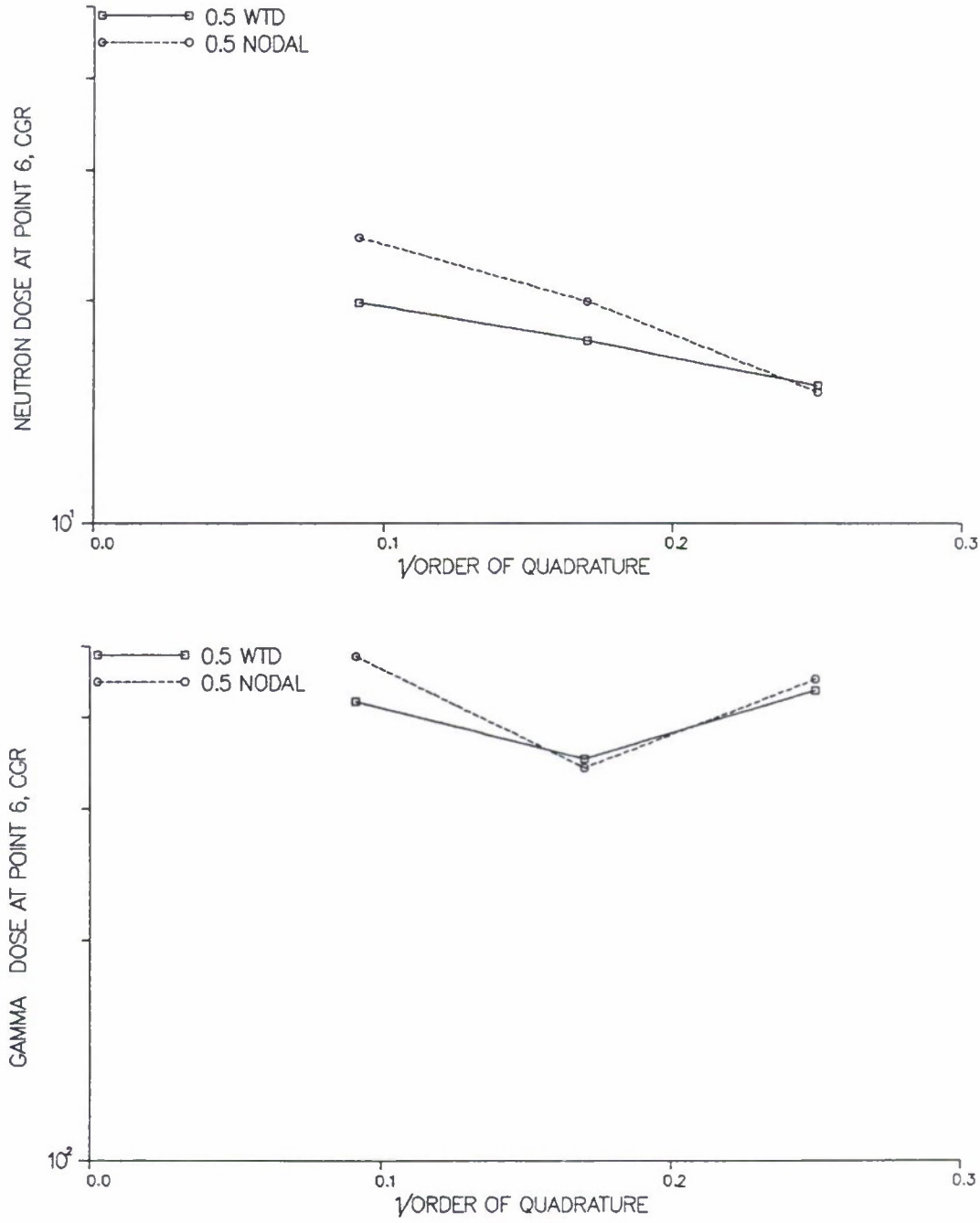

Figure 5.24 Variation of dose at Point 6 with order of quadrature and spatial method.

Table 5.6 Dose responses at selected points calculated using P_1 and P_3 scattering

		Dose (cGy)		
	Position	Neutron	Gamma	Total
P_1 scattering:	1	2.20641E+01	3.16045E+01	3.38109E+02
	2	7.65157E+01	1.93965E+03	2.01617E+03
	3	1.08190E+02	2.78644E+03	2.89463E+03
	4	4.39071E+01	5.08255E+02	5.52162E+02
	5	5.46268E+01	7.48522E+02	8.03149E+02
	6	2.43416E+01	4.83089E+02	5.07431E+02
	7	8.18385E+01	2.03069E+03	2.11253E+03
	8	1.23395E+02	3.05440E+03	3.17780E+03
	9	4.40067E+01	6.04907E+02	6.48914E+02
	10	6.98548E+01	1.37640E+03	1.44626E+03
	Position	Neutron	Gamma	Total
P_3 scattering:	1	2.19243E+01	3.03666E+02	3.25590E+02
	2	7.70841E+01	1.93632E+03	2.01340E+03
	3	1.09116E+02	2.79046E+03	2.89957E+03
	4	4.41872E+01	5.15610E+02	5.59797E+02
	5	5.52129E+01	7.78069E+02	8.33282E+02
	6	2.42431E+01	4.84742E+02	5.08986E+02
	7	8.24545E+01	2.02535E+03	2.10781E+03
	8	1.24184E+02	3.04693E+03	3.17111E+03
	9	4.43925E+01	6.25812E+02	6.70204E+02
	10	7.06992E+01	1.44725E+03	1.51795E+03

Table 5.7 Relative flux in selected energy groups at point 1 calculated using P_1 and P_3 scattering

Group	P_1 flux	P_3 flux
2	7.59E−22	5.61E−22
10	1.08E−18	9.69E−19
20	1.71E−16	1.70E−16
30	2.93E−16	2.94E−16
40	6.41E−16	6.42E−16
50	3.94E−16	3.80E−16
60	1.43E−14	1.36E−14
69	1.03E−17	1.07E−17

5.5 SUMMARY OF METHODS STUDIES

The metric building studies provided a remarkably thorough test of methods. The weighted difference method that has been the mainstay for reactor vessel calculations since the early 1970's was inferior to the newer nodal method in this application. It failed to agree closely with the highly-trusted characteristic method in some of the traverses. It showed disturbing non-physical behavior in certain locations, and it was sensitive to the choice of the model adjustment parameter.

In contrast, the nodal method gave results almost identical to the characteristic method for any value of the model adjustment parameter, theta, except in the small intervals inside the center wall and at each end of the traverses. In those intervals, the 1.0 value of theta gave the best comparison in streaming calculations, while 0.5 was slightly preferable in penetration through overhead concrete and air layers.

The scattering expansion was not important in the streaming calculations, but it was significant in the penetration cases. The expansion was more important when the nodal method was used rather than weighted difference. Similarly, the directional quadrature was more important in the penetration cases and when the nodal method was used.

Early S_6 studies of the A1 building indicated that the weighted difference method could be adjusted to give results for selected points that agreed with the more sophisticated methods. At the time of those studies, the more trusted-nodal method was too expensive for production use. The results deep inside the building were affected by 17% when the change to the finer S_{10} quadrature was made, but this brought an increase in computer memory and processor requirements that were unacceptable at that time. Accordingly, early calculations on both buildings were performed with weighted difference and S_6.

During the course of the project, increased computer memory and improved hardware and software made S_{10} a practical reality, while new programming brought the nodal method to an acceptable efficiency. New studies made practical by these advancements showed that the use of the nodal method was quite important with the finer quadrature deep inside the lower floors of the large building, just as it had been in the metric building. Accordingly, all of the production results reported in later sections were performed with those improvements. A value of 0.5 was used for the adjustable parameter.

The use of a higher order of scattering expansion was also considered. Like the finer directional quadrature, it was impractical at the beginning of the project, but it is feasible now. The metric building studies showed that the higher-order expansion could be important in the difficult case of a monodirectional source penetrating a windowless structure, but two studies of the A1 building indicated that it has negligible effect there. One may conclude that the weapon source is sufficiently multidirectional that the higher-order scattering expansion is not beneficial.

6. BUILDING A

6.1 GEOMETRIC MODELS

The A building, the main building of the Chinzei School at Nagasaki (Figs. 6.1–6.3), was a four-story rectangular structure with a half-basement under the center of the building. The exterior walls were of 10-inch reinforced concrete, built to withstand earthquakes, while the floors were of similar construction and 5 in. thick. All floors were supported by heavy concrete beams resting on concrete pillars (Fig. 6.4). The fourth-floor attic extended from the south end of the building to just past the center, leaving room for a high-ceiling auditorium at the north end.

The roof over the attic was of tile construction, supported by a wooden framework resting on wooden posts. The roof over the auditorium was of concrete slab construction, supported by a steel truss system. The entire roof and fourth-floor structure collapsed at the time of the shock wave passage, and all personnel on the third and fourth floors died on the day of the attack.[5] Since the roofing material appears to have been distributed relatively uniformly (Fig. 6.2), it was taken to have the same shielding value for the people on the lower floors before and after the collapse.

The exterior dimensions of the building, exclusive of basement, were roughly 70 m long × 17 m wide × 15 m high. The building sat on a hill about 60 feet above sea level,[13] and the first floor was taken to be at two feet above ground level, i.e. at an altitude of 62 feet or 18.9 m. The building was located southwest of the hypocenter (ground zero) at the location indicated as "18" in Fig. 6.5. For the purpose of this study, the hypocenter was taken to be 468 m from the center of the building in a direction 39 degrees clockwise from the south-to-north axis of the building. Since the epicenter (the burst position) was at an altitude of 503 m above sea level, the view of the building from the epicenter was approximately that shown in Fig. 5.22.

The exterior source was calculated assuming a horizontal air/ground interface, and so the hill could not be simulated exactly. In order to preserve the air and distance attenuation of the radiation while maintaining the correct air/ground environment, the building was moved inward to a ground range of 448 m. This perturbed the angle of the incident radiation by only about 3 degrees.

The first model, designated A1 and shown in Fig. 5.20, was constructed essentially by simplifying the Monte Carlo model constructed by Cramer and shown in Fig. 5.22. The windows were simplified, but their general shapes and sizes were retained, except that the attic windows at the north end of the building were omitted in this model. The outsets at the front doorway and at the end windows were ignored. The interior support pillars and beams were modeled in detail, but the interior walls and the basement were ignored in the A1 model. These simplifications allowed the problem to fit onto a 1 Megaword (Mw) Cray 1 using an early version of TORT. It also kept the number of mesh cells to about 100,000–thought to be important in controlling solution costs.

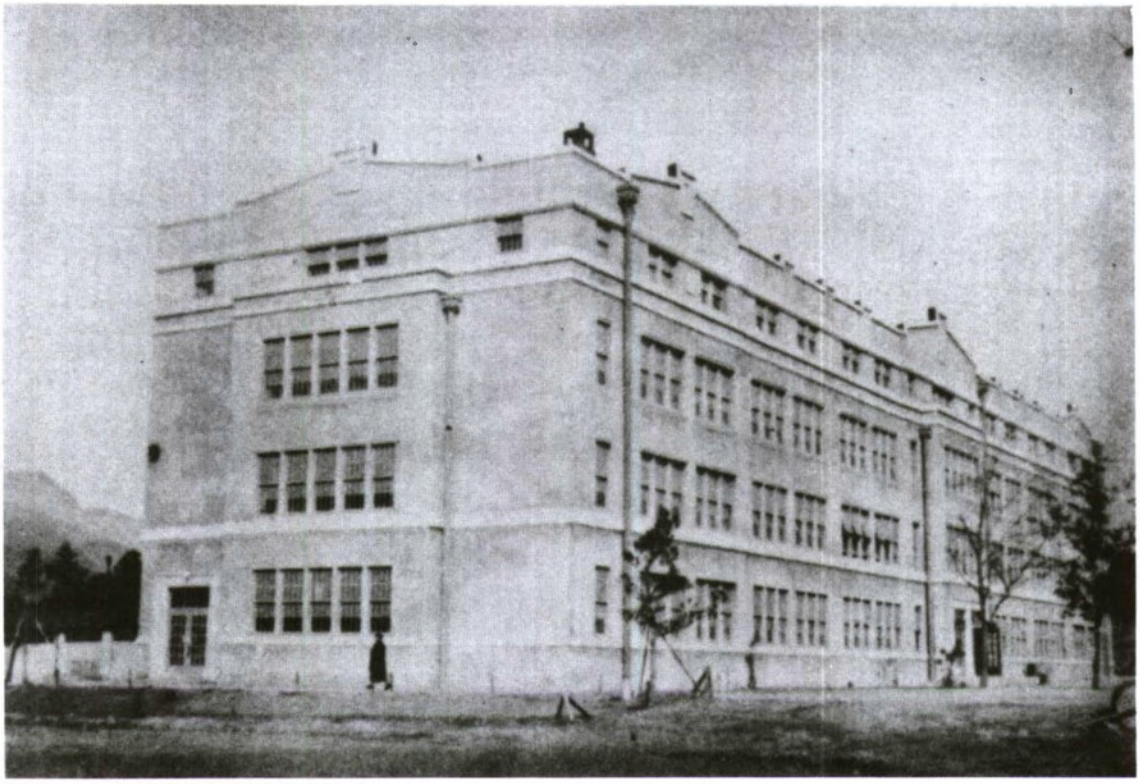

Figure 6.1 Building A4: Chinzei School main building; before the attack, looking northwest.

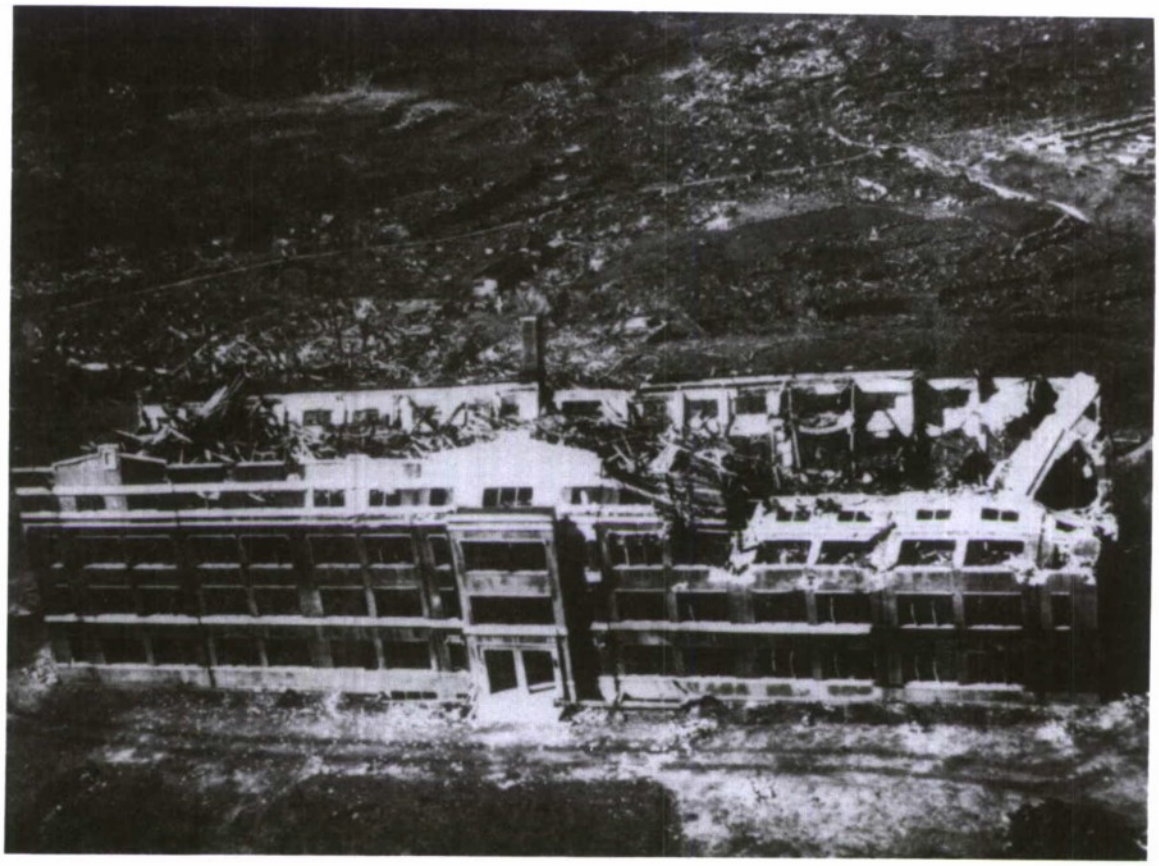

Figure 6.2 Building A4: after the attack; looking west.

Figure 6.3 Building A4: after the attack; looking northwest toward epicenter.

Figure 6.4 Building A4: Interior view showing concrete beams and pillars.

Figure 6.5 Nagasaki target area; aerial photograph looking north (Chinzei School is at area 18; Shiroyama School is at 16.) (Ranges are shown in feet.)

Although the A1 model was used for some preliminary calculations, it soon became necessary to add the basement and internal walls. Since no satisfactory information on the construction of the internal walls was available, all of the walls indicated as heavy-construction concrete were taken to be 5.5 inches thick, while all other internal walls were taken as equivalent to 2 inches of concrete. The revised model, designated A2, gave doses deep in the interior of the building as much as a factor of 2 less than A1. The mesh was expanded to about 140,000 cells, but more extensive use of external disk files allowed solution without additional memory.

Model A3 was based on new data and a thorough review of older data. Appendix A discusses the new model in detail. It used the same exterior walls, floors, and support members as the other models, but the windows were resized and repositioned based on direct scaling of file photographs. The internal walls were redesigned, based on data from several sources. The stairwells were taken to be of 5.5-inch concrete construction, and they were taken to have withstood the shock wave, based on file photographs. All other walls were taken as equivalent to 1.14 inches of concrete, based on notes in an early analysis conducted by ABCC. They were assumed to have been blown apart by the blast, and thus to offer negligible protection against radiation after the shock. The mesh was reduced to about 128,000 cells. Model A4 was identical to A3, except that the light internal walls were taken as 1.2 cm of plaster and 3.0 cm of wood, based on information by Kerr.[36]

6.2 PERSONNEL LOCATIONS

The determination of personnel locations and the incidence of fatality was made by Stohler[13] based on case interview files. Many of the cases had to be excluded from the list of "good" data for the following reasons:

- records incomplete as to whether person died or as to the cause of death,
- records insufficient to allow placement of person at the time of the attack,
- person died on the day of the attack, or
- person lived beyond the first day, but had significant mechanical or burn injuries.

The "good" case positions are shown in Table 6.1, together with the "effect," 0 for survival and 1 for radiation death, and the uncertainty in X and Y positions. In this coordinate system, the origin is at the center of the building at the surface of the first floor, X lies along the northward axis of the building, and Y lies along the westward axis. All position data in the tables are in centimeters. The positions are plotted in Figs. 6.6–6.8. For the sake of completeness, the "excluded" cases are shown in Table 6.2. Fatality and positioning uncertainty are not shown for these cases due to the various complications listed above. It should be noted that the grouping and effect data listed here are preliminary, for the purpose of evaluating the consistency of the results. Revisions may be made before a final LD50 is determined. Likewise, minor adjustments in position may be made in later analysis.

Table 6.1 Position data for building A4, good cases (Case number; effect; X,Y,Z positions; X,Y uncertainty)

Case no.	X position	Y position	Z position	X error	Y error
1	−90.00[a]	125.00	−290.52	90.00	90.00
2	−225.00	325.00	−290.52	90.00	90.00
3	135.00	−700.00	−290.52	30.00	30.00
4	210.00	−455.00	−290.52	30.00	30.00
5	85.00	−755.00	−290.52	30.00	30.00
11	2960.00	−730.00	60.00	60.00	60.00
12	2155.00	−275.00	60.00	60.00	60.00
16	1495.00	−470.00	60.00	60.00	60.00
17	3270.00	−720.00	60.00	60.00	60.00
101	−2090.00	385.00	60.00	30.00	60.00
102	−2090.00	480.00	60.00	30.00	60.00
103	−2090.00	565.00	60.00	30.00	30.00
104	−2090.00	665.00	60.00	30.00	60.00
13	1140.00	540.00	60.00	60.00	30.00
92	−410.00	−445.00	90.00	30.00	30.00
112	−740.00	−70.00	90.00	90.00	60.00
115	−420.00	−215.00	90.00	60.00	90.00
37	2810.00	−700.00	410.52	60.00	60.00
32	2400.00	−630.00	410.52	60.00	60.00
26	1580.00	−480.00	410.52	60.00	60.00
27	1555.00	−260.00	410.52	60.00	60.00
30	1670.00	−675.00	410.52	60.00	60.00
40	2975.00	540.00	410.52	60.00	60.00
43	2425.00	360.00	410.52	60.00	60.00
46	1060.00	275.00	410.52	60.00	60.00
88	−3080.00	525.00	410.52	30.00	30.00
89	−3200.00	730.00	410.52	30.00	30.00
90	−2980.00	730.00	410.52	30.00	30.00
93	−3200.00	525.00	410.52	30.00	30.00
95	−2960.00	525.00	410.52	30.00	30.00
97	−3070.00	730.00	410.52	30.00	30.00
94	−3320.00	0.00	410.52	30.00	30.00
96	−3295.00	−295.00	440.52	60.00	60.00

[a] All dimensions in centimeters.

6.3 KEY LOCATION DOSE RESULTS

It may be recalled from an earlier section that three types of doses will be presented:

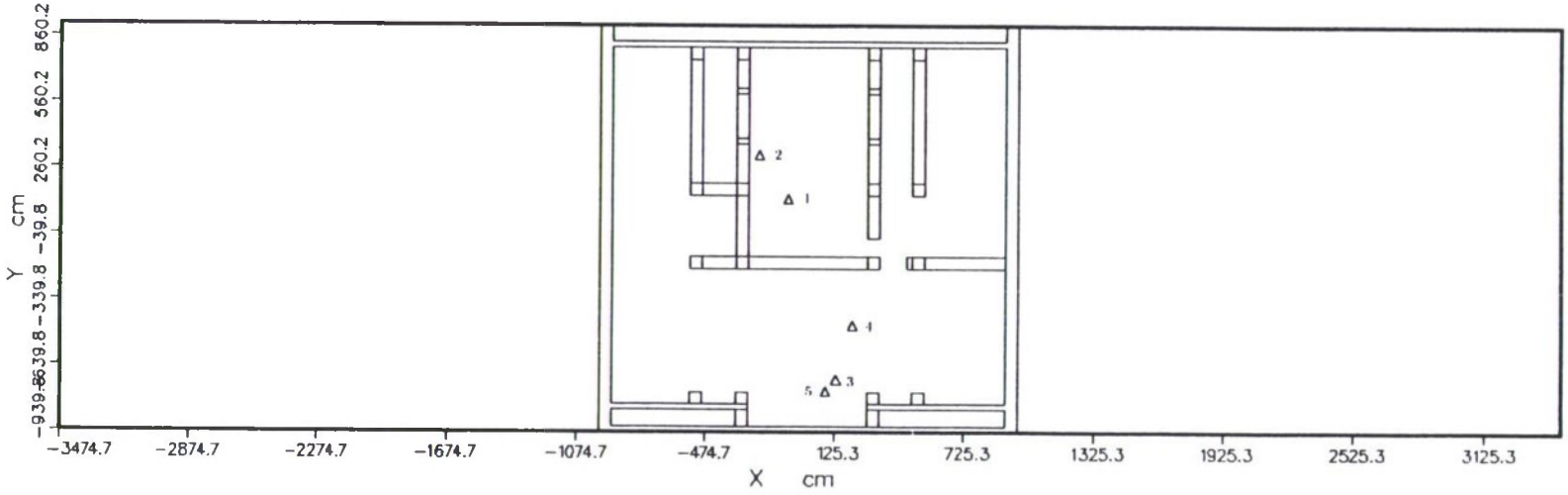

Figure 6.6 Building A4 personnel locations; basement.

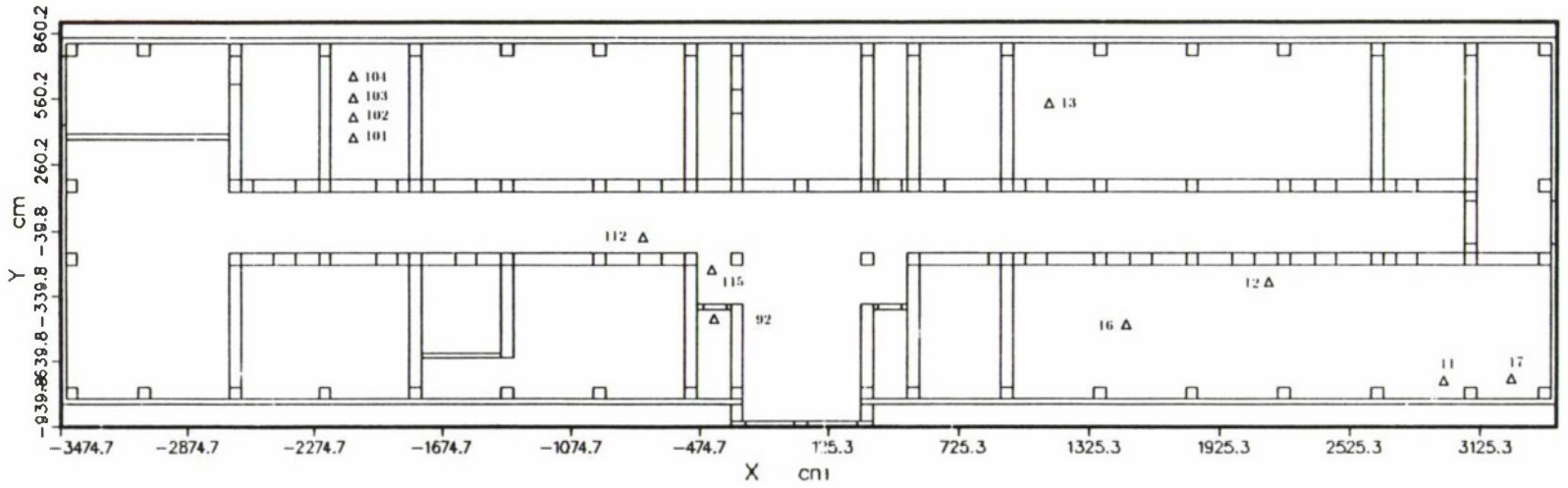

Figure 6.7 Building A4 personnel locations; first floor.

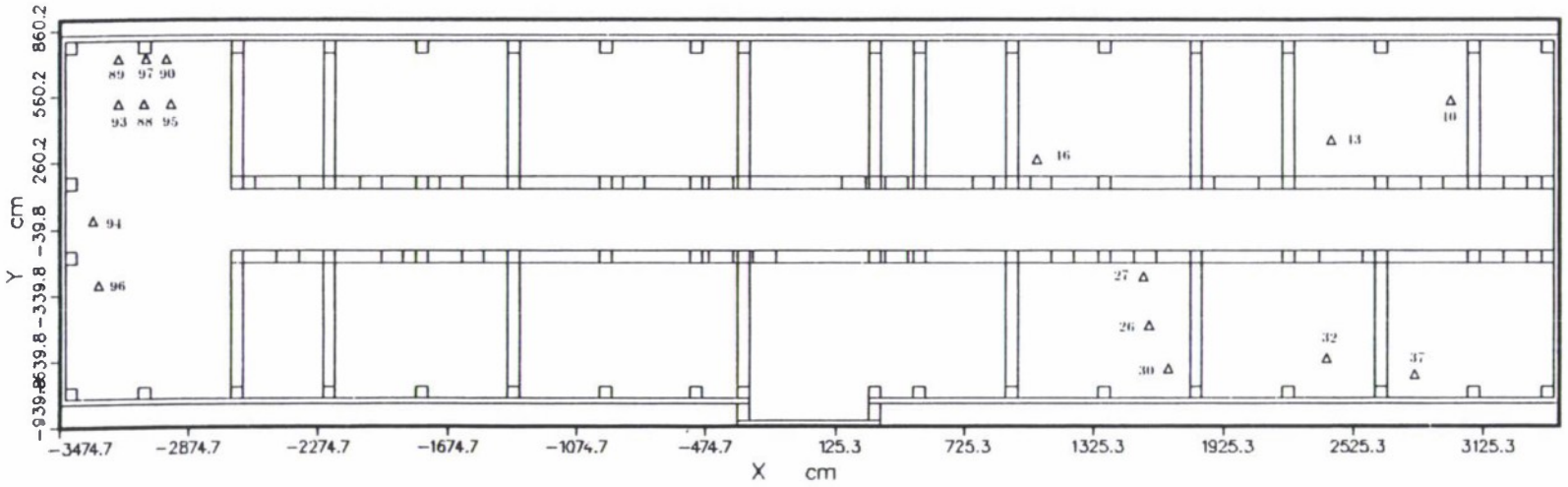

Figure 6.8 Building A4 personnel locations; second floor.

Table 6.2 Position data for building A4, excluded cases

Case no.		X position	Y position	Z position
1	6	2345.00[a]	−280.00	30.00
2	7	1180.00	−720.00	60.00
3	8	1180.00	−610.00	60.00
4	9	1180.00	−430.00	60.00
5	10	2345.00	−280.00	30.00
6	14	2670.00	−270.00	60.00
7	15	1890.00	−240.00	60.00
8	91	841.00	−670.00	60.00
9	18	185.00	−370.00	90.00
10	108	−260.00	−650.00	90.00
11	109	190.00	−720.00	90.00
12	110	−180.00	−770.00	90.00
13	105	−2140.00	510.00	60.00
14	106	−2080.00	510.00	60.00
15	107	−2160.00	450.00	60.00
16	35	3330.00	−450.00	410.52
17	36	2880.00	390.00	410.52
18	38	3330.00	−660.00	410.52
19	39	3060.00	−580.00	410.52
20	33	2290.00	−440.00	410.52
21	34	2060.00	−660.00	410.52
22	19	1500.00	−720.00	410.52
23	20	1370.00	−580.00	410.52
24	21	1280.00	−750.00	410.52
25	22	1010.00	−660.00	410.52
26	23	1030.00	−340.00	410.52
27	24	1210.00	−270.00	410.52
28	25	1720.00	−480.00	410.52
29	28	1730.00	−290.00	410.52
30	29	1330.00	−350.00	410.52
31	31	1110.00	−460.00	410.52
32	41	2670.00	510.00	410.52
33	42	2510.00	540.00	410.52
34	44	2340.00	340.00	410.52
35	45	2900.00	350.00	410.52
36	47	1120.00	590.00	410.52
37	48	1430.00	610.00	410.52
38	49	1450.00	730.00	410.52
39	50	1340.00	310.00	410.52
40	51	1580.00	310.00	410.52
41	52	1690.00	480.00	410.52
42	53	1710.00	650.00	410.52
43	54	1640.00	730.00	410.52
44	55	2670.00	670.00	791.04
45	56	2400.00	400.00	791.04
46	57	2860.00	−520.00	791.04
47	58	1690.00	−680.00	791.04
48	59	1260.00	510.00	791.04
49	60	1630.00	520.00	791.04

[a] All dimensions in centimeters.

- free-in-air soft tissue kerma (FIA)
- average small-intestine kerma (SI), and
- body-averaged bone-marrow kerma (BM).

All doses are in centiGray units. The first dose results are presented for the three points examined in the previous section:

- an "exterior" point, i.e. a point calculated at the origin of the building, but without the building materials present,
- Point 1, 155 cm above the center of the first floor, and
- Point 3, 155 cm above the first floor, in front of a window facing the weapon.

In addition to total dose, the contributions from six source components are listed separately:

- prompt gamma dose leaking directly from the weapon,
- air/ground capture gamma dose from leakage neutrons,
- early delayed gamma dose reaching the building before the shock wave,
- late delayed gamma dose reaching the building after the shock wave,
- building capture gamma dose due to neutron capture in the building, and
- prompt neutron dose due to weapon leakage.

A total of five separate computer runs were required to calculate the six results; the prompt neutron and building capture gamma data resulted from the same computer run. The three types of dose responses were obtained in parallel from the same runs.

The FIA dose response for the three positions identified above are tabulated in Table 6.3. The doses in the building range from the lethal 2586 cGy to a survivable 208 cGy. The attenuation differs for the various sources due to spectral and directional effects. Also, the late delayed gammas are attenuated less than the early delays due to the assumption that the light-construction walls have been removed by the intervening shock wave.

It may be interesting to look at attenuation factors (AF) and protection factors (PF) for these points as a measure of the building effect:

AF = ratio by which neutron or gamma dose is reduced in penetrating the building, and

PF = neutron or gamma exterior radiation dose divided by all interior dose due to that type of exterior radiation.

Table 6.3 Free-in-air doses from various sources outside building, near a window facing the source, and deep inside the first floor of building A4

	Exterior	Point 3, near window	Point 1, center of first floor
Prompt gamma	1083 cGy	295 cGy	16 cGy
Air/ground capture gamma	2695	810	59
Early delayed gamma	1881	406	29
Late delayed gamma	4389	953	83
Building capture gammas	0	25	11
All gammas	10048	2489	198
Prompt neutron	335	97	10
Total	10383	2586	208

It is readily seen that the difference between the two measures is that the building capture gamma contribution is not considered in the attenuation factor determination. The factors for the three key points are shown in Table 6.4. The total attenuation for the mixed radiation field ranged from about 4 near the windows, largely dependent upon window size and position, to about 50 in the building interior. Gammas were attenuated much more than neutrons, and capture gamma dose actually exceeded neutron dose in the center of the building.

Table 6.4 Attenuation and protection factors for building A4

	Point 3 near window	Point 1, center of first floor
AF, gamma	4.1	54
PF, gamma	4.1	54
AF, neutron	3.5	34
PF, neutron	2.7	16
AF, total	4.0	50

6.4 POSITION INTERPOLATION

The basic dose results consisted of tables of average dose for each of the mesh cells. Since some of the mesh cells were as large as 1 m on a side, dose was interpolated to the best-known location of an individual. This provided a smoother and more accurate variation of dose with position.

Direct linear interpolation had a potential disadvantage, in that a cell inside a large concrete zone, e.g. a pillar, could artificially depress the dose calculated near the surface of the pillar. If the concrete zone happened to be a wall between the weapon and the person, however, the interpolation method would produce the desired result. A compromise method was found in which two results were calculated. First, the direct-interpolation result was calculated. Then, the materials in the cells adjacent to the point were examined. If any of the cells were concrete, new interpolation cells were selected away from the concrete, and the interpolation was repeated. The maximum of the two doses was then reported as the best result. One tends, intuitively, to dislike maximum selections on the basis that they may introduce bias, but it is evident that the use here is a legitimate model, not a bias procedure. Extensive study of case-by-case results confirmed the desirable effect of this model.

6.5 DOSES AT PERSONNEL LOCATIONS

Tables of FIA dose for the same six source components are shown for all of the good cases in Table 6.5, together with the fatality effect and total dose. Case histories indicate that personnel were thrown about inside the buildings by the shock wave, but the final positions are not accurately known. Accordingly, all personnel were represented at their previous horizontal position, but at 30 cm above the floor, in determing the late delayed gamma dose. This corresponded, for example, to heights of 30.00 and 380.52 cm for the first two floors. Table 6.6 shows an estimate of the uncertainty of each component, the calculation of which is discussed in a later section. Tables 6.7–6.10 present the corresponding data for the other dose responses.

Figures 6.9–6.13 show plots of the common logarithms (base 10) of FIA dose as a function of position. To interpret these, recall that a logarithm of 2.6, for example, would correspond to a dose of approximately 4.0×10^2, etc. The source in these plots is from the direction of the lower right corner. The plots clearly show the effects of streaming through both front and back windows, shadowing by the structure, and other transport features in general agreement with expected results.

For the sake of completeness, results for the excluded cases are shown in Tables 6.11–6.13.

Table 6.5 Building A4 dose data (FIA), cGy units

Case	no.	Effect	Prompt gammas	Air/ground gammas	Early delayed gammas	Late delayed gammas	Building gammas	Total gammas	Prompt neutrons	Total dose
1	1	0	1.1	11.0	1.9	4.9	2.4	21.3	0.8	22.1
2	2	0	1.1	11.2	2.1	5.8	2.4	22.7	0.9	23.6
3	3	0	26.2	119.8	58.9	135.2	5.7	345.8	6.6	352.4
4	4	0	16.9	73.4	23.8	60.3	5.1	179.4	4.6	184.0
5	5	1	25.9	112.5	54.6	119.7	6.0	318.8	6.9	325.7
6	11	1	180.9	544.2	315.8	710.6	26.4	1777.8	60.4	1838.2
7	12	1	60.2	213.6	103.2	262.6	20.1	659.7	34.0	693.7
8	16	1	100.9	354.9	161.6	395.5	21.3	1034.2	44.8	1079.0
9	17	1	200.6	614.4	315.4	720.8	25.5	1876.7	51.0	1927.7
10	101	0	11.1	41.1	26.0	87.8	11.5	177.5	11.0	188.5
11	102	1	14.0	44.0	32.9	98.5	12.7	201.9	14.5	216.4
12	103	0	19.4	53.0	45.2	117.9	13.9	249.3	19.7	268.9
13	104	1	30.7	78.3	70.0	166.6	15.0	360.5	27.1	387.6
14	13	0	28.8	106.4	67.4	163.9	17.5	384.1	25.0	409.2
15	92	0	34.4	126.3	51.6	209.4	16.1	437.8	16.0	453.8
16	112	0	14.9	54.7	27.2	128.1	10.5	235.4	10.3	245.6
17	115	1	16.4	70.0	25.9	130.4	11.5	254.3	9.0	263.3
18	37	1	421.6	1093.8	566.1	1355.1	40.9	3477.4	105.5	3582.8
19	32	1	318.3	890.0	415.8	1049.7	40.1	2714.0	93.3	2807.3
20	26	1	141.2	549.2	238.5	605.7	35.2	1569.9	60.1	1630.0
21	27	1	99.1	407.9	179.6	473.3	32.4	1192.3	44.3	1236.6
22	30	1	303.5	845.9	446.0	1106.4	38.8	2740.7	88.9	2829.6
23	40	1	56.7	254.2	121.2	283.4	31.7	747.2	35.3	782.5
24	43	1	89.8	417.8	195.0	479.0	32.6	1214.2	38.5	1252.7
25	46	1	84.5	371.7	156.8	393.1	25.0	1031.1	30.1	1061.2
26	88	0	30.1	119.7	61.9	151.4	20.1	383.1	23.3	406.5
27	89	1	22.9	102.9	49.2	113.8	20.5	309.4	18.1	327.4
28	90	1	50.9	168.7	104.7	239.9	20.9	585.0	32.0	617.0
29	93	0	28.2	122.2	57.0	140.4	20.5	368.3	20.8	389.2
30	95	0	28.0	105.6	59.8	144.5	19.7	357.7	23.7	381.4
31	97	0	44.0	156.4	87.1	205.3	20.2	513.0	26.2	539.2
32	94	0	51.1	167.6	103.5	249.1	20.3	591.6	39.8	631.4
33	96	1	44.3	180.8	74.7	189.9	20.3	510.0	26.3	536.3

Table 6.6 FIA uncertainty, %

Case	no.	Effect	Prompt gammas	Air/ground gammas	Early delayed gammas	Late delayed gammas	Building gammas	Total gammas	Prompt neutrons	Total dose
1	1	0	7.2	6.6	6.3	5.9	7.3	6.5	11.2	6.7
2	2	0	36.3	36.7	39.0	37.6	25.1	35.9	40.2	36.0
3	3	0	10.2	13.2	12.9	13.7	1.7	12.9	3.1	12.7
4	4	0	19.9	16.3	17.7	16.9	2.6	16.6	9.6	16.4
5	5	1	9.1	14.3	15.3	17.9	1.7	15.2	2.8	14.9
6	11	1	61.6	52.9	59.1	57.5	6.8	56.1	33.6	55.3
7	12	1	12.2	13.1	10.0	8.8	2.2	10.5	7.3	10.3
8	16	1	29.8	24.3	23.4	22.5	4.8	23.6	17.1	23.4
9	17	1	28.4	25.6	38.2	33.5	3.4	30.8	21.0	30.5
10	101	0	9.9	5.7	11.7	4.1	6.1	6.1	13.9	6.5
11	102	1	19.7	10.8	19.5	10.9	6.3	12.6	20.1	13.1
12	103	0	14.9	10.6	14.5	10.5	3.1	11.2	12.5	11.3
13	104	1	31.6	35.8	29.0	23.6	4.2	27.2	13.2	26.2
14	13	0	6.3	3.9	6.0	4.7	2.6	4.7	7.1	4.8
15	92	0	15.7	13.2	15.2	11.1	5.0	12.3	12.8	12.3
16	112	0	22.7	21.3	22.2	9.5	8.2	14.5	21.8	14.8
17	115	1	31.7	27.3	28.7	29.5	16.4	28.4	24.5	28.2
18	37	1	17.2	12.7	17.5	12.7	2.1	13.9	8.7	13.8
19	32	1	34.8	24.4	30.1	28.6	2.2	27.8	14.9	27.4
20	26	1	20.8	14.9	15.5	13.2	2.6	14.6	14.7	14.6
21	27	1	7.5	7.6	6.4	4.1	1.9	5.9	6.2	5.9
22	30	1	28.1	23.9	28.1	19.4	1.4	22.9	13.8	22.6
23	40	1	17.1	19.7	20.2	20.1	2.7	19.0	10.2	18.6
24	43	1	6.8	8.1	6.8	7.1	1.3	7.2	3.1	7.1
25	46	1	2.4	3.4	5.9	3.6	4.9	3.8	5.9	3.8
26	88	0	1.8	3.8	2.3	2.1	1.0	2.6	4.0	2.7
27	89	1	14.4	11.7	14.2	14.6	1.2	12.6	10.9	12.5
28	90	1	15.6	13.7	15.1	12.8	1.9	13.3	10.3	13.2
29	93	0	3.0	3.6	3.3	4.2	0.9	3.6	3.8	3.6
30	95	0	5.9	4.7	4.2	3.4	1.2	4.0	5.7	4.1
31	97	0	28.5	21.8	26.5	26.1	0.4	24.1	20.0	23.9
32	94	0	10.4	6.2	10.6	8.6	1.7	8.2	10.6	8.3
33	96	1	7.5	8.5	4.3	3.9	2.6	5.8	5.1	5.8

Table 6.7 Building A4 dose data (SI), cGy units

Case	no.	Effect	Prompt gammas	Air/ground gammas	Early delayed gammas	Late delayed gammas	Building gammas	Total gammas	Prompt neutrons	Total dose
1	1	0	0.7	7.8	1.2	3.1	1.7	14.4	0.7	15.1
2	2	0	0.7	8.0	1.4	3.7	1.7	15.4	0.8	16.2
3	3	0	16.7	85.4	38.4	88.0	3.9	232.4	3.3	235.7
4	4	0	10.8	51.7	15.0	38.1	3.5	119.1	2.5	121.6
5	5	1	16.5	79.8	35.3	77.1	4.1	212.8	3.4	216.2
6	11	1	114.0	383.7	194.6	439.3	18.1	1149.6	26.7	1176.3
7	12	1	36.1	146.2	60.5	153.2	13.7	409.6	17.0	426.6
8	16	1	61.5	246.1	96.3	236.0	14.6	654.5	20.4	674.9
9	17	1	128.7	437.9	197.5	453.1	17.4	1234.6	22.6	1257.2
10	101	0	6.4	27.5	14.9	49.7	7.9	106.3	7.3	113.6
11	102	1	8.0	29.0	18.6	55.4	8.6	119.6	8.9	128.5
12	103	0	11.0	34.5	25.4	66.1	9.5	146.5	11.1	157.6
13	104	1	17.6	51.3	39.5	94.2	10.2	212.9	13.9	226.8
14	13	0	16.8	71.8	38.9	94.7	12.0	234.3	14.0	248.4
15	92	0	20.8	86.2	30.6	121.5	11.0	270.1	9.8	279.9
16	112	0	8.8	36.6	15.8	72.2	7.1	140.5	6.0	146.6
17	115	1	9.9	47.8	15.3	74.6	7.9	155.5	5.8	161.3
18	37	1	270.7	778.5	351.9	844.4	28.0	2273.5	44.6	2318.1
19	32	1	201.9	628.3	255.3	650.8	27.4	1763.8	40.5	1804.3
20	26	1	86.8	383.0	146.2	369.3	24.1	1009.3	29.1	1038.4
21	27	1	60.8	282.8	110.5	287.6	22.1	763.8	23.1	787.0
22	30	1	192.7	597.7	275.8	685.7	26.6	1778.5	39.1	1817.6
23	40	1	34.6	175.9	74.1	172.9	21.7	479.2	20.9	500.1
24	43	1	55.9	293.2	122.7	298.4	22.2	792.4	21.6	814.0
25	46	1	53.3	261.6	98.8	246.1	17.1	676.8	16.7	693.5
26	88	0	17.8	81.3	36.3	89.2	13.7	238.3	12.9	251.2
27	89	1	13.8	71.0	29.5	68.6	14.0	196.9	11.2	208.1
28	90	1	30.6	115.9	62.4	143.7	14.3	366.9	16.1	382.9
29	93	0	16.9	83.8	34.0	83.8	14.0	232.5	12.1	244.6
30	95	0	16.4	71.1	34.8	84.2	13.5	220.0	13.1	233.1
31	97	0	26.8	108.2	52.4	124.1	13.8	325.2	13.9	339.1
32	94	0	29.6	112.3	59.0	142.2	13.9	357.0	18.8	375.8
33	96	1	26.6	124.3	44.2	112.1	13.9	321.1	14.0	335.1

Table 6.8 Building A4 uncertainty data (SI), %

Case	no.	Effect	Prompt gammas	Air/ground gammas	Early delayed gammas	Late delayed gammas	Building gammas	Total gammas	Prompt neutrons	Total dose
1	1	0	7.6	6.6	5.9	5.5	7.4	6.5	9.2	6.6
2	2	0	36.2	37.5	38.5	37.1	25.2	36.1	31.6	35.9
3	3	0	10.7	13.7	13.4	14.3	1.7	13.5	2.5	13.3
4	4	0	20.8	17.0	18.3	17.5	2.6	17.2	6.7	17.0
5	5	1	9.6	15.0	16.2	19.1	1.7	16.0	2.1	15.8
6	11	1	63.4	54.1	60.7	59.2	6.8	57.3	24.9	56.6
7	12	1	12.9	13.6	10.4	9.4	2.2	11.1	4.1	10.8
8	16	1	30.9	25.0	24.0	23.1	4.8	24.3	12.8	23.9
9	17	1	28.5	26.0	38.9	34.2	3.4	31.0	15.5	30.7
10	101	0	9.5	6.6	11.2	3.5	6.2	6.0	10.6	6.3
11	102	1	19.3	10.3	18.8	10.5	6.3	12.0	14.4	12.2
12	103	0	14.9	10.5	14.3	10.4	3.1	11.0	8.8	10.8
13	104	1	34.2	38.6	31.2	26.1	4.2	29.7	9.1	28.4
14	13	0	6.0	4.3	5.6	4.1	2.6	4.5	5.4	4.6
15	92	0	15.9	13.4	15.2	11.5	5.1	12.6	9.6	12.5
16	112	0	22.4	22.3	21.2	9.5	8.3	14.9	16.3	15.0
17	115	1	32.0	27.5	28.5	29.8	16.4	28.4	20.8	28.2
18	37	1	17.7	13.1	18.4	13.4	2.2	14.4	6.3	14.3
19	32	1	36.2	25.3	31.1	29.5	2.2	28.6	11.0	28.2
20	26	1	21.1	15.2	15.5	13.2	2.6	14.7	10.4	14.6
21	27	1	8.0	8.1	7.1	4.8	1.9	6.5	4.5	6.5
22	30	1	29.2	24.6	29.2	20.2	1.4	23.8	9.0	23.5
23	40	1	17.7	20.6	21.2	21.2	2.8	19.9	7.2	19.4
24	43	1	7.3	8.5	7.3	7.6	1.3	7.7	2.6	7.5
25	46	1	2.6	3.4	5.8	3.6	5.0	3.8	5.2	3.9
26	88	0	1.5	4.3	1.9	2.1	1.0	2.7	2.6	2.7
27	89	1	14.2	11.8	13.9	14.3	1.2	12.4	6.6	12.1
28	90	1	16.8	14.7	15.9	13.8	2.0	14.2	7.8	13.9
29	93	0	2.8	3.9	3.1	4.1	1.0	3.6	2.0	3.5
30	95	0	5.8	5.0	3.9	3.1	1.2	3.9	4.1	3.9
31	97	0	29.4	22.3	26.9	26.5	0.4	24.3	13.0	23.8
32	94	0	10.1	6.1	10.2	8.2	1.8	7.8	7.6	7.8
33	96	1	8.5	9.1	4.3	4.2	2.6	6.4	3.7	6.3

Table 6.9 Building A4 dose data (BM), cGy units

Case	no.	Effect	Prompt gammas	Air/ground gammas	Early delayed gammas	Late delayed gammas	Building gammas	Total gammas	Prompt neutrons	Total dose
1	1	0	0.8	8.6	1.3	3.5	1.9	16.1	0.8	16.9
2	2	0	0.8	8.9	1.5	4.2	1.8	17.2	0.9	18.1
3	3	0	18.8	94.4	43.0	98.5	4.4	259.1	4.3	263.4
4	4	0	12.1	57.3	16.9	42.9	3.9	133.1	3.3	136.4
5	5	1	18.6	88.3	39.5	86.6	4.6	237.5	4.5	242.0
6	11	1	128.3	424.5	220.0	496.2	20.1	1289.1	36.1	1325.2
7	12	1	41.1	162.6	69.2	175.3	15.3	463.4	22.5	485.9
8	16	1	69.7	273.1	109.6	268.7	16.3	737.4	27.5	765.0
9	17	1	144.3	483.6	222.5	510.1	19.5	1379.9	30.7	1410.6
10	101	0	7.3	30.7	17.2	57.2	8.8	121.2	9.2	130.4
11	102	1	9.2	32.5	21.4	63.8	9.6	136.6	11.3	147.9
12	103	0	12.7	38.8	29.2	76.1	10.6	167.4	14.3	181.7
13	104	1	20.3	57.6	45.4	108.2	11.4	242.9	18.2	261.1
14	13	0	19.3	80.2	44.6	108.4	13.4	265.9	18.1	284.0
15	92	0	23.7	96.0	35.0	139.1	12.3	306.1	12.5	318.6
16	112	0	10.1	40.9	18.2	83.2	8.0	160.3	7.7	168.0
17	115	1	11.3	53.3	17.5	85.7	8.8	176.6	7.3	183.9
18	37	1	303.4	859.7	397.1	952.4	31.2	2543.8	61.1	2604.9
19	32	1	227.0	694.9	289.0	735.5	30.6	1977.0	55.2	2032.1
20	26	1	98.3	424.7	165.7	418.8	26.8	1134.3	38.8	1173.1
21	27	1	69.0	314.0	125.3	326.5	24.7	859.4	30.4	889.8
22	30	1	216.6	661.0	311.6	774.3	29.6	1993.1	53.1	2046.2
23	40	1	39.3	195.4	84.0	196.0	24.2	538.9	26.8	565.7
24	43	1	63.2	324.9	138.4	337.0	24.8	888.3	28.0	916.3
25	46	1	60.1	289.8	111.4	277.7	19.1	758.0	21.6	779.7
26	88	0	20.3	90.7	41.5	101.8	15.3	269.6	16.7	286.3
27	89	1	15.7	79.0	33.6	78.0	15.6	221.8	14.2	236.0
28	90	1	34.8	128.8	71.0	163.3	15.9	413.9	21.2	435.0
29	93	0	19.2	93.3	38.7	95.4	15.7	262.3	15.6	277.9
30	95	0	18.8	79.4	39.8	96.3	15.1	249.4	17.0	266.3
31	97	0	30.4	120.2	59.5	140.8	15.4	366.2	18.1	384.3
32	94	0	34.0	125.5	67.7	163.1	15.5	405.7	25.0	430.6
33	96	1	30.3	138.3	50.4	127.8	15.5	362.3	18.3	380.5

Table 6.10 Building A4 uncertainty data (BM), %

Case	no.	Effect	Prompt gammas	Air/ground gammas	Early delayed gammas	Late delayed gammas	Building gammas	Total gammas	Prompt neutrons	Total dose
1	1	0	7.5	6.6	6.0	5.6	7.4	6.5	9.4	6.6
2	2	0	36.2	37.4	38.6	37.2	25.2	36.1	32.6	35.9
3	3	0	10.6	13.6	13.3	14.2	1.7	13.4	2.6	13.2
4	4	0	20.6	16.9	18.2	17.3	2.6	17.1	7.2	16.9
5	5	1	9.5	14.9	16.0	18.8	1.7	15.8	2.3	15.6
6	11	1	63.0	53.9	60.4	58.8	6.8	57.1	26.7	56.2
7	12	1	12.7	13.5	10.3	9.2	2.2	11.0	4.6	10.7
8	16	1	30.7	24.9	23.8	22.9	4.8	24.1	13.7	23.7
9	17	1	28.5	25.9	38.8	34.1	3.4	30.9	16.7	30.6
10	101	0	9.6	6.5	11.2	3.6	6.2	6.0	11.0	6.3
11	102	1	19.4	10.3	18.8	10.5	6.3	12.1	15.2	12.3
12	103	0	14.9	10.5	14.3	10.4	3.1	11.0	9.4	10.8
13	104	1	33.5	38.1	30.7	25.6	4.2	29.2	9.9	27.8
14	13	0	6.1	4.3	5.7	4.2	2.6	4.5	5.6	4.6
15	92	0	15.8	13.4	15.1	11.4	5.0	12.5	10.1	12.4
16	112	0	22.4	22.1	21.3	9.5	8.2	14.8	17.1	14.9
17	115	1	31.9	27.4	28.6	29.7	16.4	28.4	21.2	28.1
18	37	1	17.6	13.1	18.2	13.2	2.2	14.3	6.8	14.1
19	32	1	35.9	25.1	30.9	29.3	2.2	28.4	11.9	27.9
20	26	1	21.0	15.1	15.5	13.2	2.6	14.7	11.2	14.6
21	27	1	7.8	8.1	6.9	4.6	1.9	6.4	4.8	6.3
22	30	1	28.9	24.5	28.9	20.1	1.4	23.6	10.0	23.3
23	40	1	17.5	20.4	21.0	21.0	2.8	19.7	7.6	19.1
24	43	1	7.2	8.4	7.2	7.5	1.3	7.6	2.6	7.4
25	46	1	2.6	3.4	5.8	3.6	5.0	3.8	5.3	3.9
26	88	0	1.6	4.3	2.0	2.1	1.0	2.7	2.8	2.7
27	89	1	14.2	11.7	13.9	14.3	1.2	12.4	7.2	12.1
28	90	1	16.5	14.5	15.7	13.5	2.0	14.0	8.3	13.7
29	93	0	2.9	3.8	3.2	4.1	1.0	3.6	2.3	3.5
30	95	0	5.8	5.0	3.9	3.1	1.2	3.9	4.4	4.0
31	97	0	29.2	22.2	26.8	26.4	0.4	24.2	14.2	23.7
32	94	0	10.1	6.1	10.3	8.3	1.8	7.8	8.2	7.9
33	96	1	8.2	8.9	4.3	4.2	2.6	6.3	3.9	6.2

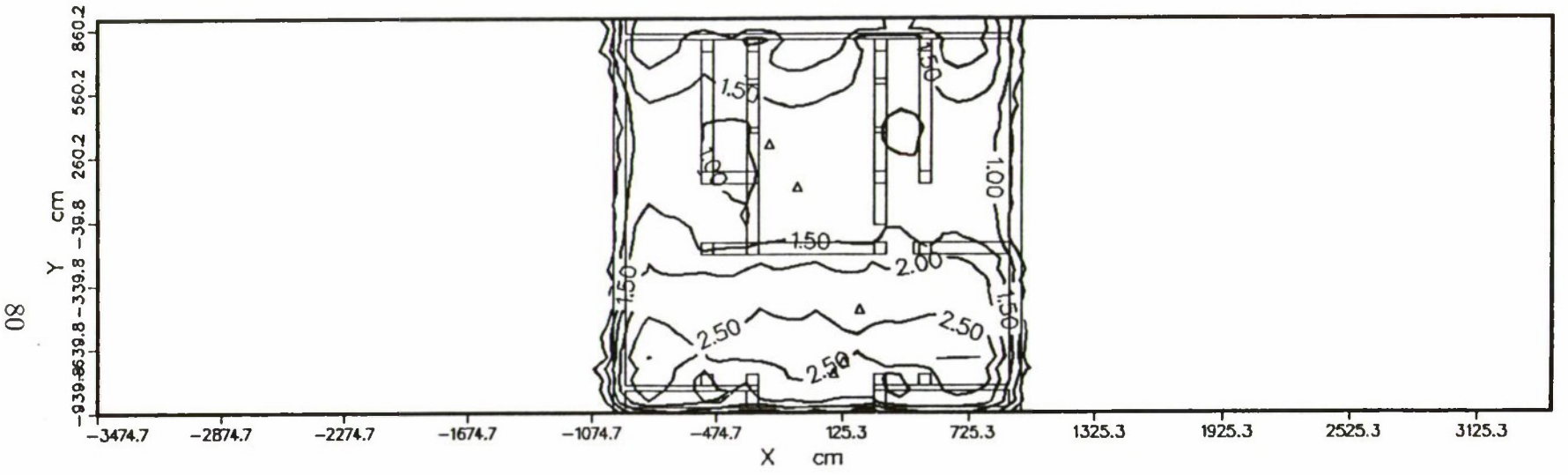

Figure 6.9 Building A4 dose distribution; 50 cm above basement floor.

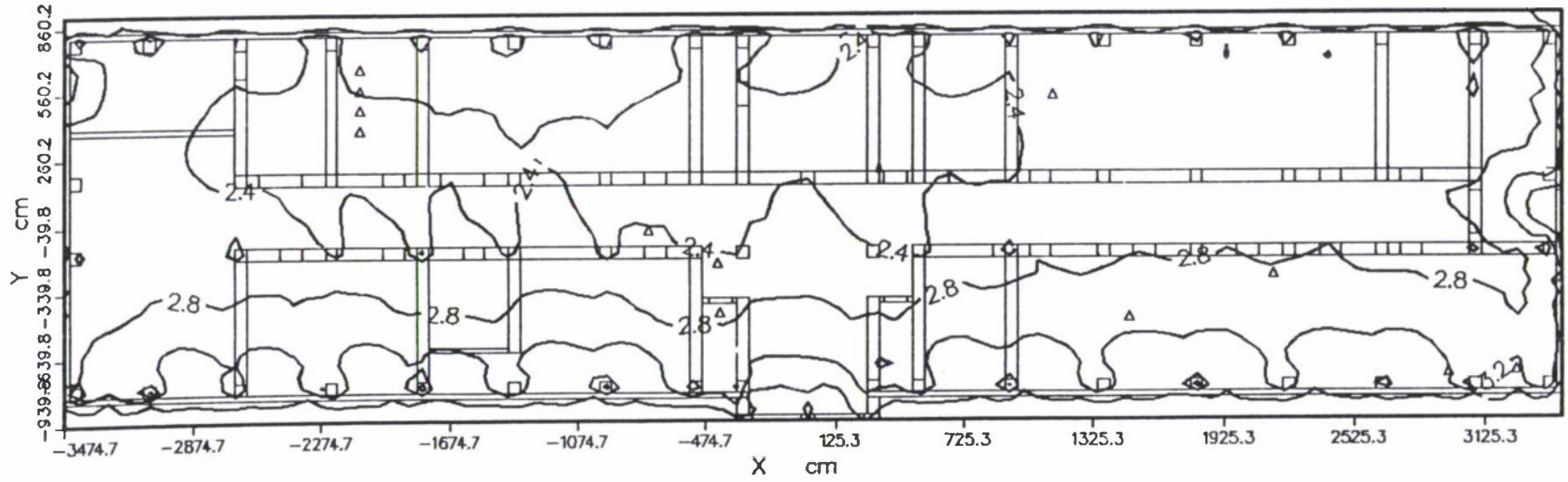

Figure 6.10 Building A4 dose distribution; 50 cm above first floor.

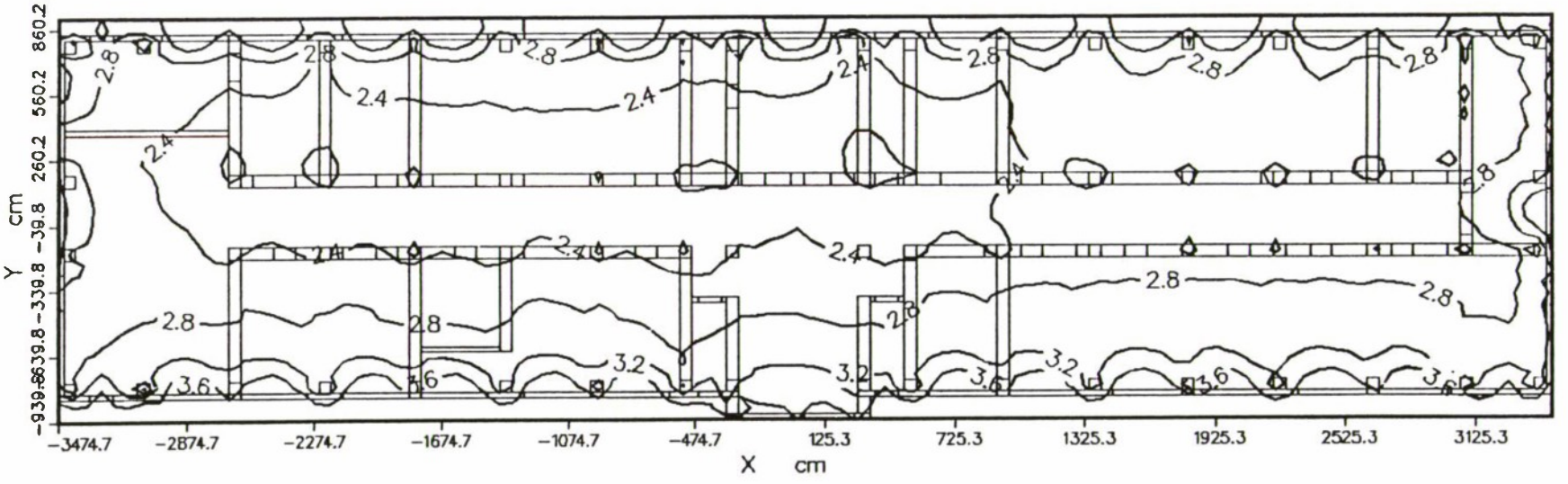

Figure 6.11 Building A4 dose distribution; 147 cm above first floor.

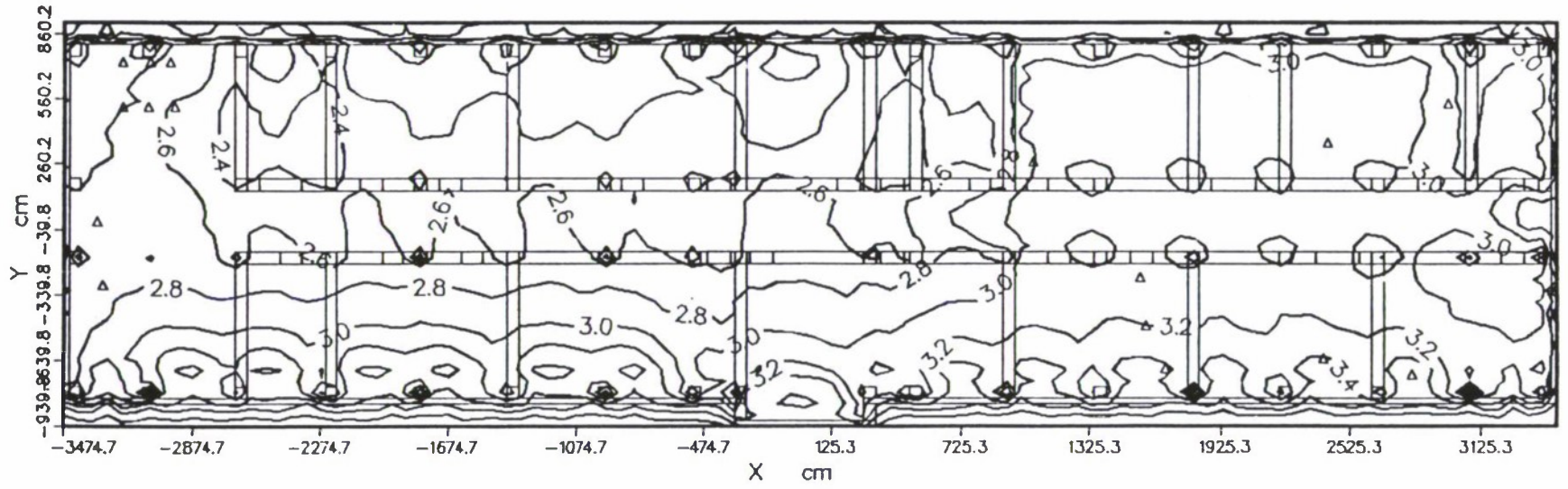

Figure 6.12 Building A4 dose distribution; 50 cm above second floor.

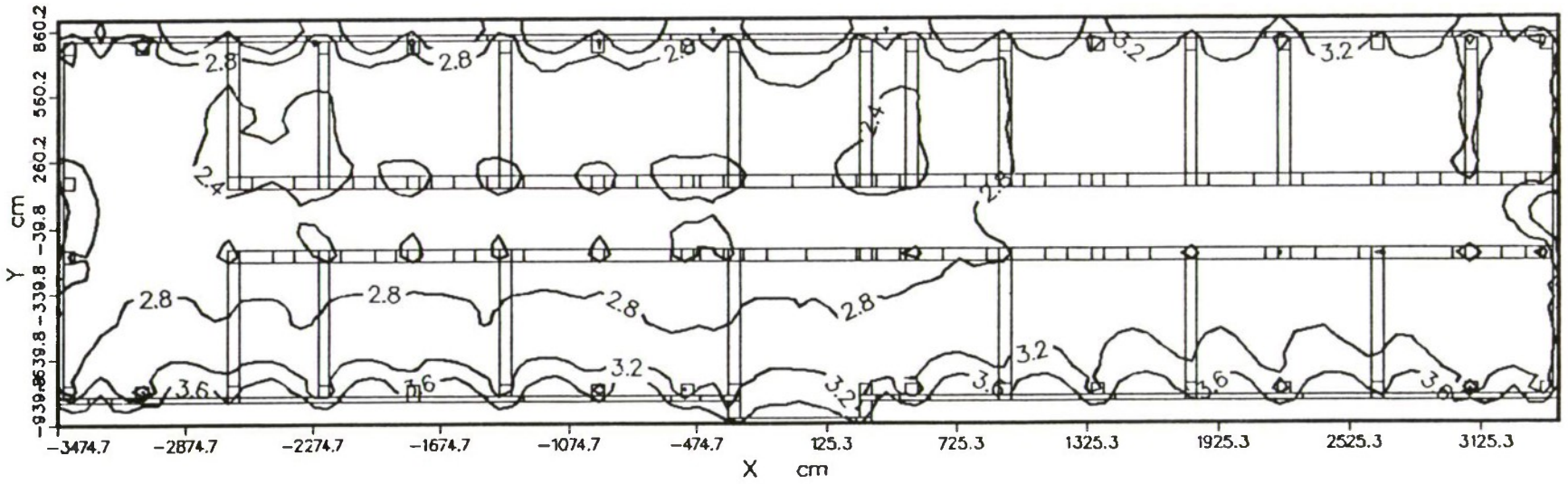

Figure 6.13 Building A4 dose distribution; 147 cm above second floor.

Table 6.11 Building A4 dose data, excluded cases (FIA), cGy units

Case	no.	Effect	Prompt gammas	Air/ground gammas	Early delayed gammas	Late delayed gammas	Building gammas	Total gammas	Prompt neutrons	Total dose
1	6	0	67.6	242.5	110.1	275.1	20.1	715.5	35.1	750.6
2	7	0	301.5	831.3	490.0	1142.5	25.2	2790.5	77.5	2868.0
3	8	0	196.0	562.3	283.4	663.1	23.9	1728.7	63.7	1792.4
4	9	0	75.6	270.7	123.1	301.4	20.5	791.3	36.7	828.1
5	10	0	67.6	242.5	110.1	275.1	20.1	715.5	35.1	750.6
6	14	0	61.9	220.3	99.6	244.9	20.6	647.3	33.6	680.9
7	15	0	65.5	230.3	107.5	260.8	19.5	683.6	35.2	718.8
8	91	0	226.8	631.0	349.6	861.0	23.7	2092.0	64.8	2156.8
9	18	0	38.1	131.2	63.2	199.5	15.6	447.7	20.7	468.4
10	108	0	151.2	469.7	226.1	528.0	22.7	1397.7	54.9	1452.7
11	109	0	144.0	390.3	243.1	571.6	23.3	1372.3	62.3	1434.6
12	110	0	305.9	822.4	458.9	1069.2	24.8	2681.1	94.5	2775.6
13	105	0	15.7	47.8	36.2	100.7	13.1	213.5	16.1	229.6
14	106	0	15.6	46.0	36.8	104.3	13.1	215.9	16.3	232.2
15	107	0	13.4	43.5	30.9	94.6	12.2	194.5	13.6	208.1
16	35	0	66.6	294.2	96.9	228.0	36.4	722.0	37.3	759.3
17	36	0	66.9	325.9	154.1	367.4	31.4	945.7	35.8	981.5
18	38	0	117.6	412.8	165.0	385.1	37.0	1117.6	46.5	1164.1
19	39	0	112.9	403.9	163.7	389.1	36.9	1106.4	54.6	1161.0
20	33	0	136.1	549.6	238.1	586.4	35.9	1546.0	58.9	1604.9
21	34	0	259.1	748.6	385.5	901.9	39.6	2334.7	85.2	2419.9
22	19	0	407.2	1110.2	552.0	1291.3	38.0	3398.7	95.0	3493.7
23	20	0	182.2	614.0	255.2	604.7	35.0	1691.2	67.4	1758.5
24	21	0	146.1	481.7	251.6	586.4	35.8	1501.6	58.7	1560.3
25	22	0	353.6	975.0	451.8	1061.2	36.3	2877.9	87.6	2965.5
26	23	0	110.5	454.8	186.8	465.6	30.0	1247.6	41.6	1289.2
27	24	0	98.2	388.8	165.1	415.5	30.2	1097.8	42.7	1140.5
28	25	0	112.3	433.8	187.1	559.8	36.6	1329.7	51.3	1381.0
29	28	0	82.6	336.6	143.9	463.5	33.3	1059.9	37.9	1097.8
30	29	0	115.6	460.1	195.5	490.0	31.5	1292.8	47.1	1339.8
31	31	0	129.8	516.4	225.5	542.9	32.7	1447.3	55.0	1502.3
32	41	0	88.9	404.6	200.3	477.5	32.4	1203.6	45.8	1249.4
33	42	0	94.2	387.2	187.9	450.1	33.6	1153.1	46.4	1199.4
34	44	0	95.4	438.7	194.7	497.9	32.2	1258.9	36.0	1295.0
35	45	0	62.5	298.0	137.3	334.1	31.1	863.0	34.0	897.0
36	47	0	95.8	394.1	183.6	436.2	29.2	1138.8	42.8	1181.6
37	48	0	105.4	425.6	198.8	475.3	30.6	1235.7	45.4	1281.1
38	49	0	116.4	455.4	209.6	495.0	30.8	1307.4	44.5	1351.8
39	50	0	83.7	363.2	157.3	410.7	27.5	1042.4	32.7	1075.2
40	51	0	86.4	390.0	170.8	447.0	29.9	1124.1	34.2	1158.4
41	52	0	86.8	374.2	166.6	458.4	31.5	1117.4	37.0	1154.4
42	53	0	87.6	340.4	166.7	461.0	33.3	1089.0	44.2	1133.2
43	54	0	101.1	386.8	200.1	490.0	32.8	1210.8	51.2	1261.9
44	55	0	541.4	1575.4	909.4	2124.6	52.8	5203.6	171.2	5374.7
45	56	0	606.8	1755.3	1008.1	2352.7	52.5	5775.4	186.9	5962.3
46	57	0	354.8	1129.9	752.2	1757.8	55.4	4050.1	172.9	4223.0
47	58	0	441.8	1205.6	739.5	1729.9	52.9	4169.7	175.1	4344.8
48	59	0	573.9	1730.0	934.3	2198.0	47.9	5484.1	158.1	5642.2
49	60	0	597.9	1778.7	982.5	2301.9	49.6	5710.5	175.9	5886.4

Table 6.12 Building A4 dose data, excluded cases (SI), cGy units

Case	no.	Effect	Prompt gammas	Air/ground gammas	Early delayed gammas	Late delayed gammas	Building gammas	Total gammas	Prompt neutrons	Total dose
1	6	0	40.9	167.0	64.7	161.8	13.7	448.2	17.3	465.5
2	7	0	192.8	591.8	305.0	711.3	17.2	1818.1	32.0	1850.1
3	8	0	123.1	395.0	171.6	401.5	16.3	1107.6	27.2	1134.8
4	9	0	45.7	186.3	72.8	177.3	14.0	496.2	17.8	513.9
5	10	0	40.9	167.0	64.7	161.8	13.7	448.2	17.3	465.5
6	14	0	37.4	151.2	58.4	143.1	14.0	404.1	16.8	420.9
7	15	0	39.5	158.1	62.9	152.0	13.3	425.7	17.3	443.0
8	91	0	143.6	446.1	214.9	528.4	16.2	1349.2	28.1	1377.3
9	18	0	22.8	89.0	36.8	115.6	10.7	275.0	11.5	286.5
10	108	0	93.5	327.8	135.4	315.5	15.5	887.8	25.9	913.6
11	109	0	88.3	268.9	143.8	338.2	15.9	855.1	29.0	884.0
12	110	0	192.1	578.0	277.5	646.6	17.0	1711.1	38.9	1750.0
13	105	0	9.0	31.5	20.4	56.7	9.0	126.6	9.6	136.2
14	106	0	8.9	30.1	20.8	58.5	8.9	127.2	9.7	136.9
15	107	0	7.7	28.9	17.5	53.2	8.3	115.6	8.4	124.0
16	35	0	41.0	203.6	58.5	137.5	24.9	465.4	21.3	486.7
17	36	0	41.1	227.2	96.1	228.4	21.4	614.2	20.4	634.6
18	38	0	74.0	289.6	101.3	236.5	25.3	726.7	24.2	750.9
19	39	0	69.4	280.1	98.0	232.5	25.2	705.3	27.5	732.8
20	33	0	83.9	384.6	146.7	359.3	24.5	999.0	28.8	1027.8
21	34	0	163.5	526.7	237.0	554.2	27.0	1508.4	38.2	1546.6
22	19	0	262.2	792.3	345.6	808.3	26.0	2234.5	40.2	2274.7
23	20	0	113.7	430.3	155.3	367.3	23.9	1090.5	31.2	1121.7
24	21	0	91.2	336.8	154.8	360.9	24.5	968.1	28.7	996.8
25	22	0	226.3	693.0	280.2	656.8	24.9	1881.1	38.1	1919.2
26	23	0	68.8	318.9	116.1	286.9	20.5	811.2	21.9	833.0
27	24	0	60.5	269.4	100.9	252.1	20.6	703.4	22.0	725.4
28	25	0	68.7	300.0	113.7	340.1	25.0	847.7	26.9	874.6
29	28	0	50.7	232.3	88.1	282.3	22.7	676.1	21.4	697.5
30	29	0	71.8	321.5	120.8	300.4	21.5	836.0	23.8	859.9
31	31	0	79.6	360.2	138.6	332.2	22.3	932.9	26.8	959.7
32	41	0	54.8	283.5	124.6	296.3	22.1	781.4	24.5	805.8
33	42	0	58.3	269.7	115.7	276.5	23.0	743.2	25.0	768.2
34	44	0	60.0	309.4	123.3	311.6	22.0	826.2	20.8	847.0
35	45	0	38.4	207.2	85.1	206.6	21.2	558.6	19.7	578.3
36	47	0	59.7	276.3	113.7	270.1	19.9	739.8	22.6	762.4
37	48	0	65.9	298.6	123.3	294.4	20.9	803.2	23.7	826.9
38	49	0	73.4	321.6	130.8	308.6	21.1	855.4	23.2	878.5
39	50	0	52.6	254.4	98.4	254.9	18.8	679.2	18.4	697.5
40	51	0	54.0	273.2	107.2	277.7	20.4	732.4	19.4	751.9
41	52	0	54.1	261.4	103.6	284.0	21.5	724.6	21.2	745.8
42	53	0	53.9	235.9	101.6	281.3	22.8	695.4	24.5	719.9
43	54	0	62.1	269.3	121.9	298.9	22.4	774.7	26.5	801.2
44	55	0	344.5	1116.1	570.6	1332.9	36.2	3400.2	71.8	3472.0
45	56	0	386.8	1244.6	634.0	1479.4	35.9	3780.6	76.4	3857.1
46	57	0	217.7	788.0	465.8	1088.3	37.9	2597.7	72.9	2670.7
47	58	0	275.4	842.0	453.7	1061.0	36.2	2668.3	72.5	2740.9
48	59	0	366.9	1230.1	589.3	1385.0	32.7	3603.9	66.2	3670.1
49	60	0	381.1	1262.3	617.7	1446.4	33.9	3741.5	72.2	3813.7

Table 6.13 Building A4 dose data, excluded cases (BM), cGy units

Case	no.	Effect	Prompt gammas	Air/ground gammas	Early delayed gammas	Late delayed gammas	Building gammas	Total gammas	Prompt neutrons	Total dose
1	6	0	46.5	185.6	73.9	184.8	15.3	506.2	22.9	529.1
2	7	0	216.2	653.6	344.0	802.1	19.2	2035.1	44.0	2079.1
3	8	0	138.7	437.3	194.7	455.5	18.2	1244.4	37.1	1281.6
4	9	0	51.9	207.1	83.1	202.5	15.6	560.2	23.7	583.9
5	10	0	46.5	185.6	73.9	184.8	15.3	506.2	22.9	529.1
6	14	0	42.5	168.1	66.8	163.7	15.7	456.8	22.2	479.0
7	15	0	44.9	175.8	71.9	173.9	14.9	481.4	22.9	504.3
8	91	0	161.5	493.2	243.0	597.6	18.1	1513.4	38.3	1551.7
9	18	0	26.0	99.2	42.2	132.6	11.9	311.9	14.9	326.8
10	108	0	105.7	363.3	154.1	359.1	17.3	999.5	34.6	1034.1
11	109	0	100.0	298.8	164.0	385.8	17.8	966.3	38.8	1005.1
12	110	0	216.4	639.7	314.9	733.9	18.9	1923.7	53.5	1977.3
13	105	0	10.4	35.3	23.5	65.3	10.0	144.6	12.2	156.8
14	106	0	10.3	33.8	23.9	67.4	10.0	145.4	12.4	157.8
15	107	0	8.8	32.3	20.1	61.4	9.3	132.0	10.6	142.6
16	35	0	46.4	226.2	66.6	156.5	27.7	523.4	27.5	550.9
17	36	0	46.6	252.1	108.5	258.1	23.9	689.2	26.4	715.6
18	38	0	83.4	320.8	114.8	267.8	28.2	815.0	31.8	846.7
19	39	0	78.6	310.9	111.6	264.9	28.1	794.1	36.4	830.5
20	33	0	94.9	426.3	166.1	407.2	27.3	1121.8	38.3	1160.1
21	34	0	184.0	582.9	268.1	627.1	30.2	1692.3	51.7	1743.9
22	19	0	293.8	874.7	389.5	910.9	29.0	2497.7	55.1	2552.8
23	20	0	128.3	476.6	176.2	416.8	26.7	1224.6	41.9	1266.5
24	21	0	102.9	373.3	175.2	408.3	27.3	1086.8	38.1	1124.9
25	22	0	253.9	765.6	316.4	741.8	27.7	2105.4	51.9	2157.3
26	23	0	77.8	353.3	131.2	324.8	22.8	909.9	28.7	938.6
27	24	0	68.4	299.1	114.5	286.4	23.0	791.3	29.0	820.3
28	25	0	78.0	333.2	129.2	386.1	27.9	954.4	35.3	989.7
29	28	0	57.5	258.2	100.0	320.3	25.3	761.4	27.8	789.1
30	29	0	81.2	356.4	136.8	340.5	24.0	938.8	31.5	970.3
31	31	0	90.2	399.3	157.0	376.5	24.9	1048.0	35.7	1083.6
32	41	0	62.1	314.4	140.7	334.7	24.7	876.6	31.9	908.5
33	42	0	65.9	299.4	131.0	313.0	25.6	834.9	32.6	867.5
34	44	0	67.7	342.6	138.8	351.6	24.5	925.3	26.8	952.1
35	45	0	43.6	230.0	96.3	233.8	23.7	627.3	25.4	652.7
36	47	0	67.4	306.3	128.5	305.3	22.3	829.8	29.5	859.3
37	48	0	74.4	331.0	139.3	332.7	23.3	900.8	31.1	931.9
38	49	0	82.7	356.0	147.5	348.2	23.5	957.9	30.3	988.3
39	50	0	59.3	282.1	111.1	288.2	21.0	761.7	23.8	785.5
40	51	0	61.0	302.9	120.9	313.8	22.8	821.4	25.2	846.6
41	52	0	61.2	290.0	117.1	321.0	24.0	813.2	27.4	840.6
42	53	0	61.1	262.0	115.2	318.7	25.4	782.4	31.7	814.1
43	54	0	70.3	298.9	138.2	338.6	25.0	871.1	34.7	905.8
44	55	0	387.3	1234.1	643.6	1503.5	40.3	3808.8	98.0	3906.8
45	56	0	434.7	1376.0	715.1	1668.6	40.1	4234.5	104.9	4339.4
46	57	0	246.9	873.7	527.2	1231.8	42.3	2921.9	99.5	3021.3
47	58	0	311.0	933.1	514.3	1202.7	40.4	3001.4	99.4	3100.8
48	59	0	412.0	1359.2	664.1	1561.1	36.5	4032.9	90.4	4123.3
49	60	0	428.3	1395.3	696.6	1631.4	37.8	4189.4	99.1	4288.5

7. BUILDING C

7.1 GEOMETRIC MODEL

The C building, the south wing of the Shiroyama School at Nagasaki (Fig. 7.1), was a three-story rectangular structure built entirely of reinforced concrete. The roof and floors were all of slab construction, supported by a framework of concrete beams and girders resting on pillars. The east end of the building faced the blast directly, and Fig. 7.1, taken soon after the attack, shows that it was heavily damaged. That end of the building collapsed several days later.

The exterior dimensions of the building were 9 m wide by 56 m long by 13 m high. The building sat on a hill about 80 feet above sea level,[13] and the first floor was taken to be 2 feet above ground level, i.e. at an altitude of 82 feet or 25.0 m. The building was located west of the hypocenter at the location indicated by "16" in Fig. 6.5. For the purpose of this study, the hypocenter was taken to be 515 m from the center of the building in a direction 4.5 degrees counterclockwise from the west-to-east axis of the building. The view of the building from the weapon site was from an upward angle approximately as shown in Fig. 7.1, but from a direction almost aligned with the length of the building, i.e. to the left of the observer position used for that photograph. As in the A-building study, the distance and air attenuation were preserved by artificially moving the building inward to a ground range of 491 m.

The first model, designated C1, was based largely on information from the USSBS report.[1] It had walls, windows, roof, floor, and supporting structure in full detail. Enough of the passageway to the north buildings was modeled to give some shadowing at the rear of the building. Lacking other data, the east and west walls were given windows similar to those of the south wall. No internal walls were represented.

The second model, C2, illustrated in Fig. 7.2, used additional information from ORNL file photographs and sketches associated with the USSBS study, as well as a photograph from Ref. 37. The windows of this model were sized and positioned based on data scaled from the photographs. The windows in the east and west ends were removed, based on another photograph. Internal walls were added according to a file sketch. The stairwells and passageway to the north wing were redesigned according to additional data. This model used about 84,000 mesh cells. The final model, C3, used the same structure as C2, but the internal wall composition was based on the Kerr data as described in the previous section. A detailed description of the model is given in Appendix B.

7.2 PERSONNEL LOCATIONS

The personnel locations were selected and categorized into "good" cases and "excluded" cases in the same manner as the Building A cases. The locations, position uncertainty, and fatality effect data, directly analogous to the Building A

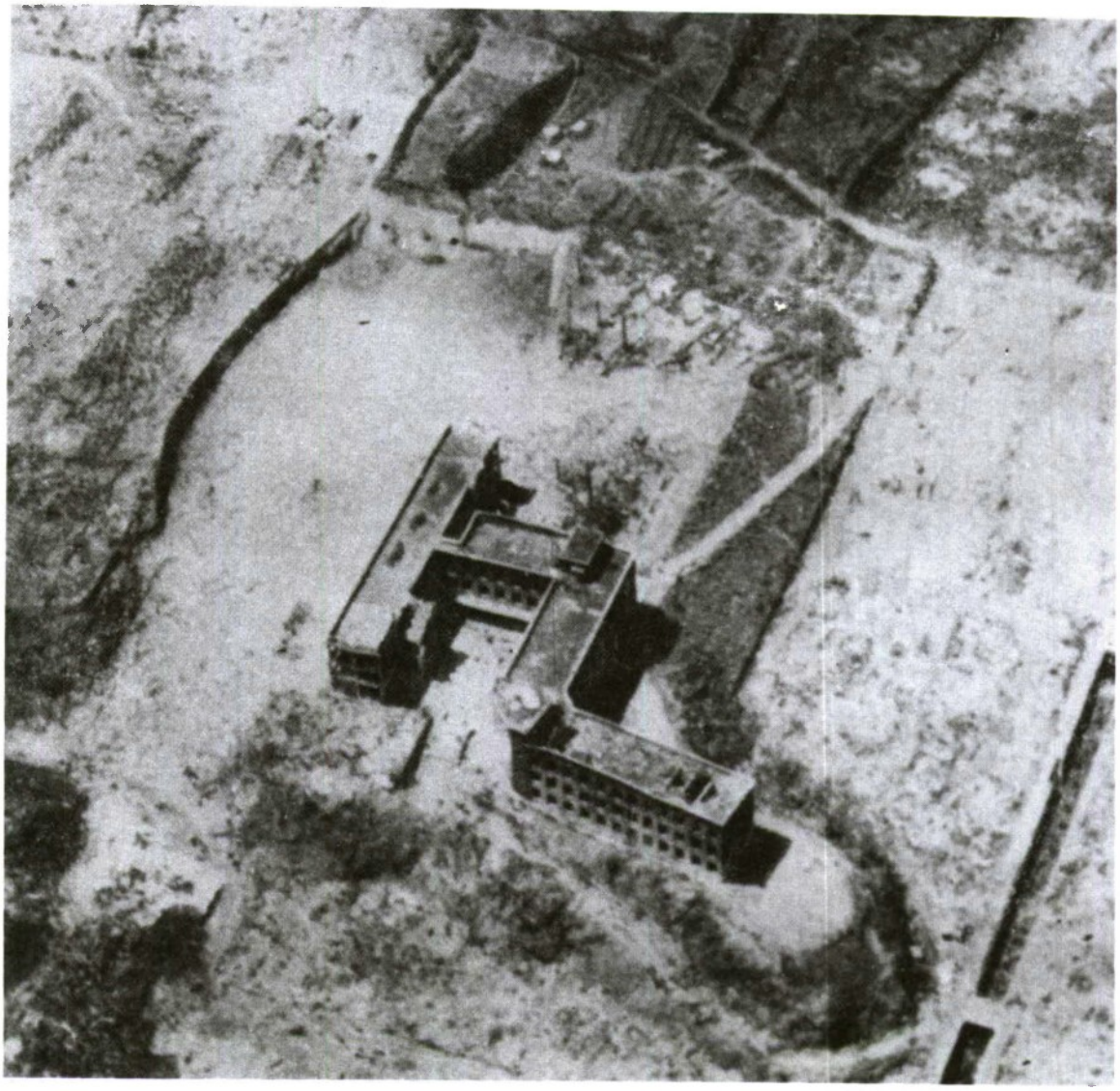

Figure 7.1 Shiroyama School Complex after attack; looking southwest.

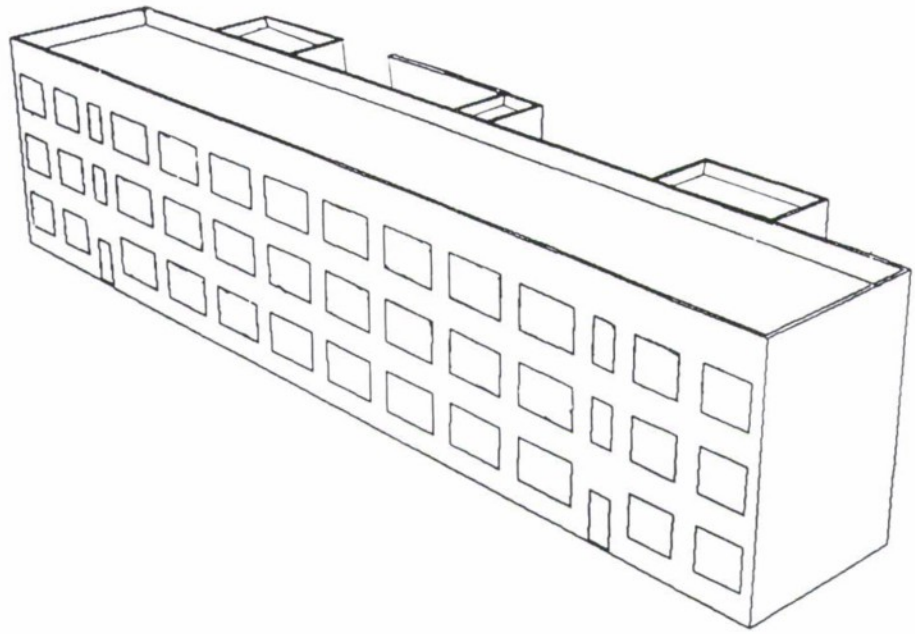

Figure 7.2 Discrete ordinates model of Building C.

data, for the good cases are shown in Table 7.1. The locations are plotted in Figs. 7.3 and 7.4. The excluded case positions are shown in Table 7.2.

7.3 KEY LOCATION DOSE RESULTS

As in the case of Building A, the doses at three selected locations will be examined, together with the associated protection factors and attenuation factors:

- an "exterior" point,
- Point 1, deep inside the second floor, and
- Point 5, near a window at the east end of the building.

The FIA gamma and neutron doses are shown in Table 7.3. The attenuation and protection factors, shown in Table 7.4, are all lower than the Building A factors. This is due partly to the presence of only two layers of concrete above the personnel and partly to the fact that all of the personnel locations in the building were exposed directly to the windows in the south wall. The relationships between gamma and neutron attenuation and between attenuation factors and protection factors are approximately as before.

Table 7.1 Position data for building C3, good cases (case number; effect, X,Y,Z positions; X,Y uncertainty

Case no.	X position	Y position	Z position	X error	Y error
12	190.00[a]	−135.00	456.24	60.00	60.00
19	225.00	−345.00	456.24	60.00	30.00
75	130.00	50.00	456.24	30.00	30.00
95	435.00	75.00	456.24	60.00	30.00
98	645.00	−105.00	456.24	60.00	30.00
18	−290.00	75.00	456.24	30.00	30.00
58	−240.00	−360.00	456.24	60.00	30.00
69	−470.00	−360.00	456.24	60.00	30.00
76	−415.00	−225.00	456.24	60.00	60.00
103	−470.00	60.00	456.24	60.00	30.00
104	−195.00	−230.00	456.24	60.00	30.00
105	−690.00	60.00	456.24	60.00	30.00
36	−1310.00	25.00	456.24	90.00	60.00
62	−1030.00	25.00	456.24	60.00	60.00
111	−1045.00	−135.00	456.24	60.00	60.00
117	390.00	−375.00	456.24	60.00	30.00
39	790.00	−290.00	456.24	30.00	60.00
80	−680.00	−185.00	456.24	60.00	60.00
81	−670.00	−360.00	456.24	60.00	30.00
82	1100.00	55.00	456.24	60.00	60.00
106	665.00	−290.00	456.24	60.00	30.00
112	460.00	−275.00	456.24	90.00	30.00
52	2125.00	55.00	822.00	60.00	60.00
113	2700.00	55.00	822.00	30.00	60.00
42	1560.00	20.00	822.00	60.00	30.00
56	1315.00	20.00	822.00	60.00	30.00
65	1325.00	−390.00	822.00	30.00	30.00
114	1180.00	20.00	822.00	60.00	30.00
94	115.00	−135.00	822.00	60.00	30.00
110	275.00	−135.00	822.00	60.00	30.00
10	−810.00	−380.00	822.00	30.00	30.00
17	−365.00	−135.00	822.00	60.00	30.00
30	−390.00	−380.00	822.00	60.00	30.00
31	−265.00	−380.00	822.00	60.00	30.00
53	−250.00	−160.00	822.00	60.00	30.00
88	−110.00	−170.00	822.00	60.00	30.00
21	−1310.00	−350.00	822.00	60.00	30.00
23	−1700.00	−375.00	822.00	60.00	30.00
32	−1250.00	65.00	822.00	60.00	30.00
44	−1440.00	−365.00	822.00	60.00	30.00
48	−1545.00	20.00	822.00	60.00	30.00
27	−2600.00	−270.00	822.00	60.00	60.00
43	−2415.00	−30.00	822.00	60.00	60.00
46	−2400.00	205.00	822.00	60.00	60.00
47	−2600.00	205.00	822.00	60.00	60.00
86	−2615.00	−25.00	822.00	60.00	60.00
91	−2235.00	210.00	822.00	60.00	60.00
38	−120.00	−370.00	822.00	30.00	30.00
41	2520.00	75.00	822.00	60.00	30.00
51	2340.00	75.00	822.00	60.00	30.00
54	2120.00	270.00	822.00	60.00	30.00
90	−2210.00	−25.00	822.00	60.00	30.00
101	1685.00	−170.00	822.00	60.00	30.00
78	−645.00	−170.00	822.00	60.00	30.00
87	−645.00	−370.00	822.00	60.00	30.00
109	−115.00	45.00	822.00	30.00	30.00
118	645.00	0.00	822.00	60.00	60.00
40	−1010.00	−360.00	822.00	30.00	30.00
49	−820.00	−45.00	822.00	30.00	60.00
73	1425.00	25.00	822.00	30.00	60.00

[a] All dimensions in centimeters.

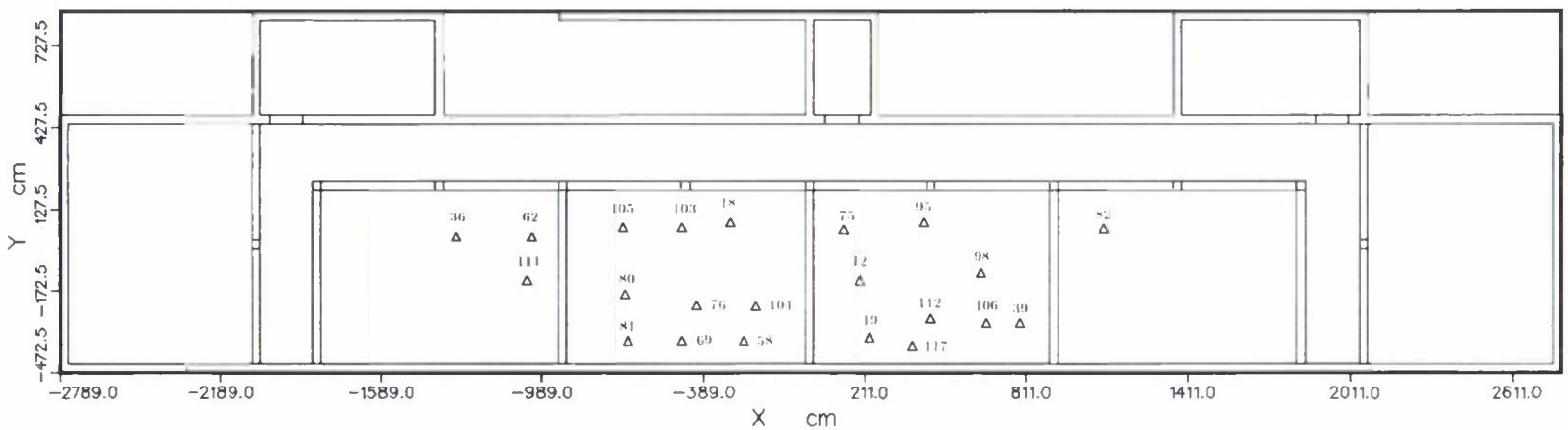

Figure 7.3 Building C3 personnel locations; second floor.

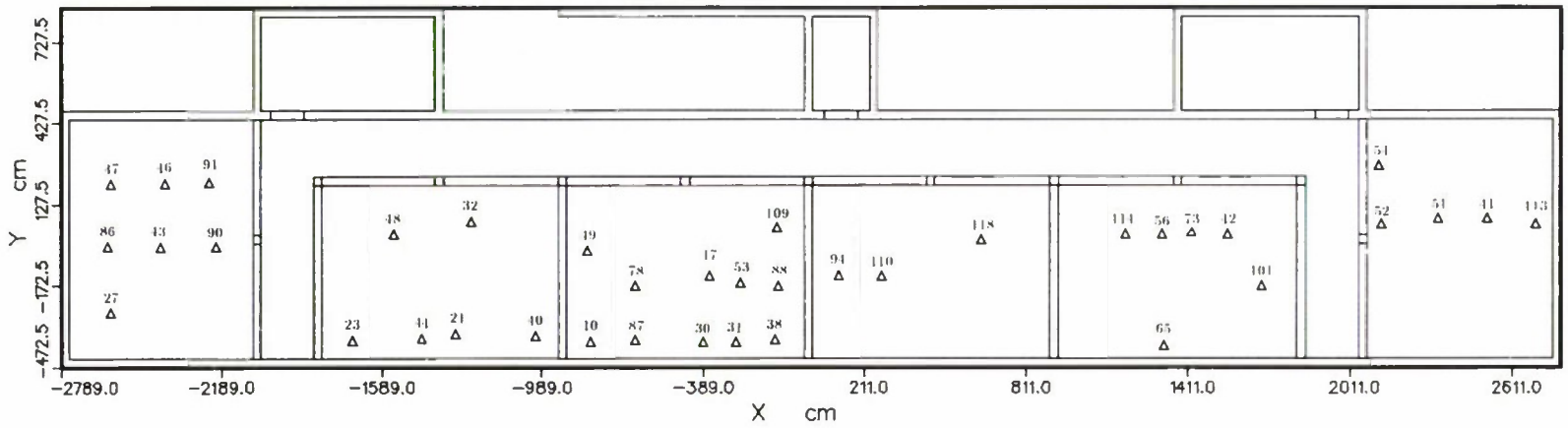

Figure 7.4 Building C3 personnel locations; third floor.

Table 7.2 Position data for building C3, excluded cases

Case no.		X position	Y position	Z position
1	15	1685.00[a]	135.00	456.24
2	68	1425.00	38.00	456.24
3	70	1272.00	38.00	456.24
4	72	1757.00	−170.00	456.24
5	60	373.00	−135.00	456.24
6	71	−140.00	125.00	456.24
7	107	−1408.00	−116.00	456.24
8	7	2690.00	−373.00	822.00
9	26	2431.00	−236.00	822.00
10	33	2664.00	286.00	822.00
11	34	2394.00	255.00	822.00
12	64	2487.00	−387.00	822.00
13	97	2251.00	−374.00	822.00
14	99	2164.00	−371.00	822.00
15	100	2301.00	−242.00	822.00
16	115	2637.00	−88.00	822.00
17	116	2637.00	−229.00	822.00
18	5	1042.00	−358.00	822.00
19	63	1169.00	−371.00	822.00
20	96	1654.00	22.00	822.00
21	102	1539.00	−157.00	822.00
22	6	497.00	−342.00	822.00
23	24	390.00	−336.00	822.00
24	35	500.00	−120.00	822.00
25	84	715.00	−202.00	822.00
26	93	771.00	−69.00	822.00
27	119	622.00	−214.00	822.00
28	20	−715.00	28.00	822.00
29	79	−557.00	−170.00	822.00
30	108	−1057.00	−69.00	822.00
31	25	−2416.00	−245.00	822.00
32	83	−2208.00	−245.00	822.00

[a] All dimensions in centimeters.

Table 7.3 Free-in-air doses from various sources outside building, near a window, and deep inside the second floor of building C3

	Exterior	Point 5, near window	Point 1, center of second floor
Prompt gamma	770 cGy	328 cGy	24 cGy
Air/ground capture gamma	2230	895	142
Early delayed gamma	1407	548	45
Late delayed gamma	3283	1286	176
Building capture gammas	0	23	22
All gammas	7690	3080	409
Prompt neutron	230	115	15
Total	7920	3195	424

Table 7.4 Attenuation and protection factors for building C3

	Point 5, near window	Point 1, center of second floor
AF, gamma	2.5	20
PF, gamma	2.5	20
AF, neutron	2.0	15
PF, neutron	1.7	6.2
AF, total	2.5	19

7.4 DOSE AT PERSONNEL LOCATIONS

Tables of FIA dose for the six source components, interpolated as before, together with fatality effect and uncertainty data, are shown in Tables 7.5 and 7.6. As before, the personnel were assumed to have been thrown into the prone position by the shock wave. Accordingly, heights of 426.24 and 732.00 were used for the late delayed gamma calculation. The corresponding data for the other responses are shown in Tables 7.7–7.10.

The common logarithm of FIA dose is plotted as a function of position in Figs. 7.5–7.8. In these figures, the source is from the right side of the figure, incident upon a wall with no windows. An area of low dose can be seen immediately behind

Table 7.5 Building C3 dose data (FIA), cGy units

Case	no.	Effect	Prompt gammas	Air/ground gammas	Early delayed gammas	Late delayed gammas	Building gammas	Total gammas	Prompt neutrons	Total dose
1	12	1	69.8	270.1	127.0	343.8	24.0	834.7	38.4	873.1
2	19	1	162.6	497.5	284.3	699.2	25.1	1668.7	60.6	1729.3
3	75	1	47.0	197.9	82.5	253.3	23.1	603.8	25.3	629.0
4	95	0	50.6	197.5	91.8	290.1	23.7	653.8	30.2	684.0
5	98	1	57.6	229.3	108.7	339.6	24.7	759.8	35.3	795.2
6	18	1	37.0	156.6	69.4	232.3	21.1	516.3	22.8	539.1
7	58	1	164.6	498.6	289.8	722.0	23.7	1698.7	57.5	1756.3
8	69	1	130.8	428.9	197.5	495.2	23.2	1275.5	42.0	1317.5
9	76	0	93.5	328.5	156.7	413.4	22.4	1014.5	42.8	1057.4
10	103	0	42.1	170.4	78.5	230.5	20.8	542.3	25.7	568.0
11	104	0	70.1	247.2	125.6	363.5	23.4	829.9	39.5	869.3
12	105	1	43.6	175.8	79.6	237.3	21.3	557.5	24.9	582.4
13	36	1	40.2	161.2	73.0	222.4	19.7	516.5	24.3	540.8
14	62	1	37.1	153.3	65.1	245.0	21.2	521.7	21.6	543.3
15	111	1	49.2	193.8	86.4	289.0	21.8	640.2	28.4	668.6
16	117	1	97.1	335.0	160.5	395.2	24.9	1012.7	43.5	1056.1
17	39	1	82.8	289.8	145.4	443.7	26.6	988.4	43.7	1032.2
18	80	1	69.9	262.1	124.2	320.7	22.5	799.4	38.7	838.1
19	81	1	151.0	467.6	272.1	650.4	23.3	1564.4	55.6	1620.0
20	82	1	47.9	191.6	90.9	286.0	25.2	641.5	29.9	671.5
21	106	1	119.0	373.7	207.2	548.7	25.8	1274.4	53.3	1327.7
22	112	1	129.5	431.1	204.3	537.3	24.9	1327.3	51.4	1378.7
23	52	1	175.0	659.8	296.5	718.9	35.0	1885.1	61.2	1946.3
24	113	1	76.3	295.9	132.3	309.3	32.9	846.6	51.0	897.6
25	42	1	133.7	548.3	256.1	680.9	32.7	1651.7	52.5	1704.2
26	56	1	165.6	627.5	282.2	727.3	33.2	1835.7	56.4	1892.1
27	65	1	172.0	598.1	272.6	664.8	33.0	1740.5	61.7	1802.2
28	114	1	168.4	627.6	277.8	710.3	34.0	1818.2	59.0	1877.2
29	94	1	165.3	640.3	290.1	719.2	32.8	1847.6	60.7	1908.3
30	110	1	171.8	619.2	280.6	696.2	32.1	1800.0	64.4	1864.4
31	10	1	252.3	818.7	423.8	994.7	30.5	2520.0	71.8	2591.8
32	17	1	155.0	599.8	277.0	701.1	29.9	1762.7	58.8	1821.6
33	30	1	247.1	794.3	401.3	949.4	30.1	2422.2	70.1	2492.3
34	31	1	232.7	749.9	410.7	979.2	30.4	2402.8	76.7	2479.5
35	53	1	140.7	545.2	253.0	676.1	30.6	1645.7	58.7	1704.4
36	88	1	133.3	509.6	222.3	709.5	31.7	1606.4	52.1	1658.6
37	21	1	242.5	783.4	401.3	976.7	27.7	2431.6	70.5	2502.1
38	23	1	236.7	772.4	403.1	948.1	27.8	2388.1	68.9	2457.0
39	32	1	127.0	508.7	228.3	614.3	28.2	1506.6	45.8	1552.4
40	44	1	165.5	579.3	271.6	653.4	27.3	1697.0	59.0	1756.1
41	48	1	146.3	548.5	236.9	603.0	26.8	1561.5	47.9	1609.4
42	27	1	153.5	550.1	260.9	619.7	24.1	1608.2	58.3	1666.5
43	43	1	131.9	499.3	234.8	585.7	24.2	1475.8	50.4	1526.3
44	46	1	117.6	452.7	214.7	542.3	24.2	1351.4	49.0	1400.5
45	47	1	135.4	497.8	226.5	546.2	23.3	1429.2	50.3	1479.5
46	86	1	145.0	545.0	242.3	575.4	23.3	1531.0	49.7	1580.8
47	91	1	106.8	398.6	185.1	539.3	24.4	1254.1	46.8	1300.9
48	38	1	150.3	523.9	266.8	729.9	31.2	1702.2	61.3	1763.5
49	41	1	106.8	429.6	209.5	488.5	34.0	1268.3	60.2	1328.6
50	51	1	147.0	587.7	281.8	664.9	34.3	1715.7	65.0	1780.7
51	54	1	204.2	724.8	347.8	856.3	34.9	2168.0	72.0	2240.0
52	90	1	101.7	390.0	182.0	548.0	24.9	1246.6	44.5	1291.1
53	101	1	131.2	509.0	235.0	722.6	34.0	1631.7	56.2	1687.9
54	78	1	169.6	615.3	274.0	671.0	30.1	1760.0	62.4	1822.4
55	87	1	209.7	689.9	367.3	861.9	29.9	2158.6	73.4	2232.0
56	109	1	118.4	467.1	198.9	665.0	31.1	1480.6	42.9	1523.5
57	118	1	137.6	541.9	257.4	677.7	33.4	1648.0	56.3	1704.3
58	40	1	134.6	480.4	234.4	679.9	29.4	1558.7	55.8	1614.6
59	49	1	150.4	591.4	260.2	647.3	30.8	1680.1	50.6	1730.7
60	73	1	158.1	612.1	278.0	722.0	32.8	1802.9	54.7	1857.7

Table 7.6 Building C3 uncertainty data (FIA), %

Case	no.	Effect	Prompt gammas	Air/ground gammas	Early delayed gammas	Late delayed gammas	Building gammas	Total gammas	Prompt neutrons	Total dose
1	12	1	14.9	10.5	13.7	11.8	2.0	11.6	12.6	11.7
2	19	1	18.5	16.1	15.5	15.2	0.7	15.6	7.1	15.3
3	75	1	3.8	4.1	4.8	3.7	0.7	3.9	3.7	3.9
4	95	0	7.9	5.4	8.1	6.3	0.7	6.2	7.7	6.3
5	98	1	8.4	7.9	7.8	7.0	1.3	7.3	6.6	7.3
6	18	1	2.8	1.4	2.6	3.5	0.7	2.6	3.5	2.6
7	58	1	17.7	15.6	14.3	14.1	1.1	14.7	7.6	14.5
8	69	1	30.6	23.7	30.0	29.6	0.7	27.2	14.1	26.8
9	76	0	29.4	23.8	25.8	23.7	1.6	24.1	13.1	23.7
10	103	0	9.6	7.2	9.8	6.8	0.6	7.3	9.1	7.4
11	104	0	14.5	8.9	15.7	9.6	1.9	10.5	10.3	10.5
12	105	1	2.6	3.1	2.9	3.1	0.6	2.9	3.4	3.0
13	36	1	12.7	12.1	10.8	8.9	2.6	10.2	9.1	10.2
14	62	1	11.5	10.5	10.8	6.3	2.6	8.3	9.1	8.4
15	111	1	14.4	12.2	14.1	11.2	3.2	11.9	13.6	11.9
16	117	1	26.9	21.3	25.5	26.5	0.8	24.0	11.4	23.5
17	39	1	20.9	14.5	25.0	14.5	1.2	16.2	12.5	16.1
18	80	1	17.4	10.9	16.5	15.3	2.3	13.9	12.6	13.8
19	81	1	21.6	18.0	18.9	19.6	1.1	18.9	9.4	18.6
20	82	1	6.2	9.2	7.1	7.0	1.8	7.4	5.0	7.3
21	106	1	26.6	23.1	24.0	20.3	1.2	21.9	9.8	21.4
22	112	1	16.3	12.4	14.6	14.7	0.9	13.9	7.0	13.6
23	52	1	8.4	6.9	10.6	6.3	1.0	7.3	15.3	7.5
24	113	1	5.3	6.2	8.2	7.9	0.4	6.8	3.1	6.6
25	42	1	5.8	6.1	7.2	3.1	0.2	4.9	4.3	4.9
26	56	1	3.2	3.3	5.1	5.5	1.5	4.4	4.4	4.4
27	65	1	12.9	12.2	10.4	15.4	0.2	13.0	8.1	12.8
28	114	1	5.8	3.8	2.7	1.7	0.7	2.9	4.4	3.0
29	94	1	2.5	1.2	1.7	2.0	2.3	1.7	5.2	1.8
30	110	1	4.8	3.2	3.1	2.9	0.3	3.2	4.2	3.2
31	10	1	2.7	3.1	4.0	6.2	1.1	4.4	6.2	4.4
32	17	1	6.6	3.3	3.3	2.5	0.6	3.2	4.0	3.2
33	30	1	8.5	7.1	13.1	13.5	0.3	10.7	12.1	10.7
34	31	1	10.7	9.8	8.6	9.1	0.7	9.3	6.5	9.2
35	53	1	3.6	4.0	6.1	2.2	1.4	3.5	4.4	3.5
36	88	1	5.4	5.0	7.1	3.2	3.1	4.5	7.6	4.6
37	21	1	6.9	4.8	10.1	10.7	0.5	8.2	8.8	8.2
38	23	1	3.3	3.5	4.3	6.1	1.6	4.6	7.8	4.7
39	32	1	6.6	5.0	4.2	2.2	1.4	3.8	3.9	3.8
40	44	1	14.8	12.6	15.1	15.6	0.5	14.2	7.8	14.0
41	48	1	5.0	3.3	3.1	2.5	0.4	3.1	4.4	3.1
42	27	1	8.4	7.4	11.0	10.5	0.8	9.2	5.6	9.1
43	43	1	7.7	6.2	4.2	4.0	0.8	5.0	3.2	5.0
44	46	1	6.9	4.3	5.4	5.1	0.9	5.0	2.1	4.9
45	47	1	1.2	2.7	3.7	3.2	1.7	2.9	3.3	2.9
46	86	1	5.6	5.1	4.7	4.7	1.7	4.9	4.6	4.9
47	91	1	4.3	3.6	6.5	3.4	0.9	3.9	5.2	4.0
48	38	1	11.8	9.7	13.2	11.1	1.2	10.9	8.6	10.8
49	41	1	9.9	11.3	12.5	12.4	0.9	11.5	4.0	11.2
50	51	1	8.3	4.5	2.8	3.4	0.6	4.1	1.5	4.0
51	54	1	13.0	9.1	14.0	8.0	1.7	9.7	17.4	10.0
52	90	1	11.8	11.5	11.6	6.5	1.1	9.1	8.2	9.1
53	101	1	10.5	7.8	9.7	0.9	1.8	5.1	9.3	5.2
54	78	1	4.4	2.6	2.7	2.6	0.8	2.8	3.9	2.8
55	87	1	13.6	11.1	13.6	14.2	0.6	12.9	7.4	12.7
56	109	1	4.1	4.1	4.1	3.5	1.1	3.8	4.2	3.8
57	118	1	3.2	3.4	4.8	3.3	0.8	3.5	4.0	3.5
58	40	1	7.5	6.6	10.7	8.0	1.9	7.8	8.5	7.8
59	49	1	5.5	4.4	5.0	3.3	1.3	4.1	8.2	4.2
60	73	1	7.5	5.5	6.1	4.5	0.6	5.3	7.8	5.3

Table 7.7 Building C3 dose data (SI), cGy units

Case	no.	Effect	Prompt gammas	Air/ground gammas	Early delayed gammas	Late delayed gammas	Building gammas	Total gammas	Prompt neutrons	Total dose
1	12	1	42.1	186.0	76.1	203.6	16.4	524.3	19.6	543.9
2	19	1	101.6	349.0	174.2	427.6	17.2	1069.6	26.7	1096.3
3	75	1	28.6	136.4	49.9	150.8	15.8	381.5	15.2	396.7
4	95	0	30.4	134.9	54.7	171.3	16.2	407.5	16.9	424.5
5	98	1	34.4	157.0	64.9	201.5	16.9	474.8	18.9	493.7
6	18	1	22.2	106.9	41.5	137.9	14.4	322.8	13.8	336.6
7	58	1	103.4	350.9	178.3	444.5	16.2	1093.2	25.0	1118.3
8	69	1	83.0	303.8	122.1	306.0	15.8	830.8	20.0	850.8
9	76	0	57.3	228.3	94.1	247.8	15.3	642.9	20.2	663.1
10	103	0	25.3	116.3	46.7	136.3	14.2	338.8	14.6	353.4
11	104	0	42.1	169.0	74.2	214.5	16.0	515.9	19.6	535.5
12	105	1	26.3	120.3	47.7	140.9	14.6	349.7	14.4	364.2
13	36	1	24.2	109.9	43.5	131.6	13.5	322.6	13.8	336.5
14	62	1	22.4	104.8	39.0	145.8	14.5	326.6	13.4	340.0
15	111	1	29.7	132.8	51.4	171.6	14.9	400.4	15.8	416.2
16	117	1	60.1	234.0	97.0	238.7	17.0	646.9	21.4	668.2
17	39	1	50.3	199.7	86.5	264.3	18.2	619.0	22.2	641.2
18	80	1	41.9	180.1	73.7	189.3	15.4	500.4	19.0	519.4
19	81	1	94.5	328.4	167.0	400.0	15.9	1005.7	24.4	1030.1
20	82	1	28.7	130.9	54.5	167.5	17.2	398.9	17.4	416.2
21	106	1	73.3	259.2	125.0	330.4	17.6	805.5	24.7	830.1
22	112	1	80.5	301.7	123.8	324.3	17.0	847.3	23.6	870.9
23	52	1	110.5	464.2	185.7	448.7	23.9	1233.0	30.2	1263.3
24	113	1	46.1	200.6	78.8	183.9	22.4	531.8	26.5	558.3
25	42	1	83.4	383.8	160.2	422.5	22.3	1072.3	27.0	1099.3
26	56	1	105.0	441.9	177.3	453.0	22.7	1200.0	28.4	1228.4
27	65	1	108.6	420.4	169.1	410.9	22.5	1131.5	29.8	1161.3
28	114	1	106.3	440.7	173.4	439.0	23.2	1182.6	29.4	1212.0
29	94	1	103.3	448.9	180.6	443.9	22.4	1199.2	29.4	1228.6
30	110	1	107.7	432.9	173.4	427.0	21.9	1162.9	30.4	1193.3
31	10	1	160.5	580.0	265.6	623.5	20.8	1650.5	31.7	1682.2
32	17	1	97.0	420.5	172.5	433.5	20.4	1143.8	27.9	1171.7
33	30	1	157.7	563.0	251.8	596.0	20.5	1589.0	31.0	1620.0
34	31	1	146.7	528.1	255.3	609.0	20.8	1559.9	33.2	1593.1
35	53	1	87.1	379.8	155.9	414.6	20.9	1058.4	28.1	1086.5
36	88	1	83.1	355.1	137.1	437.6	21.7	1034.6	26.4	1061.0
37	21	1	154.3	554.5	251.3	610.7	18.9	1589.8	30.3	1620.2
38	23	1	150.3	546.4	252.2	593.1	19.0	1561.0	29.9	1590.9
39	32	1	79.8	356.6	143.2	381.5	19.3	980.3	23.5	1003.8
40	44	1	104.1	406.9	168.0	403.6	18.7	1101.2	27.0	1128.2
41	48	1	92.5	385.3	148.2	374.6	18.3	1019.0	23.6	1042.6
42	27	1	96.2	385.4	161.3	382.8	16.5	1042.2	25.6	1067.8
43	43	1	82.9	349.7	146.6	364.1	16.5	959.9	23.5	983.5
44	46	1	73.4	316.2	133.2	334.8	16.5	874.2	23.1	897.3
45	47	1	85.3	349.1	140.8	338.1	15.9	929.3	23.1	952.4
46	86	1	91.9	383.7	151.9	360.3	15.9	1003.8	22.9	1026.7
47	91	1	66.4	276.7	113.3	331.5	16.7	804.6	22.5	827.1
48	38	1	93.2	364.7	163.4	449.5	21.4	1092.2	29.0	1121.2
49	41	1	64.9	295.9	128.0	297.2	23.2	809.3	29.7	838.9
50	51	1	91.3	411.2	175.3	412.2	23.4	1113.4	31.3	1144.7
51	54	1	128.4	509.3	216.5	530.6	23.9	1408.6	33.7	1442.2
52	90	1	63.1	270.3	112.0	338.1	17.0	800.5	21.9	822.4
53	101	1	81.3	353.9	144.7	444.8	23.2	1047.9	28.5	1076.4
54	78	1	106.4	430.9	169.2	412.4	20.6	1139.4	29.0	1168.4
55	87	1	131.8	484.5	227.4	534.0	20.4	1397.9	32.1	1430.1
56	109	1	74.4	326.1	123.9	413.2	21.3	958.7	23.3	982.1
57	118	1	85.6	378.0	160.2	417.1	22.9	1063.7	28.3	1092.1
58	40	1	83.4	333.9	143.2	417.7	20.1	998.3	26.8	1025.0
59	49	1	94.8	415.8	163.4	403.0	21.0	1098.0	25.6	1123.6
60	73	1	100.0	430.9	174.9	449.5	22.4	1177.7	27.7	1205.4

Table 7.8 Building C3 uncertainty data (SI), %

Case	no.	Effect	Prompt gammas	Air/ground gammas	Early delayed gammas	Late delayed gammas	Building gammas	Total gammas	Prompt neutrons	Total dose
1	12	1	15.0	10.5	13.4	11.7	2.0	11.5	8.2	11.4
2	19	1	19.5	16.8	16.3	15.7	0.7	16.3	4.7	16.0
3	75	1	4.0	4.3	5.0	3.9	0.7	4.0	2.1	4.0
4	95	0	7.8	5.4	7.8	6.2	0.7	6.0	4.0	5.9
5	98	1	8.4	8.2	7.8	7.0	1.3	7.4	3.9	7.3
6	18	1	2.7	1.4	2.3	3.2	0.7	2.3	2.0	2.3
7	58	1	18.4	16.1	14.9	14.7	1.1	15.3	4.6	15.1
8	69	1	31.8	24.3	31.3	30.8	0.7	28.0	9.2	27.6
9	76	0	30.8	24.7	26.9	24.9	1.7	25.1	8.7	24.6
10	103	0	9.4	7.2	9.4	6.4	0.6	7.1	4.7	7.0
11	104	0	15.0	9.0	16.2	10.2	1.9	10.8	6.1	10.6
12	105	1	2.6	3.5	2.8	3.0	0.6	3.0	1.8	3.0
13	36	1	12.9	12.4	10.8	9.1	2.7	10.5	5.2	10.3
14	62	1	11.9	11.0	10.9	6.6	2.7	8.7	4.6	8.6
15	111	1	14.1	12.3	13.5	11.0	3.3	11.7	7.8	11.5
16	117	1	28.2	22.0	26.8	27.6	0.9	24.8	7.5	24.2
17	39	1	21.7	15.0	26.0	15.4	1.2	16.9	7.3	16.5
18	80	1	17.8	11.0	16.6	15.5	2.3	13.8	8.5	13.6
19	81	1	22.5	18.6	19.6	20.3	1.1	19.5	6.5	19.2
20	82	1	6.7	9.8	7.6	7.0	1.8	7.8	2.5	7.5
21	106	1	28.2	24.2	25.3	21.7	1.3	23.2	5.9	22.7
22	112	1	17.2	13.0	15.3	15.5	0.9	14.4	4.5	14.2
23	52	1	8.4	7.0	10.1	6.0	1.0	7.1	9.7	7.2
24	113	1	5.3	6.5	8.7	8.3	0.4	7.1	2.3	6.9
25	42	1	6.1	6.4	7.6	3.3	0.2	5.2	2.6	5.1
26	56	1	3.0	3.3	5.1	5.5	1.5	4.3	2.4	4.3
27	65	1	13.8	12.8	10.3	15.4	0.2	13.2	5.4	13.0
28	114	1	5.9	3.8	2.5	1.6	0.7	2.9	2.8	2.9
29	94	1	2.7	1.3	1.5	1.9	2.3	1.7	2.9	1.7
30	110	1	5.0	3.3	3.1	3.1	0.3	3.3	2.7	3.3
31	10	1	2.7	3.0	3.9	5.9	1.2	4.2	4.0	4.2
32	17	1	7.0	3.4	3.3	2.5	0.6	3.3	2.4	3.3
33	30	1	8.0	7.0	12.8	13.3	0.4	10.3	8.3	10.2
34	31	1	11.1	10.1	8.9	9.1	0.7	9.5	4.3	9.4
35	53	1	3.5	4.1	6.3	2.4	1.4	3.7	2.5	3.6
36	88	1	5.2	5.1	6.9	3.2	3.2	4.5	3.8	4.5
37	21	1	7.1	4.8	9.9	10.6	0.5	8.0	6.1	8.0
38	23	1	3.3	3.4	4.3	5.9	1.6	4.5	5.1	4.5
39	32	1	7.3	5.3	4.6	2.4	1.5	4.2	2.2	4.1
40	44	1	15.2	12.9	15.6	16.0	0.5	14.5	5.0	14.2
41	48	1	5.1	3.3	2.9	2.7	0.4	3.1	2.7	3.1
42	27	1	8.6	7.7	11.2	10.9	0.8	9.4	3.8	9.3
43	43	1	8.4	6.5	4.7	4.2	0.8	5.4	2.1	5.3
44	46	1	7.7	4.5	5.8	5.3	0.9	5.2	1.4	5.1
45	47	1	1.0	2.8	3.8	3.3	1.8	3.0	2.1	2.9
46	86	1	5.8	5.2	4.8	4.8	1.7	5.0	3.1	5.0
47	91	1	4.5	3.5	6.7	3.8	1.0	4.1	2.9	4.1
48	38	1	12.1	9.9	13.5	11.1	1.3	10.9	5.2	10.8
49	41	1	10.3	11.8	13.3	13.2	0.9	12.1	2.9	11.8
50	51	1	9.1	4.7	2.9	3.6	0.6	4.3	1.0	4.2
51	54	1	12.9	9.2	13.7	8.0	1.8	9.6	10.8	9.7
52	90	1	12.0	11.8	11.9	6.5	1.1	9.4	4.9	9.3
53	101	1	10.7	7.9	9.7	0.8	1.8	5.2	5.2	5.2
54	78	1	4.5	2.7	2.7	2.7	0.9	2.8	2.5	2.8
55	87	1	14.0	11.4	14.0	14.4	0.7	13.1	5.0	12.9
56	109	1	4.1	4.1	4.1	3.5	1.2	3.8	2.3	3.7
57	118	1	3.6	3.6	5.1	3.4	0.8	3.7	2.3	3.7
58	40	1	7.4	6.6	10.6	8.1	1.9	7.8	4.8	7.7
59	49	1	5.3	4.3	4.7	3.0	1.3	3.9	4.9	3.9
60	73	1	7.5	5.5	5.9	4.4	0.6	5.2	4.9	5.2

Table 7.9 Building C3 dose data (BM), cGy units

Case	no.	Effect	Prompt gammas	Air/ground gammas	Early delayed gammas	Late delayed gammas	Building gammas	Total gammas	Prompt neutrons	Total dose
1	12	1	47.9	206.8	86.7	232.1	18.3	591.8	25.7	617.5
2	19	1	114.5	386.5	197.1	483.8	19.2	1201.1	36.1	1237.2
3	75	1	32.5	151.7	56.8	171.8	17.6	430.4	19.5	449.8
4	95	0	34.7	150.3	62.5	195.5	18.1	460.9	21.9	482.8
5	98	1	39.3	174.8	74.0	229.6	18.8	536.5	24.6	561.1
6	18	1	25.3	119.0	47.3	157.2	16.0	364.8	17.6	382.5
7	58	1	116.4	388.3	201.5	502.2	18.1	1226.5	34.0	1260.4
8	69	1	93.2	336.0	137.9	345.6	17.7	930.4	26.7	957.1
9	76	0	64.9	253.3	107.0	281.6	17.1	724.0	27.0	750.9
10	103	0	28.8	129.6	53.2	155.5	15.8	383.0	18.8	401.8
11	104	0	47.9	188.1	84.7	244.6	17.9	583.2	25.9	609.1
12	105	1	29.9	133.9	54.3	160.7	16.2	395.0	18.6	413.6
13	36	1	27.6	122.5	49.6	150.1	15.0	364.8	17.8	382.6
14	62	1	25.5	116.8	44.5	166.1	16.1	369.1	17.1	386.1
15	111	1	33.8	147.9	58.6	195.5	16.6	452.4	20.4	472.8
16	117	1	68.0	259.4	110.1	270.9	19.0	727.4	28.3	755.6
17	39	1	57.1	221.9	98.6	300.7	20.3	698.6	29.2	727.8
18	80	1	47.7	200.2	84.0	215.8	17.2	565.0	25.2	590.2
19	81	1	106.5	363.6	188.8	452.0	17.8	1128.6	33.0	1161.6
20	82	1	32.8	145.8	62.1	191.4	19.2	451.4	22.4	473.7
21	106	1	82.9	287.6	141.9	375.1	19.7	907.2	33.0	940.2
22	112	1	90.9	334.3	140.5	368.0	19.0	952.6	31.7	984.3
23	52	1	124.5	514.2	209.6	506.6	26.7	1381.6	40.0	1421.5
24	113	1	52.5	223.8	90.0	210.0	25.1	601.2	34.6	635.8
25	42	1	94.3	425.5	180.9	477.7	24.9	1203.3	35.5	1238.8
26	56	1	118.2	489.5	200.1	511.7	25.3	1344.8	37.5	1382.3
27	65	1	122.3	465.7	191.1	464.7	25.2	1268.9	39.6	1308.5
28	114	1	119.8	488.3	195.9	496.7	25.9	1326.6	38.9	1365.5
29	94	1	116.6	497.5	204.1	502.3	25.0	1345.5	39.1	1384.6
30	110	1	121.5	479.9	196.3	483.8	24.5	1306.0	40.6	1346.6
31	10	1	180.3	641.3	299.4	702.6	23.2	1846.8	42.9	1889.7
32	17	1	109.4	466.0	194.9	490.3	22.8	1283.4	37.2	1320.6
33	30	1	177.0	622.5	283.7	671.4	22.9	1777.6	41.9	1819.5
34	31	1	165.1	584.5	288.2	687.3	23.2	1748.3	45.1	1793.4
35	53	1	98.6	421.4	176.5	469.7	23.4	1189.6	37.4	1227.0
36	88	1	93.9	394.0	155.3	495.2	24.2	1162.5	34.8	1197.3
37	21	1	173.4	613.2	283.3	688.5	21.1	1779.5	41.3	1820.8
38	23	1	168.9	604.3	284.2	668.6	21.2	1747.2	40.6	1787.8
39	32	1	90.0	395.3	161.7	431.2	21.5	1099.7	30.9	1130.5
40	44	1	117.3	450.7	189.9	456.3	20.8	1235.0	36.3	1271.3
41	48	1	104.2	426.9	167.3	423.4	20.5	1142.3	31.3	1173.6
42	27	1	108.5	427.1	182.4	432.9	18.4	1169.2	34.6	1203.8
43	43	1	93.5	387.7	165.6	411.5	18.4	1076.6	31.4	1108.1
44	46	1	82.9	350.8	150.6	378.8	18.4	981.5	30.8	1012.3
45	47	1	96.1	387.0	159.0	382.3	17.8	1042.2	30.9	1073.1
46	86	1	103.4	425.0	171.4	406.6	17.7	1124.1	30.7	1154.8
47	91	1	75.0	307.3	128.5	375.4	18.6	904.8	29.9	934.6
48	38	1	105.4	404.6	185.1	508.5	23.8	1227.4	38.6	1266.0
49	41	1	73.8	329.0	145.3	337.5	25.9	911.5	39.2	950.7
50	51	1	103.2	455.9	198.2	466.1	26.1	1249.5	41.6	1291.1
51	54	1	144.7	564.1	244.6	599.8	26.6	1579.7	45.0	1624.7
52	90	1	71.4	300.2	126.9	382.6	19.0	900.1	29.0	929.1
53	101	1	91.9	392.9	163.9	503.6	25.9	1178.2	37.5	1215.7
54	78	1	120.0	477.6	191.4	467.0	23.0	1279.0	38.8	1317.8
55	87	1	148.5	536.5	256.9	603.1	22.8	1567.7	43.5	1611.2
56	109	1	83.9	361.7	140.1	467.0	23.7	1076.5	30.4	1106.9
57	118	1	96.8	419.3	181.1	472.4	25.5	1195.1	37.4	1232.5
58	40	1	94.3	370.6	162.3	472.7	22.4	1122.4	35.6	1157.9
59	49	1	106.8	460.7	184.3	455.3	23.5	1230.5	33.8	1264.3
60	73	1	112.6	477.3	197.2	507.9	25.0	1320.0	36.6	1356.5

Table 7.10 Building C3 uncertainty data (BM), %

Case	no.	Effect	Prompt gammas	Air/ground gammas	Early delayed gammas	Late delayed gammas	Building gammas	Total gammas	Prompt neutrons	Total dose
1	12	1	14.9	10.5	13.4	11.7	2.0	11.5	9.0	11.4
2	19	1	19.3	16.6	16.1	15.6	0.7	16.1	5.3	15.8
3	75	1	4.0	4.2	5.0	3.8	0.7	4.0	2.4	3.9
4	95	0	7.8	5.4	7.9	6.2	0.7	6.1	4.6	6.0
5	98	1	8.3	8.1	7.8	7.0	1.3	7.4	4.4	7.2
6	18	1	2.7	1.4	2.4	3.2	0.7	2.4	2.2	2.4
7	58	1	18.2	16.0	14.7	14.6	1.1	15.2	5.2	14.9
8	69	1	31.5	24.1	31.0	30.6	0.7	27.8	10.2	27.3
9	76	0	30.5	24.5	26.6	24.6	1.7	24.9	9.6	24.3
10	103	0	9.4	7.2	9.5	6.5	0.6	7.1	5.5	7.0
11	104	0	14.8	9.0	16.0	10.1	1.9	10.7	6.8	10.6
12	105	1	2.6	3.5	2.8	3.1	0.6	3.0	2.1	3.0
13	36	1	12.8	12.4	10.8	9.0	2.7	10.4	5.8	10.2
14	62	1	11.8	10.9	10.9	6.5	2.7	8.6	5.2	8.5
15	111	1	14.1	12.2	13.6	11.0	3.2	11.7	8.7	11.6
16	117	1	27.9	21.8	26.5	27.4	0.9	24.6	8.2	24.0
17	39	1	21.4	14.9	25.7	15.2	1.2	16.7	8.2	16.4
18	80	1	17.7	11.0	16.5	15.4	2.3	13.8	9.3	13.6
19	81	1	22.3	18.5	19.5	20.2	1.1	19.4	7.1	19.1
20	82	1	6.6	9.7	7.5	7.0	1.8	7.7	2.9	7.5
21	106	1	27.8	24.0	25.0	21.4	1.3	22.9	6.7	22.3
22	112	1	17.0	12.9	15.1	15.3	0.9	14.3	5.1	14.0
23	52	1	8.4	7.0	10.2	6.1	1.0	7.1	10.6	7.2
24	113	1	5.3	6.4	8.6	8.2	0.4	7.0	2.4	6.8
25	42	1	6.0	6.3	7.5	3.3	0.2	5.1	2.9	5.1
26	56	1	3.0	3.3	5.1	5.5	1.5	4.3	2.7	4.3
27	65	1	13.6	12.7	10.3	15.4	0.2	13.1	5.9	12.9
28	114	1	5.9	3.8	2.5	1.6	0.7	2.9	3.1	2.9
29	94	1	2.6	1.2	1.5	1.9	2.3	1.7	3.3	1.7
30	110	1	4.9	3.3	3.1	3.0	0.3	3.3	3.0	3.3
31	10	1	2.7	3.0	3.9	5.9	1.1	4.2	4.5	4.2
32	17	1	6.9	3.4	3.3	2.5	0.6	3.3	2.7	3.3
33	30	1	8.1	7.0	12.9	13.3	0.4	10.3	9.1	10.3
34	31	1	11.0	10.0	8.8	9.1	0.7	9.4	4.8	9.3
35	53	1	3.5	4.1	6.3	2.3	1.4	3.6	2.9	3.6
36	88	1	5.3	5.0	6.9	3.2	3.2	4.5	4.5	4.5
37	21	1	7.0	4.8	10.0	10.6	0.5	8.0	6.7	8.0
38	23	1	3.3	3.4	4.3	5.9	1.6	4.5	5.6	4.5
39	32	1	7.1	5.2	4.5	2.4	1.5	4.1	2.5	4.0
40	44	1	15.1	12.9	15.4	15.9	0.5	14.4	5.6	14.1
41	48	1	5.1	3.3	3.0	2.6	0.4	3.1	3.0	3.1
42	27	1	8.6	7.7	11.1	10.8	0.8	9.3	4.2	9.2
43	43	1	8.2	6.4	4.6	4.1	0.8	5.3	2.3	5.2
44	46	1	7.5	4.5	5.7	5.3	0.9	5.2	1.5	5.1
45	47	1	1.0	2.8	3.8	3.3	1.8	2.9	2.4	2.9
46	86	1	5.8	5.2	4.8	4.8	1.7	5.0	3.4	4.9
47	91	1	4.4	3.5	6.6	3.7	1.0	4.1	3.3	4.0
48	38	1	12.0	9.9	13.4	11.1	1.2	10.9	5.9	10.8
49	41	1	10.2	11.7	13.1	13.0	0.9	12.0	3.1	11.6
50	51	1	8.9	4.7	2.9	3.5	0.6	4.2	1.1	4.1
51	54	1	12.9	9.2	13.7	7.9	1.7	9.6	11.9	9.7
52	90	1	12.0	11.7	11.9	6.5	1.1	9.3	5.5	9.2
53	101	1	10.6	7.9	9.7	0.8	1.8	5.2	5.9	5.2
54	78	1	4.4	2.7	2.6	2.6	0.8	2.8	2.7	2.8
55	87	1	13.9	11.3	13.9	14.3	0.7	13.0	5.6	12.8
56	109	1	4.1	4.1	4.0	3.5	1.2	3.8	2.7	3.7
57	118	1	3.5	3.6	5.0	3.4	0.8	3.7	2.6	3.6
58	40	1	7.4	6.6	10.6	8.0	1.9	7.8	5.5	7.7
59	49	1	5.3	4.3	4.7	3.0	1.3	3.9	5.5	4.0
60	73	1	7.5	5.5	5.9	4.4	0.6	5.2	5.4	5.2

the wall. The effect of radiation streaming through the open windows on the south wall and across the rooms is evident in all of the plots. The complicated contours around the passageway and stairwells are also evident, but no cases were located there.

Results for the excluded cases are shown in Tables 7.11–7.13.

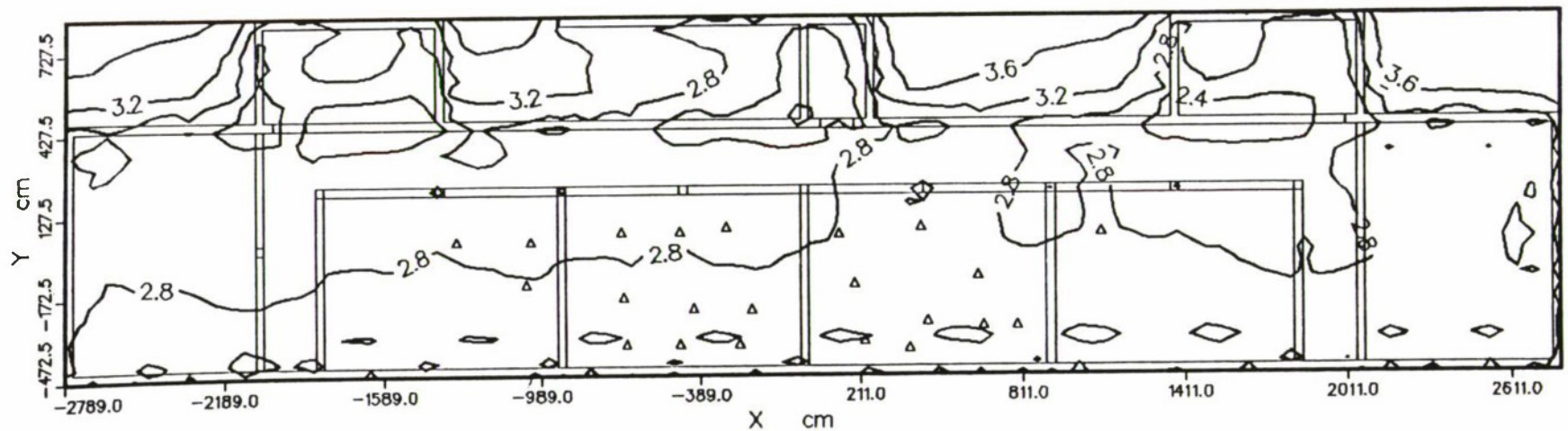

Figure 7.5 Building C3 dose distribution; 48 cm above second floor.

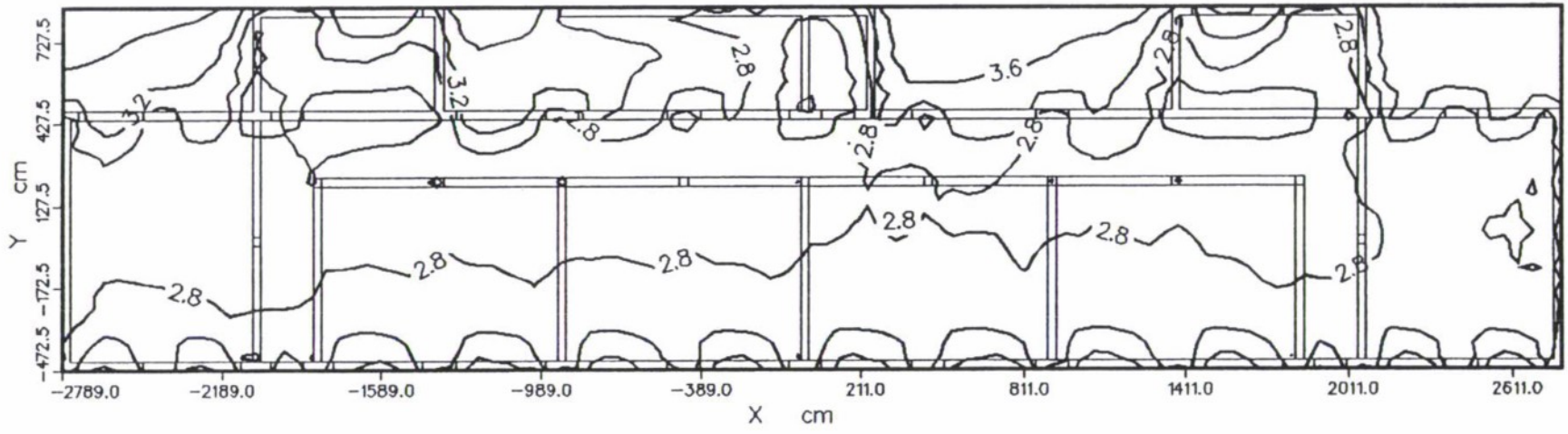

Figure 7.6 Building C3 dose distribution; 150 cm above second floor.

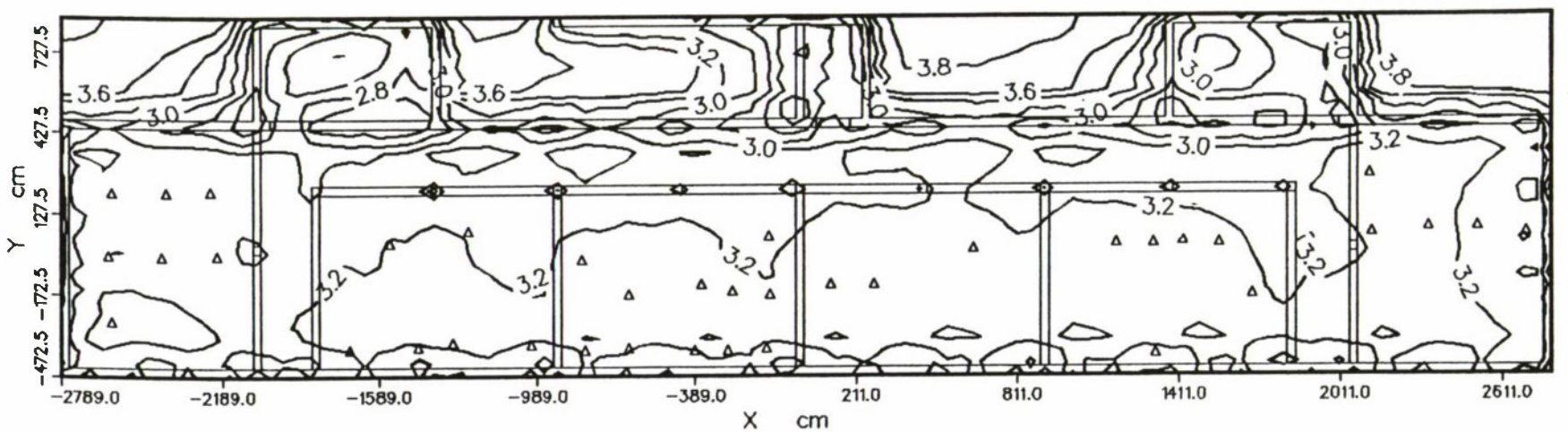

Figure 7.7 Building C3 dose distribution; 48 cm above third floor.

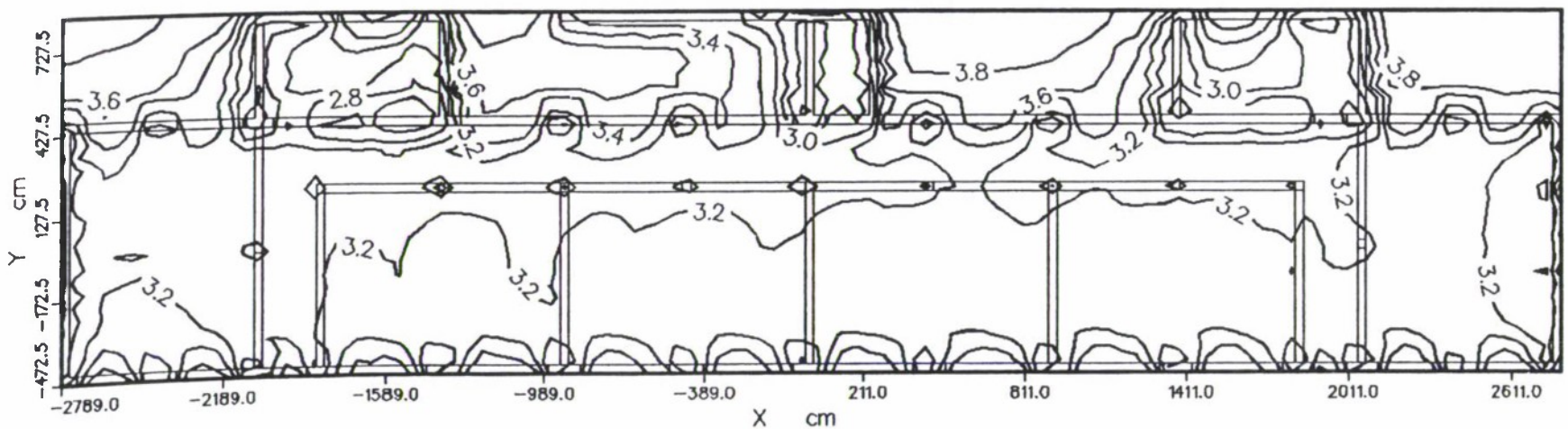

Figure 7.8 Building C3 dose distribution; 150 cm above third floor.

Table 7.11 Building C3 dose data, excluded cases (FIA), cGy units

Case	no.	Effect	Prompt gammas	Air/ground gammas	Early delayed gammas	Late delayed gammas	Building gammas	Total gammas	Prompt neutrons	Total dose
1	15	0	27.6	123.6	52.3	213.6	22.1	439.2	18.6	457.9
2	68	0	41.1	170.4	77.3	252.6	23.3	564.7	26.6	591.3
3	70	0	42.8	181.6	80.8	243.8	24.4	573.5	26.9	600.3
4	72	0	43.9	174.4	78.3	311.7	25.9	634.1	28.5	662.6
5	60	0	69.0	267.4	119.6	326.7	24.0	806.6	37.2	843.8
6	71	0	30.3	131.3	55.4	208.4	21.2	446.5	19.1	465.6
7	107	0	58.8	234.3	102.8	274.4	19.8	690.1	30.6	720.7
8	7	0	104.2	366.8	196.8	441.0	33.7	1142.6	63.8	1206.3
9	26	0	169.5	638.6	318.3	750.2	34.6	1911.1	77.9	1989.0
10	33	0	95.0	345.4	175.8	410.5	33.0	1059.6	62.4	1122.0
11	34	0	169.3	657.6	327.1	785.1	34.6	1973.8	75.4	2049.2
12	64	0	223.9	717.3	376.4	862.5	34.8	2214.8	78.3	2293.2
13	97	0	221.7	749.3	403.5	928.1	35.8	2338.4	81.5	2419.9
14	99	0	277.4	883.0	466.4	1090.6	36.2	2753.6	85.5	2839.1
15	100	0	179.0	675.2	324.7	770.3	35.5	1984.7	76.3	2060.9
16	115	0	89.2	352.2	166.5	385.6	33.4	1026.9	56.8	1083.7
17	116	0	102.0	371.5	185.3	431.4	34.2	1124.4	63.9	1188.2
18	5	0	277.5	892.4	468.5	1139.2	34.4	2812.0	84.8	2896.8
19	63	0	236.7	770.2	412.6	977.1	33.6	2430.2	82.5	2512.7
20	96	0	125.1	503.1	221.8	670.9	32.8	1553.8	47.5	1601.3
21	102	0	152.2	590.0	286.2	732.4	33.2	1794.0	63.8	1857.8
22	6	0	261.3	835.1	415.9	1020.4	32.2	2564.9	77.4	2642.3
23	24	0	190.2	660.8	311.2	758.0	31.9	1952.2	69.5	2021.7
24	35	0	168.5	626.2	292.5	731.7	32.4	1851.2	63.6	1914.8
25	84	0	153.7	567.5	265.3	750.3	33.6	1770.4	64.6	1835.0
26	93	0	134.9	515.3	233.0	708.3	34.1	1625.6	53.6	1679.3
27	119	0	168.6	624.1	305.2	781.4	33.0	1912.2	69.9	1982.1
28	20	0	138.8	547.9	239.9	621.9	30.2	1578.6	49.4	1628.1
29	79	0	168.8	620.1	278.7	679.9	29.7	1777.2	61.1	1838.3
30	108	0	122.0	467.6	207.8	631.0	29.3	1457.7	47.2	1504.9
31	25	0	164.1	586.0	284.8	702.1	24.6	1761.5	61.8	1823.2
32	83	0	118.1	435.2	207.9	611.1	26.0	1398.4	51.8	1450.2

Table 7.12 Building C3 dose data, excluded cases (SI), cGy units

Case	no.	Effect	Prompt gammas	Air/ground gammas	Early delayed gammas	Late delayed gammas	Building gammas	Total gammas	Prompt neutrons	Total dose
1	15	0	16.5	84.0	31.0	126.2	15.1	272.9	13.0	285.9
2	68	0	24.6	116.3	46.0	149.0	15.9	351.8	15.8	367.6
3	70	0	25.8	124.7	48.6	144.5	16.7	360.3	16.2	376.5
4	72	0	26.2	118.5	46.0	184.3	17.7	392.7	17.2	409.9
5	60	0	41.9	184.8	71.7	194.4	16.4	509.1	19.2	528.3
6	71	0	18.2	89.4	32.9	123.2	14.5	278.3	12.7	291.0
7	107	0	35.9	162.4	61.8	164.2	13.6	437.8	15.8	453.6
8	7	0	63.1	251.0	117.7	264.6	23.0	719.4	30.7	750.2
9	26	0	104.4	446.0	195.7	460.3	23.6	1230.0	35.3	1265.3
10	33	0	57.0	234.8	104.4	243.5	22.5	662.2	30.1	692.3
11	34	0	104.6	460.3	202.8	485.3	23.7	1276.7	34.5	1311.1
12	64	0	141.5	505.9	234.0	537.0	23.7	1442.1	35.3	1477.4
13	97	0	139.2	527.2	250.7	577.8	24.4	1519.4	36.7	1556.1
14	99	0	176.0	624.7	291.4	682.3	24.7	1799.2	37.8	1837.1
15	100	0	111.1	472.9	200.5	474.4	24.2	1283.2	35.1	1318.3
16	115	0	53.8	240.5	100.1	231.4	22.8	648.6	28.5	677.1
17	116	0	61.5	253.1	110.5	256.8	23.3	705.2	30.9	736.1
18	5	0	175.7	630.9	292.2	708.9	23.5	1831.2	37.0	1868.2
19	63	0	148.8	541.5	255.5	604.5	23.0	1573.3	36.3	1609.6
20	96	0	78.4	351.7	138.2	417.1	22.4	1007.8	25.4	1033.2
21	102	0	94.4	411.9	177.5	450.8	22.7	1157.2	30.6	1187.8
22	6	0	166.3	590.9	260.1	635.6	22.0	1674.8	34.0	1708.8
23	24	0	119.4	464.2	192.3	467.0	21.8	1264.7	31.8	1296.5
24	35	0	105.7	438.7	182.0	450.8	22.1	1199.3	30.2	1229.5
25	84	0	95.3	394.9	162.7	458.8	23.0	1134.6	30.9	1165.5
26	93	0	84.2	358.9	144.3	437.9	23.3	1048.7	27.8	1076.4
27	119	0	104.5	435.5	188.2	478.7	22.5	1229.3	32.3	1261.6
28	20	0	87.1	384.2	149.9	385.0	20.6	1026.8	25.1	1051.9
29	79	0	106.1	435.3	173.0	420.5	20.3	1155.2	28.6	1183.8
30	108	0	76.2	325.6	128.7	390.8	20.0	941.3	24.2	965.5
31	25	0	102.7	410.8	176.1	433.3	16.8	1139.6	26.9	1166.5
32	83	0	73.0	301.9	126.9	375.5	17.8	895.1	24.4	919.5

Table 7.13 Building A4 dose data, excluded cases (BM), cGy units

Case	no.	Effect	Prompt gammas	Air/ground gammas	Early delayed gammas	Late delayed gammas	Building gammas	Total gammas	Prompt neutrons	Total dose
1	15	0	18.9	93.7	35.4	144.0	16.9	308.8	16.3	325.1
2	68	0	28.0	129.6	52.5	170.0	17.8	397.9	20.3	418.2
3	70	0	29.4	138.8	55.4	164.8	18.6	407.0	20.7	427.7
4	72	0	29.9	132.1	52.6	210.1	19.8	444.4	22.0	466.4
5	60	0	47.6	205.4	81.6	221.4	18.3	574.1	25.2	599.3
6	71	0	20.8	99.7	37.6	140.6	16.2	314.8	16.0	330.9
7	107	0	40.7	180.4	70.3	186.8	15.1	493.2	20.7	513.9
8	7	0	71.7	279.4	134.0	301.0	25.7	811.8	40.7	852.5
9	26	0	118.2	494.5	221.5	521.3	26.3	1381.8	47.5	1429.3
10	33	0	65.0	261.7	119.1	277.8	25.2	748.6	39.9	788.5
11	34	0	118.4	510.2	229.3	548.9	26.4	1433.1	46.3	1479.4
12	64	0	159.2	559.8	264.1	606.0	26.5	1615.7	47.5	1663.2
13	97	0	156.9	583.7	283.1	652.1	27.3	1703.1	49.4	1752.4
14	99	0	197.9	690.9	328.6	769.2	27.6	2014.2	51.2	2065.4
15	100	0	125.6	524.2	226.8	536.9	27.0	1440.5	47.0	1487.5
16	115	0	61.3	267.9	113.9	263.6	25.5	732.2	37.5	769.7
17	116	0	70.0	282.0	125.9	292.8	26.0	796.8	40.9	837.7
18	5	0	197.6	697.8	329.7	799.9	26.2	2051.1	50.2	2101.4
19	63	0	167.7	599.5	288.7	683.0	25.6	1764.5	49.1	1813.6
20	96	0	88.5	390.0	156.3	471.4	25.0	1131.2	33.2	1164.4
21	102	0	106.7	456.8	200.7	510.3	25.3	1299.9	40.7	1340.6
22	6	0	186.8	653.5	293.3	717.2	24.5	1875.4	46.0	1921.4
23	24	0	134.6	514.2	217.5	528.3	24.3	1418.9	42.7	1461.5
24	35	0	119.2	486.3	205.7	510.3	24.7	1346.1	40.2	1386.3
25	84	0	107.8	438.2	184.4	520.0	25.6	1275.9	41.2	1317.1
26	93	0	95.2	398.3	163.4	495.4	26.0	1178.3	36.4	1214.7
27	119	0	118.1	483.0	213.0	542.3	25.1	1381.5	43.2	1424.8
28	20	0	98.3	425.8	169.3	435.6	23.0	1151.9	33.1	1185.0
29	79	0	119.6	482.3	195.6	475.6	22.7	1295.7	38.2	1333.9
30	108	0	86.1	361.4	145.7	441.9	22.3	1057.4	31.8	1089.2
31	25	0	115.8	455.2	199.1	490.0	18.7	1278.8	36.4	1315.2
32	83	0	82.6	335.2	143.9	425.1	19.9	1006.7	32.5	1039.2

8. EVALUATION OF RESULTS

8.1 TRANSITION RANGE CASES

In this section, we examine a "transition range," defined as the dose range from the lowest dose causing death to the highest dose survived. While the limits of this range obviously depend upon the sample population, certain valid information can be obtained from it. The range limits are summarized in Table 8.1, together with the arithmetic and geometric means of the limits. Values are shown for Building A, Building C, and for the composite of the two buildings. Table 8.2 gives the ratio of SI and BM doses to FIA dose for the mean values. The BM/FIA ratio for the composite geometric mean dose is 0.70, while the corresponding ratio of SI dose to FIA dose is 0.61.

While none of the tabulated results are a true LD50 evaluation, it is apparent that the LD50 parameter should lie within the transition range, given a sufficient sample size and barring statistical mishap. Accordingly, we note that a very old reference by Goldstein[18] estimates an LD50 equivalent to 350–500 cGy in modern units. A 1950 estimate was equivalent to 450 cGy. More recent estimates have ranged from 217 to 634 cGy, in terms of FIA dose. These values lie within our transition zone, 216 to 1057 cGy, as expected. This is a preliminary confirmation of the new data.

The individual cases in the transition ranges for the two buildings, sorted by FIA dose, are listed in Tables 8.3 and 8.4. Building A provided a broad case distribution ranging from well below the lowest fatal dose to well above the highest survival dose. The doses in Building C were not so well distributed, however. The two lowest doses were about 540 cGy, and both of those cases were fatalities. At the other end, two survivors had doses approaching twice the highest doses survived in Building A.

These high doses were hardly independent, however. In fact, they were located side by side. In a letter dated 10 December 1986, Stohler[13] states, "In the Shiroyama cases, there seems to be an almost casual positioning in the Y-direction, since it had little effect on the shielding between the case history and the hypocenter." Accordingly, we examined the effect of an arbitrary movement of these two cases 1 m away from the windows. The results, shown in Table 8.5, indicate that this movement reduces the highest dose from 1057 cGy to 763 cGy. It must be noted, however, that the y uncertainty assigned to the two cases is only 0.3 m, so a 1 m error must be considered improbable.

Table 8.1 Transition range data

Building	Response	Dose (cGy)			
		Bottom of range	Top of range	Arithmetic mean	Geometric mean
A	FIA	216	631	424	369
A	SI	128	376	252	219
A	BM	148	431	289	253
C	FIA	539	1057	798	755
C	SI	336	663	500	472
C	BM	382	751	567	536
A+C	FIA	216	1057	636	478
A+C	SI	128	663	396	291
A+C	BM	148	751	448	333

Table 8.2 Transition range dose ratios

Building	Response	Ratio	
		Arithmetic mean	Geometric mean
A	SI/FIA	0.59	0.59
A	BM/FIA	0.68	0.69
C	SI/FIA	0.63	0.63
C	BM/FIA	0.71	0.71
A+C	SI/FIA	0.62	0.61
A+C	BM/FIA	0.70	0.70

Table 8.3 Building A transition range cases FIA dose (cGy)

Case no.		Effect	Total dose
1	102	1	216.4
2	112	0	245.6
3	115	1	263.3
4	103	0	268.9
5	5	1	325.7
6	89	1	327.4
7	3	0	352.4
8	95	0	381.4
9	104	1	387.6
10	93	0	389.2
11	88	0	406.5
12	13	0	409.2
13	92	0	453.8
14	96	1	536.3
15	97	0	539.2
16	90	1	617.0
17	94	0	631.4

Table 8.4 Building C transition range FIA dose (cGy)

Case no.		Effect	Total dose
1	18	1	539.1
2	36	1	540.8
3	62	1	543.3
4	103	0	568.0
5	105	1	582.4
6	75	1	629.0
7	111	1	668.6
8	82	1	671.5
9	95	0	684.0
10	98	1	795.2
11	80	1	838.1
12	104	0	869.3
13	12	1	873.1
14	113	1	897.6
15	39	1	1032.2
16	117	1	1056.1
17	76	0	1057.4

Table 8.5 Building C, arbitrary relocation of two key cases

Cases	Total FIA dose, cGy	Dose, cGy in relocated position[a]
104	869	702
76	1057	763

[a]Relocated position is 1 m from the standard position in the direction away from the south wall.

It is also possible to find systematic differences between the two buildings that could be important. The Building A personnel were predominantly male machine shop trainees, while Building C contained predominantly young female students. They may have differed in their response to radiation exposure. The exposure in Building A included radiation streaming directly from the weapon through windows on the east and north sides of the building. Personnel were located throughout the building, and many were exposed to this direct radiation as well as to backscattered radiation and penetration through overhead floors. All line-of-sight paths in Building C were blocked by the east wall, however. All of the radiation reaching the personnel had penetrated thick concrete layers or scattered through a sharp angle to enter the windows. Accordingly, systematic spectral and geometric differences between the two radiation environments existed, and they could be significant.

Systematic errors in building modeling could also be involved. For example, it was found that the results for personnel exposed to streaming through the windows are very sensitive to the size and location of the windows. Errors in floor thickness, concrete composition, and other details could also be significant. While the models were constructed with great attention to these details, some error is inherent in the process. Of course, ordinary random error in dose calculation and random variation in biological response are present in such comparisons.

The transition range cases for the combination of Buildings A and C are combined in Table 8.6

8.2 CROSSOVER CASE ANALYSIS

Away from a closely regulated laboratory situation, dose calculations involve significant error, and a major portion of this error derives from so many sources that it can be considered random. To examine the effect of random error in the calculations, let us consider a hypothetical radiation effect having a precise

Table 8.6 Combined buildings A&C transition range FIA dose (cGy)

Case no.		Effect	Total dose
1	102	1	216.4
2	112	0	263.3
3	115	1	263.3
4	103	0	268.9
5	5	1	325.7
6	89	1	327.4
7	3	0	352.4
8	95	0	381.4
9	104	1	387.6
10	93	0	389.2
11	88	0	406.5
12	13	0	409.2
13	92	0	453.8
14	96	1	536.3
15	18	1	539.1
16	97	0	539.2
17	36	1	540.8
18	62	1	543.3
19	103	0	568.0
20	105	1	582.4
21	90	1	617.0
22	75	1	629.0
23	94	0	631.4
24	111	1	668.6
25	82	1	671.5
26	95	0	684.0
27	12	1	693.7
28	40	1	782.5
29	98	1	795.2
30	80	1	838.1
31	104	0	869.3
32	12	1	873.1
33	113	1	897.6
34	39	1	1032.2
35	117	1	1056.1
36	76	0	1057.4

threshold, i.e. one having effect 0 below a dose LT and effect 1 above it. If the dose could be calculated precisely in this perfect world, the results would align on either side of LT as illustrated in Fig. 8.1a. The effect of dose error, however, would be to cause misplotting of each dose to some extent, as depicted in Fig. 8.1b. The result would be a transition zone in which a mixture of effects would be observed, as illustrated in Fig. 8.1c. The boundaries of the zone would depend somewhat upon chance, but that is not the important point. Within the zone, valuable information about the dose error can be obtained.

If we now consider the irradiation of a uniform continuous distribution of subjects along the dose line, the result, in the absence of dose error, would be 100% probability of effect 0 below LT and 100% probability of effect 1 above it. The effect of dose error would be to blur each probability about LT, as depicted conceptually in Fig. 8.2a. This is clearly just the continuous analog of Fig. 8.1c. Well away from LT, the effect of cases displaced to lower doses would be balanced by other cases displaced to higher doses. Near LT, however, no such balance exists. Some cases with effect 0 would be falsely displaced above LT, and they would result in a sloped distribution near LT, as shown. (The actual distributions would be smooth curves, of course, not line segments as conceptually illustrated.) A comparable effect would displace cases with effect 1 below LT, of course. In the resulting transition zone, "0" cases displaced upward past LT or "1" cases displaced downward past LT can be readily identified, and the resulting population of "crossover cases" would be distributed roughly as depicted in Fig. 8.2b. This distribution would be directly related to the pointwise dose error, although it would not necessarily be the identical distribution.

One may note that, in a real event, variability in biological response would occur together with dose error. Thus, the effects of dose error and biological response would be intermingled in a single observation, and only a composite would be observed.

Returning to Fig. 8.2c, we see that, if a value of LT were known, the standard deviation of the crossover distribution could be calculated as:

$$s = \left[\sum_i (d_i - LT)^2 / n \right]^{1/2}$$

where: i = index of crossover case,
d = calculated dose of i'th case, and
n = total number of crossover cases.

The threshold value, LT, is not known *a piori*, of course, but we can estimate a value for it by finding the value that minimizes s. For a given set of observations, that search yields both LT and the minimum standard deviation of the distribution, s, which can be related to the composite of dose error and biological variability. The standard deviations for the Building A alone, and then for A and C combined, are shown in Table 8.7. The result for Building C, taken by itself, is not a valid indicator because of the lack of low-dose cases indicated earlier, and it is not listed.

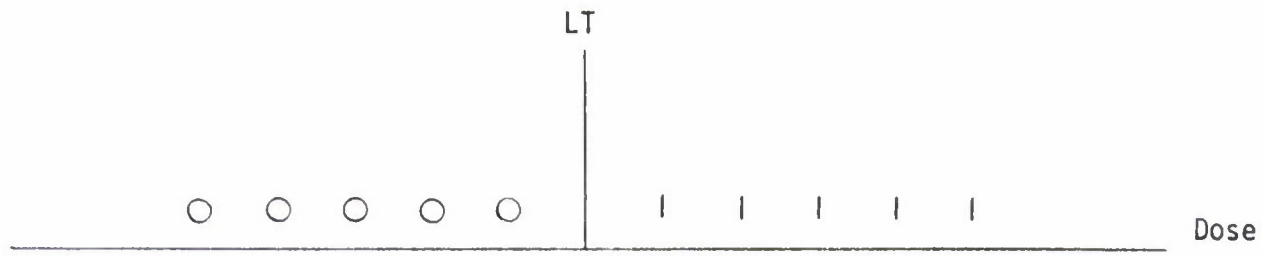

A. Observations Without Error

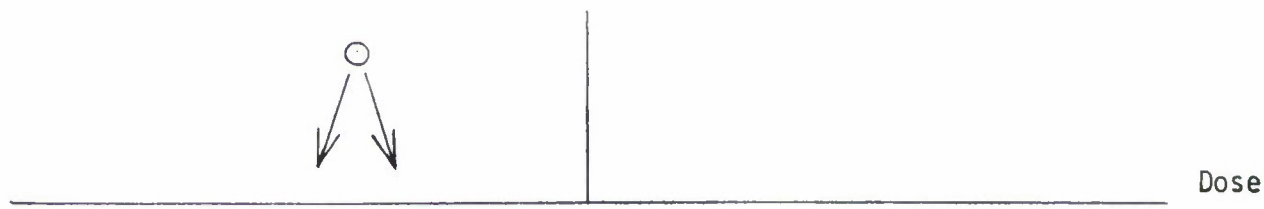

B. The Effect of Dose Error

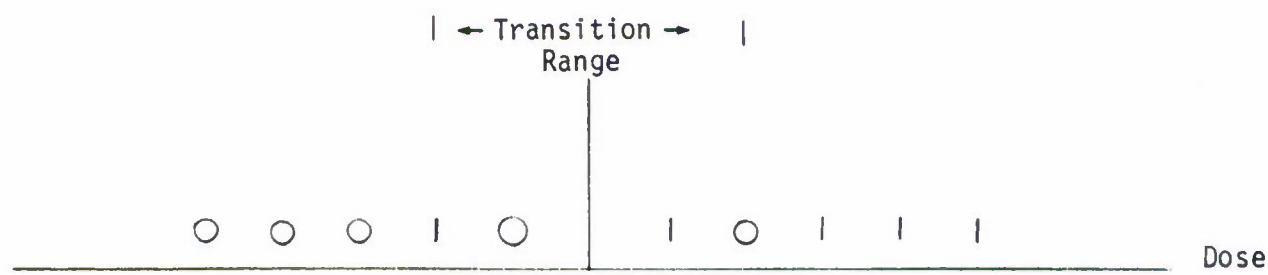

C. Observations with Dose Error and Biological Variability

Figure 8.1 Results of individual dose observations.

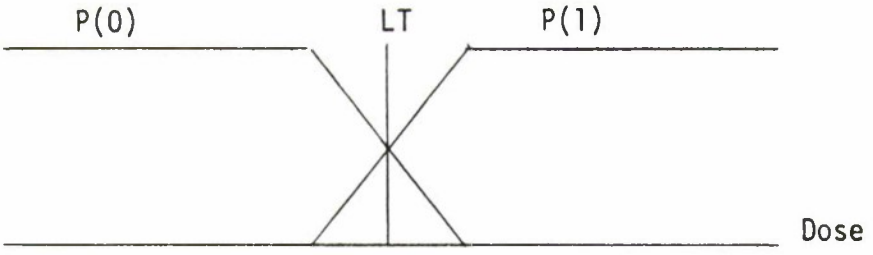

A. Probability of Finding 0's or 1's at a Given Calculated Dose

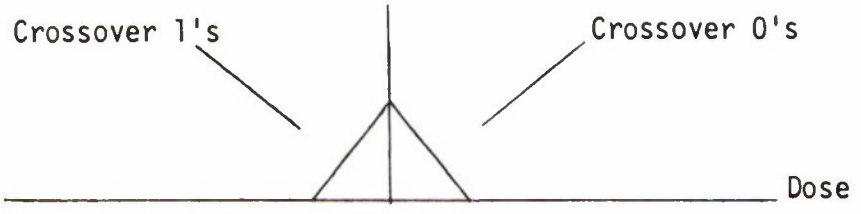

B. Density of Crossover Cases

Figure 8.2 Conceptual probability distribution of results.

Table 8.7 Standard deviations from crossover analysis

Building(s)	Standard deviation, %
A	31
A&C	50
A&C with arbitrary repositioning	39

The optimum value of s is 31% for Building A, but 50% for the combination of both buildings. The table also shows that s would be reduced to 39% by the arbitrary repositioning of the two cases noted earlier. This does not necessarily mean that those results are wrong, of course, but it shows that the differences can be due to a few exceptional cases.

It could be speculated that a crossover fit performed in logarithmic space, where errors would be treated as relative rather than absolute, might produce a smaller standard deviation, but the comparison between log and linear fits in Table 8.8 indicate otherwise. All of the standard deviations were increased by this treatment.

Table 8.8 Comparison of crossover data obtained from linear and log fits

	Standard deviation, %	
Buildings	Linear	Log
A	31	35
A&C	50	65
A&C with arbitrary repositioning	39	55

Since the cases for Building A spanned the range from low to high dose, they are a valid indication of the crossover distribution. The cases and deviations about LT are shown in Table 8.9. The table also shows the calculated positional uncertainty, but no particular correlation between deviation and that uncertainty is evident. Table 8.10 summarizes the distribution of deviations and compares them with a Gaussian distribution. The distribution is only slightly flatter than the standard Gaussian distribution.

The effect of dose error in dose-effect correlation is quite analogous to the effect of a detector of finite response width in observing a spectrum or to the "straggling"

Table 8.9 Building A crossover case summary

Case	FIA dose, cGy	Deviation from LT, cGy	Position uncertainty, %
102	216	−177	13
115	263	−133	28
5	326	−70	15
89	327	−69	13
104	388	−8	26
88	406	+10	3
13	409	+13	5
92	454	+58	12
97	539	+143	24
94	631	+235	8

Table 8.10 Building A crossover distribution

Bracket limits	Population	Cumulative %	Standard distribution
$0.0 - 1.0\ \sigma$	6	60	68
$1.0 - 2.0\ \sigma$	3	90	95
$2.0 - \infty$	1	100	100

effect seen in charged-particle transport. In the latter case, all charged particles of a given type and energy have the same range into a given shield material, in first principle. In detail, various random effects cause blurring of particle density in the neighborhood of the range similar to the crossover curve of Fig. 8.2a.

It was possible to simulate the effects of an arbitrary blurring in a computer experiment. Doses in the interval (0,LT) were selected at random, and then a random Gaussian blurring of known fractional standard deviation (FSD) was simulated. The distribution of the crossover cases and the FSD of the crossover distribution are shown in Table 8.11. Two solutions with very different numbers of samples confirm the good convergence of the process. An FSD of 0.38 in the dose data produced an FSD of 0.31 in the crossovers, approximately that observed in Building A. The distribution of the calculated crossovers was slightly more peaked than the observed result, as shown in the table, and it may be suspected, accordingly, that the pointwise error distribution is more peaked than the standard Gaussian assumed in the simulation. One may also conclude that the FSD of the error distribution is somewhat larger than the FSD of the crossover distribution.

It should be noted that the statistical procedures used in the determination of the LD50 parameter are entirely independent of the analysis shown here. The sole purpose of the present analysis is to provide a basis for evaluating the uncertainty analysis that is to follow.

Table 8.11 Results of a theoretical crossover modeling

	Calculation with 100,000 samples	Calculation with 1,000,000 samples	Observed
FSD of dose data	0.38	0.38	–
FSD of crossovers	0.3083	0.3127	–
Crossovers in range:			
0 – 0.5 FSD	0.4278	0.4246	–
0 – 1.0 FSD	0.7062	0.7049	0.60
0 – 1.5 FSD	0.8872	0.8637	–
0 – 2.0 FSD	0.9458	0.9442	0.90

8.3 COMPARISON WITH OTHER EVALUATIONS

It is possible to compare the observed dose variability with estimates of biological variability alone. Young[38] cites a study by Morris[39] indicating that a 50% random dose error would double the slope of the mortality curve. If we assume that it would similarly double the standard deviation of the composite dose variability, and that random dose error is not correlated with biological variability, then a unique value for the biological variability, 29%, can be calculated. If the composite crossover FSD of 38% as found above for Building A is accepted, removing the 29% biological effect leaves a dose error of 25%. If the data for both buildings are considered together, a dose error of 54% is implied. Of course, these results are directly dependent upon the assumption of biological variability.

8.4 DOSE UNCERTAINTY COMPONENTS

The uncertainty in each individual dose calculation can be considered to be a composite of the following contributions:

- external fluence — the total uncertainty in calculating the fluence at the exterior boundary of the building,
- building transport — the uncertainty in calculating the fluence at an interior point, given the external fluence,
- position — the uncertainty in locating the position of the individual at the time of the attack, and
- response function — the uncertainty in calculating the appropriate kerma, given the fluence and position.

The variability from case to case is affected by building transport errors, location errors, and, to some lesser extent, by the response function errors. It would not be affected by an error in the magnitude of the external fluence, however.

8.5 SOURCE UNCERTAINTY BY COMPARISON WITH INTEGRAL DATA

Science Applications International Corporation (SAIC) has conducted an extensive evaluation of the accuracy of dose calculations in conjunction with their study of personnel in wooden houses at the time of the attack,[6,38,40,41] and this study has included comparisons of various integral activation data with modern calculations. Based on this study, Woolson indicated on 29 October 1986 that an uncertainty of ±15% in integral dose was appropriate for prompt radiation and ±10% was appropriate for delayed radiation.[42] (This is a 1-sigma uncertainty, i.e. at the 67% confidence level, as all uncertainties in this document will be unless otherwise stated.) In a later report, an uncertainty of ±14% was stated for the delayed radiation, together with a 5% bias.[7]

8.6 SOURCE UNCERTAINTY BY ANALYTICAL EVALUATION

An evaluation of prompt dose uncertainty has also been made by Lillie *et al.* by combining the best estimates of the uncertainty in primitive input information, i.e. weapon yield, weapon positioning, air and soil composition, and cross section data, as well as uncertainty in the air transport process.[43] Their paper contained a misinterpretation of weapon yield uncertainty, but Lillie provided a corrected copy of the tables.[44] The corrected data indicated an uncertainty of ±18% at 700 m ground range, decreasing slightly with distance, for the Nagasaki weapon. From this, we estimate 17% uncertainty at the range of the buildings being studied. The good agreement with the SAIC estimate is evident.

8.7 UNCERTAINTY DUE TO THE BUILDING TRANSPORT PROCESS

In a previous section, various tests of the mechanics of the building transport process were discussed. The neutron calculations were found to be quite accurate in comparison with measurements performed on the experimental building. The gamma doses tended to agree within 17% in areas touched by the direct source, although larger errors were noted behind obstacles. The calculation in the experimental building was especially difficult due to direct radiation from the source that reached the building without collision. Because of this, the result was sensitive to the detailed description of the source. At Nagasaki, fluence reaching the building had been repeatedly scattered in air. Thus, it entered the building along many paths and from many directions, representing an easier computational problem. Accordingly, we expect the uncertainty applicable to typical locations in the Nagasaki buildings to be lower.

In the methods comparisons, it was found that the nodal spatial treatment agreed well with the most trusted procedure, the characteristic method. No basis for a numerical error estimate applicable to either method was found, however. The studies of Building A showed that the S_{10} directional quadrature should be used, but those studies, again, did not yield an error estimate. The uncertainty due to the scattering expansion was found to be quite small, since varying it had negligible

effect. The comparison of dose in the center of the A1 building with the Monte Carlo result agreed within 19%, and much of the difference must be attributed to imperfect convergence of the Monte Carlo process.

Some allowance must be made for uncertainty in building construction details, material composition, and moisture content. There is no numerical basis for estimating and combining the several effects, but they would appear to be no more severe in the Nagasaki buildings than in the experimental building. Accordingly, we assume that the 17% experimental value applies to uncertainty at typical locations due to all building transport effects.

8.8 UNCERTAINTY DUE TO PERSONNEL LOCATION

In earlier sections, the uncertainties in the X and Y positions of each case were listed. When the interpolation was performed for each dose component, the uncertainty of that component due to position was also evaluated. If x represents the estimated uncertainty in coordinate X, for example, the doses at $X+x$ and $X-x$ were evaluated. Since these repositionings were equally likely but mutually exclusive events, they were completely correlated. Thus, the absolute value of the deviations in the $+x$ and $-x$ directions from the central value were averaged arithmetically. The Y uncertainty was similarly treated. Since X and Y uncertainties were completely uncorrelated, they were combined by squares. Thus, the information in the main body of the error tables such as 6.6 and 7.6 corresponds to the formulation:

$$U^m(X,Y) = \left\{ \left[|d^m(X+x,Y) - d^m(X,Y)| + |d^m(X-x,Y) - d^m(X,Y)| \right]^2 + \left[|d^m(X,Y+y) - d^m(X,Y)| + |d^m(X,Y-y) - d^m(X,Y)| \right]^2 \right\}^{1/2} \times \left\{ \frac{1}{2d^m(X,Y)} \right\}$$

where

$d^m(X,Y)$ = m^{th} component of dose at location (X,Y), and
$U^m(X,Y)$ = uncertainty in m^{th} component of dose at location (X,Y).

The uncertainty in total dose is found by adding the components linearly:

$$U_i^T = \left\{ \frac{\sum_m U^m(X_i,Y_i) d^m(X_i,Y_i)}{\sum_m d^m(X_i,Y_i)} \right\}$$

where:

U_i^T = uncertainty in total dose at position i

This summing is appropriate, since the position errors for each type are highly correlated; e.g. moving the location away from the window tends to reduce all the doses in a typical situation. It may also be noted that the partitioning into six dose types was somewhat arbitrary, and this type of summing provides a result that is independent of the method of partitioning.

The calculation of a composite uncertainty to represent each building is somewhat arbitrary–neither the sum nor the average of dose over the individual cases is meaningful in this context, and so the uncertainty in those measures is not meaningful. We know intuitively that relative measures of uncertainty should be used in preference to absolute measures, since low doses are as important as high doses in the statistical analysis. Accordingly, the composite value quoted at the bottom of the uncertainty tables is a root-mean-square (RMS) average of the relative errors:

$$\overline{U}^T = \left[\left(\sum_i U_i^T \right) / N \right]^{1/2}$$

where:

$\overline{U}^T$ = composite relative error in the total dose, and

N = number of positions in sample.

As the tables in the previous sections show, the results were 19% for Building A and 10% for Building C. These data reflect the fact that the spatial dose gradients in the vicinity of the personnel in Building C were relatively small. Many of the most uncertain cases in Building A were at the rear of the building, where the gradients were much larger. The positional uncertainty for the composite of all cases was 14%. If the single worst case had been excluded, the uncertainty would have been 13%.

8.9 UNCERTAINTY DUE TO DOSE RESPONSE DETERMINATION

The effect of uncertainty in the FIA response function has been estimated as 2% for gammas and 5% for neutrons.[8] The gamma dose predominates in these calculations, so the 2% value is applicable to the combined total. The internal doses, i.e. the SI and BM doses, are susceptible to other uncertainties, however. The Monte Carlo calculation that resulted in the response functions had statistical convergence on the order of 2%. Uncertainty in modeling the human form apply, and cross section uncertainty is a contributor. This study did not consider the directional asymmetry of organ response, but that is also a significant effect. Reference 7 lists several examples of variation due to horizontal rotation, of which the kerma in bone marrow of a standing male is most applicable to this study. The data listed fall within a range of ±3% for prompt gamma dose and ±5% for delayed gammas. The 1-sigma uncertainty would be less than the complete range of data, of course.

Related studies suggested a 6% uncertainty in dose to the bone marrow due to these various effects,[8] and that value is accepted for use in this study.

8.10 SYSTEMATIC BIAS

Certain systematic features of the calculation could bias the results. For example, the delayed-gamma source, by far the largest contributor to total dose, had numerous false negative values. These were removed during the processing, and this might bias the result upward slightly. The treatment of bone marrow and small intestine dose as isotropic point responses could possibly be a source of bias. It is reasonable to assume that the azimuthal orientation in the horizontal plane would be a random error, as it was treated earlier in this section, but the sensitivity to polar angle, i.e. the angle with the vertical, might be less random. Almost all of the personnel were positioned upright before the shock wave, and the early radiation component reached those personnel from an upward angle. The importance of this polar angle effect is not known.

The importance of a variation of dose with height was explored by a calculation in which the isotropic response was distributed along a vertical plane approximating the size of the torso. This had an entirely negligible effect, indicating that the vertical variation of the dose was adequately represented by a point at midheight. If the true response were found to vary significantly as a function of height, however, the vertical distribution might be significant. Data from which to judge this matter are not available, however.

8.11 OVERALL UNCERTAINTY

The external source uncertainty tends to affect all cases in roughly equal proportion, while the other uncertainties tend to be random effects from case to case. The SI and BM doses involve uncertainties not present in the FIA dose determination. These considerations lead to the summary of Table 8.12, listing first, the composite case-to-case uncertainty, and then the overall uncertainty. The individual uncertainties have been combined as uncorrelated errors.

Assuming that the "SI or BM" uncertainty best represents the uncertainty in the mortality risk, we can compare the random uncertainty estimate, 23%, with the dose variability deduced from the crossover analysis. The uncertainty estimate is in excellent agreement with the 25% variability deduced for Building A. The variability deduced for the combination of Buildings A and C, however, is significantly larger.

Table 8.12 Overall dose uncertainty (%)

	FIA dose	SI or BM dose
Random uncertainty		
Building transport process	17	17
Personnel location error	14	14
Dose response, including orientation effects	2	6
Total random uncertainty	22	23
Correlated uncertainty		
External Source	20	20
Overall uncertainty		
Composite	30	30

Note: These uncertainties combine as squares, since they are statistically independent.

9. SUMMARY AND CONCLUSIONS

The objective of the effort was to determine the radiation doses to occupants of two reinforced concrete buildings during the World War II nuclear attack on Nagasaki, and that objective was accomplished. Previous work had determined the fluence in the vicinity of the buildings. A parallel effort determined the locations of the occupants and the physiological consequences of the radiation exposure. This study constructed radiation models of the buildings, calculated the radiation inside the buildings, and determined the dose to each occupant. Future studies are to derive a new value of the LD50 dose from these data.

The dose calculation centered about a three-dimensional discrete ordinates code, TORT, constructed especially for this study. The validity of TORT was tested in comparisons with various alternate methods of calculation and with an experimental simulation of the concrete buildings. Various internal parameters and procedures were compared in order to find the most suitable combinations.

The construction of analytical models of the buildings was particularly difficult, since the buildings were heavily damaged by the attack and were later demolished. Various post-war records and photographs were pieced together to form the best composite. Of all the details, the size and position of the windows were the most important, and the existence of high-quality glossy photographs was particularly important.

In this report, preliminary analysis of the data, especially the relationship of fatality to dose received, indicates general validity of the results and provides an indication of the composite effects of random error in the dose calculation and variability in the biological response. Using an estimate of the biological variability, a value for the observed random dose error was isolated. The value was 25% for Building A alone, but it increased to 54% when both buildings were combined, due to systematic differences in the results.

An uncertainty analysis indicated random case-to-case uncertainties of 22% in FIA dose and 23% in SI or BM dose. Including the consistent 20% uncertainty in the external fluence gave overall uncertainty of 30% for all dose types. The use of numerous cases in deducing a single parameter like the LD50 would mitigate the effect of the random component, of course, driving the persistent error toward the 20% value.

10. ACKNOWLEDGEMENTS

The authors wish to acknowledge the special contributions of R. W. Young, Defense Nuclear Agency, for his patient support of this project; of R. L. Stohler, Dikewood Division, Kaman Sciences, for his extraordinary help in locating building construction details and personnel locations; of S. N. Cramer, ORNL, for his assistance in locating construction details and in performing several Monte Carlo calculations to be compared with these results; of J. C. Ryman, Martin Marietta Energy Systems, Inc., for the appendix describing his response functions; and of the numerous others cited as individuals in the references for their comments and unpublished memoranda used in this study. The contributions of A. C. Alford and S. A. Raby in preparing the manuscript are also acknowledged.

APPENDIX A
BUILDING A MODEL CONSTRUCTION

The main source of information used for our modeling of Building A was a report compiled by the United States Strategic Bombing Survey, (USSBS) Physical Damage Division.[1] Figure 17 of this reference shows the construction of the building. The reference also includes 29 photographs of the building. Glossy prints of these photographs are available in ORNL files,[36] and they provide better detail. The files also contain sketches of the internal layout of the building, apparently the result of the USSBS study. Additional USSBS information is found in the "Building and Protection Studies" section of Ref. 2. The ORNL files also contain unpublished case histories and blueprints assembled in conjunction with the Atomic Bomb Casualty Commission (ABCC) study.[3] Both the blueprints and case histories contain considerable architectural detail. Unfortunately, the information is often contradictory and in disagreement with USSBS information. The USSBS photographs often settle the issue in favor of their descriptions. Thus, the USSBS information is considered the more reliable in cases of conflict. Stohler[13] provided several sketches of the internal layout from Dikewood files, and these were in good agreement with the ORNL sketches.

Figure A.1 shows a drawing of the north portion of the building. The building center is at the center of the outset seen at the left of the figure. The dimensions, based on Ref. 1, are assumed to refer to the centers of the reinforced concrete columns and to the outside of the 10-inch reinforced concrete walls. The dimensions for the south end of the building are the same as those for the north end, with the overall building size being 55 feet by 228 feet (17 m $\times$ 70 m).

All floors in the model are 5-inch reinforced concrete slabs.[1] The surface of the first floor is assumed to be 2 feet above ground level. Penetrations for stairways are ignored. An auditorium at the north end of the third floor extends upward past the fourth floor to the roof. The basement extends under only the central portion of the building. The distance between floors is 11.5 feet.[1] The distance from the top of the fourth floor to the top of the roof is also represented as 11.5 feet. Reference 1 indicates that this distance was 13.5 feet, but photographic evidence indicates otherwise. Reference 1 indicates that the steel trusses over the auditorium were above the fourth floor windows, while photographs show that the trusses and windows overlapped. The fact that the fourth floor was demolished by the shock wave may account for the apparent inaccuracies in the generally-reliable USSBS data.

In the south part of the fourth floor, a ceiling is placed 8 feet above the floor. It is assumed arbitrarily to be equivalent to 1 inch of wood. The wooden fourth-floor posts are extended above the ceiling to the roof in lieu of detailed information about the wooden roof trusses in that area. The roof above the auditorium is represented as 2 inches of concrete, while the rest of the roof is represented as 2 inches of tile having the compositon of earth.[2] A 3-foot parapet having the same thickness as the outer walls extends above the roof level on all sides, making the overall building height 49 feet (15 m) above the first-floor surface. The front entrance to the building is located in an architectural outset shown in Fig. A.1. This detail

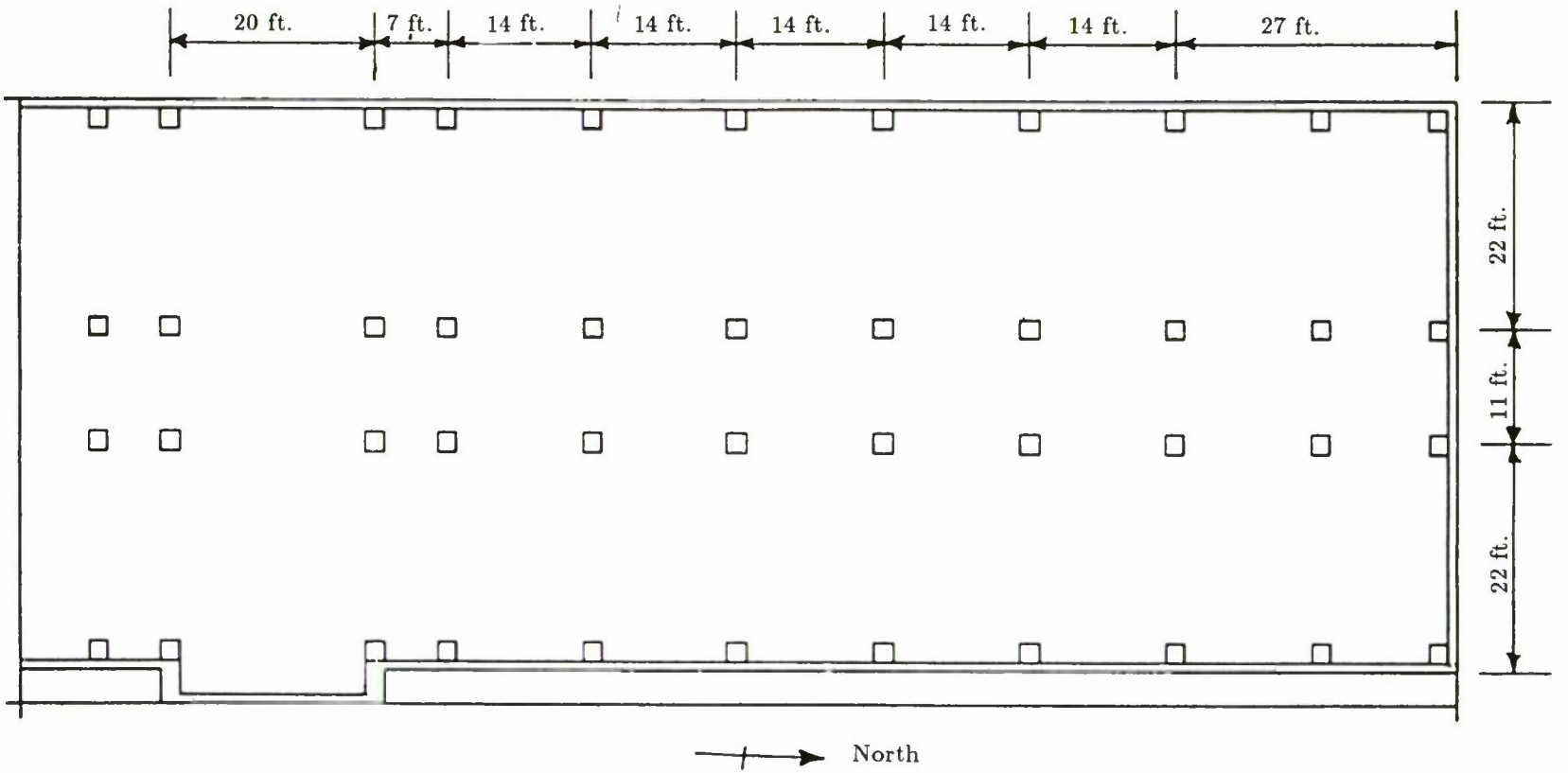

Figure A1. Building dimensions.

is included because satisfactory modeling of this area is needed to represent the radiation environment of the people in the basement. The short walls at the side of the outset are included in a zone 22 inches wide, but a density factor reduces the effective thickness to 5 inches.

The largest concrete columns were 23 inches by 30 inches, while the wooden posts were only 8 inches by 8 inches. In order to conserve mesh intervals, all columns and posts in the building are represented by zones 22 inches by 22 inches in horizontal dimension. Density factors are used to place the correct amount of material in the zones.

The building had three different sizes of reinforced concrete beams. These were 10 inches wide by 14 inches high (unhaunched), 13 inches by 20 inches (haunched), and 13 inches by 18 inch (haunched). In our model, all beams are represented in zones 19 inches high. The beams that attach to columns are represented in the column zone width, 22 inches, while the 10-inch-wide beams are represented in their true width. Density factors are used to adjust to the correct amount of material. At the intersection of 10-inch by 14-inch beams and 13-inch by 20-inch beams, the larger beams actually continue through. In our model, however, 10-inch by 14-inch beams continue through the larger beams, since they have a higher density factor. This is not considered an important issue, however. The beams and columns in our model are shown in Figs. A.2 through A.5. The 10-inch by 14-inch beam centers are assumed to be equally spaced between the centers of the central columns and the outside of the external walls. The steel lattice supporting the roof of the auditorium has been omitted from our model, since its construction is so open as to offer little obstruction to radiation.

Figures A.6 through A.10 show floor plans for the building, while Figs. A.11 through A.15 give some additional dimensions. Reference 1 gives a height of 7 feet for windows on the first three floors and in the basement, and Ref. 2 indicates a height above the floor of 1 m. The model uses dimensions based on scaling of several photographs, however. The windows on the first three floors are 6.25 feet high and 3.25 feet above the floor. The tops of the windows are aligned with the bottoms of the beams in our model. On the fourth floor, the windows are 3 feet 10 inches high.[1] In our model, these windows are aligned with the 8-foot ceiling, making the bottoms of the windows 4 feet 2 inches above the floor. Tests showed the size and location of the windows to be one of the most important parameters in the modeling.

The ABCC blueprints indicate two types of interior walls, heavy concrete walls and light-construction walls similar to U.S. home construction. The light walls, constructed of metal or wooden lath and plaster, were destroyed by the blast and fire. These light walls are assumed to be equivalent to 1.12 cm of plaster and 3.0 of wood, based on data from Kerr.[35] They are the walls cross-hatched in the plan views.

The blueprints indicate that a large number of the thick walls were located throughout the building. The heavy walls are taken to be 5.5 inches of concrete, and we concluded that a 5.5-inch wall would not disappear without leaving sections that would be visible in the photographs. The internal basement walls can be seen in the USSBS photographs to have survived intact, and they were accepted

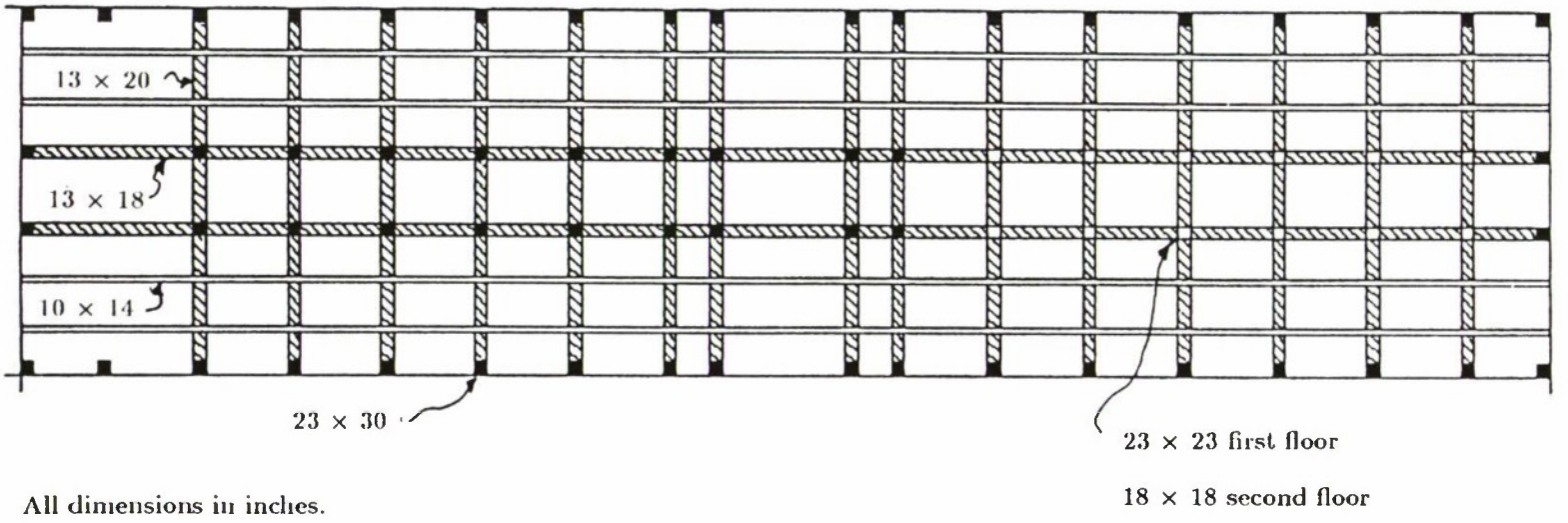

Figure A.2 Columns and beams on the first and second floors (supporting the second and third floors).

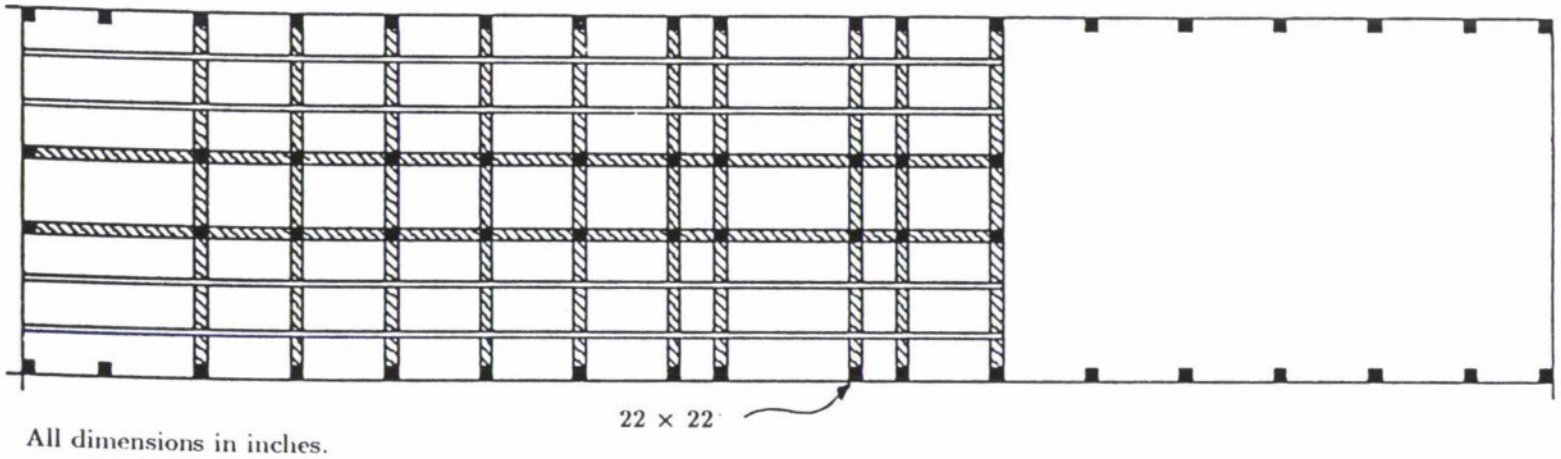

Figure A.3 Columns and beams on the third floor (supporting the fourth floor).

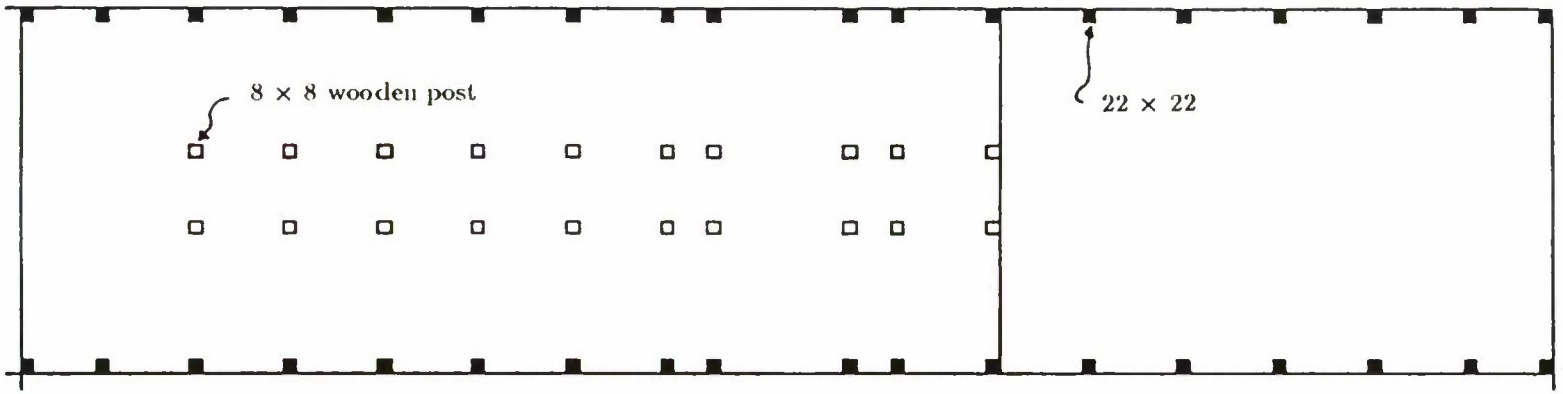

All dimensions in inches.

Figure A.4 Columns and posts on the fourth floor.

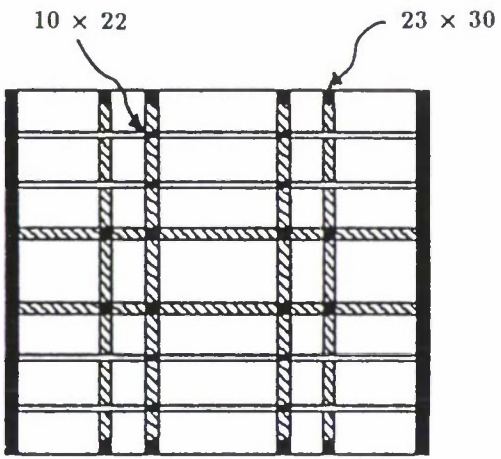

All dimensions in inches.

Figure A.5 Columns and beams in the basement (supporting the first floor).

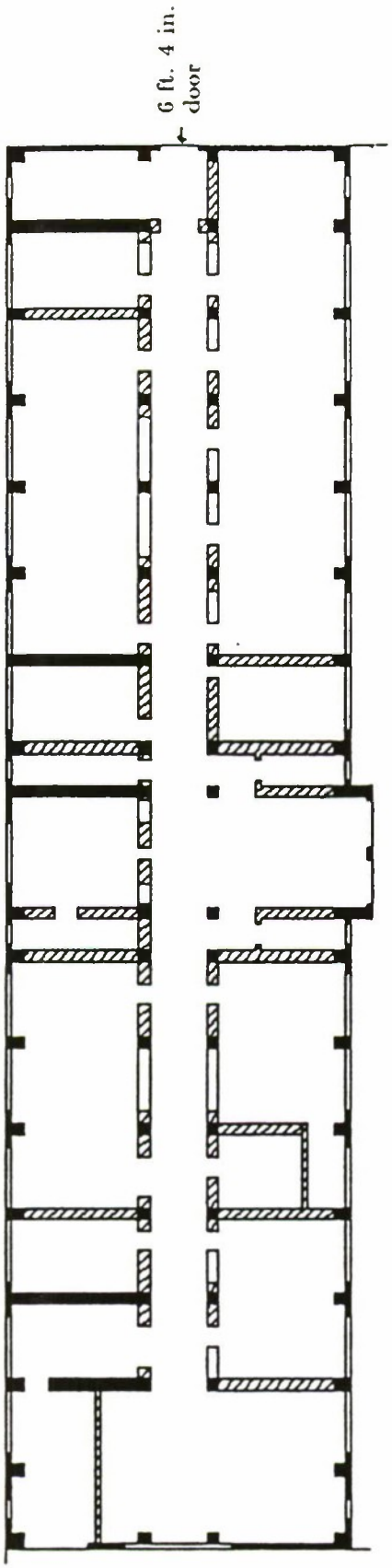

Figure A.6 First floor plan.

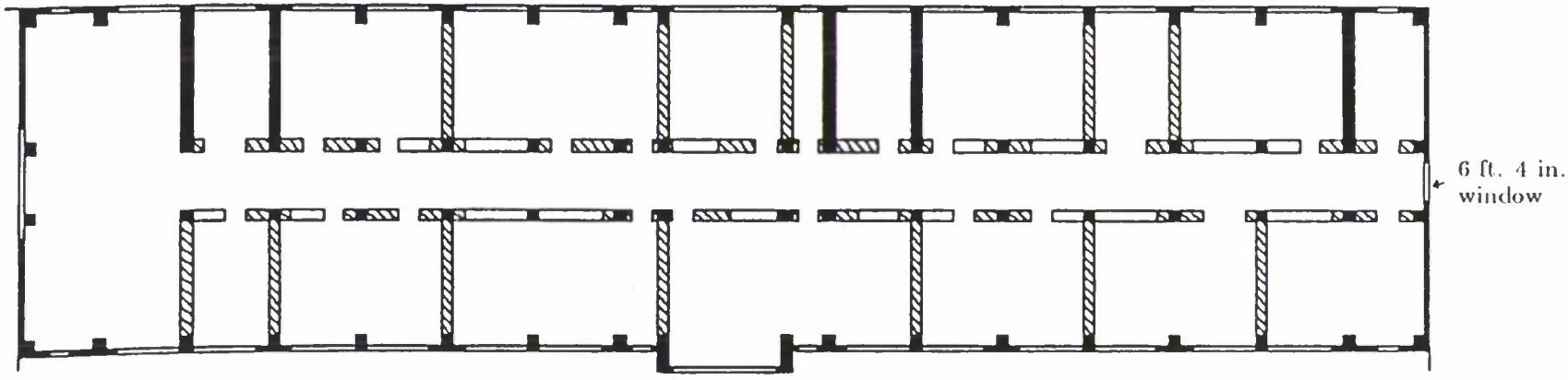

Figure A.7 Second floor plan.

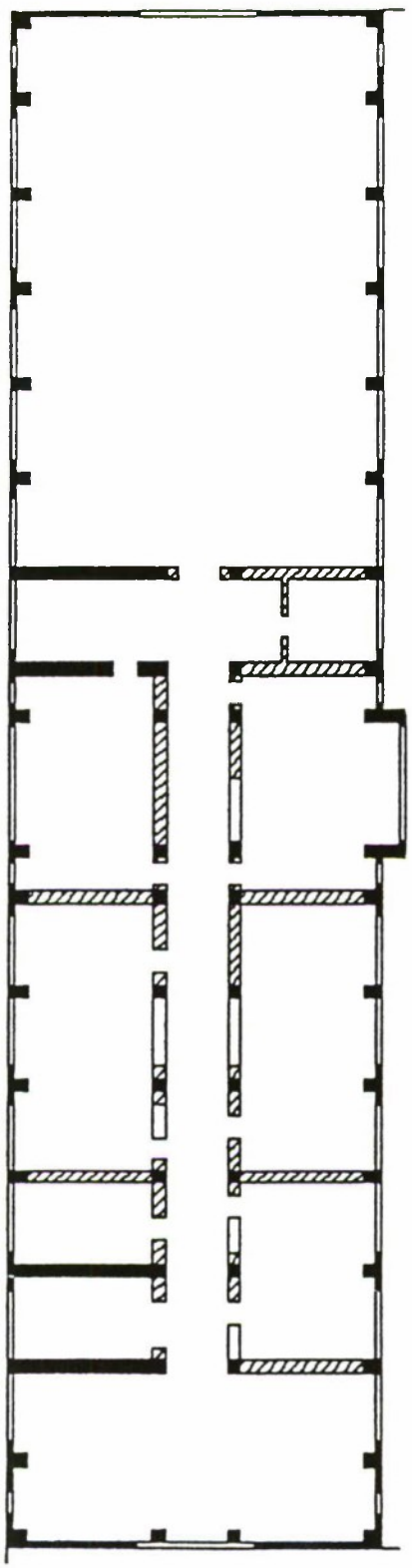

Figure A.8 Third floor plan.

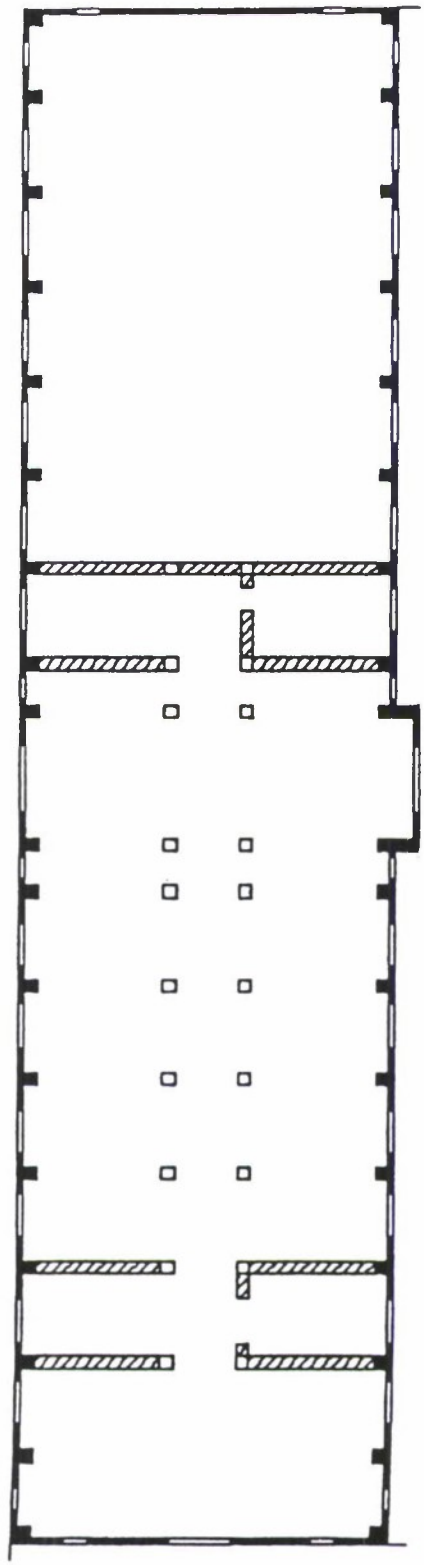

Figure A.9 Fourth floor plan.

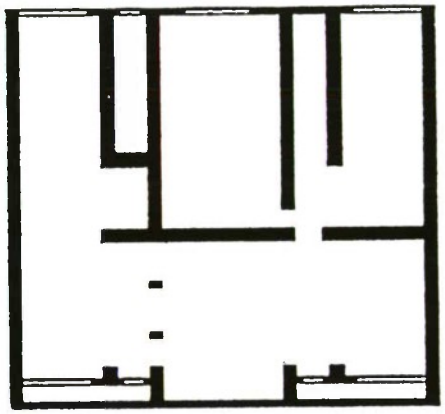

Figure A.10 Basement plan.

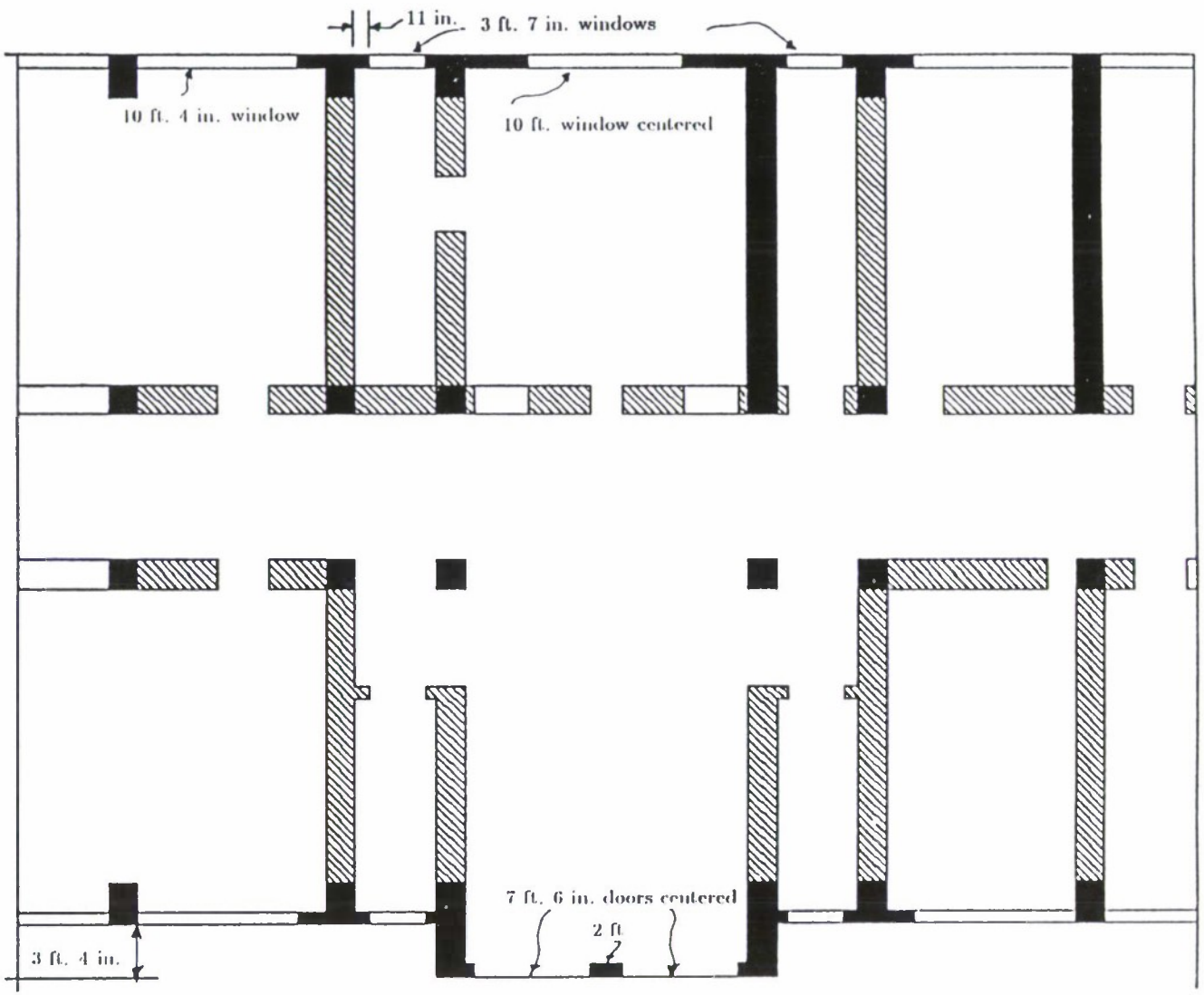

Figure A.11 Dimensions for the first floor-center.

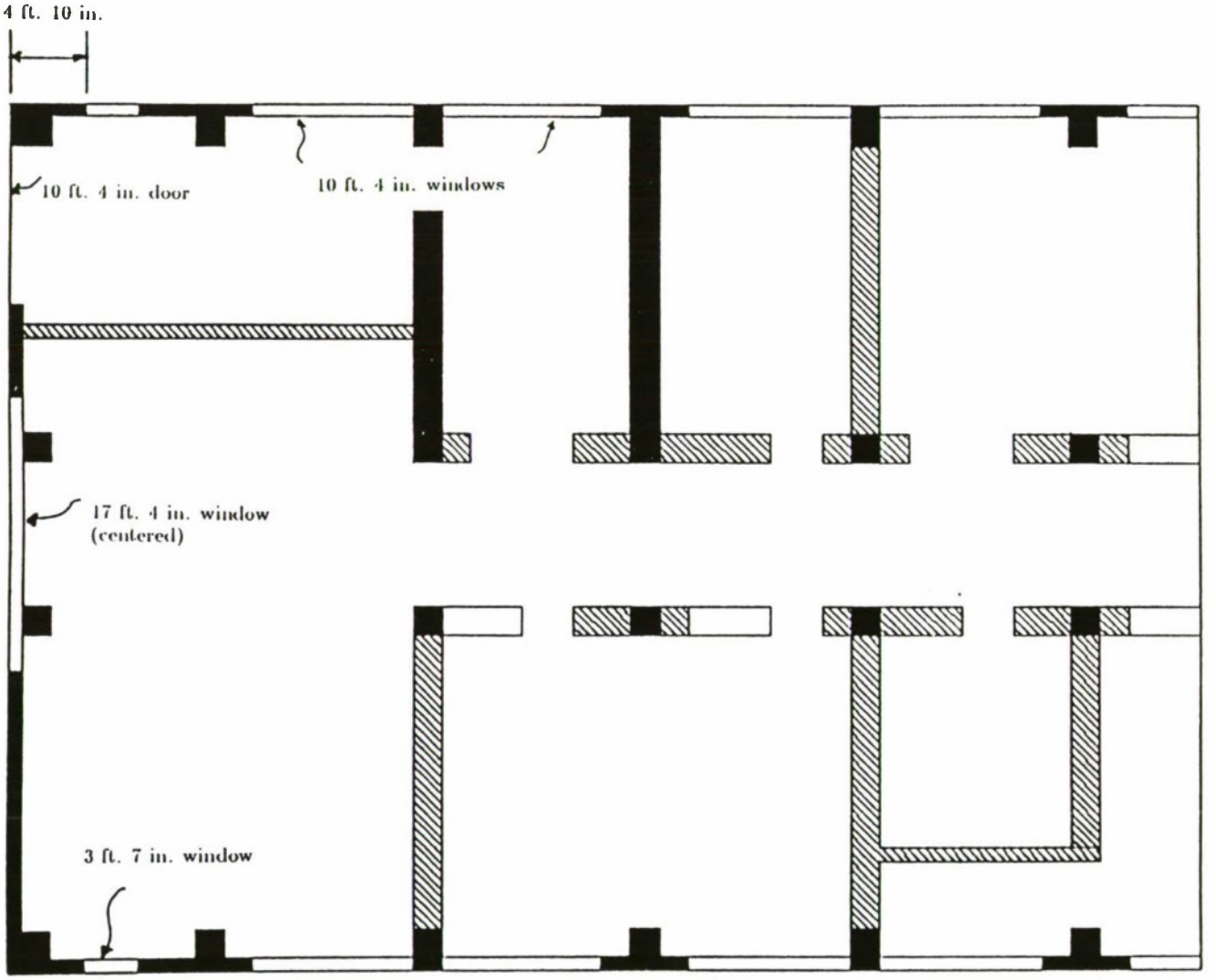

Figure A.12 Dimensions for the first floor–south end.

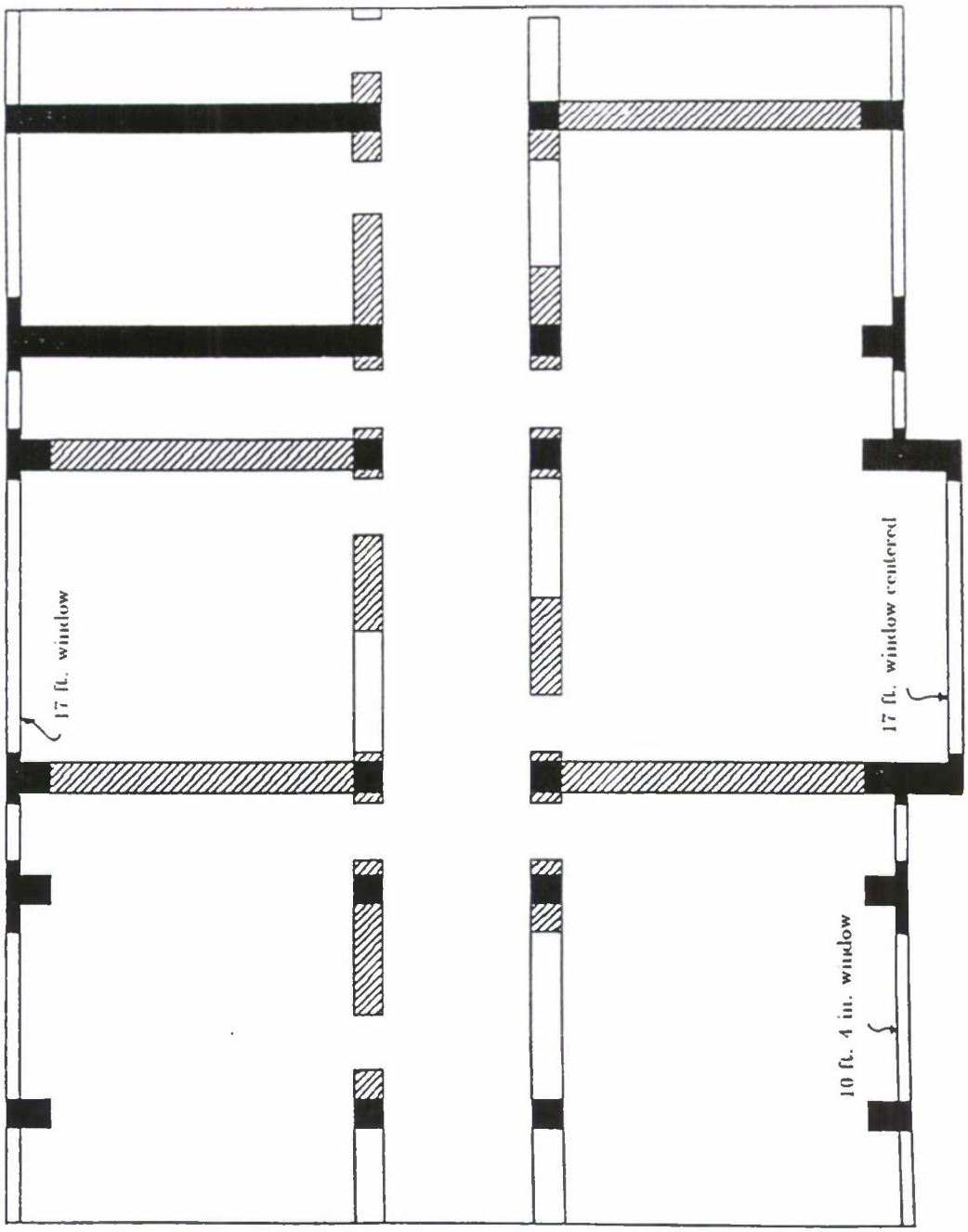

Figure A.13 Dimensions for the second floor.

Figure A.13 Dimensions for the second floor.

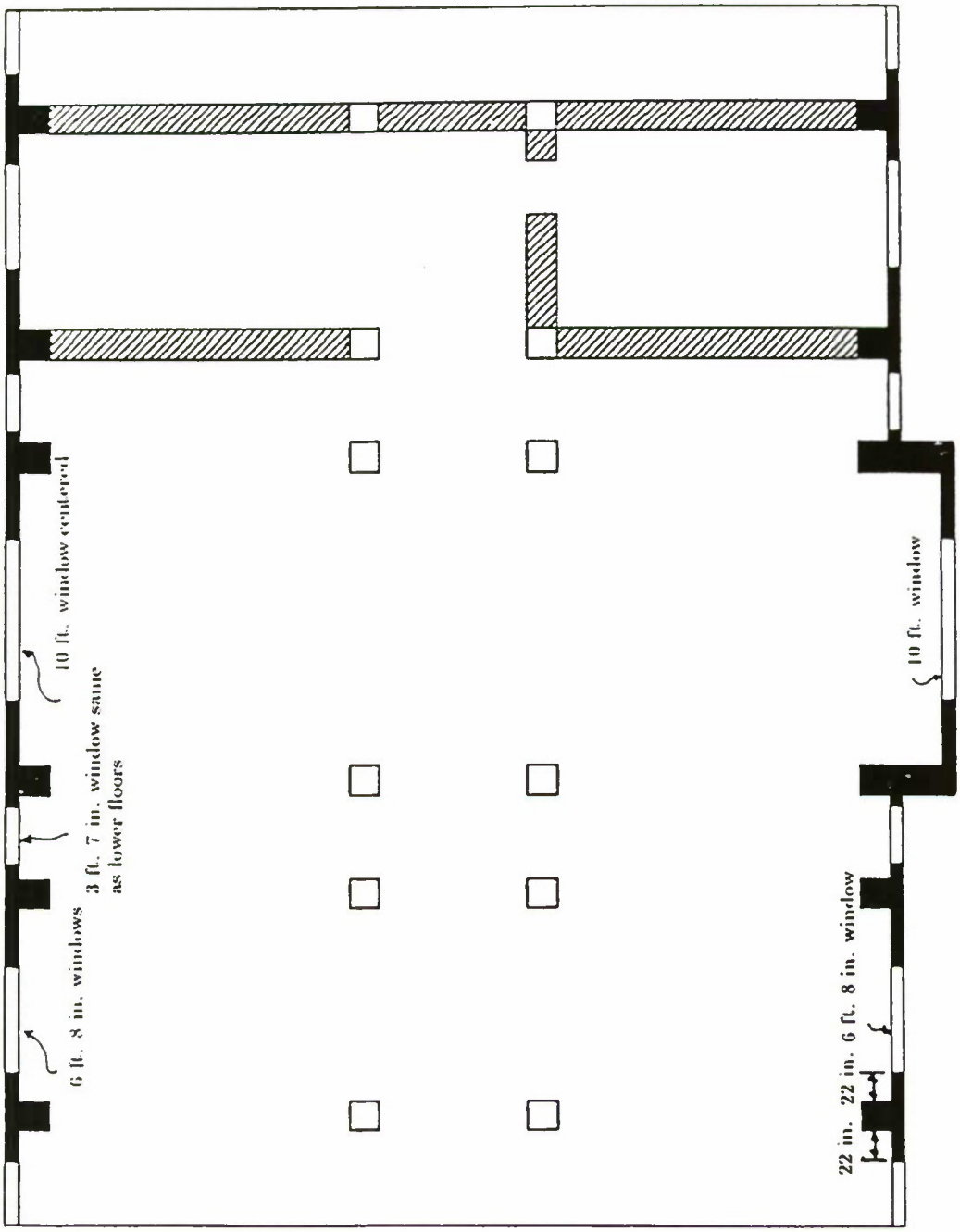

Figure A.14 Dimensions for the fourth floor–center.

Figure A.14 Dimensions for the fourth floor–center.

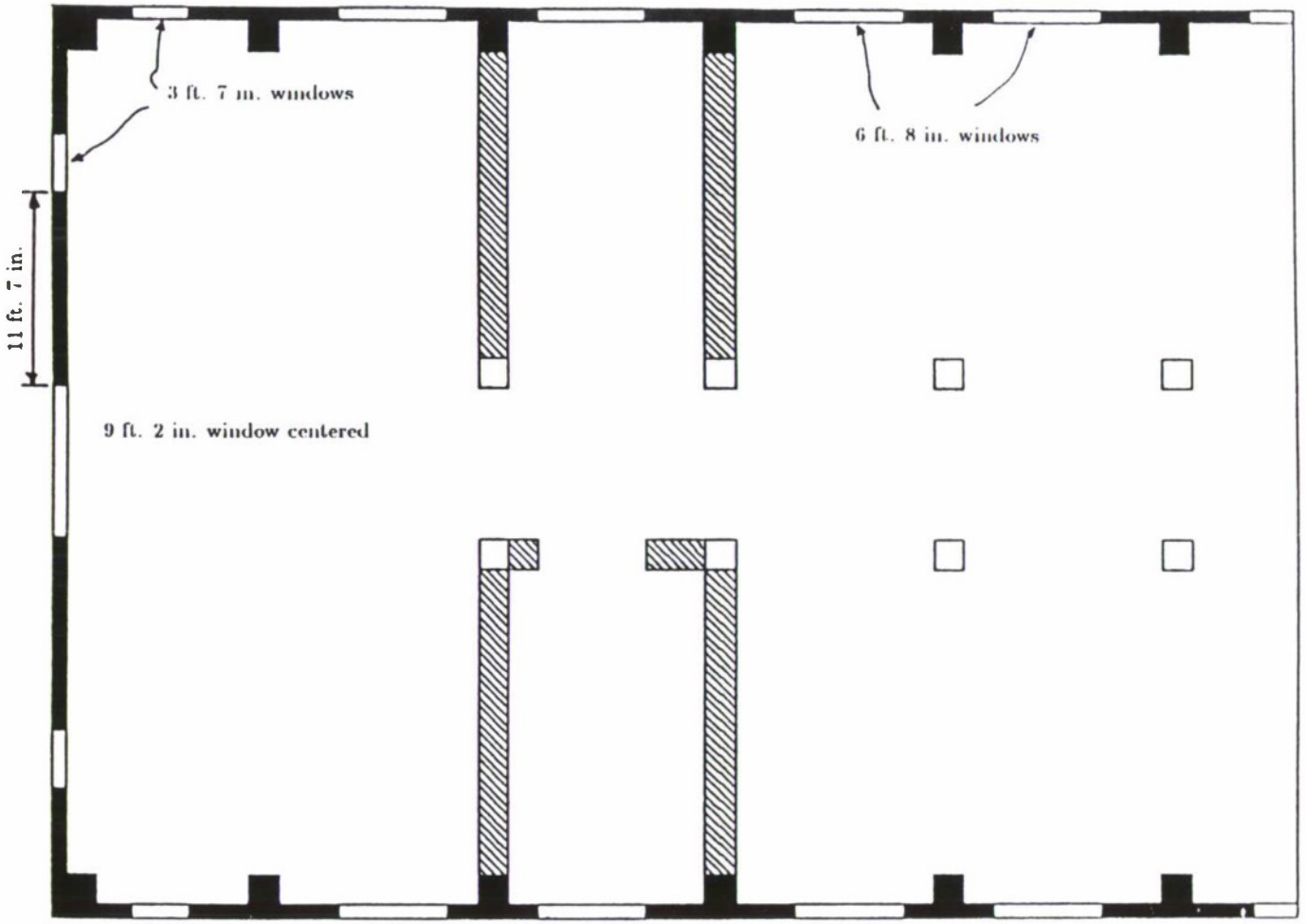

Figure A.15 Dimensions for the fourth floor–south end.

as heavy construction. Above the basement, however, only internal walls at the stairwells remain in the photographs. Accordingly, they were assumed to be heavy construction, while the others were assumed to be of the light construction. The heavy concrete walls are shaded dark in the plan views, as are the outer walls and the columns.

The interior wall layouts represented a composite of all of the information sources, with dimensions based on the USSBS report. The interior walls are located in the same mesh intervals that described the pillars, with appropriate density factor adjustments. The doors and windows in the interior walls, based on the ABCC blueprints, are quite approximate, using only the mesh required for other purposes. All door tops are aligned with the tops of the windows. Both interior and exterior door and window locations are filled with air in our model, ignoring glass and wood material that might be present.

The basement wall layout generally follows the ABCC blueprint, except for a wall extending westward from the north edge of the doorway outset. This wall was not shown in the other data sources, and a photograph of the area indicates conclusively that it was not present. The windows and doors shown by the blueprint in the west wall are not consistent with the photographs, and they were revised accordingly.

The first floor layout generally followed the blueprint, except that an open machine room in the northeast quadrant, in which several persons were located, is not in the blueprint. It was added, based on the other data sources. It was similarly necessary to adjust the second-floor blueprint layout using the USSBS and Stohler sketches, in order to eliminate conflicts between room layout and locations reported by the case histories. The third and fourth floors were based on the sketches.

APPENDIX B
BUILDING C MODEL CONSTRUCTION

The main sources of information used for the modeling of the structure of Building C were a report by the United States Strategic Bombing Survey (USSBS) Physical Damage Division[1] and associated ORNL photographs. One photograph from Ref. 37 was also helpful. Only Building 2, the southmost building of the complex, was modeled, since all of the cases of interest to this study were located there. Figure 7.2 shows a perspective view of the model.

Figure B.1 shows a plan view of the building and some dimensions from Ref. 1. Only the passageway to the north wing and the southmost wall of that wing were included in the model. The two external stairwells on the north side of the building were modeled, although the stairways inside were not. All of the dark walls in Fig. 2 are 12 inches thick. All structural components in the model are reinforced concrete. The overall size of the building, exclusive of stairwells and passageway, was 31 feet by 185 feet (9 m by 56 m).

The roof and floors were 5.5-inch slabs resting on a structure of concrete beams, girders, and columns. The distance from the top of the first-floor slab to the top of the second-floor slab was 12.5 feet. For the second and third floors, the heights were 12 feet and 13.5 feet, respectively. A 3.5-foot parapet wall 9 inches thick rose above the roof, making the building height 42 feet (13 m) above the first floor surface. The first floor surface was assumed to be at an elevation of 2 feet above ground level. Reference 3 gave conflicting values of 8 inches and 4.5 inches for the wall and floor thicknesses, respectively, and this was repeated in Ref. 45. The USSBS value was retained due to the general reliability of their information, however.

The interior columns in the building were 12 inches square on the third floor and 13 inches square on the second floor. We are primarily interested in these floors, since no cases of interest were on the first floor. In order to simplify the mesh, all interior columns are modeled as 12 inches by 13 inches, as shown in Fig. B.2.

The roof slab was supported with 12-inch-wide by 14-inch-high transverse beams and 12-inch by 21-inch longitudinal girders, while the third floor slab was supported by 13-inch by 13-inch beams and 11-inch by 19.5-inch girders. This was simplified in the model, making all beams and girders the same width as the pillars shown in Fig. B.2. The height of the beams and girders supporting the roof was modeled as 17.5 inches, while the height of the second- and third-floor supports was modeled as 16.5 inches.

The sizes and locations of the windows and doors, shown in Figs. B.3 and B.4, were estimated from photographs. All windows were modeled with a height of 7 feet. On the first and second floors, the tops of the windows were aligned with the bottoms of the beams. On the third floor, a 17-inch gap was placed between the beams and the windows because the third floor had a false ceiling. The doors on the second and third floors are the same height as the tops of the windows, while the doors on the first floor are 8 feet high. A photograph of the west wall indicates that it did not have windows or doors, and it was so modeled. No comparable

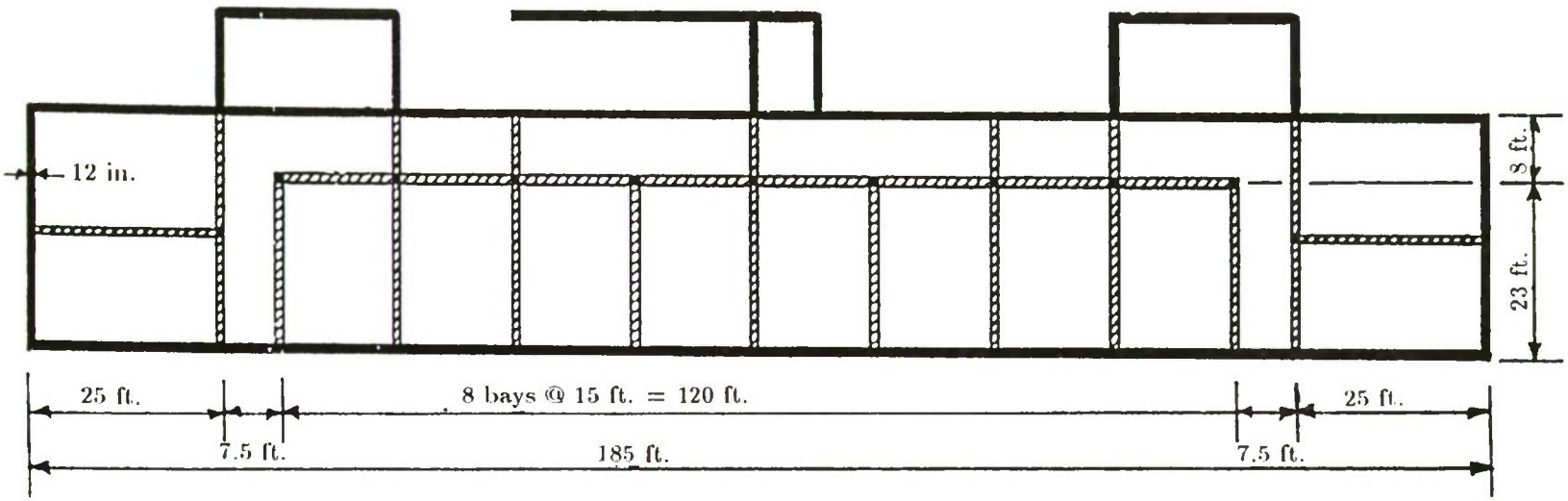

Figure B.1 Plan view with overall dimensions.

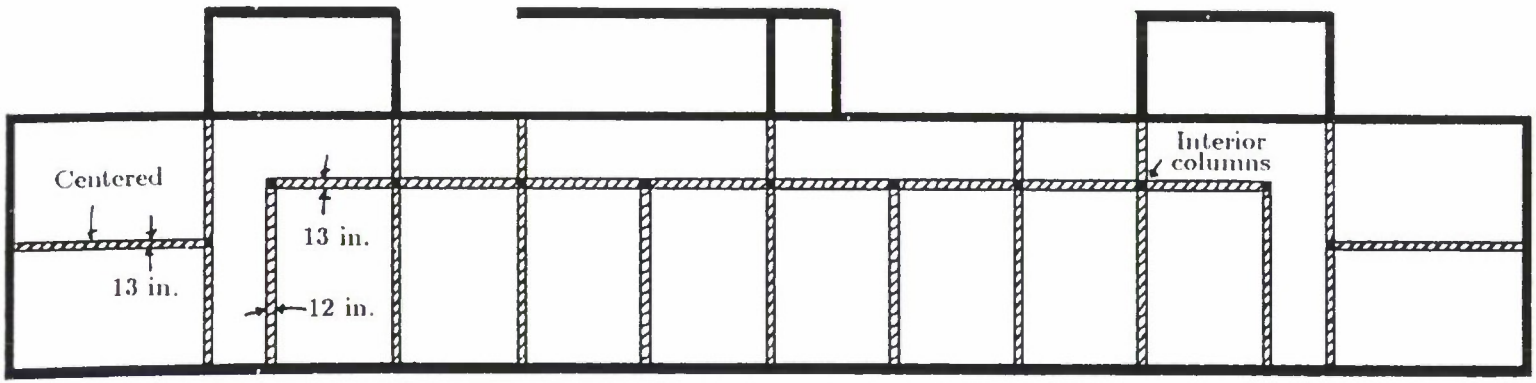

Figure B.2 Beams and interior columns.

information was found concerning the east wall, however. Photographs taken soon after the attack indicate that it was blown away by the direct impact of the blast, and later, the entire east end of the building collapsed. For this purpose, the east wall was modeled as identical to the west wall.

The interior walls shown in Figs. B.3 and B.4 are represented in zones the same thickness as the beams, but their density factors adjust the amount of material to match the light-wall construction of Building A. Their locations are based on sketches from the ORNL files and from Stohler.[13] ABCC shielding summaries also gave some internal details, but they were not a consistent or reliable source of data. Nothing is known about interior windows or doors, and no attempt was made to model them.

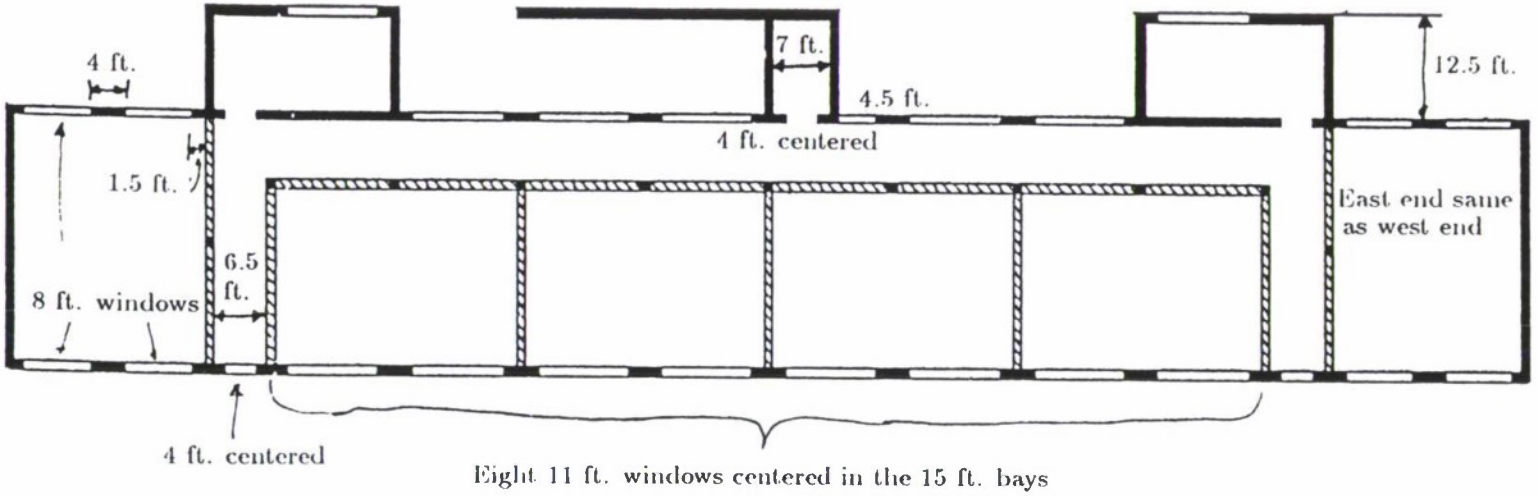

Figure B.3 Window and door locations for second and third floor.

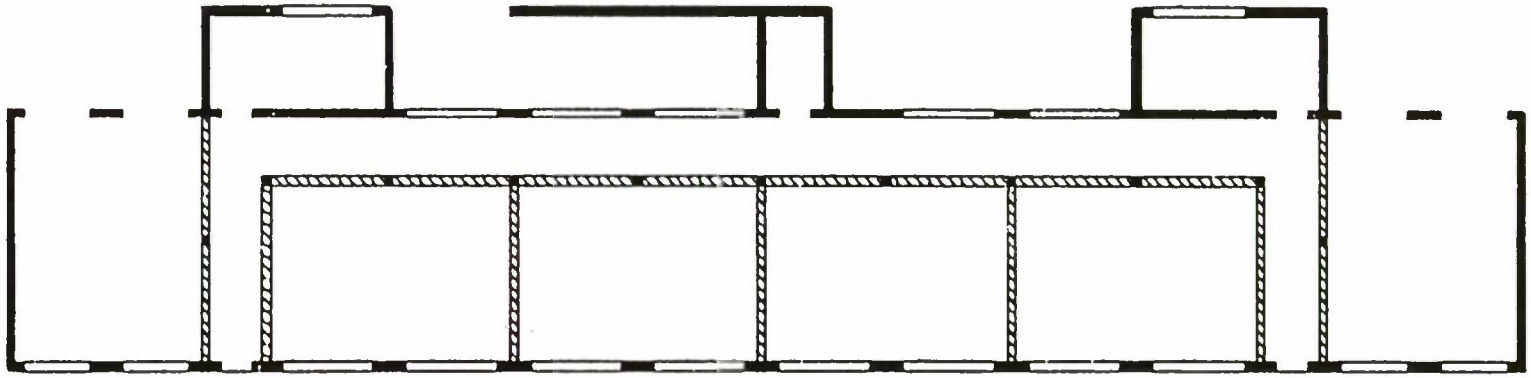

Figure B.4 Window and door locations for the first floor.

APPENDIX C
SELF-SHIELDED FLUENCE-TO-DOSE CONVERSION FACTORS FOR THE SMALL INTESTINE AND ACTIVE MARROW OF A 57 KG HUMAN PHANTOM

Contributed by J. C. Ryman[12]

Self-shielded fluence-to-dose conversion factors for both neutron and gamma-ray exposure have been developed for the small intestine and active marrow of a 57-kg human phantom[46] nominally representing a Japanese adult. The conversion factor for the small intestine (averaged over the wall and contents) should be useful for estimating a mid-line dose. The conversion factors were computed both for the VITAMIN-E group structure [47] (174 neutron and 38 gamma groups) and for the new Defense Nuclear Agency (DNA) library broad group structure[48] (46 neutron and 23 gamma groups).

The conversion factors were derived from adjoint Monte Carlo transport calculations using a modified version of the MORSE-SGC/S code[49] which incorporates the phantom geometry, a fictitious scattering model, and some in-group energy biasing techniques developed by SAIC.[50] In each transport calculation, an adjoint neutron or gamma-ray source uniformly distributed in either the small intestine or active marrow was selected uniformly from the VITAMIN-E neutron or gamma-ray group structure. For each calculation, a leakage file was written in which leakage coordinates, direction cosines, and leakage group were saved for each leakage particle as well as the source group for the particle or its adjoint parent.

The next step of the conversion factor calculations used an unpublished folding code which coupled the adjoint Monte Carlo leakage data to forward DOT-IV[10] angular fluence data. The angular fluence data had been processed by the JPVISA code,[51] a modified version of the VISA code from the Vehicle Code System.[25]

The basic quantity computed by the folding code is the fluence in detector group g_d at the organ of interest caused by the incident angular fluence in group g_s at a coupling surface surrounding the phantom. Specifically,

$$\overline{\Phi} = \int_{A_s} dA \int_{\hat{n}\cdot\overline{\Omega}} d\overline{\Omega}\; J^*_{g_d g_s}(\bar{r},\overline{\Omega})\; \Phi_{g_s}(\bar{r},\overline{\Omega})\;, \tag{1}$$

where

$J_{g_d g_s}$ = the adjoint leakage current in group g_s due to an adjoint source in group g_d,
Φ_{g_s} = the forward fluence incident on the coupling surface A_s, and
$\hat{n}$ = the outward normal to the coupling surface.

If the incident fluence is isotropic, it is easy to see that the fluence term comes outside the innermost integral of the Eq. (1). Furthermore, if one assumes the phantom does not perturb the external radiation field, the fluence at a point can be

used. Then, the fluence term also comes outside the area integral over the coupling surface to give

$$\overline{\Phi}_{g_s g_d} = \frac{\Phi_{g_s}(\bar{r}_d)}{4\pi} \int_{A_s} dA \int_{\hat{n}\cdot\overline{\Omega}} d\overline{\Omega} J^*_{g_d g_s}(\bar{r}, \overline{\Omega}) \,. \tag{2}$$

The fluence in detector group g_d due to a unit fluence incident on the phantom in group g_s is just

$$\frac{\overline{\Phi}_{g_s g_d}}{\Phi_{g_s}(\bar{r}_d)} = \frac{1}{4\pi} \int_{A_s} dA \int_{\hat{n}\cdot\overline{\Omega}} d\overline{\Omega}\, J^*_{g_d g_s}(\bar{r}, \overline{\Omega}) \,. \tag{3}$$

Thus, for isotropic exposure of a phantom which does not perturb the external radiation field, the organ fluence due to a source in a given incident group depends only on the adjoint leakage current.

In this work, the adjoint leakage current from an upright phantom was folded with the DOT-IV fluence 1 m above the surface at a radial distance of 700 m from the Nagasaki atomic bomb detonation. This was done for convenience, since the original folding code was designed to couple with DOT-IV fluence data, but the results are independent of the phantom orientation and external fluence.

The organ dose in group g_d due to an incident fluence in group g_s is given by

$$\overline{D}_{g_s g_d} = \overline{\Phi}_{g_s g_d} R_{g_d} \,, \tag{4}$$

where R_{g_d} is the response per unit fluence for group g_d.

The dose to all detector (organ) groups due to an incident fluence in group g_s is just

$$\overline{D}_{g_s} = \sum_{g_d} \overline{D}_{g_s g_d} = \sum_{g_d} \overline{\Phi}_{g_s g_d} R_{g_d} \,. \tag{5}$$

The self-shielded fluence-to-dose conversion factor for fluence incident in group g_s is

$$R_{g_s} = \frac{\overline{D}_{g_s}}{\Phi_{g_s}(\bar{r}_d)} \,, \text{ or} \tag{6a}$$

$$R_{g_s} = \sum_{g_d} R_{g_d} \left[\frac{1}{4\pi} \int_{A_s} dA \int_{\hat{n}\cdot\overline{\Omega}} d\overline{\Omega}\, J^*_{g_d g_s}(\bar{r}, \overline{\Omega}) \right] \tag{6b}$$

For convenience, the quantity actually scored by the folding code (due to its original design) is $\overline{D}_{g_s}$. The Monte Carlo estimates of $\overline{D}_{g_s}$, the associated fractional standard deviations, and the incident fluences are written to a data file for further analysis.

These data are written separately for direct neutron dose, for autogamma dose [dose due to (n,γ) reactions within the phantom], for gamma dose due to the primary gamma rays at Nagasaki, and the gamma dose due to the secondary gamma rays at Nagasaki. Again, the use of all these data files is a consequence of the original design of the folding code.

An auxiliary program was written to combine the direct neutron dose and the autogamma dose to yield the total neutron dose. Another auxiliary program was used to compute the fine-group and broad-group conversion factors for the total neutron dose and for the gamma dose. The gamma dose was computed using both the primary and secondary gamma fluence from the DOT-IV Nagasaki calculations. The results were the same, verifying the independence of the conversion factors from the fluence used for the folding.

The fine-group organ dose response functions were computed with the VEL module of the AMPX cross-section code system,[52] using a flat flux weighting function. The point response function data input to the VEL module were as follows. Soft tissue response functions were used for the small intestine. The gamma soft tissue response was a dose response computed from the mass energy-absorption coefficients of Hubbell[53] and the total soft tissue composition of Kerr.[19] The neutron soft tissue response was a kerma response computed from the kerma factors of Caswell, Coyne, and Randolph[54] and the bulk (total – lung) soft tissue composition of Kerr.[19] The neutron and gamma active marrow responses were dose responses from Kerr and Eckerman,[55] who derived the responses from Monte Carlo calculations based on measured pathlength distributions in bone marrow. It should be noted that the skull red marrow has a different response than the remainder of the red marrow. A separate MORSE calculation was made for each marrow response function, followed by a separate folding run for each. An auxiliary program combined the marrow doses for the skull and other marrow using a mass weighting.

The self-shielded fluence-to-dose conversion factors are shown in Tables C-1 to C-8. The fractional standard deviations were estimated by propagation of error from the individual folding code runs. The groups with no values are due to the fact that the DOT-IV calculations for the Nagasaki weapon had no source in those groups. With no fluence in those groups, the folding code could not estimate a dose. Since the conversion factors do not depend on dose, this problem will be fixed in a future version of the folding code.

Table C-1. Fluence-to-dose conversion factors for small intestine for the gamma groups of the VITAMIN-E group structure

Group	Conversion factor (Gy/(#/cm^2))	(FSD)[a]
175	0.0	(0.0)
176	2.54437E−11	(0.021)
177	2.17819E−11	(0.025)
178	1.80636E−11	(0.020)
179	1.60993E−11	(0.023)
180	1.51869E−11	(0.020)
181	1.39337E−11	(0.020)
182	1.36722E−11	(0.018)
183	1.28657E−11	(0.026)
184	1.20975E−11	(0.019)
185	1.11520E−11	(0.021)
186	1.00856E−11	(0.021)
187	9.07689E−12	(0.023)
188	8.33114E−12	(0.021)
189	7.08459E−12	(0.020)
190	6.17101E−12	(0.020)
191	5.10822E−12	(0.026)
192	4.40563E−12	(0.022)
193	4.05948E−12	(0.025)
194	3.47112E−12	(0.025)
195	2.63700E−12	(0.016)
196	2.29586E−12	(0.022)
197	1.92595E−12	(0.022)
198	1.59832E−12	(0.026)
199	1.52857E−12	(0.021)
200	1.40811E−12	(0.020)
201	1.21322E−12	(0.024)
202	9.96423E−13	(0.022)
203	6.73658E−13	(0.022)
204	4.43208E−13	(0.021)
205	3.32738E−13	(0.023)
206	2.18772E−13	(0.021)
207	1.76981E−13	(0.026)
208	1.65301E−13	(0.021)
209	1.34693E−13	(0.029)
210	7.81556E−14	(0.043)
211	1.23834E−14	(0.178)
212	0.0	(0.0)

[a]Fractional standard deviation.

Table C-2. Fluence-to-dose conversion factors for small intestine for the gamma groups of the DNA group structure

Group	Conversion factor (Gy/(#/cm^2))	(FSD)[a]
47	2.54437E−11	(0.021)
48	2.17819E−11	(0.025)
49	1.80636E−11	(0.020)
50	1.56431E−11	(0.015)
51	1.38029E−11	(0.013)
52	1.24816E−11	(0.016)
53	1.06188E−11	(0.015)
54	8.70402E−12	(0.016)
55	7.08459E−12	(0.020)
56	6.17101E−12	(0.020)
57	4.88339E−12	(0.019)
58	3.67116E−12	(0.018)
59	2.52329E−12	(0.013)
60	1.68316E−12	(0.014)
61	1.06869E−12	(0.016)
62	5.96841E−13	(0.018)
63	3.32738E−13	(0.023)
64	2.11807E−13	(0.018)
65	1.46937E−13	(0.018)
66	7.81556E−14	(0.043)
67	1.23834E−14	(0.178)
68	0.0	(0.0)

[a]Fractional standard deviation.

Table C-3. Fluence-to-dose conversion factors for small intestine for the neutron groups of the VITAMIN-E group structure

Group	Conversion factor (Gy/(#/cm^2))	(FSD)[a]
1	0.0	(0.0)
2	0.0	(0.0)
3	4.42479E−11	(0.048)
4	4.51694E−11	(0.036)
5	4.33242E−11	(0.039)
6	4.27242E−11	(0.039)
7	4.21154E−11	(0.049)
8	4.27255E−11	(0.046)
9	3.74525E−11	(0.043)
10	4.02298E−11	(0.043)
11	3.86614E−11	(0.037)
12	3.70819E−11	(0.042)
13	3.40594E−11	(0.037)
14	3.59060E−11	(0.044)
15	3.54100E−11	(0.044)
16	3.18678E−11	(0.037)
17	3.41120E−11	(0.042)
18	2.97542E−11	(0.048)
19	2.88498E−11	(0.044)
20	2.67231E−11	(0.047)
21	2.69863E−11	(0.044)
22	2.46493E−11	(0.058)
23	2.47135E−11	(0.048)
24	2.63137E−11	(0.045)
25	2.48529E−11	(0.045)
26	2.46581E−11	(0.042)
27	2.21414E−11	(0.044)
28	2.29078E−11	(0.056)
29	2.27017E−11	(0.050)
30	2.12169E−11	(0.041)
31	1.85487E−11	(0.052)
32	1.75093E−11	(0.057)
33	1.56630E−11	(0.053)
34	1.43891E−11	(0.056)
35	1.26648E−11	(0.053)
36	1.20322E−11	(0.058)
37	1.25019E−11	(0.055)
38	1.09472E−11	(0.048)
39	9.66563E−12	(0.055)
40	1.03335E−11	(0.048)
41	1.01624E−11	(0.057)
42	1.00884E−11	(0.055)
43	1.01095E−11	(0.055)
44	9.75417E−12	(0.057)
45	9.34009E−12	(0.057)
46	8.86232E−12	(0.058)

Table C-3. Cont'd

Group	Conversion factor (Gy/(#/cm^2))	(FSD)[a]
47	7.58663E−12	(0.056)
48	7.30488E−12	(0.065)
49	7.45984E−12	(0.054)
50	6.38049E−12	(0.045)
51	6.56702E−12	(0.052)
52	5.76149E−12	(0.059)
53	6.05276E−12	(0.061)
54	5.54435E−12	(0.058)
55	4.54551E−12	(0.059)
56	4.62878E−12	(0.060)
57	3.76953E−12	(0.063)
58	4.15118E−12	(0.051)
59	3.71892E−12	(0.070)
60	3.80444E−12	(0.059)
61	3.07058E−12	(0.056)
62	2.79354E−12	(0.055)
63	2.85634E−12	(0.061)
64	2.96580E−12	(0.061)
65	2.88713E−12	(0.049)
66	2.76421E−12	(0.059)
67	2.85763E−12	(0.059)
68	2.46808E−12	(0.057)
69	2.33994E−12	(0.053)
70	2.30250E−12	(0.053)
71	2.24134E−12	(0.051)
72	2.36070E−12	(0.047)
73	2.09126E−12	(0.048)
74	1.99989E−12	(0.047)
75	1.88229E−12	(0.045)
76	1.77609E−12	(0.047)
77	1.51679E−12	(0.047)
78	1.60896E−12	(0.043)
79	1.57381E−12	(0.045)
80	1.71316E−12	(0.040)
81	1.54315E−12	(0.038)
82	1.59033E−12	(0.046)
83	1.56136E−12	(0.039)
84	1.58210E−12	(0.048)
85	1.55507E−12	(0.039)
86	1.38720E−12	(0.039)
87	1.52472E−12	(0.040)
88	1.43205E−12	(0.038)
89	1.47022E−12	(0.043)
90	1.40876E−12	(0.041)
91	1.36063E−12	(0.035)
92	1.29027E−12	(0.040)
93	1.36047E−12	(0.041)

Table C-3. Cont'd

Group	Conversion factor (Gy/(#/cm^2))	(FSD)[a]
94	1.34194E−12	(0.043)
95	1.37674E−12	(0.042)
96	1.34659E−12	(0.043)
97	1.42570E−12	(0.040)
98	1.35244E−12	(0.042)
99	1.32928E−12	(0.049)
100	1.36184E−12	(0.045)
101	1.32520E−12	(0.041)
102	1.21979E−12	(0.043)
103	1.29522E−12	(0.035)
104	1.20533E−12	(0.046)
105	1.29055E−12	(0.046)
106	1.24790E−12	(0.054)
107	1.18092E−12	(0.049)
108	1.30713E−12	(0.050)
109	1.23003E−12	(0.053)
110	1.19652E−12	(0.051)
111	1.22206E−12	(0.049)
112	1.24750E−12	(0.047)
113	1.14652E−12	(0.046)
114	1.13094E−12	(0.041)
115	1.15171E−12	(0.051)
116	1.15124E−12	(0.048)
117	1.15011E−12	(0.058)
118	1.11169E−12	(0.044)
119	1.24713E−12	(0.046)
120	1.18530E−12	(0.049)
121	1.13735E−12	(0.052)
122	1.16307E−12	(0.048)
123	1.14076E−12	(0.057)
124	1.09607E−12	(0.048)
125	1.14910E−12	(0.051)
126	1.00037E−12	(0.053)
127	1.13319E−12	(0.048)
128	1.15030E−12	(0.044)
129	1.14642E−12	(0.037)
130	1.13313E−12	(0.049)
131	1.12774E−12	(0.048)
132	1.02503E−12	(0.051)
133	1.04544E−12	(0.049)
134	1.15589E−12	(0.052)
135	1.14043E−12	(0.038)
136	1.13927E−12	(0.047)
137	1.14658E−12	(0.055)
138	1.16589E−12	(0.049)
139	1.08463E−12	(0.052)
140	1.15295E−12	(0.047)

Table C-3. Cont'd

Group	Conversion factor (Gy/(#/cm^2))	(FSD)[a]
141	1.18003E−12	(0.045)
142	1.02812E−12	(0.049)
143	1.14310E−12	(0.048)
144	1.16320E−12	(0.055)
145	1.13710E−12	(0.052)
146	1.18145E−12	(0.045)
147	1.05459E−12	(0.051)
148	1.15248E−12	(0.059)
149	1.07909E−12	(0.060)
150	1.11896E−12	(0.057)
151	1.16562E−12	(0.060)
152	1.12867E−12	(0.061)
153	1.12573E−12	(0.063)
154	1.15893E−12	(0.055)
155	1.17005E−12	(0.058)
156	1.05645E−12	(0.057)
157	1.16203E−12	(0.050)
158	1.13582E−12	(0.048)
159	1.23231E−12	(0.060)
160	1.13328E−12	(0.060)
161	1.05479E−12	(0.064)
162	1.12572E−12	(0.057)
163	1.16023E−12	(0.063)
164	1.19840E−12	(0.066)
165	1.13535E−12	(0.063)
166	1.14258E−12	(0.067)
167	1.09565E−12	(0.061)
168	1.23650E−12	(0.051)
169	1.10013E−12	(0.058)
170	1.18481E−12	(0.056)
171	1.15314E−12	(0.050)
172	1.14718E−12	(0.057)
173	1.11550E−12	(0.059)
174	1.07661E−12	(0.026)

[a]Fractional standard deviation.

Table C-4. Fluence-to-dose conversion factors for small intestine for the neutron groups of the DNA group structure

Group	Conversion factor (Gy/(#/cm^2))	(FSD)[a]
1	0.0	(0.0)
2	4.42653E−11	(0.023)
3	4.24236E−11	(0.031)
4	4.27255E−11	(0.046)
5	3.95093E−11	(0.034)
6	3.86614E−11	(0.037)
7	3.56085E−11	(0.028)
8	3.56642E−11	(0.031)
9	3.29619E−11	(0.028)
10	2.93133E−11	(0.033)
11	2.68514E−11	(0.032)
12	2.48921E−11	(0.028)
13	2.27886E−11	(0.021)
14	1.85487E−11	(0.052)
15	1.63094E−11	(0.039)
16	1.31766E−11	(0.030)
17	1.02623E−11	(0.024)
18	9.63942E−12	(0.034)
19	7.46533E−12	(0.025)
20	5.73649E−12	(0.026)
21	4.03183E−12	(0.027)
22	2.99309E−12	(0.044)
23	2.89995E−12	(0.034)
24	2.80975E−12	(0.042)
25	2.37294E−12	(0.032)
26	2.23354E−12	(0.028)
27	1.72346E−12	(0.020)
28	1.57343E−12	(0.019)
29	1.38076E−12	(0.014)
30	1.33467E−12	(0.016)
31	1.23825E−12	(0.019)
32	1.17517E−12	(0.026)
33	1.16008E−12	(0.024)
34	1.16247E−12	(0.032)
35	1.10989E−12	(0.027)
36	1.13517E−12	(0.020)
37	1.12165E−12	(0.019)
38	1.12104E−12	(0.028)
39	1.15932E−12	(0.031)
40	1.09711E−12	(0.029)
41	1.14873E−12	(0.028)
42	1.13114E−12	(0.028)
43	1.12428E−12	(0.029)
44	1.14561E−12	(0.032)
45	1.14223E−12	(0.029)
46	1.10611E−12	(0.046)

[a]Fractional standard deviation.

Table C-5. Fluence-to-dose conversion factors for active marrow for the gamma groups of the VITAMIN-E group structure

Group	Conversion factor (Gy/(#/cm^2))	(FSD)[a]
175	0.0	(0.0)
176	2.76975E−11	(0.020)
177	2.40363E−11	(0.018)
178	2.00033E−11	(0.020)
179	1.80087E−11	(0.016)
180	1.67893E−11	(0.017)
181	1.61556E−11	(0.017)
182	1.51092E−11	(0.019)
183	1.36573E−11	(0.015)
184	1.31250E−11	(0.017)
185	1.21200E−11	(0.018)
186	1.11968E−11	(0.017)
187	9.82968E−12	(0.017)
188	8.97637E−12	(0.018)
189	8.11379E−12	(0.016)
190	6.81641E−12	(0.017)
191	5.74608E−12	(0.018)
192	5.02395E−12	(0.019)
193	4.51041E−12	(0.018)
194	3.85413E−12	(0.017)
195	2.97273E−12	(0.017)
196	2.56679E−12	(0.021)
197	2.17829E−12	(0.022)
198	1.89034E−12	(0.020)
199	1.68466E−12	(0.020)
200	1.61204E−12	(0.019)
201	1.48918E−12	(0.020)
202	1.15072E−12	(0.021)
203	8.05203E−13	(0.018)
204	5.31460E−13	(0.019)
205	3.74349E−13	(0.022)
206	2.55099E−13	(0.017)
207	1.96619E−13	(0.020)
208	1.76317E−13	(0.024)
209	1.49430E−13	(0.022)
210	1.01923E−13	(0.034)
211	5.34765E−14	(0.076)
212	1.05579E−14	(0.266)

[a]Fractional standard deviation.

Table C-6. Fluence-to-dose conversion factors for active marrow for the gamma groups of the DNA group structure

Group	Conversion factor (Gy/(#/cm^2))	(FSD)[a]
47	2.76975E−11	(0.020)
48	2.40363E−11	(0.018)
49	2.00033E−11	(0.020)
50	1.73990E−11	(0.011)
51	1.56324E−11	(0.013)
52	1.33912E−11	(0.011)
53	1.16584E−11	(0.013)
54	9.40303E−12	(0.012)
55	8.11379E−12	(0.016)
56	6.81641E−12	(0.017)
57	5.51500E−12	(0.014)
58	4.07726E−12	(0.012)
59	2.83742E−12	(0.013)
60	1.93708E−12	(0.013)
61	1.26354E−12	(0.015)
62	7.13955E−13	(0.014)
63	3.74349E−13	(0.022)
64	2.45352E−13	(0.015)
65	1.60185E−13	(0.016)
66	1.01923E−13	(0.034)
67	5.34765E−14	(0.076)
68	1.05579E−14	(0.266)

[a]Fractional standard deviation.

Table C-7. Fluence-to-dose conversion factors for active marrow for the neutron groups of the VITAMIN-E group structure

Group	Conversion factor (Gy/(#/cm^2))	(FSD)[a]
1	0.0	(0.0)
2	0.0	(0.0)
3	4.90983E−11	(0.036)
4	4.80411E−11	(0.042)
5	4.66447E−11	(0.030)
6	4.68141E−11	(0.033)
7	4.69254E−11	(0.033)
8	4.59783E−11	(0.035)
9	4.34712E−11	(0.037)
10	4.15742E−11	(0.043)
11	4.05194E−11	(0.035)
12	4.19088E−11	(0.043)
13	3.67198E−11	(0.038)
14	4.05229E−11	(0.033)
15	3.81671E−11	(0.040)
16	3.75383E−11	(0.035)
17	3.56267E−11	(0.045)
18	3.48711E−11	(0.042)
19	3.32731E−11	(0.041)
20	3.28078E−11	(0.036)
21	3.12096E−11	(0.041)
22	2.99176E−11	(0.050)
23	3.15811E−11	(0.048)
24	2.84992E−11	(0.041)
25	3.09480E−11	(0.042)
26	2.97036E−11	(0.038)
27	2.78766E−11	(0.040)
28	2.63610E−11	(0.042)
29	2.82307E−11	(0.036)
30	2.52829E−11	(0.037)
31	2.48775E−11	(0.040)
32	2.55333E−11	(0.048)
33	2.24493E−11	(0.047)
34	2.11753E−11	(0.049)
35	1.92744E−11	(0.046)
36	1.81644E−11	(0.048)
37	1.78348E−11	(0.045)
38	1.74141E−11	(0.041)
39	1.79490E−11	(0.042)
40	1.60429E−11	(0.053)
41	1.61954E−11	(0.045)
42	1.50961E−11	(0.044)
43	1.56772E−11	(0.045)
44	1.49732E−11	(0.046)
45	1.47034E−11	(0.045)
46	1.46098E−11	(0.043)

Table C-7. Cont'd.

Group	Conversion factor (Gy/(#/cm^2))	(FSD)[a]
47	1.35025E−11	(0.038)
48	1.26887E−11	(0.045)
49	1.31040E−11	(0.045)
50	1.17497E−11	(0.044)
51	1.18851E−11	(0.050)
52	1.05308E−11	(0.044)
53	1.06568E−11	(0.045)
54	1.02252E−11	(0.045)
55	9.44896E−12	(0.041)
56	8.95572E−12	(0.042)
57	8.50982E−12	(0.045)
58	8.75727E−12	(0.048)
59	8.19262E−12	(0.051)
60	7.65990E−12	(0.043)
61	6.81323E−12	(0.054)
62	6.89246E−12	(0.050)
63	6.64835E−12	(0.059)
64	5.85522E−12	(0.053)
65	5.66732E−12	(0.054)
66	6.34261E−12	(0.050)
67	5.64074E−12	(0.055)
68	5.48825E−12	(0.047)
69	4.94732E−12	(0.053)
70	5.29605E−12	(0.052)
71	4.73731E−12	(0.046)
72	4.75779E−12	(0.047)
73	4.65832E−12	(0.054)
74	4.65990E−12	(0.052)
75	4.11635E−12	(0.043)
76	4.08718E−12	(0.055)
77	3.73276E−12	(0.059)
78	3.49964E−12	(0.057)
79	3.45663E−12	(0.044)
80	3.23814E−12	(0.048)
81	3.07157E−12	(0.052)
82	3.10337E−12	(0.054)
83	2.89203E−12	(0.044)
84	2.76673E−12	(0.051)
85	2.67858E−12	(0.054)
86	2.78679E−12	(0.053)
87	2.68393E−12	(0.050)
88	2.70912E−12	(0.044)
89	2.81578E−12	(0.053)
90	2.56645E−12	(0.039)
91	2.23228E−12	(0.040)
92	2.44824E−12	(0.049)
93	2.11703E−12	(0.045)

Table C-7. Cont'd.

Group	Conversion factor (Gy/(#/cm^2))	(FSD)[a]
94	2.07564E−12	(0.051)
95	2.18811E−12	(0.046)
96	1.97123E−12	(0.045)
97	2.05588E−12	(0.047)
98	2.10458E−12	(0.050)
99	1.88462E−12	(0.047)
100	1.96036E−12	(0.048)
101	1.87502E−12	(0.040)
102	1.76856E−12	(0.046)
103	1.62745E−12	(0.048)
104	1.78236E−12	(0.042)
105	1.64214E−12	(0.046)
106	1.55363E−12	(0.047)
107	1.53444E−12	(0.042)
108	1.47979E−12	(0.041)
109	1.48426E−12	(0.045)
110	1.44458E−12	(0.041)
111	1.42984E−12	(0.042)
112	1.46637E−12	(0.039)
113	1.25906E−12	(0.047)
114	1.33730E−12	(0.037)
115	1.23139E−12	(0.044)
116	1.21647E−12	(0.041)
117	1.29778E−12	(0.042)
118	1.21228E−12	(0.046)
119	1.23846E−12	(0.042)
120	1.23603E−12	(0.041)
121	1.18269E−12	(0.042)
122	1.24332E−12	(0.043)
123	1.22018E−12	(0.044)
124	1.18863E−12	(0.042)
125	1.15241E−12	(0.039)
126	1.17079E−12	(0.037)
127	1.08815E−12	(0.041)
128	1.14093E−12	(0.038)
129	1.16179E−12	(0.046)
130	1.14600E−12	(0.036)
131	1.09427E−12	(0.039)
132	1.10861E−12	(0.044)
133	1.06081E−12	(0.052)
134	1.06852E−12	(0.046)
135	1.13883E−12	(0.050)
136	1.10895E−12	(0.050)
137	1.11202E−12	(0.052)
138	1.02283E−12	(0.046)
139	1.13531E−12	(0.040)
140	1.17031E−12	(0.048)

Table C-7. Cont'd.

Group	Conversion factor (Gy/(#/cm^2))	(FSD)[a]
141	1.12091E−12	(0.051)
142	1.18897E−12	(0.049)
143	1.19951E−12	(0.046)
144	1.11665E−12	(0.037)
145	1.18488E−12	(0.041)
146	1.14658E−12	(0.047)
147	1.21072E−12	(0.057)
148	1.18468E−12	(0.056)
149	1.14856E−12	(0.053)
150	1.19076E−12	(0.052)
151	1.13242E−12	(0.048)
152	1.15544E−12	(0.047)
153	1.09781E−12	(0.045)
154	1.17467E−12	(0.058)
155	1.18501E−12	(0.039)
156	1.21015E−12	(0.044)
157	1.24011E−12	(0.048)
158	1.22425E−12	(0.044)
159	1.20979E−12	(0.064)
160	1.24265E−12	(0.054)
161	1.29748E−12	(0.051)
162	1.32389E−12	(0.041)
163	1.27645E−12	(0.054)
164	1.20749E−12	(0.051)
165	1.23500E−12	(0.054)
166	1.23361E−12	(0.055)
167	1.39133E−12	(0.053)
168	1.32057E−12	(0.050)
169	1.29433E−12	(0.049)
170	1.12878E−12	(0.053)
171	1.26077E−12	(0.052)
172	1.26615E−12	(0.054)
173	1.21827E−12	(0.060)
174	1.22696E−12	(0.020)

[a]Fractional standard deviation.

Table C-8. Fluence-to-dose conversion factors for active marrow for the neutron groups of the DNA group structure

Group	Conversion factor (Gy/(#/cm^2))	(FSD)[a]
1	0.0	(0.0)
2	4.77256E−11	(0.022)
3	4.68691E−11	(0.023)
4	4.59783E−11	(0.035)
5	4.20663E−11	(0.033)
6	4.05194E−11	(0.035)
7	3.93793E−11	(0.029)
8	3.93744E−11	(0.026)
9	3.66064E−11	(0.028)
10	3.40921E−11	(0.029)
11	3.20286E−11	(0.027)
12	3.05351E−11	(0.026)
13	2.75761E−11	(0.017)
14	2.48775E−11	(0.040)
15	2.35291E−11	(0.034)
16	1.95904E−11	(0.026)
17	1.66980E−11	(0.021)
18	1.50188E−11	(0.028)
19	1.30776E−11	(0.019)
20	1.06013E−11	(0.021)
21	8.44389E−12	(0.021)
22	6.83539E−12	(0.041)
23	6.10584E−12	(0.033)
24	6.00044E−12	(0.037)
25	5.24720E−12	(0.029)
26	4.71911E−12	(0.028)
27	3.96213E−12	(0.024)
28	2.97272E−12	(0.024)
29	2.38021E−12	(0.016)
30	1.91054E−12	(0.018)
31	1.57731E−12	(0.018)
32	1.35767E−12	(0.023)
33	1.23570E−12	(0.021)
34	1.22936E−12	(0.028)
35	1.18309E−12	(0.022)
36	1.13168E−12	(0.018)
37	1.10547E−12	(0.018)
38	1.16312E−12	(0.029)
39	1.14654E−12	(0.024)
40	1.18713E−12	(0.029)
41	1.14366E−12	(0.023)
42	1.22125E−12	(0.025)
43	1.27210E−12	(0.024)
44	1.28195E−12	(0.028)
45	1.23743E−12	(0.027)
46	1.22037E−12	(0.045)

[a]Fractional standard deviation.

REFERENCES

1. "Effects of the Atomic Bomb on Nagasaki, Japan," U.S.Strategic Bombing Survey (USSBS) Report (June 1947). ORNL files also include glossy photos and room layout sketches apparently from the USSBS study.
2. "Medical Effects of Atomic Bombs," Report of the Joint Commission for the Investigation of the Effects of the Atomic Bomb in Japan, USAEC Report NP-3041 (July 1951).
3. Atomic Bomb Casualty Commission (ABCC) Radiation Shielding Summaries (c. 1954). A collection of unpublished studies relating personnel positions with exposure. Also, a set of construction blueprints. In custody of G.D.Kerr, Oak Ridge National Laboratory, Oak Ridge, TN.
4. William E. Loewe, "Perspectives on Radiation Dose Estimates for A-Bomb Survivors," pp. 630–638 in *Proceedings of the American Nuclear Society Topical Conference on Theory and Practices in Radiation Protection and Shielding*, (April 1987) ISBN:0-89448-132-0.
5. S. Levin, "LD50 for Healthy Young Adults Acutely Irradiated with Low LET Whole-Body Radiation," Unpublished Manuscript Draft (March 1987).
6. W. A. Woolson *et al.*, "House Shielding Models for Japanese A-Bomb Survivors." pp. 600-609 in *Proceedings of the American Nuclear Society Topical Conference on Theory and Practices in Radiation Protection and Shielding*, (April 1987) ISBN:0-89448-132-0.
7. William C. Roesch, Editor, "US-Japan Joint Reassessment of Atomic Bomb Radiation Dosimetry in Hiroshima and Nagasaki: Final Report," Radiation Effect Research Foundation, 5-2 Hijiyama Park, Minami-ku, Hiroshima, 732, Japan. Vol. 1, Ch. 2-3 (1987).
8. J. V. Pace, III, Computing and Telecommunications Division, Martin Marietta Energy Systems, P.O. Box 2008, Oak Ridge, TN 37831, personal communication.
9. M. L. Gritzner, Science Applications International Corporation, P.O.Box 2351, La Jolla, CA 92038, personal communication.
10. W. A. Rhoades and R. L. Childs, *An Updated Version of the DOT 4 One- and Two-Dimensional Neutron/Photon Transport Code,* ORNL-5851 (July 1982).
11. W. A. Rhoades and R. L. Childs, *The TORT Three-Dimensional Discrete Ordinates Neutron/Photon Transport Code,* ORNL-6268 (November 1987).
12. J. C. Ryman, Computing and Telecommunications Division, Martin Marietta Energy Systems, P.O. Box 2008, Oak Ridge, TN 37831, personal communication.
13. R. L. Stohler, Dikewood Division, Kaman Sciences, 1613 University Boulevard NE, Albuquerque, NM 87102, personal communication.
14. D. T. Ingersoll, R. W. Roussin, and C. Y. Fu, *DABL-69: A Broad-Group Neutron/Photon Cross-Section Library for Defense Nuclear Applications,* ORNL/TM-10568 (to be released).
15. R. W. Roussin, "DNA Broad-Group ANISN Libraries Based on VITAMIN-E," Internal Letter, Oak Ridge National Laboratory (August 28, 1985)

16. "VITAMIN E – A Coupled 174-Neutron, 38-Gamma-Ray Multigroup Cross-Section Library for Deriving Application-Dependent Working Libraries for Radiation Transport Calculations," RSIC Data Library Collection DLC-113 (December 1984).

17. D. E. Bartine, J. R. Knight, J. V. Pace, III, and R. W. Roussin, *Production and Testing of the DNA Few-Group Coupled Neutron-Gamma Cross-Section Library,* ORNL/TM-4840 (1977).

18. H. Goldstein, "The Attenuation of Gamma Rays and Neutrons in Reactor Shields," Nuclear Development Corporation of America, White Plains, New York, pp. 10-11 (May 1, 1957).

19. G. D. Kerr, *Photon and Neutron Fluence-to-Kerma Conversion Factors for ICRP-1975 Reference Man Using Improved Elemental Compositions for Bone and Marrow of the Skeleton,* ORNL/TM-8318 (1982).

20. S. N. Cramer, Engineering Physics and Mathematics Division, Oak Ridge National Laboratory, P.O. Box 2008, Oak Ridge, TN 37831.

21. B. S. Hopkins and J. C. Bailar, Jr., "General Chemistry for Colleges," pp. 512-513, D. C. Heath and Company, Boston (1951).

22. "Handbook of Chemistry and Physics, Thirty-Sixth Edition," pp. 494-495, Chemical Rubber Publishing Company, Cleveland (1954).

23. R. L. Childs and J. V. Pace, III, "GRTUNCL: First Collision Source Program," Computing and Telecommunications Division, Martin Marietta Energy Systems, P.O. Box 2008, Oak Ridge, TN 37831, unpublished memorandum.

24. W. W. Engle, Jr., *ANISN, A One-Dimensional Discrete Ordinates Transport Code with Anisotropic Scattering,* Oak Ridge Gaseous Diffusion Plant Report K-1693 (March 1967).

25. W. A. Rhoades *et al., Vehicle Code System (VCS) User's Manual,* ORNL-TM-4648 (August 1974).

26. W. A. Rhoades *et al., Development of a Code System for Determining Radiation Protection of Armored Vehicles (The VCS Code),* ORNL/TM-4664 (October 1974).

27. J. L. Thompson, M. B. Emmett, and H. L. Dodds, Jr., *Development and Evaluation of DOTTOR, A Computer Code to Couple Two-Dimensional to Three-Dimensional Discrete Ordinates Calculations,* ORNL/TM-9919 (April 1986).

28. W. A. Rhoades *et al.,* "Applications of the Three-Dimensional Oak Ridge Transport Code," pp. 225–238 in *Proc. Am. Nucl. Soc. Topical Meeting on Reactor Physics and Shielding*, Chicago (September 17–19, 1984).

29. M. B. Emmett, *The MORSE Monte Carlo Radiation Transport Code System,* ORNL-4972 (February 1975).

30. R. L. Childs and W. A. Rhoades, "The Extension of the Linear Nodal Method to Large Concrete Buildings," *Trans. Am. Nucl. Soc.* **50**, 475-477 (November 1985).

31. R. L. Childs and W. A. Rhoades, "The Linear Characteristic Method in XYZ Geometry," *Trans. Am. Nucl. Soc.* **55**, 352-354 (November 1987).

32. F. J. Muckenthaler *et al., Verification Experiment of the Three-Dimensional Oak Ridge Transport Code (TORT),* ORNL/TM-9528 (December 1985).

33. W. A. Rhoades *et al.,* "Analysis of the TORT Validation Experiment," *Trans. Am. Nucl. Soc.* **50**, 473-475 (November 1985).

34. S. N. Cramer, "DNA Concrete Building Study," Oak Ridge National Laboratory Internal Letter to D. T. Ingersoll (November 7, 1984).

35. S. N. Cramer and J. S. Tang, "Variance Reduction Methods Applied to Deep-Penetration Monte Carlo Problems," ORNL/TM-9643 (January 1986).

36. G. D. Kerr, Health and Safety Division, Oak Ridge National Laboratory, P.O. Box 2008, Oak Ridge, TN 37831, personal communication.

37. Hiroshima and Nagasaki: The Physical, Medical, and Social Effects of the Atomic Bombings, The Committee for the Compilation of Materials on Damage Caused by the Atomic Bombs in Hiroshima and Nagasaki, Translated by Eisei Ishikawa and David L. Swain, Basic Books, Inc., New York (1981).

38. R. W. Young, Defense Nuclear Agency, Washington D.C., "Human Mortality From Uniform Low-LET Radiation," paper presented to the NATO RSG V Meeting on LD50, Gosport, UK (11 May 1987).

39. M. D. Morris, Engineering Physics and Mathematics Division, Oak Ridge National Laboratory, P.O. Box 2008, Oak Ridge, TN 37831, private communication.

40. D. C. Kaul *et al.,* "Calculation of Dose in Quartz for Comparison with Thermoluminescent Dosimetry Measurements," pp. 620–629 in *Proceedings of the American Nuclear Society Topical Conference on Theory and Practices in Radiation Protection and Shielding,* (April 1987) ISBN:0-89448-132-0.

41. M. L. Gritzner, S. D. Egbert, and W. A. Woolson, "House Shielding Models for Japanese A-Bomb Survivors," pp. 600-609 in *Proceedings of the American Nuclear Society Topical Conference on Theory and Practices in Radiation Protection and Shielding,* (April 1987) ISBN:0-89448-132-0.

42. W. A. Woolson, Science Applications International Corporation, P.O.Box 2351, La Jolla, CA 92038, personal communication.

43. R. A. Lillie *et al.,* "Sensitivity/Uncertainty Analysis for the Hiroshima Dosimetry Reevaluation Effort," pp. 139-148 *Proceedings of the American Nuclear Society Topical Conference on Theory and Practices in Radiation Protection and Shielding,* (April 1987) ISBN:0-89448-132-0.

44. R. A. Lillie, Engineering Physics and Mathematics Division, Oak Ridge National Laboratory, P.O. Box 2008, Oak Ridge, TN 37831, personal communication.

45. Ashley W. Oughterson and Shields Warren, Medical Effects of the Atomic Bomb in Japan, McGraw-Hill (1956).

46. M. Cristy and K. F. Eckerman, *Specific Absorbed Fractions of Energy at Various Ages from Internal Photon Sources. I. Methods,* ORNL/TM-8381/V1 (April 1987).

47. C. R. Weisbin, R. W. Roussin, J. J. Wagschal, J. E. White, and R. Q. Wright, *VITAMIN-E: An ENDF/B-V Multigroup Cross-Section Library for LMFBR Core and Shield, LWR Shield, Dosimetry and Fusion Blanket Technology,* ORNL-5505 (ENDF-274) (Februrary 1979).

48. D. T. Ingersoll, "Draft Specifications for Updated DNA Few Group Cross Section Library," (April 26, 1985), enclosure with letter to W. H. Scott, SAIC (April 29, 1985).

49. J. T. West, T. J. Hoffman, and M. B. Emmett, *MORSE-SGC/S for the SCALE System,* Sect. F9 of *SCALE: A Modular Code System for Performing Standardized Computer Analyses for Licensing Evaluation,* NUREG/CR-0200 (ORNL/NUREG/CSD-2/V2/R2) (Rev. December 1984).

50. W. H. Scott and V. E. Staggs, "Adjoint Energy Biasing and Thermal Neutron Diffusion in the MORSE and VCS Codes," SAI-133-81-384-LJ (November 9, 1981).

51. J. V. Pace, III, "JPVISA," informal notes, personal communication to J. S. Tang, April 22, 1983.

52. N. M. Greene *et al., AMPX: A Modular Code System for Generating Coupled Multigroup Neutron-Gamma Libraries from ENDF/B,* ORNL/TM-3706 (Rev. December 1978).

53. J. H. Hubbell, "Photon Mass Attenuation and Energy-Absorption Coefficients from 1 keV to 20 MeV," *Int. J. Appl. Radiat. Isot.* **33**, 1269 (1982).

54. R. S. Caswell, J. J. Coyne, and M. L. Randolph, "Kerma Factors for Neutron Energies Below 30 MeV," *Radiat. Res.* **83**, 217 (1980).

55. G. D. Kerr and K. F. Eckerman, "Neutron and Photon Fluence-to-Dose Conversion Factors for Active Marrow of the Skeleton," pp. 133-145 in *Proc. Fifth Symp. on Neutron Dosimetry,* H. Schraube, G. Burger, and J. Booz, Editors, Vol. 1, EUR 9762 EN, Commission of the European Communities, Luxembourg (1985).

INTERNAL DISTRIBUTION

1. R. G. Alsmiller
2. B. R. Appleton
3. Y. Y. Azmy
4. D. E. Bartine
5–9. R. L. Childs
10. S. N. Cramer
11. M. B. Emmett
12. W. W. Engle, Jr.
13. C. Y. Fu
14–18. D. T. Ingersoll
19. J. O. Johnson
20. G. D. Kerr
21. R. A. Lillie
22. F. C. Maienschein
23. J. V. Pace III
24. S. A. Raby
25–29. W. A. Rhoades
30. J. C. Ryman
31. R. T. Santoro
32. C. O. Slater
33. R. M. Westfall
34. J. J. Dorning (consultant)
35. R. M. Haralick (consultant)
36–37. Laboratory Records Department
38. Laboratory Records, ORNL–RC
39. Document Reference Section
40. Central Research Library
41. ORNL Patent Section

EXTERNAL DISTRIBUTION

42. Office of the Assistant Manager for Energy Research and Development, DOE-ORO, Oak Ridge, TN 37831
43. D. Auton, Defense Nuclear Agency, ATTN: STRP, 6801 Telegraph Road, Alexandria, VA 22310
44. S. Levin, P.O. Box 547, Espanola, NM 87532.
45. R. L. Stohler, Dikewood Division, Kaman Sciences Corporation, 6400 Uptown Blvd. NE, Suite 300E, Albuquerque, NM 87110
46. R. W. Young, Defense Nuclear Agency, ATTN: STRP, 6801 Telegraph Road, Alexandria, VA 22310

47–372. Defense Nuclear Agency Transport Distribution (AU)

373–382. Office of Scientific and Technical Information, P.O. Box 62, Oak Ridge, TN 37830

☆ U.S. GOVERNMENT PRINTING OFFICE: 1989 648-119/00014